

# Modulation, Pre-Equalization and Pulse Shaping for PCM Voiceband Channels

*Nader Sheikholeslami Alagha*



Department of Electrical and Computer Engineering  
McGill University  
Montreal, Canada

December 2001

---

A thesis submitted to the Faculty of Graduate Studies and Research in partial fulfillment of the requirements for the degree of Doctor of Philosophy.

© 2001 Nader Sheikholeslami Alagha

## Abstract

For the past few decades, analog voiceband modems have been used extensively to carry digital information over the Public Switched Telephone Network (PSTN). Conventional voiceband modems treat the PSTN as an analog communication channel. However, today's PSTN is mostly a digital network except for the basic telephone services provided via analog subscriber lines. The conventional model of analog voiceband channels is no longer adequate to characterize the physical connection between terminals with direct digital access to the network and voiceband modems connected to analog subscriber lines. Such a connection requires a different model in each direction. There are now international modem standards which support rates of up to 56 kbits/s for the down-stream channel.

This dissertation examines the more challenging part of the voiceband communication channel, i.e., the up-stream direction connecting an analog subscriber to the digital network. The major source of distortion on the up-stream channel is quantization error caused by analog-to-digital conversion performed as part of the encoding to Pulse-Code Modulation (PCM) process. A bandpass filter prior to the PCM encoder restricts the bandwidth while the sampling rate of the PCM encoder is predetermined by the network. Signalling in the presence of such constraints lead to theoretical problems as well as practical concerns in modem design.

Communication models that characterize PCM voiceband channels are developed. We investigate modulation design and related issues including index mapping, constellation design and constellation probability assignment to match the pre-determined structure of the detector at the receiver, i.e., the PCM encoder at the central office.

We develop a framework for transmitter structures that can avoid or reduce Inter-Symbol Interference (ISI) at the receiver in order to sidestep the limited bandwidth of the up-stream channels and the fixed sampling rate of the up-stream channel. Techniques employed include linear filtering, spectral shaping and precoding to reduce the ISI, while limiting the average transmitted signal power. A filterbank structure for pre-equalizing channels with spectral nulls is also described.

A new method for pulse shaping design is proposed. The new pulse shaping filters provide a compatible design that can be used for the up-stream PCM channel as well as to the cascade of the up-stream and the down-stream channels.

Compared to conventional modem design, the proposed modulation and pre-equalization techniques together allow for an increase of the data transmission rates in the up-stream direction of up to 50%.

## Résumé

Depuis quelques dizaines d'années, les modems téléphoniques analogiques servent dans une large mesure à acheminer des informations numériques sur le réseau téléphonique public commuté (RTPC). Les modems téléphoniques conventionnels traitent le RTPC comme une voie de communication analogique. Or, le RTPC actuel est surtout un réseau numérique, hormis les services téléphoniques de base fournis par le truchement des lignes d'abonnés analogiques. Le modèle traditionnel de voie téléphonique analogique ne suffit plus à caractériser la connexion matérielle entre les terminaux à accès numérique direct au réseau et les modems téléphoniques branchés aux lignes d'abonnés analogiques. Une telle connexion nécessite un modèle différent dans chaque direction. Il existe maintenant des recommandations internationales de modem fondées sur les caractéristiques de la voie aval acheminant des débits pouvant atteindre 56 kbit/s.

Cet essai porte sur la portion la plus délicate de la voie de communication téléphonique, soit la direction amont reliant l'abonné analogique au réseau numérique. La source majeure de distorsion de la voie amont est l'erreur de quantification causée par la conversion analogique-numérique réalisée au cours du codage en modulation par impulsions codées (MIC). Un filtre passe-bande précédant le codeur MIC limite la largeur de bande de la voie alors que le taux d'échantillonnage du codeur MIC est prédéterminé par le réseau. La signalisation en présence de telles limites pose de nombreux problèmes théoriques et des difficultés pratiques dans la conception du modem.

Nous élaborons des modèles de communication pour caractériser les voies téléphoniques MIC. La conception de la modulation et les enjeux associés, y compris la cartographie des indices, la conception de la constellation et l'affectation de la probabilité de constellation, sont étudiées afin de correspondre à la structure prédéterminée du détecteur au récepteur, c'est-à-dire le codeur MIC au bureau central.

Pour contourner la largeur de bande limitée et le taux d'échantillonnage fixe de la voie amont, nous créons un cadre de conception de l'émetteur qui évite ou réduit le brouillage intersymbole au récepteur. Parmi les techniques utilisées, mentionnons la mise en forme spectrale et le précodage afin de réduire le brouillage intersymbole tout en maintenant une limite sur la puissance moyenne du signal émis. Nous proposons aussi une structure de banc de filtres afin de précorriger les voies avec une phase non minimum ou des extinctions spectrales.

Nous proposons aussi une nouvelle méthode de conception de la mise en forme des impulsions. Les nouveaux filtres de mise en forme des impulsions ont un design compatible qui peut être appliqué à la voie MIC amont ainsi qu'à la cascade de voies amont et aval.

Comparées à la conception du modem conventionnel, les techniques de modulation et de précorrection proposées permettent ensemble d'accroître jusqu'à 50% les débits de transmission de données en amont.

## Acknowledgments

I would like to express my sincere gratitude to my supervisor, Professor Peter Kabal for his patient and friendly support during the course of my Ph.D. studies. His contributions to this thesis and my education are highly appreciated.

The financial support of this research was mainly provided by Professor Kabal via a grant from the Natural Sciences and Engineering Research Council of Canada. I would like to thank Professor Kabal and recognize NSERC for this support.

My special thanks go to the members of the Telecommunications and Signal Processing Laboratory including the present graduate students and others who have graduated from this lab in the past few years. I have many good memories from the TSP Lab and have had many inspiring conversations with other students. Professor Kabal has provided the leadership and set the tone for such a friendly environment.

I would like to thank Sylviane Duval for her editorial comments regarding this dissertation. I am greatly thankful to Paul Mercier and Martin Côté, my colleagues at EMS Technologies Canada, for the French translation of the thesis abstract. My special thanks go to Marin Côté for his generous support of my studies since the beginning of my work at EMS.

I am indebted to my parents for encouraging me to pursue my studies. I am thankful to my father for being such a supportive friend in all stages of my life. I am grateful to my mother for being such a caring person at home and an excellent teacher at school.

My journey towards graduate studies was inspired by many individuals: those scholars who care so much for education and educating people to create a better society. Among them, my special gratitude goes to Dr. Jalil Mostashari. Just remembering his words has helped me overcome many difficulties in this journey. I would like to thank him for being such an inspiring figure in my life.

Last but not least, I am greatly thankful to my dear wife, Firouzeh, for her unconditional support of my studies in the past two years. I greatly appreciate her patience, care and encouragements.

---

# Contents

<b>1</b>	<b>Introduction</b>	<b>1</b>
1.1	Data transmission over voiceband channels . . . . .	1
1.2	PSTN: A hybrid communication network . . . . .	2
1.3	Related work . . . . .	4
1.4	Our research objectives . . . . .	5
1.5	Thesis organization . . . . .	6
<b>2</b>	<b>The PCM Voiceband Channel Characteristics</b>	<b>7</b>
2.1	Subscriber access to the PSTN . . . . .	7
2.2	Subscriber loop interface circuit . . . . .	7
2.3	Subscriber loop characteristics . . . . .	8
2.3.1	Hybrid Circuits . . . . .	11
2.3.2	Characteristics of the filters in the line circuit . . . . .	11
2.3.3	PCM encoding and decoding . . . . .	13
2.3.4	Non-uniform Quantizer . . . . .	17
2.3.5	Multiplexing . . . . .	19
2.4	Power Constraints of the PCM channel . . . . .	19
2.5	Capacity of PCM voiceband channels . . . . .	21
2.6	PCM Modems . . . . .	22
2.6.1	Digital network imperfections . . . . .	22
2.7	The down-stream PCM channel . . . . .	24
2.8	The up-stream PCM channel . . . . .	24
2.8.1	Synchronization . . . . .	25
2.8.2	Signal mapping and constellation design . . . . .	26
2.8.3	Channel Pre-equalization . . . . .	26
2.8.4	Echo cancellation . . . . .	26
2.8.5	Channel Coding . . . . .	26

---

2.9	End-to-end PCM voiceband channels . . . . .	26
2.9.1	Synchronization . . . . .	27
2.9.2	Channel estimation . . . . .	27
2.9.3	Channel Equalization . . . . .	27
<b>3</b>	<b>Modulation Design for the Up-Stream PCM Channel</b>	<b>28</b>
3.1	Modulation scheme . . . . .	28
3.2	Optimal signal levels . . . . .	31
3.2.1	Performance criterion . . . . .	33
3.2.2	Remarks . . . . .	36
3.2.3	Performance results . . . . .	37
3.2.4	How to choose detector thresholds . . . . .	41
3.2.5	Bit-to-symbol mapping . . . . .	43
3.3	Non-uniform probability distributions for constellation points . . . . .	51
3.3.1	Maximizing the entropy . . . . .	51
3.3.2	Examples of maximum entropy distributions for a PAM signal . . . . .	52
3.3.3	Channel capacity for non-uniform PAM modulation . . . . .	53
3.3.4	The Huffman algorithm for bit-to-symbol mapping . . . . .	57
3.4	Chapter Summary . . . . .	61
<b>4</b>	<b>Transmitter Design for the Up-stream PCM Channel</b>	<b>64</b>
4.1	Optimal transmitter filter design . . . . .	65
4.1.1	Peak distortion criterion . . . . .	67
4.1.2	Mean-Square Error (MSE) criterion . . . . .	68
4.2	Optimal transmitting filter design for the up-stream PCM channels . . . . .	71
4.2.1	Observations and remarks . . . . .	76
4.3	Spectrum shaping and filtering . . . . .	80
4.3.1	Methods of Spectrum Shaping . . . . .	82
4.3.2	Spectrum shaping by inserting redundant symbols . . . . .	83
4.4	Precoding: combined filtering and spectral shaping . . . . .	92
4.4.1	Tomlinson-Harashima Precoding . . . . .	92
4.4.2	Precoding design for the up-stream PCM channels . . . . .	96
4.4.3	Linear block-by-block pre-filtering . . . . .	97
4.5	Concluding Remarks . . . . .	102

---

<b>5</b>	<b>Filterbank Structures for ISI Channel Pre-Equalization</b>	<b>104</b>
5.1	Signal design based on non-uniform sampling . . . . .	104
5.1.1	Pre-equalizer design for the up-stream PCM channel . . . . .	108
5.2	Non-maximally decimated filterbanks . . . . .	108
5.2.1	IIR implementation of the FIR filters . . . . .	113
5.2.2	Average transmitted power . . . . .	114
5.3	Performance Comparison . . . . .	115
5.4	Remarks . . . . .	118
<b>6</b>	<b>A New Family of Pulse Shaping Filters</b>	<b>119</b>
6.1	Pulse shaping filters for voiceband PCM channels . . . . .	119
6.2	Nyquist filters . . . . .	120
6.2.1	Nyquist Filters with compensated phase . . . . .	122
6.3	Extension of Nyquist's first criterion . . . . .	123
6.3.1	Square-root Nyquist filters . . . . .	123
6.3.2	Phase compensated square-root raised-cosine filter . . . . .	124
6.3.3	Special Case: Full excess bandwidth . . . . .	126
6.3.4	Eye pattern diagram . . . . .	127
6.3.5	SNR degradation . . . . .	128
6.4	Generalized Raised-Cosine Filters . . . . .	132
6.4.1	Nyquist filter design using phase compensation . . . . .	132
6.5	Design examples . . . . .	134
6.5.1	Nyquist filters with smoother spectra . . . . .	134
6.5.2	Nyquist filters with reduced ISI due to truncation . . . . .	136
6.6	Remarks . . . . .	139
<b>7</b>	<b>Concluding Remarks</b>	<b>141</b>
7.1	Contributions . . . . .	143
7.2	Future Work . . . . .	144
<b>A</b>	<b>Optimal Linear Transmitter Structure</b>	<b>146</b>
<b>B</b>	<b>Optimal MMSE Transmitting Filters</b>	<b>148</b>
B.1	Transmitting filter with infinite length impulse response . . . . .	148
B.2	Finite Impulse Response . . . . .	150
<b>C</b>	<b>Inner boundaries of the eye pattern for the square-root filter</b>	<b>152</b>

---

D The impulse response of $H_{sqrt}(f)$	154
References	155

# List of Figures

1.1	Schematic graph network access via PSTN . . . . .	3
2.1	Subscriber loop access via line interface circuits at the central office. . . . .	8
2.2	The T-equivalent circuit for a unit length segment of a subscriber line . . . . .	9
2.3	The magnitude response of subscriber lines with a 26-AWG cable. . . . .	10
2.4	Magnitude response of a loaded line . <i>vs.</i> an unload line . . . . .	10
2.5	Measurement results of the magnitude response of several subscriber lines. . . . .	12
2.6	A circuit model of a hybrid coupler . . . . .	13
2.7	Example of the frequency response of a send filter. . . . .	14
2.8	Frequency response of the overall send-receive filter is compared with Recommendation G.712 requirements. . . . .	15
2.9	Empirical results as provided in Recommendation V.56. . . . .	16
2.10	Bit allocation in a $\mu$ -Law codeword. . . . .	18
2.11	A channel bank multiplexing 24 voice channels to a DS1 stream. . . . .	20
2.12	Three types of PCM channels. . . . .	23
2.13	The Up-stream PCM Channel . . . . .	25
3.1	A schematic model for the Up-stream PCM channel. . . . .	28
3.2	In the up-stream PCM channel the ADC at the central office is interpreted as a detector .	30
3.3	Placement of the signal points relative to the thresholds . . . . .	32
3.4	Two examples of conditional probabilities of the received signal. . . . .	35
3.5	Performance results of 32-PAM modulation designed for the up-stream PCM channels. . .	38
3.6	Performance results for non-uniform 64-PAM modulation designed for the up-stream PCM channels. . . . .	40
3.7	Performance results for the non-uniform 128-PAM designed for the up-stream PCM channels.	40
3.8	Performance results for non-uniform PAM modulation with an average of $-12$ dBm0 signal power. . . . .	41
3.9	The average transmitted bit-rate as a function of symbols per frame on a PCM channel. .	43

---

3.10	The average Hamming distance between indices of adjacent points is shown as a function of $K$ for a 58-PAM modulation . . . . .	45
3.11	Bit-to-symbol mapping based on hybrid natural-Gray encoding. . . . .	47
3.12	Compare the average Hamming distance generated by the natural index mapping with that generated by the Hybrid Gray-Natural index mapping . . . . .	49
3.13	Probability of bit error for a 58-PAM modulation over a PCM up-stream channel. . . . .	50
3.14	Probability distribution of the PAM symbols. The average signal power is $-10$ dBm0 . . . . .	54
3.15	Probability distribution of the PAM symbols. The average signal power is $-12$ dBm0. . . . .	54
3.16	Probability of symbol error for PAM constellations with a maximum entropy distribution and uniform probability distribution. . . . .	55
3.17	Transmitted bit rates of PAM modulation over a PAM channel. . . . .	55
3.18	Channel capacity of a Gaussian channel with a continuous input signal and a PAM-modulated input signal. . . . .	58
3.19	Probability distributions of a constellation point with Huffman bit assignments compared to the maximum entropy distributions. . . . .	62
3.20	Transmitted bit-rates as a function of SNR for three different probability distributions: maximum entropy, the Huffman algorithm and uniform distributions. . . . .	62
4.1	The general structure of an optimal transmitter filter. . . . .	66
4.2	A discrete-time model of the up-stream PCM channel. . . . .	67
4.3	The magnitude response of the channel equivalent filter as discussed in Example 1. . . . .	72
4.4	The impulse response of the channel discussed in Example 1. . . . .	72
4.5	Pole-zero plot of a channel filter of Example 1. . . . .	73
4.6	Signal-to-interference ratio as a function of the average transmitted power . . . . .	73
4.7	Probability of symbol error for several PAM signals as a function of signal-to-interference ratio. . . . .	75
4.8	Probability of symbol error as a function of SNR. . . . .	75
4.9	Channel characteristics in Example 2. . . . .	77
4.10	Pole-zero plot of a channel filter. . . . .	78
4.11	Signal-to-ISI ratio as a function of the average transmitted power in Example 2. Compared to Example 1, a significant increase in the average transmitted power is required to obtain the same SIR. . . . .	78
4.12	Probability of symbol error for several PAM signals as a function of signal-to-interference ratio. . . . .	79
4.13	Probability of symbol error as a function of SNR. . . . .	79

4.14	Spectrum shaping cascaded with an optimal filtering to control MMSE while maintaining the limit on the average transmitted power. . . . .	80
4.15	Spectrum shaping by inserting redundant symbols into a block of data symbols. . . . .	84
4.16	Power spectrum including spectral null . . . . .	87
4.17	Transmitter design for a channel with spectral null at DC. . . . .	88
4.18	Spectrum shaping reduces the average transmitted power. . . . .	90
4.19	Average transmitted power as a function of the block size for a 90-PAM signal. . . . .	91
4.20	Data transmission rate as a function of transmitted power . . . . .	91
4.21	Tomlinson-Harashima Precoder. . . . .	93
4.22	A TH-precoder can be viewed as combined filtering and spectrum shaping. . . . .	94
4.23	A precoding followed by linear filter at the transmitter. . . . .	97
4.24	A block-by-block inverse filtering. . . . .	98
4.25	Redundancy insertion in a block of symbols to control the transmitted power. . . . .	100
4.26	The average signal power as a function of the block size. . . . .	101
4.27	Comparing the power gain of two inverse filters. . . . .	102
5.1	Signal design for a bandlimited channel with non-uniform symbol timing distribution. . .	106
5.2	Signal design for a channel with $W = 3500$ Hz bandwidth and sampling rate of $1/T_s=8000$ Hz. . . . .	107
5.3	A non-maximally decimated structure as a channel pre-equalizer. . . . .	109
5.4	A set of FIR filters can partially invert the channel filter. . . . .	110
5.5	Power gain as a function of the effective symbol rate for $H(z) = 1 - z^{-1}$ . . . . .	116
5.6	Power gain as a function of the effective symbol rate for $H(z) = 1 - z^{-2}$ . . . . .	117
5.7	Power gain as a function of the effective symbol rate for $H(z) = (1+z^{-1})(1-e^{j0.8\pi}z^{-1})(1-e^{-j0.8\pi}z^{-1})$ . . . . .	117
6.1	Pulse shaping filter design for PCM channels. . . . .	121
6.2	Piece-wise linear phase compensator for square-root raised-cosine filter. . . . .	125
6.3	Normalized impulse responses of the square-root raised-cosine filter with $\alpha=1$ , (dashed line). The phase compensated filter has a delayed impulse response (solid line). . . . .	127
6.4	Binary eye patterns for a raised-cosine filter and a square-root raised-cosine filter. .	129
6.5	Eye patterns (4 level PAM) for a raised-cosine filter and a square-root raised-cosine filter. . . . .	130
6.6	Binary eye patterns for a raised-cosine filter and a phase compensated square-root raised-cosine filter. . . . .	131
6.7	Polynomials $P_n(x)$ to generate the generalized raised-cosine filter. . . . .	136

---

6.8	Impulse responses of generalized raised-cosine filters generated by $P_1(x)$ and $P_3(x)$ are compared. . . . .	137
6.9	Inner boundaries of the eye diagram for several generalized raised-cosine filters with $\alpha = 1$ .	138

# List of Tables

3.1	Huffman algorithm for bit-to-signal mapping. The bit sequence associated with each constellation is presented. . . . .	61
5.1	Comparison of decimation rates and the average filterbank power gain. . . . .	115
6.1	Comparison of several generalized raised-cosine filters with $\alpha = 1$ . . . . .	135
6.2	Nyquist filter design to reduce ISI due to truncation. . . . .	140

# Glossary

		<i>First appears on page</i>
<b>ADC</b>	Analog to Digital Converter	2
<b>ADSL</b>	Asymmetric Digital Subscriber Line	1
<b>AWGN</b>	Additive White Gaussian Noise	21
<b>BER</b>	Bit Error Rate	45
<b>CODEC</b>	Encoder and Decoder	17
<b>CRTC</b>	Canadian Radio and Telecommunication Commission	19
<b>DAC</b>	Digital-to-Analog Converter	11
<b>DLC</b>	Digital Loop Carrier	8
<b>FCC</b>	Federal Communication Commission	19
<b>HGN</b>	Hybrid Gray-Natural (index mapping)	46
<b>ICI</b>	Inter-Channel Interference	108
<b>ISDN</b>	Integrated Service Digital Network	1
<b>ISI</b>	Inter-Symbol Interference	22
<b>ISP</b>	Internet Service Provider	2
<b>(M)MSE</b>	(Minimum) Mean Square Error	67
<b>PSTN</b>	Public Switched Telephone Network	1
<b>PAM</b>	Pulse Amplitude Modulation	29
<b>PSD</b>	Power Spectrum Density	68
<b>SER</b>	Symbol Error Rate	37
<b>SIR</b>	Signal to Interference (ISI) Ratio	71
<b>SNR</b>	Signal to Noise Ratio	21
<b>SQNR</b>	Signal to Quantization Noise Ratio	17
<b>TH-precoder</b>	Tomlinson-Harashima precoder	92

# Chapter 1

## Introduction

### 1.1 Data transmission over voiceband channels

For the past few decades, data transmission over the Public Switched Telephone Network (PSTN) has been an active area of scientific research as well as product development. Although the PSTN was originally designed for voice communications, its worldwide reach and relatively low service cost have made it convenient to also use the PSTN for data communication.

Conventional telephone service provides a limited bandwidth to each user. The bandwidth of a telephone channel is limited to frequencies ranging approximately from 200 Hz to 3600 Hz. Apart from limited bandwidth, a telephone channel has other effects on the transmitted voiceband signal such as non-linear phase and amplitude distortion, crosstalk from the signals present on the adjacent wires, and signal echo. Several recommendations have been developed (or are being developed) by international standards bodies to characterize the impairments of telephone circuits and to provide guidelines for voiceband modem design.

Over the past few years, it has been repeatedly predicted that network access via telephone lines would be replaced by new services based on emerging technologies. Despite all these predictions, voiceband modems are still used by the majority of home computer users and small business owners for data communications and network access. There is no doubt that the demand for more reliable and efficient information access will bring changes to this situation. Several competing technologies are available to provide the solution to the so-called “last mile problem”, that is, how to connect customers premises to the broadband network in a more flexible and affordable way. Services such as Integrated System Digital Network (ISDN) and Asymmetric Digital Subscriber Line (ADSL) are two examples of digital data transmission over the twisted-pair subscriber lines. Compared to voiceband modems, these technologies require investment by the telephone companies to install special equipment at the central offices. Depending on the distance between user

premises and the serving central office, some users may not be able to use such services.

Other technologies for network access such as coaxial cable, wireless access, direct satellite access and fiber optic lines are available. Technologies developed for each of these media have shown merits for particular applications. However, there seems to be no universal technology for all locations and all applications.

Among all access technologies, the “plain old telephone service” provides the widest access coverage in the world. A voiceband modem connected to any phone line can reach millions of other modems connected to the PSTN. Therefore, it is desirable to investigate new techniques to reach the maximum achievable data transmission rates over voiceband channels.

## 1.2 PSTN: A hybrid communication network

In most parts of the world, the public switched telephone network has evolved towards a digital communication network. The interconnections among central offices are based on fully digital transmission via electrical cable, radio links, and increasingly, fiber optic cables. There are many traffic sources such as Internet Service Providers (ISP) and medium to large size businesses which have a direct digital connection to the PSTN. The only remaining analog links are the *analog subscriber loops* providing subscribers with basic telephone services. Figure 1.1 shows a schematic diagram of the telephone network. As shown in this figure, subscribers such as D1 or D2 use technologies such as ISDN or even radio links for direct digital access to the PSTN, whereas other telephone users are connected to the network via an analog subscriber loop. Since the rest of the network carries only digital data, the analog signal received must be converted to a stream of binary digits. The conversion scheme used at the central office is known as Pulse Code Modulation (PCM) encoding. The analog signal is passed through a band-limited filter followed by a sampler and subsequent Analog-to-Digital Converter (ADC). A non-uniform encoding rule ( $\mu$ -law or A-Law) is used to map each sample to an 8-bit codeword. The output of the PCM encoder is a stream of bits constructed from codewords. To reconstruct the analog signal, the bit stream is passed through a PCM decoder. The PCM encoding and decoding processes add signal distortion. Although the distortion caused by the PCM encoding process is tolerable for voice signals, it has a significant impact on the performance of voiceband modems. In fact, quantization distortion is the predominant source of data transmission errors over voiceband PCM channels.

Until the early 1990s, it was widely believed that voiceband modems had reached their maximum theoretical limits in terms of data transmission rate. The theoretical limit was based on a linearized model of the voiceband channels. In this model, a voiceband channel was essentially viewed as an analog medium where the quantization distortion caused by the PCM encoding and decoding process was treated as additive noise.

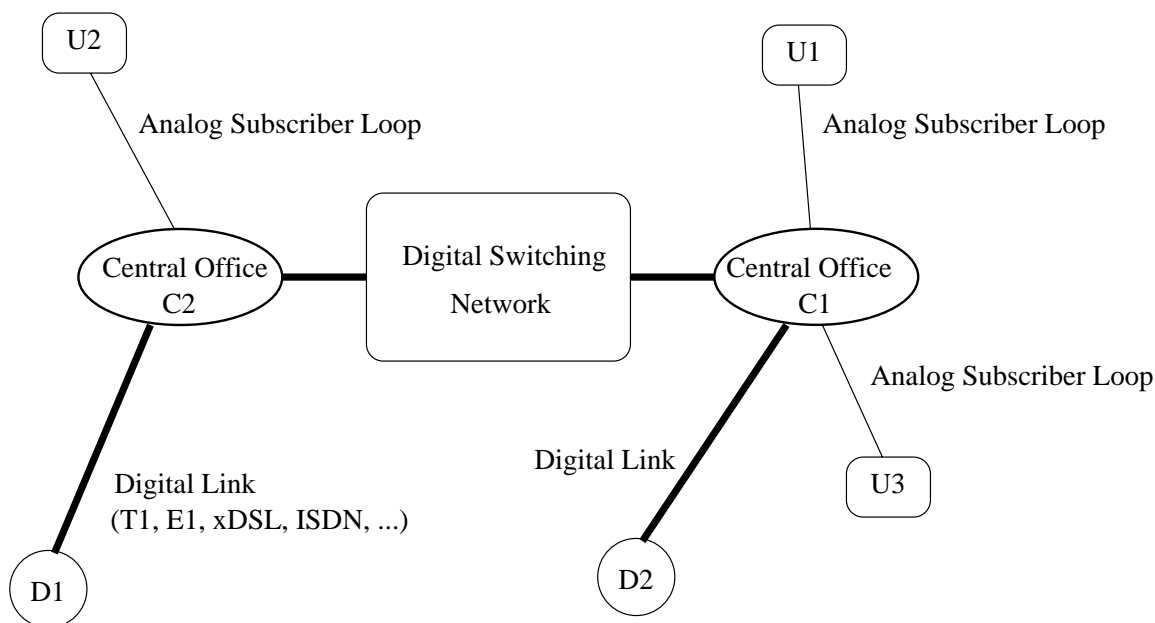


**Fig. 1.1** Schematic graph network access via PSTN

However, the conventional model of voiceband channels is not adequate to describe the different network access scenarios over the PSTN. Analog subscriber loops can be part of three different types of connections. One type is a connection from a digital source (D1 in Fig. 1.1) to an analog subscriber. A signal flowing in this direction is not distorted by quantization error since it does not pass through any PCM encoder. We refer to the channel model associated with this connection as the *down-stream* PCM channel. The second type of connection begins with an analog subscriber and ends with a digital user. We call the corresponding channel the *up-stream* PCM channel. This channel includes a PCM encoder with an analog input signal and a digital bit stream at the output. The third type of connection starts from an analog subscriber, passes through a PCM encoder and decoder and ends with another analog subscriber line. We refer to this channel as an *end-to-end* PCM voiceband channel. Communication models describing these three types of channels are different.

In a down-stream PCM channel, where the transmitted signal is not distorted by quantization error at the central office, the maximum achievable information rate is higher than the 33 kbits/s provided by state of the art analog voiceband modems. There are now international modem standards for down-stream PCM channels that can support rates of up to 56 kbits/s.

For the up-stream PCM channel, the presence of analog-to-digital conversions as part of the PCM encoder is a major source of signal distortion. Furthermore, the bandwidth of the up-stream channel is limited by a bandpass filter ahead of the PCM encoder. The bandpass filter, followed by

the PCM encoder, acts as the receiver front-end for the up-stream channel. The characteristics of this receiver, including the sampling rate, sample timing and detection process are pre-determined by the network.

An end-to-end PCM voiceband channel consists of two channels; an up-stream PCM channel followed by a down-stream PCM channel. Compared to the up-stream and the down-stream channels, achieving a higher transmission rate over an end-to-end PCM channel is more difficult since the end points do not have direct access to the digital data stream.

### 1.3 Related work

Theoretical studies as well as industrial R&D led to a significant increase in achievable data-rates on voiceband channels. Data transmission rates increased from 300 bits/s in the mid 1950s to rates of up to 33.6 kbits/s in early 1990s. This advancement was mainly due to improved channel modelling and the invention of sophisticated techniques for mitigating the channel impairments<sup>1</sup>. Many of these techniques were examined by standards bodies to develop recommendations and guidelines for voiceband modems. The Series V Recommendations from ITU-T<sup>2</sup> have global acceptance in modem development. Recommendation V.34 [2] was the last recommendation for voiceband modem design that considered the conventional view of additive noise for the quantization error [3].

Although the development of the V.34 Standard seemed to be the end of the voiceband modem era, an interesting observation regarding the PCM voiceband channels created a new wave of research and development on voiceband modem design. Instead of ignoring the underlying structure of signal conversions in the PCM encoders and decoders, this structure can be employed in order to reduce the distortion caused by these conversions.

To obtain a higher data rate over a PCM voiceband channel, the quantization distortion causing symbol detection errors should be avoided. Voiceband modems designed to achieve this goal are known as PCM modems. The idea of PCM voiceband modems was first investigated in [4]. This work was followed by [5] which establishes a method for equalizer design for PCM modems. The error correction method to combat echo was described in [6]. Many of these published articles have companion patents [7, 8, 9, 10, 11]. A report on the actual system design based on the idea of PCM modems is described in [12].

The first recommendation on PCM modems, known as Recommendation V.90, was completed in 1998 [13]. Recommendation V.90 uses a spectrum shaping known as convolutional spectrum shaping [14] to reduce the power density of the transmitted signal at certain frequencies.

---

<sup>1</sup>A comprehensive review of earlier work on voiceband modems is presented in [1].

<sup>2</sup>International Telecommunication Union–Telecommunication Standardization Sector.

Recommendation V.90 provides asymmetrical data rates in two directions. During the development of Recommendation V.90, the support of higher data-rates in the up-stream PCM channel was proposed [15, 16]. Due to technical uncertainties on several issues such as channel equalization, channel coding, signal mapping and constellation design, the ITU-T committee did not reach an agreement on a new standard for the up-stream PCM channels [17]. As a result, the conventional voiceband transmission techniques based on Recommendation V.34 were adopted for the up-stream direction.

There is ongoing work by an ITU-T study group to develop new recommendation to achieve higher transmission rates over the up-stream PCM channels<sup>3</sup>. For data transmission over the up-stream PCM channels, a technique based on convolutional spectrum shaping [14] [13] and a linear filtering is proposed [18].

## 1.4 Our research objectives

The main objective of our research is to identify methods of obtaining higher rates of reliable data transmission over voiceband PCM channels. We particularly target the up-stream PCM channel, where the pre-determined structure of the receiver front-end creates several theoretical, as well as practical, problems in the modem design.

We first need to identify alternative models of data transmission over a PCM channel. We characterize sources of impairment in the PCM channel and develop strategies to avoid or minimize the impact of distortions on the data transmission performance.

There are several constraints imposed by the telephone network on the up-stream PCM channel receiver as well as the transmitted signal. We investigate methods of modulation design which are compliant with network requirements and match the pre-determined structure of the receiver. We investigate design techniques in constellation design, index mapping and constellation probability assignment that can improve the system performance under a transmitted power constraint.

Due to limited bandwidth and fixed sampling rate, the up-stream PCM channel creates inter-symbol interference (ISI) at the receiver. In order to eliminate or reduce the impact of ISI on the system performance, we investigate methods of compensating for the channel at the transmitter. Since there is no direct access to the receiver front-end of the up-stream channel, the channel compensation must be performed entirely at the transmitter. We examine the existing techniques, such as those proposed for the V.92 Standard and investigate alternative methods to improve the system performance by reducing the impact of the ISI at the receiver.

An appropriate design of pulse shaping filters prevents ISI due to signal modulation. We

---

<sup>3</sup>The new recommendation from ITU-T is called V.92 with a feature for higher bit-rates in the up-stream directions.

investigate the design of pulse shaping filters that can be used in two different scenarios: in an up-stream channel where the receiver front-end is fixed, and end-to-end PCM channels where the transmitter and receiver filters are a pair of matched filters.

## 1.5 Thesis organization

In Chapter 2, an overview of data transmission over the PCM voiceband channels is presented. We examine the characteristics of different components of PCM channels. The conventional model of data transmission over voiceband channel is compared to the hybrid model of connection between analog subscribers and the digital network.

Chapter 3 describes the choice of a modulation scheme that is compatible with the predetermined structure of the receiver in the up-stream PCM channel. We investigate several problems related to the constellation design, index mapping and non-equally-probable signalling for up-stream PCM channels. The modulation performance, with an average power constraint in the presence of additive Gaussian noise and residual inter-symbol interference, is analyzed.

Chapter 4 describes the linear distortion due to the channel and receiver filters. We describe linear transmitter filter design procedure which minimizes certain optimization criteria such as the peak distortion error or the mean-square error. A unified approach is employed to define several transmitter structures. These transmitter structures include combinations of optimal linear filtering and spectral shaping. We also describe precoding techniques to compensate for the PCM channel in the transmitter while maintaining an average transmitted power constraint.

In Chapter 5, a non-maximally decimated filterbank structure is introduced to compensate for the channel at the transmitter. The channel model can be a non-minimum phase filter and its frequency response may contain spectral nulls. The merits and limitations of such a filterbank structure for channel pre-equalization are investigated.

Chapter 6 describes new methods of designing pulse shaping Nyquist filters. We introduce a general relationship between the phase and amplitude response of bandlimited Nyquist filters. Using this relationship, we show that a bandlimited zero-phase Nyquist filter can always be split into two cascaded matched filters, such that each one is also a Nyquist filter. We explain how the new pulse shaping filters can be used for the up-stream PCM channel as well as the end-to-end PCM channels. We also introduce a new family of Nyquist filters. The standard raised-cosine spectra can be considered as a special case of this family. Compared to raised-cosine filters, the generalized raised-cosine filters provide more flexibility and control in the filter design.

In Chapter 7, concluding remarks, contributions and future research directions are discussed.

## Chapter 2

# The PCM Voiceband Channel Characteristics

This chapter describes a more detailed communication model of PCM voiceband channels. Three different connection scenarios are considered: the down-stream direction, the up-stream direction and end-to-end connections. We describe different constituents of a voiceband telephone network that contribute to the overall characteristics of the PCM channels.

### 2.1 Subscriber access to the PSTN

In a telephone network, the physical connection to customer premises is provided by a pair of twisted copper wires known as a *subscriber loop* or a *subscriber line*. A subscriber loop is used for signalling operations such as dialing, ringing and the off-hook indicator as well as for bi-directional voiceband signal transmission [19]. As shown in Fig. 2.1, at both ends of a subscriber loop, a hybrid circuit separates the receiving and transmitting signal paths by converting a two-wire link to a four-wire connection.

### 2.2 Subscriber loop interface circuit

The interface between the analog subscriber loop and a digital central office switching system is provided by a line interface circuit. A line circuit provides several functionalities such as power supply, over-voltage protection, ringing for incoming calls, monitoring the line status (supervision), coding/decoding, hybrid and testing [19]. Figure 2.1 shows the components of the line circuit that directly affect a voiceband transmitted signal. The actual locations of the line interface circuits depend on the telephone network and the associated loop plant. In the majority of existing

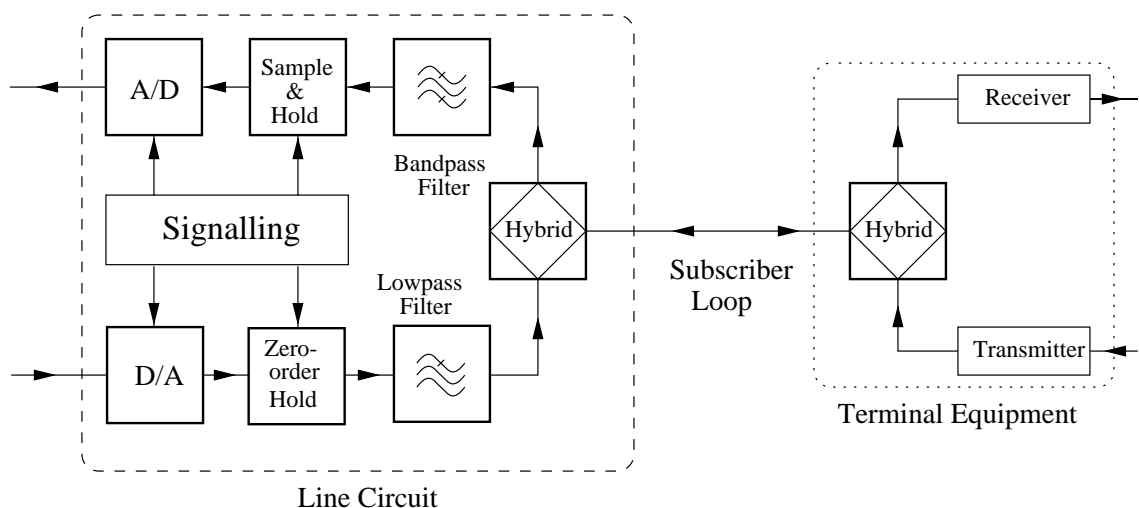


**Fig. 2.1** Subscriber loop access via line interface circuits at the central office.

telephone networks, the line interface circuit cards are installed at the central office. In some cases, line circuits are installed as part of a digital loop carrier (DLC) in a remote switching terminal[20]. The data transmission between a DLC and the central office is carried over twisted-pair or fiber-optic connections. By employing DLCs, the actual length of each analog subscriber loop is shortened and many signal transmission impairments over long analog subscriber loops are mitigated.

### 2.3 Subscriber loop characteristics

A subscriber loop cable has electrical characteristics that introduce changes to the carried signal. The theory of transmission line can be used to quantify signal distortions. As with any other transmission line, the electrical characteristics of a twisted pair of copper wires can be described by a set of parameters known as the line primary constants [19]. The primary constants consist of series inductance  $L$ , shunt capacitance  $C$ , shunt conductance  $G$  and series resistance  $R$ . The primary constants are all defined per unit length of cable. Figure 2.2 shows a lumped circuit element model of a segment of transmission line. The actual requirements of twisted copper lines used in subscriber loops are described in several standards and guideline documents. Nominal values for these parameters can be found in [19], [21] and [22]. The transfer function of a transmission line is obtained by solving a set of partial differential equations describing the current and voltage at each point of the line as a function of time and distance [23]. A set of secondary parameters known as *propagation constants* and *characteristic impedance* are computed to simplify the voltage and

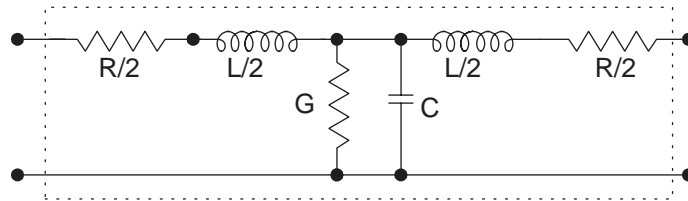


**Fig. 2.2** The T-equivalent circuit for a unit length segment of a subscriber line

current expressions:

$$\begin{aligned}\gamma &= \alpha + j\beta = \sqrt{(R + j\omega L)(G + j\omega C)} \\ Z_0 &= \sqrt{\frac{R + j\omega L}{G + j\omega C}}\end{aligned}\quad (2.1)$$

For a given load impedance  $Z_L$ , the transfer function and the input impedance of the line are determined as follows [21]:

$$T(\omega) = \frac{Z_L}{Z_L \cosh(\gamma d) + Z_0 \sinh(\gamma d)} \quad (2.2)$$

$$Z_{in}(\omega) = Z_0 \frac{Z_L + Z_0 \tanh(\gamma d)}{Z_0 + Z_L \tanh(\gamma d)} \quad (2.3)$$

where  $d$  is the length of the line. If the line consists of several segments with different electrical characteristics, the input impedance of each part is the load of the preceding segment, and the overall transfer function is the product of the transfer functions of cascaded segments. A more detailed analysis and examples including unterminated lines (bridged-tap sections) or lines with extra series inductance (loading coils) can be found in [21] and [23].

In order to show the filtering effect of the subscriber lines, we consider a set of lines with the same cable characteristics composed of wires with 26 American-Wire-Gauge (AWG)<sup>1</sup>. The line termination consists of a 600  $\Omega$  resistance. Figure 2.3 shows the frequency responses of different cable lengths. It is evident that the signal attenuation becomes more significant at higher frequencies for longer cables.

For subscriber lines longer than 5.5 km (18 kft), the signal attenuation is significant even at frequencies as low as 1 kHz, causing unacceptable distortion to the transmitted voice signal. A compensation for the line characteristics can be achieved by inserting several series inductors along the line.

A set of appropriately chosen series inductors (loading coils) can be used to compensate for

<sup>1</sup>AWG is a measure of wire diameter. Typical gauges are 19, 22, 24 and 26. The wire diameter decreases by increasing AWG [20].

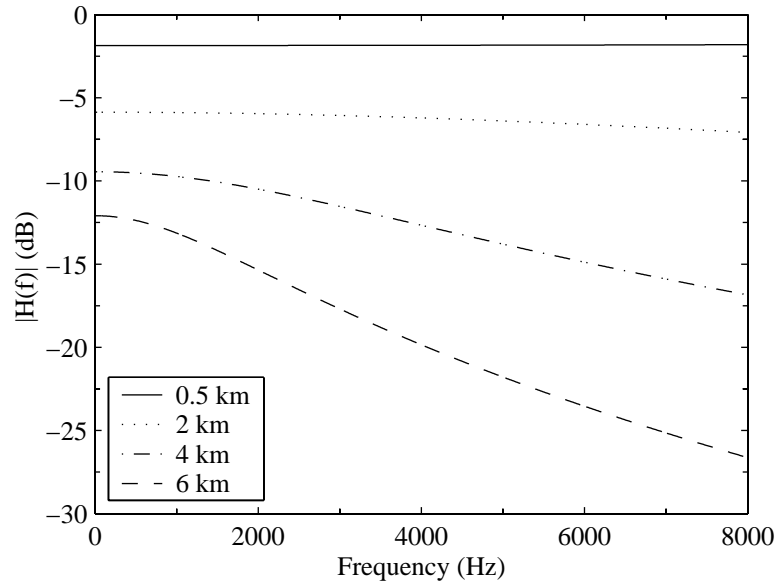


**Fig. 2.3** The magnitude response of subscriber lines with a 26-AWG cable. The magnitude response is shown for different cable lengths. The terminal load is set to a  $600 \Omega$  resistance.

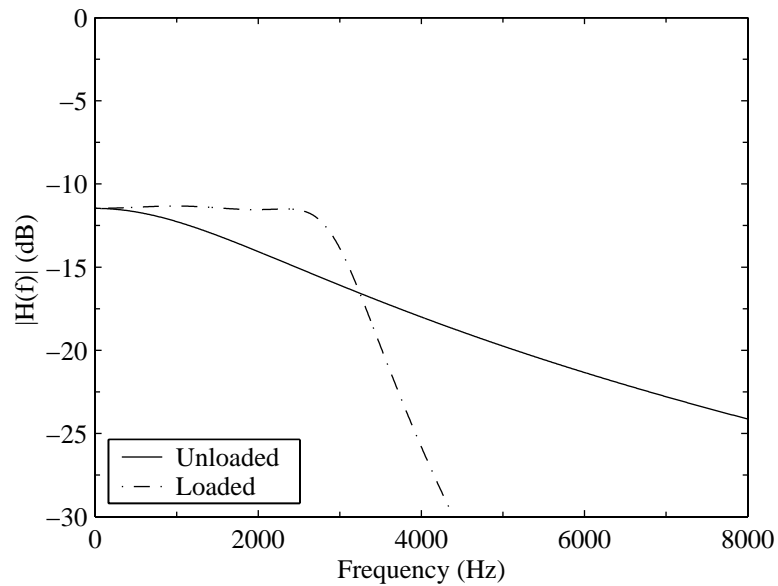


**Fig. 2.4** Magnitude response of a 5.5 km (18 kft) long unloaded subscriber line with a 26-AWG cable is compared with that of a loaded line with the same characteristics and the same length. The loaded line contains two 88 mH loading coils which are inserted at 1.83 km (6 kft) from each end.

the signal attenuation in the lower frequency range (100–2500 Hz). The disadvantage of this compensation is that the loading coils create a lowpass frequency response where signals with frequency components higher than the cutoff frequency will be significantly attenuated. This attenuation reduces the channel bandwidth and the maximum data transmission rate. Figure 2.4 shows an example of a compensated line. In this example, the total length of the line is 5.5 km (18 kft) and there are two 88 mH loading coils inserted 1.83 km (6 kft) from each end.

For simulation and testing purposes, there have been studies that identify the transmission impairment conditions encountered on the telephone networks in most countries. For example, Recommendation V.56 series from the ITU-T provides network models to be used in the evaluation and comparison of voiceband modems [24]. Figure 2.5 shows the measurement results of the frequency response for several subscriber lines, as given in [24]. In each case, a resistive load of 600  $\Omega$  is used.

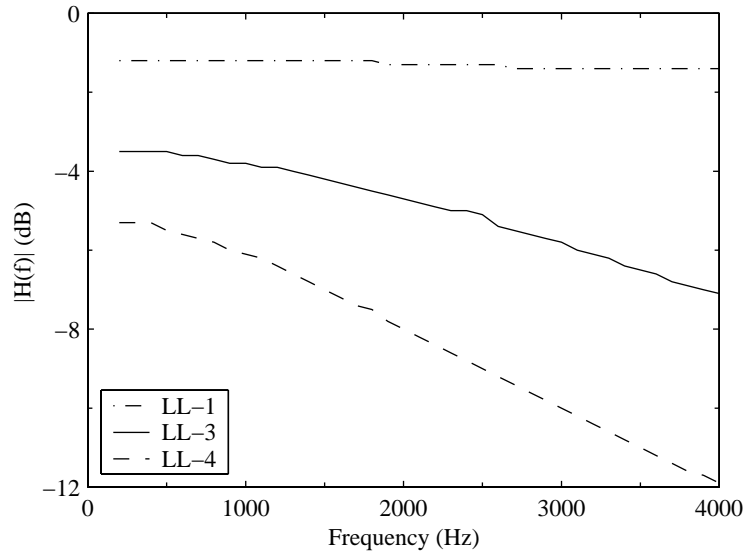
### 2.3.1 Hybrid Circuits

In a public telephone network, access to the central office for a majority of users is provided via a pair of twisted copper wires. Since the send and receive signals share the same pair of wires, this connection is called *two-wire* transmission. *Four-wire* transmission is where separate pairs of wires are used for transmitting and receiving signals. At the central office as well as the user premises, a circuit known as a *hybrid coupler* (or simply “hybrid”) is used as an interface between two-wire and four-wire connections. A hybrid circuit can be implemented in several ways. In many telephone sets, the hybrid circuit is implemented using transformers with line impedance matching to achieve a maximum energy transfer to the line and a minimum leakage from the transmitter to the receiver. Figure 2.6 shows the functionality of a hybrid using active components. Ideally, the hybrid circuit should prevent any energy leakage from the local transmitter to the local receiver. In practice, the line impedance varies from line to line. It is infeasible to choose one impedance that matches all subscriber lines. We can only choose a compromised impedance value that provides a reasonable match for most lines. As shown in Fig. 2.6, the signal from the transmitter to the subscriber line attenuates in the impedance voltage divider.

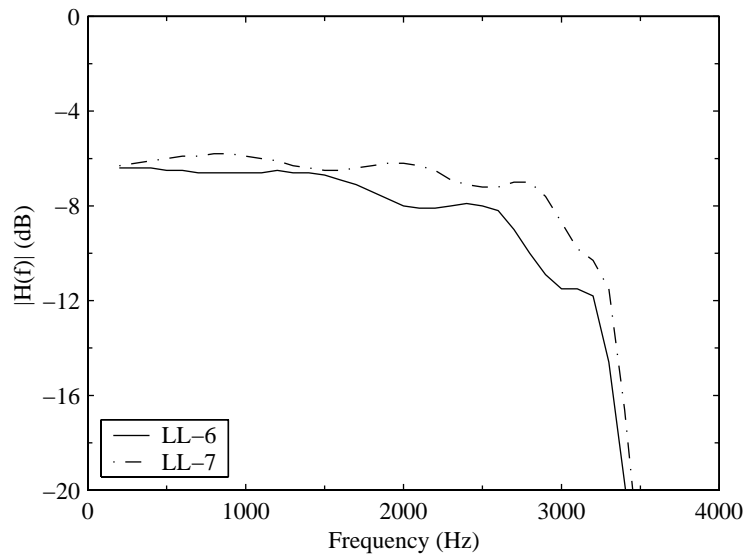
### 2.3.2 Characteristics of the filters in the line circuit

Among other tasks, a line circuit performs filtering on the received and transmitted voiceband signals. As shown in Fig. 2.1, there are two filters used in a line circuit: one prior to the ADC circuit, and one following the Digital-to-Analog Converter (DAC).

The bandpass anti-aliasing filter prior to the sampler is referred to as a send filter. The send filter limits the bandwidth of the input signal to avoid aliasing in the sampled signal. This filter



(a) Magnitude response of several unloaded subscriber lines. The wire diameter for all these cases is 0.41 mm. EIA LL-1 is 0.61 km long, EIA LL-3 is 2.13 km long and EIA LL-4 is 3.66 km long.



(b) Magnitude response of two loaded lines. The loading coils are 88 mH. The line shown as EIA LL-6 includes four loading coils and the line shown as LL-7 includes five loading coils.

**Fig. 2.5** Measurement results of the magnitude response of several subscriber lines as reported in [24].

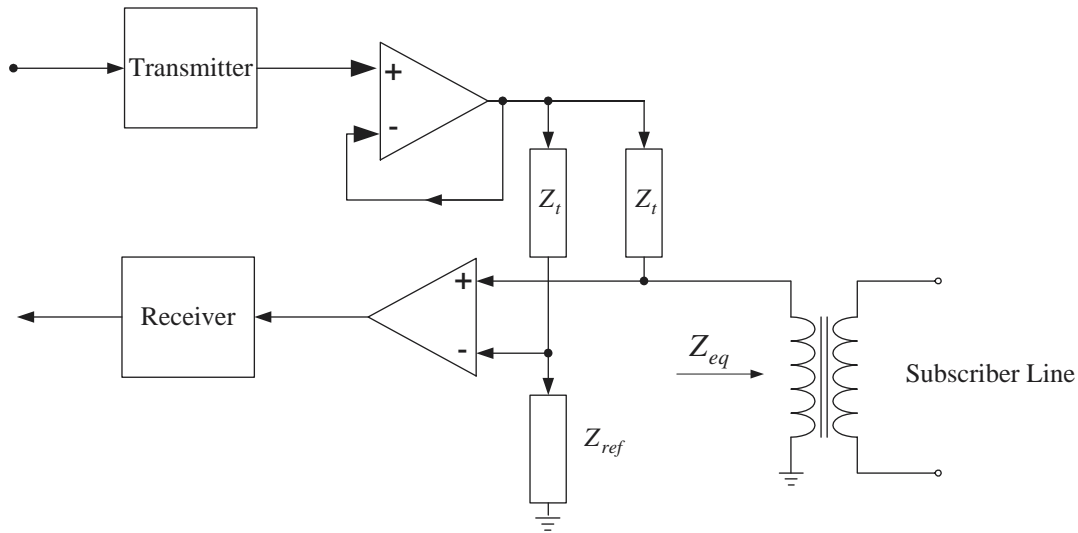


**Fig. 2.6** A circuit model of a hybrid coupler

also attenuates the low frequency interferences from power lines.

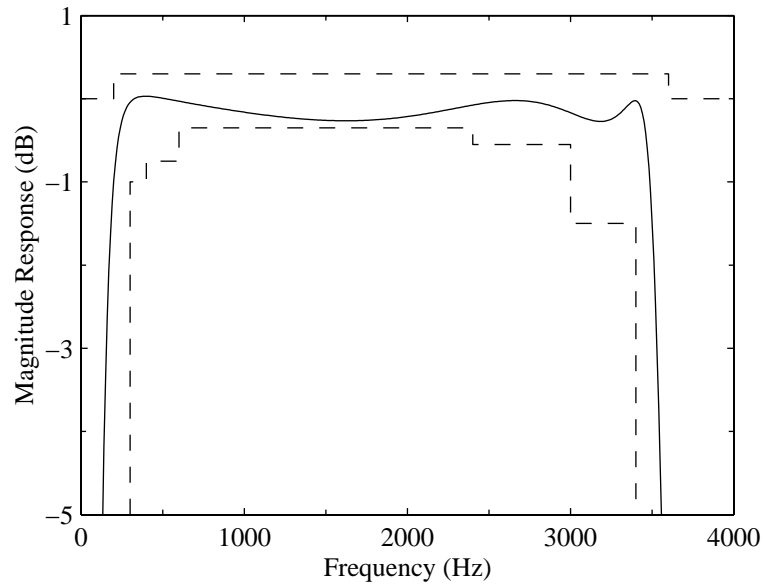
The lowpass reconstructing filter following the DAC circuit is referred to as a receive filter. This filter is used to suppress out-of-band frequency components in the reconstructed signal.

The send and receive filters should meet certain requirements in terms of their magnitude response and group delay. These requirements are specified in standard references such as ITU-T Recommendation G.712 [25]. Recommendation G.712 specifies a range for the attenuation and group delay for the send and receive filters (digital to analog channel), as well as the overall frequency response of the cascade of both filters (analog-to-analog channel). Figures 2.7 shows a design example of a send filter (prior to the ADC circuit) that satisfies the requirements of Recommendation G.712. The filter consists of a 5<sup>th</sup>-order elliptic lowpass filter cascaded with a bi-quad highpass filter. The same lowpass elliptic filter is used as the receive filter (following the DAC). Figure 2.8 shows the overall response of the send and receive filters.

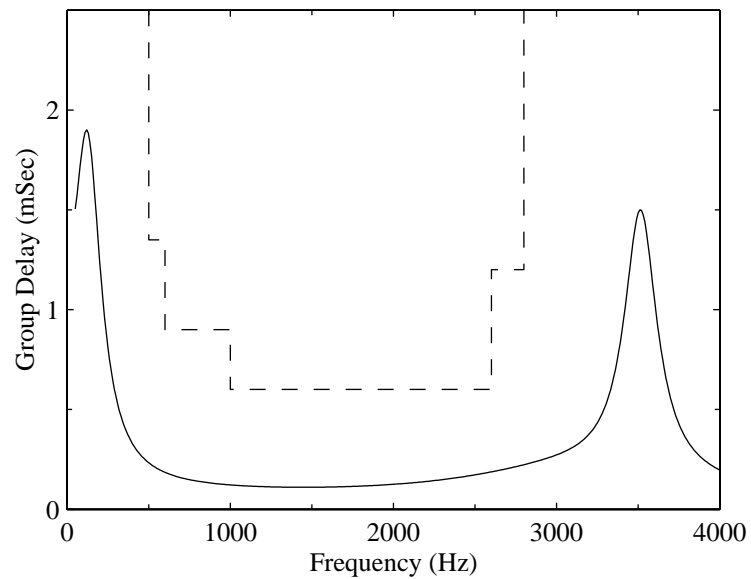
Some design specifications for send and receive filters can be found in [20]. Some empirical measurements of the frequency response of these filters are reported in [24]. For example, Fig. 2.9 presents some of the measurement results for several subscriber lines, as reported in [24].

### 2.3.3 PCM encoding and decoding

In a line circuit, the signal received from an analog subscriber loop is converted into a stream of binary digits. The encoding scheme used for digital telephone networks is Pulse Code Modulation (PCM). Conceptually, a PCM encoder performs three operations:

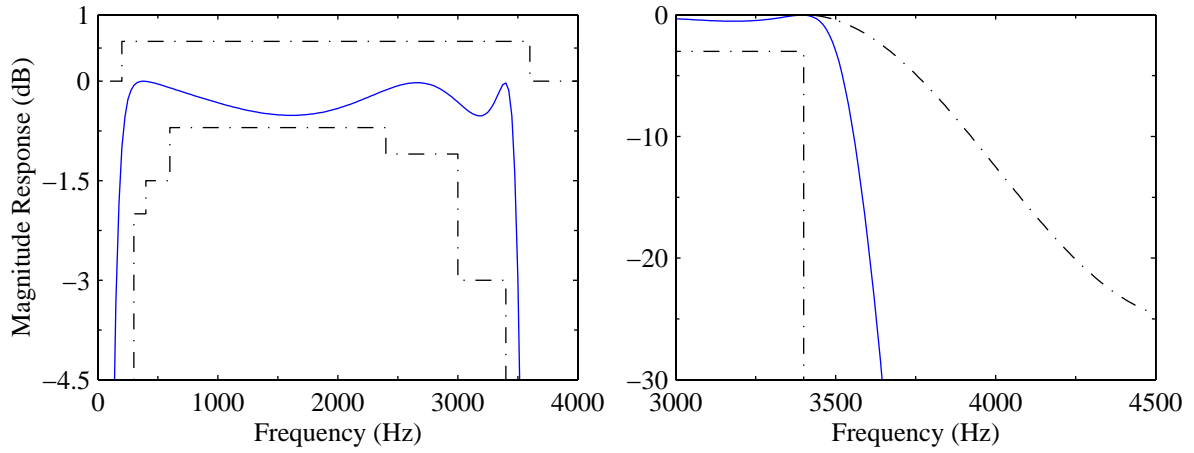


(a) Magnitude response of a send filter (solid line) is compared with the bounds provided by Recommendation G.712 (dashed lines).

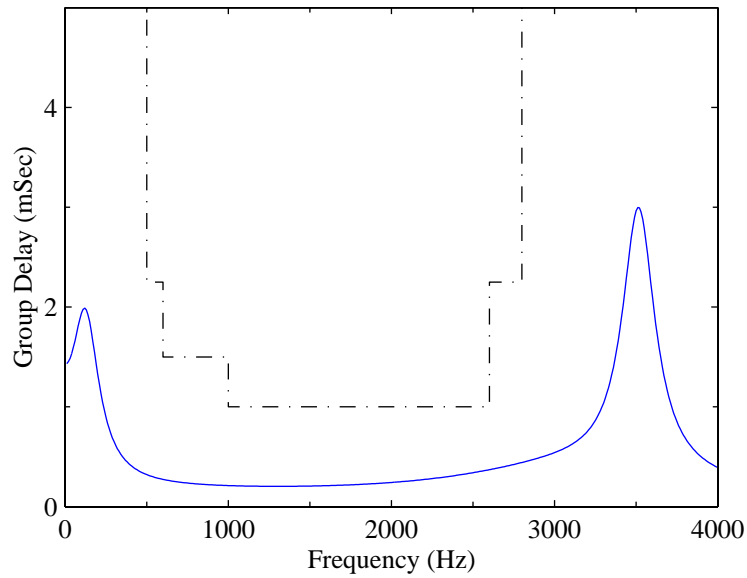


(b) Group delay of a send filter (solid line) is compared with the bound provided by Recommendation G.712 (dashed line).

**Fig. 2.7** Example of the frequency response of a send filter. The filter consists of a  $5^{th}$ -order lowpass elliptic filter cascaded with a highpass bi-quad filter.

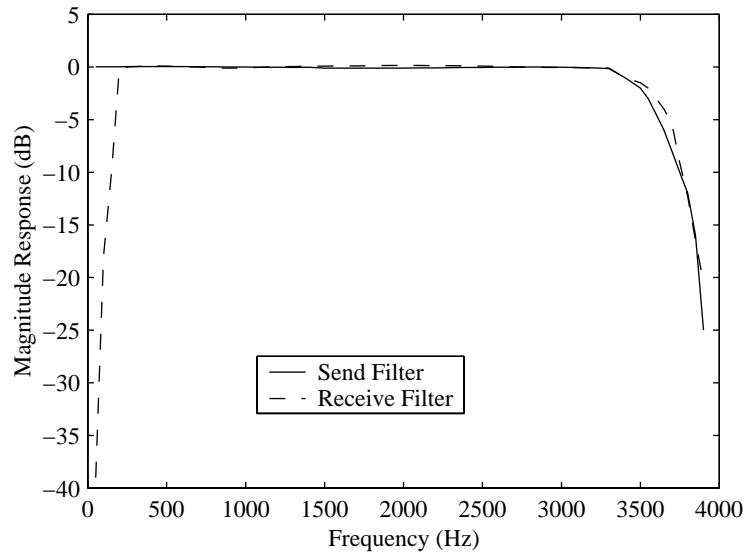


(a) Overall magnitude response of the cascade send and receive filter is compared with the bounds of Recommendation G.712.

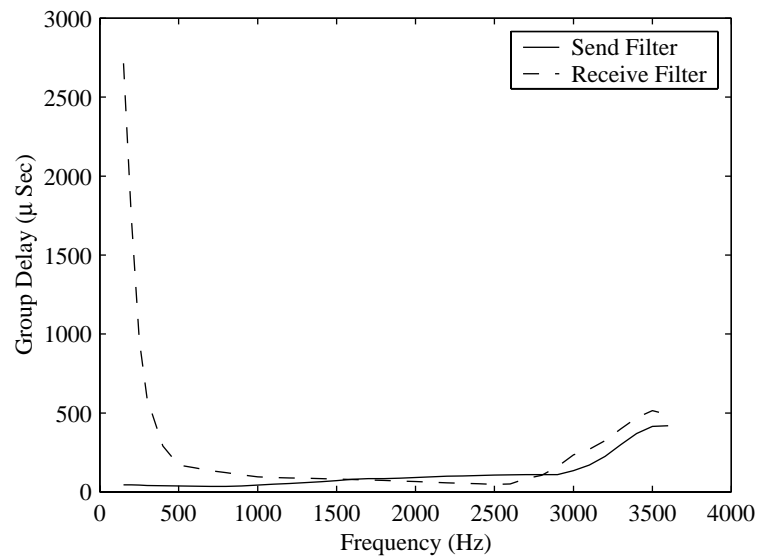


(b) Overall group delay of the cascade of send and receive filter is compared with the requirements given in Recommendation G.712.

**Fig. 2.8** Frequency response of the overall send-receive filter is compared with Recommendation G.712 requirements.



(a) Measured magnitude responses of send and receive filters.



(b) Measured group delays of send and receive filters.

**Fig. 2.9** Empirical results as provided in Recommendation V.56.

1. sampling the input waveform,
2. quantizing the samples, and
3. representing each quantizer level with a binary index.

The continuous-time analog signal at the input of the PCM encoder is sampled at 8000 samples/sec. Each sample is represented by an 8-bit codeword. A practical device for implementing this process is a sample-and-hold circuit followed by an Analog-to-Digital Converter (ADC) circuit [26, p. 187]. The ADC maps each sample into a binary codeword representing a quantized amplitude closest to the input.

A PCM decoder restores the analog waveform corresponding to the PCM encoded bit stream. The input bit stream to a PCM decoder is parsed into 8-bit codewords. As part of PCM decoder, a DAC circuit converts each 8-bit codeword into an amplitude. The discrete-time reconstructed amplitudes are converted to a continuous-time waveform. An example of a physical device which performs such conversions is zero-order-hold followed by a lowpass filter [26, p. 187].

### 2.3.4 Non-uniform Quantizer

The tandem operation of a PCM enCOder and a DECOder (CODEC), in terms of representing a discrete-time sample by a quantized amplitude, can be viewed conceptually as scalar quantization<sup>2</sup>. A codec is characterized by two finite sets of amplitudes: decision boundaries and output levels. A CODEC approximates each input sample falling between two adjacent decision boundaries with an amplitude taken from the set of output levels. The approximation error manifests itself as signal distortion in the reconstructed waveform.

For a given bit resolution (i.e., the number of quantization output levels), the goal of a CODEC design is to specify the decision boundaries and the output levels of a quantizer that minimize certain error criteria. For voice telephony, a CODEC should provide a robust quantization performance over a wide range of input signals and signal levels. The performance of a quantizer can be measured in terms of Signal-to-Quantization Noise Ratio (SQNR)<sup>3</sup>.

There are requirements imposed on a CODEC performance in terms of lower bounds (masks) for the SQNR with respect to the input signal power. Recommendation G.712 defines several masks for SQNR for different input test signals [25]. These requirements cannot be satisfied by an 8-bit uniform quantizer (equal spacing between decision boundaries).

By choosing smaller quantizer steps for small signals and large steps for large signals, we can obtain a more robust quantizer. Non-uniform spacing between quantization levels can be

---

<sup>2</sup>Here, we assume that the digital network is transparent from the viewpoint of signal transmission.

<sup>3</sup>Note that a robust quantizer does not necessarily provide the maximum SQNR for a given number of bits but it maintains a level of performance for a larger dynamic range of the input signal.

achieved by using a non-linear compression characteristic  $F(\cdot)$  prior to a uniform quantizer, then expand the quantized levels using the inverse function  $F^{-1}(\cdot)$ . The compressor characteristic  $F(\cdot)$  is referred to as (**compressing and expanding**) companding law.

Two companding laws specified in Recommendation G.711 [27] are the  $\mu$ -Law and the A-Law<sup>4</sup>. The compression characteristic function for the  $\mu$ -Law quantizers can be expressed as:

$$F(x) = x_{\max} \frac{\log(1 + \mu|x|/x_{\max})}{\log(1 + \mu)} \operatorname{sgn}(x) \quad (2.4)$$

where  $\operatorname{sgn}(x)$  is the sign of  $x$ . The inverse characteristic equation is:

$$F^{-1}(\hat{x}) = x_{\max} \frac{1}{\mu} [(1 + \mu)^{|\hat{x}|/x_{\max}} - 1] \operatorname{sgn}(\hat{x}) \quad (2.5)$$

The actual characteristics of a  $\mu$ -law (and also an A-Law) CODEC are completely specified in Recommendation G.711. In this recommendation, the companding laws are approximated as piece-wise linear functions. For  $\mu = 255$ , the  $\mu$ -Law companding function is approximated by 15 linear segments (In fact, there are 16 segments but the two segments close to the center have the same slope). Each segment specifies 16 output levels.

As shown in Fig. 2.10, each 8-bit codeword at the output of encoder consists of three parts. The most significant bit in each codeword represents the sign bit. The next three bits give the segment index and the last four bits identify one of 16 possible output levels in each segment.

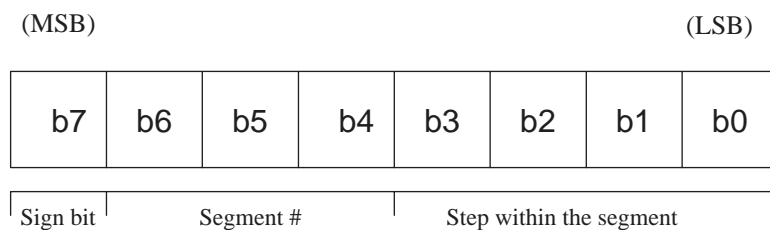


**Fig. 2.10** Bit allocation in a  $\mu$ -Law codeword.

For the  $\mu$ -Law quantizer, the positive decision levels  $X(1)$  to  $X(128)$  as well as the output levels  $Y(0^+)$  to  $Y(127)$  are specified as:

$$X(16i + j + 1) = 2^{(i+1)}(j + 17) - 33 \quad \text{for } 0 \leq i \leq 7, 0 \leq j \leq 15 \quad (2.6)$$

$$Y(16i + j) = 2^{(i+1)}(j + 16.5) - 33 \quad \text{for } 0 \leq i \leq 7, 0 \leq j \leq 15. \quad (2.7)$$

<sup>4</sup>Here, we only give the relationship for  $\mu$ -Law. A-Law companding and its approximation is described in [22, pp. 621-627].

Note that the  $\mu$ -Law quantizer has a mid-tread characteristic, i.e., zero is one of the allowed output levels. Since there are 256 possible output levels in total and the quantizer is symmetrical; two output levels are assigned to the same value:

$$Y(0^+) = Y(0^-) = 0$$

Since the quantizer is symmetrical, negative decision levels are specified as:

$$\begin{aligned} X(-i) &= -X(i) && \text{for } 1 \leq i \leq 128 \\ Y(-i) &= -Y(i) && \text{for } 0 \leq i \leq 127. \end{aligned} \tag{2.8}$$

The outer levels  $X(-128)$  and  $X(128)$  are virtual decision boundaries corresponding to the amplitude of a 3.17 dBm0 sinusoid, that is, a sine-wave with a normalized amplitude  $X(128) = 8159$  will have a power of 3.17 dBm0<sup>5</sup>.

### 2.3.5 Multiplexing

The output of a PCM encoder is a 64 kbits/s DS0 bit stream corresponding to each voice channel [20]. The bit rate DS0 is the lowest rate in the hierarchy of data multiplexing in the switched digital network. For example, in Fig. 2.11, a channel bank comprising 24 voice channels is depicted. The outputs of these channels are encoded at 64 kbits/s DS0 rates and multiplexed into a 1.54 Mbits/s DS1 stream<sup>6</sup> [20].

## 2.4 Power Constraints of the PCM channel

Each country has certain regulations and guidelines for the electrical characteristics of terminal equipment connected to a subscriber loop<sup>7</sup>. The regulations are imposed to prevent any damage to the network. Any equipment for loop terminal use must pass several certification tests in order to be connected to the network. One particular requirement concerns the signal power transmitted over the subscriber loop. The average power applied to a loop in the voice frequency band (200 Hz – 4000 Hz) should be limited to  $-13$  dBm under all conditions when averaged over a period of 3 seconds<sup>8</sup> [19]. The average power limitation reduces the maximum data transmission rate.

<sup>5</sup>dBm0 is a power measure with respect to a (virtual) reference point, known as zero Transmission Level Point (TLP) [22, p.23].

<sup>6</sup>The digital multiplexing rates given here are based on North American Standards.

<sup>7</sup>For example, the Federal Communication Commission (FCC) in the United States, and the Canadian Radio and Telecommunication Commission (CRTC) in Canada govern these regulations.

<sup>8</sup>There are ongoing discussions to relax the power constraint

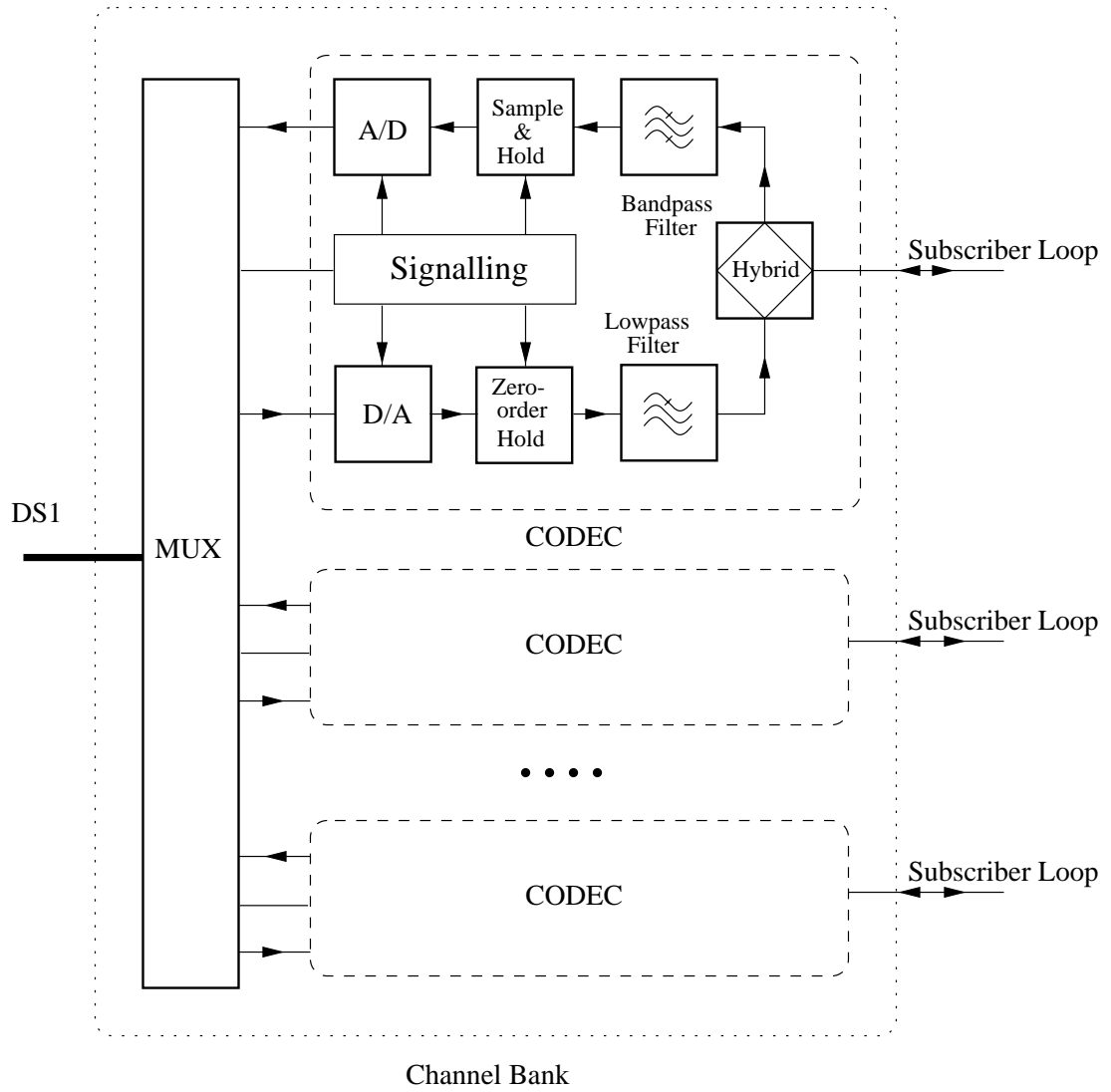


Fig. 2.11 A channel bank multiplexing 24 voice channels to a DS1 stream.

## 2.5 Capacity of PCM voiceband channels

A conventional design of voiceband modems targets data transmission between two terminals connected to analog subscriber lines. In this design, the voiceband channel is treated as an analog communication medium, where the underlying sources of channel impairment are modeled as additive distortions. For an end-to-end PCM voiceband channel, the main source of distortion is signal quantization in the analog-to-digital conversion. The quantization distortion can be approximated as Additive White Gaussian Noise (AWGN) under certain conditions [4, 28]:

- the transmitted signal contains independent, identically-distributed random symbols,
- the symbol timing is independent of the sampling clock at the PCM encoder, and
- the number of quantization levels is large.

Under the AWGN assumption of the quantization noise, the voiceband channel capacity can be computed using Shannon's classical results [29]:

$$C = W \log_2(1 + \text{SNR}) \quad \text{bits/sec} \quad (2.9)$$

where  $W$  is the bandwidth and SNR is the Signal-to-Noise power Ratio. For a typical PCM voiceband channel,  $W$  is in the 3–3.5 kHz range. In a PCM channel, the dominant source of distortion is the quantization error. The SQNR for an 8-bit non-uniform A-law or  $\mu$ -law quantizer is in the 33–39 dB range. For the given nominal values of the SQNR and the channel bandwidth, the capacity of a voiceband channel computed from Eq. (2.9) is in the 33 to 45 kbits/s range. Based on the AWGN model of distortions in voiceband channels, there are several recommendations and guidelines developed by international standards bodies such as the ITU-T to design voiceband modems. For example, Recommendation V.34 provides data transmission rates up to 33.6 kbits/s on ordinary telephone lines [2].

In the absence of quantization error, the maximum information rate on a PCM voiceband channel is limited by the channel bandwidth and the PCM codeword length<sup>9</sup>. The Nyquist theory indicates that the maximum symbol rate for data transmission with no inter-symbol interference is limited to

$$D = 2W \quad \text{symbols/sec.} \quad (2.10)$$

Since each symbol at the output of PCM encoder is represented by eight bits, the maximum channel bit rate is  $16W$  bits/sec. For a typical PCM channel, the bandwidth is limited to 3–3.5

---

<sup>9</sup>Here, we ignore any other sources of noise. In Chapter 3, we revisit the maximum achievable rate of an up-stream PCM channel.

kHz. Hence the channel bit rate can theoretically reach 48–56 kbits/sec. Compared to achievable rates using V.34 modems, there is a potential increase of data transmission rate on the PCM voiceband channels by 50%–70%.

## 2.6 PCM Modems

The idea of PCM modems was first introduced in [4]. Assuming an ideal bandlimited filter model for the overall PCM voiceband channel, [4] specifies a set of pulse shaping filters to ensure zero Inter-Symbol Interference (ISI) in a subset of the sampling instants (say 6 samples out of every 8), prior to ADC at the central office<sup>10</sup>. Such signalling is feasible only if the transmitter modem is synchronized to the network clock at the central office. If the transmitted symbols are selected from the set of PCM CODEC output levels, there will be no quantization distortion added to the subset of samples. The PCM decoder (located at the central office serving the destination end user) does not add any significant distortion to the reconstructed signal, except for a band-limiting filter at the receiver. In [4], it is suggested to use a maximum likelihood sequence detection algorithm (e.g., Viterbi Algorithm) to combat ISI at the receiver.

Although the idea of using PCM modems for end-to-end PCM channels is appealing in theory, it is challenging to implement in practice. The connection between two end-users as shown in Fig. 2.12(c) consists of two separate links, an up-stream PCM channel and a down-stream PCM channel with different characteristics. Without side information from within the digital switched telephone network, it is difficult, if not impossible, to solve problems such as synchronization, echo cancellation and channel equalization for the end-to-end PCM channel.

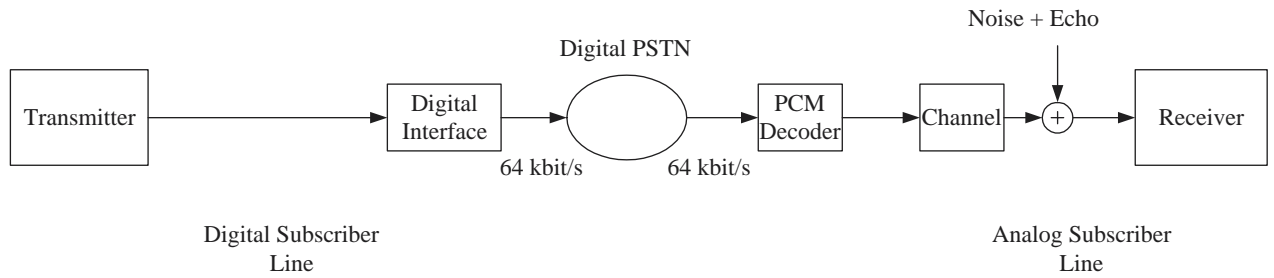
As discussed in Section 1.2, there are alternative scenarios for network connection over a PCM voiceband channel. Figure 2.12 shows three types of connection over a PCM voiceband channel. In the next sections, we describe the issues related to PCM modem design for each channel.

### 2.6.1 Digital network imperfections

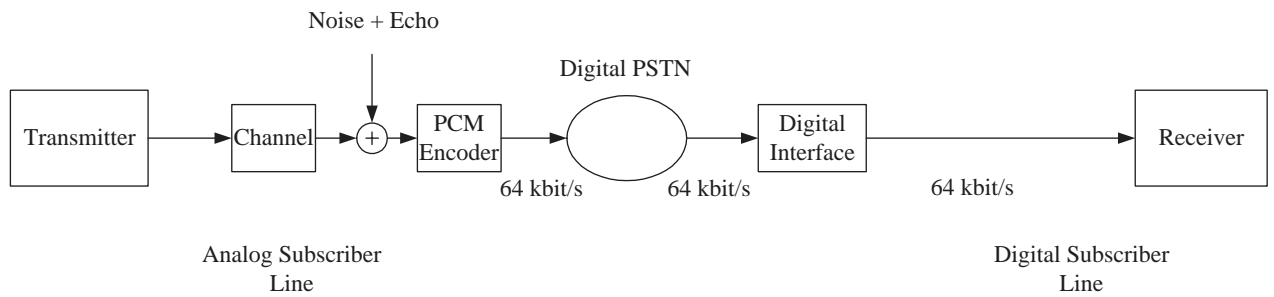
Before we describe different connections over a PCM channel, we should note that some voiceband channels are not qualified to be considered as PCM channels. The model we consider for a voiceband PCM channel does not include any signal distortion within the digital network. It is implicitly assumed that the digital network provides a 64 kbits/s data transmission rate between a pair of PCM encoders and decoders. However, there are some possible sources of distortion in the digital network. For example, in the North American standard of digital multiplexing hierarchy, the least significant bit of each codeword of a fraction of voice channels is reserved (*robbed*) for

---

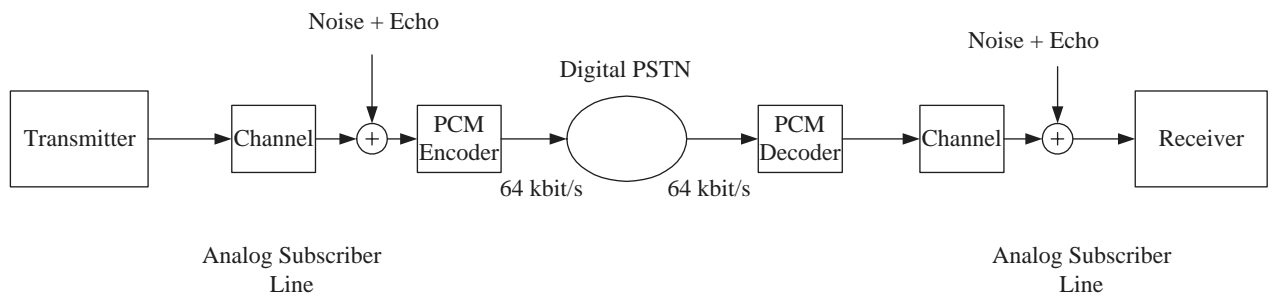
<sup>10</sup>This method is described in Chapter 5 in more detail.



(a) The down-stream PCM Channel.



(b) The up-stream PCM Channel.



(c) The end-to-end PCM Channel.

**Fig. 2.12** A PCM modem is used to transmit/receive data over one of the following channels: (a) a down-stream PCM channel, (b) an up-stream PCM channel, (c) an end-to-end PCM channel.

signaling and supervisory information [20]. Robbed-bit signalling reduces the maximum transmission rate over the PCM channels. A PCM modem should detect the use of robbed-bit signaling on a PCM channel and adjust the transmission rate accordingly<sup>11</sup>.

Digital data conversion is another example of signal distortion in a digital network. The digital data conversion can be due to

1.  $\mu$ -law to A-law conversion or vice versa,
2. conversion to other encoding standards such as ADPCM and back to PCM, or
3. conversion to an analog signal and back to digital (multiple encoding in one channel).

If a voiceband channel contains any of these data conversions, our underlying assumption about quantization error model will no longer be valid, hence, a PCM modem cannot be used for that channel.

## 2.7 The down-stream PCM channel

Figure 2.12(a) shows a down-stream PCM channel. While the transmitter modem is connected to the PSTN via a digital subscriber line (e.g., T1 link or ISDN), the receiver is connected to an analog subscriber line.

There is no quantization error due to analog-to-digital conversion. The ultimate information rate over this channel is  $8 \text{ bits/symbol} \times 8000 \text{ symbols/sec} = 64 \text{ kbits/sec}$ . However, due to the non-uniform distribution of the symbol levels as well as the limited bandwidth of the reconstruction filter at the central office, the maximum achievable rate is around  $56 \text{ kbits/s}$ . Recommendation V.90 [13] provides guidelines for designing PCM modems in the down-stream direction to achieve rates of up to  $56 \text{ kbits/s}$ <sup>12</sup>.

## 2.8 The up-stream PCM channel

Figure 2.12(b) shows an up-stream PCM channel connecting an analog subscriber to the digital network. There are many applications that require data transmission over an up-stream PCM channel. These applications include: uploading files, sending Email with attachments and Internet video-conferencing.

---

<sup>11</sup>Note that the Robbed-bit signalling is no longer a common signalling method. Instead, signalling scheme known as Common channel signalling is employed[20].

<sup>12</sup>This number is limited to  $53 \text{ kbits/s}$  in North America, due to regulatory power constraints which are expected to change in the near future.

Recommendation V.90 uses a conventional analog data transmission (based on the Recommendation V.34) in the up-stream direction [13] which does not exploit the maximum transmission rate of the up-stream channel<sup>13</sup>.

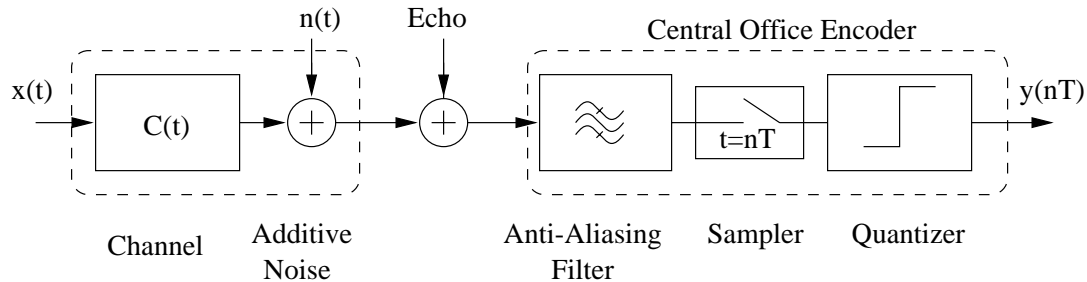


Fig. 2.13 The Up-stream PCM Channel

Figure 2.13 shows components of an up-stream PCM channel. An analog signal  $x(t)$  generated by the transmitting modem passes through the subscriber loop and reaches the central office where a PCM encoder samples the received signal and converts the sample into binary codewords. Each codeword corresponds to a quantized level  $y(nT)$ .

Compared to the down-stream PCM channel, modem design for the up-stream PCM channel is a more challenging task, primarily due to the quantization distortion at the PCM encoder. Unlike an analog modem, a PCM modem in the up-stream direction treats the PCM encoder at the central office as the receiver front-end that includes a bandpass filter, a sampler and a signal level detector (the quantizer). The choice of receiver analog filter, sampling rate, sample timing and symbol detector are constrained by the network hardware. Some of technical challenges associated with the up-stream PCM modem are:

### 2.8.1 Synchronization

In an up-stream channel, the PCM encoder acts as the receiver front-end. Since the sampling time is controlled by the telephone network, the transmitter should be synchronized to the sampling clock of the line circuit. This arrangement is unconventional since the transmitter has no direct access to the sampling clock at the receiver.

The symbol timing recovery in the down-stream direction can be used as a reference clock for the transmitter. The down-stream symbol timing is useful to the up-stream transmitter only if the encoder and decoder at the central office share the same timing clock<sup>14</sup> (see Fig. 2.11).

<sup>13</sup>There is ongoing work on a new Recommendation called V.92 that provides guidelines for designing PCM modems in the up-stream direction.

<sup>14</sup>In the development of the V.92 recommendation, the same assumption has been considered.

### 2.8.2 Signal mapping and constellation design

In the up-stream PCM channel, the symbol detector at the receiver is a scalar quantizer. As we will describe in Chapter 3, the appropriate choice of modulation scheme is a baseband Pulse Amplitude Modulation (PAM). Issues related to the optimal constellation design and bit-to-symbol mapping should be investigated.

### 2.8.3 Channel Pre-equalization

The anti-aliasing filter at the central office, along with the subscriber loop filtering effect limit the frequency band of the up-stream channel to the 300–3600 Hz range. While the channel bandwidth is restricted to about 3300 Hz, the sampling frequency at the central office is fixed at 8000 Hz. As a result, the received samples are distorted by Inter-symbol Interference (ISI). Since there is no access to the receiver front-end, the compensation for the channel linear distortion must be implemented entirely at the transmitter.

### 2.8.4 Echo cancellation

As shown in Fig. 2.1, the PCM up-stream and down-stream links share the same pair of wires. Ideally, a hybrid circuit should provide isolation between the two directions of transmissions. In practice however, there is an echo path from the down-stream link to the up-stream channel. Although, there are conventional methods for echo cancellation in analog voiceband modems, echo cancellation in up-stream PCM modem requires further consideration, due to the non-linear characteristics of PCM quantizer.

### 2.8.5 Channel Coding

Since there are always residual ISI and error induced by echo, it is important to analyze the system performance to characterize the potential error correcting coding gain on the up-stream PCM channel. According to the result of such an analysis, we should decide on the use and the type of coding over the up-stream channels.

## 2.9 End-to-end PCM voiceband channels

An end-to-end PCM channel is shown in Fig. 2.12(c). This channel consists of a cascade of an up-stream and a down-stream channel. From the end users point of view, there is no information available in the channel output regarding the PCM CODEC, the underlying sampling and the CODEC filters individually. It is difficult to acquire this information from the end points. Some challenging problems on and end-to-end PCM channels can be identified as:

**2.9.1 Synchronization**

Since there is no access to the signal at the central office for the transmitter modem nor the receiver modem, it is not straightforward to synchronize the modems to the sampling clock of the ADC at the central office. Without such synchronization, the underlying structure of the PCM channel is not visible to the end users.

**2.9.2 Channel estimation**

Since there is no access to the digital stream of bits at the central office, the up-stream and the down-stream channel filters involved in an end-to-end channel cannot be estimated separately.

**2.9.3 Channel Equalization**

Without any information from within the network, channel compensation can only be performed based on partial knowledge about the up and down-stream channels composing the end-to-end channel.

Problems described above become much simpler if we assume that there are some assistance available from within the digital network to obtain the channel characteristics and the network timing information. For example, an end-to-end PCM connection between two analog end-users can be established via a third party who has direct access to the digital network and provides both end-users the channel characteristics and the symbol timing. In fact, in this approach, the end-to-end PCM channel is decoupled into an up-stream channel and a down-stream channel.

## Chapter 3

# Modulation Design for the Up-Stream PCM Channel

Following the general review of PCM voiceband channels presented in Chapter 2, this chapter focuses on data transmission issues related to the up-stream PCM channel and investigates the choice of modulation scheme suitable for the up-stream PCM channels. Considering the transmit power limitation over the voiceband channel, we discuss a constellation design to minimize the probability of error, and maximize the bit-rate at a given signal-to-noise ratio.

### 3.1 Modulation scheme

The choice of modulation scheme for the up-stream PCM channel is mainly influenced by the structure of the front-end receiver, i.e., the PCM encoder at the central office. Figure 3.1 shows a model of the up-stream PCM channel. The PCM encoder converts the received signal into a 64 kbits/s DS0 digital data stream. The DS0 rate is clearly the upper bound of the data

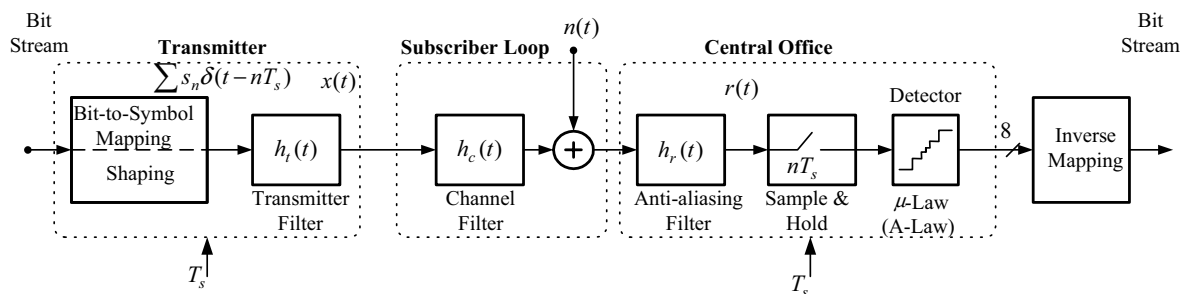


**Fig. 3.1** A schematic model for the Up-stream PCM channel.

transmission rate over a PCM voiceband channel. Each 8-bit codeword at the ADC output should represent a distinct transmitted symbol to achieve a DS0 data rate over this channel.

The ADC operates as a threshold detector, or in communications terms, as a one-dimensional slicer. Figure 3.2 shows schematically the relationship between the ADC decision boundaries and the received signal at the ADC input. As shown in this figure, different transmitted symbols are expected to generate different signal levels at the ADC input. Each signal level corresponds to a constellation point in a one-dimensional signal space. The choice of modulation scheme for the up-stream PCM channel should be compliant with such a detector.

The natural choice of modulation for the up-stream channel is baseband Pulse Amplitude Modulation<sup>1</sup> (PAM). A PAM transmitted signal can be represented as:

$$x(t) = \sum_{i=-\infty}^{\infty} a_i h_t(t - iT_s) \quad (3.1)$$

where  $h_t(t)$  is the impulse response of the transmitting filter<sup>2</sup> and  $a_i$ 's are the transmitted symbols taking values from a one-dimensional PAM symbol alphabet. In a PCM channel, the symbol rate is 8000 samples per second. We assume that the transmitting modem is synchronized with the sampling clock at the central office. The up-stream transmitter can achieve such synchronization by extracting the symbol timing information from the received signal in the down-stream direction. The correct symbol timing of the transmitter can be determined during a training phase and be adjusted prior to data transmission<sup>3</sup>.

A PCM encoder has an 8-bit output word-length corresponding to a maximum of 256 input decision intervals. However, in the presence of noise and other distortions, a subset of symbol levels is chosen in order to increase the minimum distance between consecutive signal levels. At the output of the anti-aliasing filter in the PCM encoder, the received signal can be expressed as:

$$\begin{aligned} r(t) &= x(t) \otimes h_c(t) \otimes h_r(t) + n(t) \otimes h_r(t) \\ &= \sum_{i=-\infty}^{\infty} a_i h(t - iT_s) + \eta(t) \end{aligned} \quad (3.2)$$

where ' $\otimes$ ' denotes the linear convolution and  $h(t)$  is the overall impulse response of three cascaded filters: the transmitting filter, channel filter and receiving filter. Unless otherwise stated, we assume that these filters are linear and time-invariant over the time period of data transmission.

---

<sup>1</sup>Note that a multi-dimensional modulated signal, such as Quadrature Amplitude Modulation, cannot be detected by a single slicer.

<sup>2</sup>For the optimum detection of the PAM signal, the transmitter and (channel-) receiver filters should be matched to one another. The design of transmitter filter will be discussed in the next chapters.

<sup>3</sup>We assume the PCM encoder and decoder share a common network clock [20].

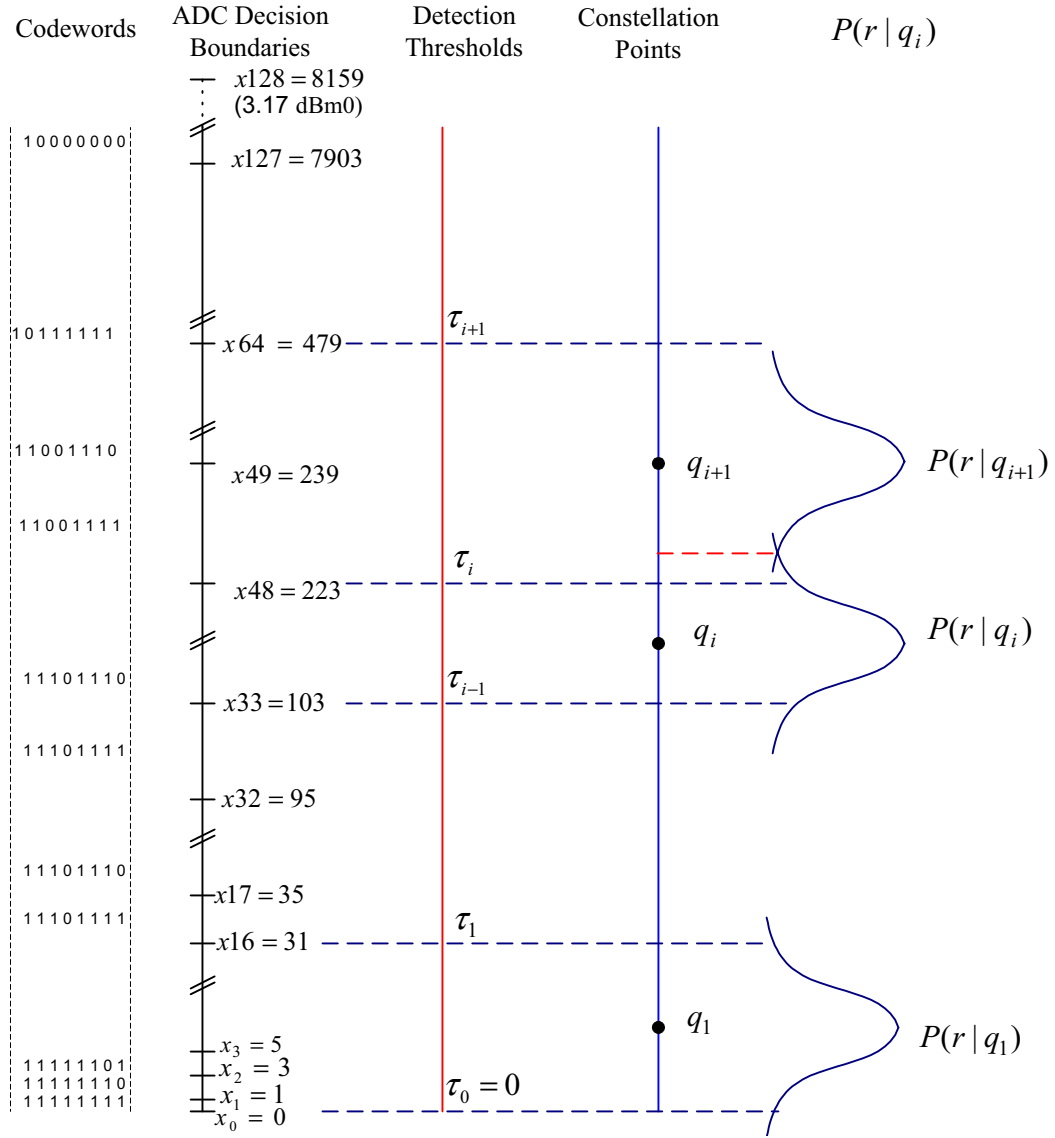


**Fig. 3.2** In order to avoid quantization error in the up-stream PCM channel, the ADC at the central office is employed as a slicer. One or more codewords represent a transmitted symbol.

The impulse response of the overall filter is determined by convolving the impulse responses of three cascaded filters. The additive noise component  $\eta(t)$ , represents the thermal noise as well as other additive distortions, such as cross-talk from the adjacent wire lines and echo (should it not be mitigated by an echo canceller). The discrete-time signal at the input of the ADC can be represented as:

$$r(nT_s + t_0) = \sum_{i=-\infty}^{\infty} a_i h(nT_s - iT_s + t_0) + \eta(nT_s + t_0) \quad (3.3)$$

To simplify the signal presentation, we use a discrete time notation with a normalized symbol rate:

$$r[n] = \sum_{i=-\infty}^{\infty} a_i h[n - i] + \eta[n] \quad (3.4)$$

$$= a_{n-n_0} h[n_0] + \sum_{\substack{i=-\infty \\ i \neq n_0}}^{\infty} a_i h[n - i] + \eta[n] \quad (3.5)$$

Equation (3.5) identifies two sources of distortion affecting the symbol detection result; additive noise and Inter-Symbol Interference (ISI) caused by the memory of the overall impulse response  $h[n]$ . In Eq. (3.5), we consider the time offset  $n_0$  to compensate for the delay of the overall channel filter  $h[n]$ . The value of  $n_0$  identifies the optimal sampling time of the pulse shape  $h[n]$  with respect to a reference time. In the absence of noise and ISI, each sample  $r[n]$  represents a transmitted symbol  $a_{n-n_0}$  scaled by the filter gain  $h[n_0]$ . In the presence of noise and ISI, the signal levels corresponding to different symbol alphabets should be chosen such that the probability of symbol error is minimized. We will discuss the optimal selection of signal alphabets for a given set of detector thresholds in the next section.

### 3.2 Optimal signal levels

For a given set of detector threshold levels, chosen from the ADC decision boundaries, we wish to determine the optimal PAM symbol alphabet that minimizes the probability of symbol error. Consider a set of  $2N$  one-dimensional signal levels that is positioned symmetrically about zero. In the absence of noise and ISI, the desired signal levels at the input of the ADC are denoted as  $\{q_{-N}, q_{-(N-1)}, \dots, q_{-1}, q_1, \dots, q_{(N-1)}, q_N\}$ . Note that the  $q_i$ 's represent the symbol alphabet at the input of ADC at the receiver.

Let us define a set of detector thresholds,

$$\{-\infty, -\tau_{(N-1)}, \dots, \tau_0 = 0, \dots, \tau_{(N-1)}, \infty\},$$

in ascending order that identify  $2N$  decision intervals. A sample that falls between  $\tau_{i-1}$  and  $\tau_i$  is detected as symbol  $q_i$ . The two outmost intervals are semi-infinite. We consider two virtual detector thresholds  $\pm\tau_N$  for these two regions. The use of these virtual thresholds will be described below. Figure 3.3 shows the placement of the signal levels together with the detector thresholds. Except for  $\pm\tau_N$ , all other threshold levels are chosen from the set of ADC decision levels<sup>4</sup>. If more than one codeword at the ADC output represents a transmitted symbol (i.e.  $2N \leq 256$ ), only a subset of ADC decision levels will be used as detector thresholds.

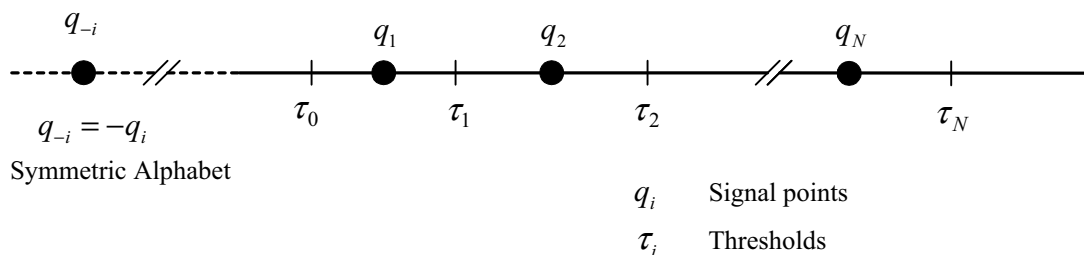


**Fig. 3.3** Placement of the signal points relative to the thresholds

Each constellation point  $q_i$  corresponds to a transmitted PAM symbol. We denote  $P(q_i)$  as the probability of transmitting  $q_i$ . In a conventional data transmission system, each point in the constellation is equally likely to be transmitted. This corresponds to a uniform probability distribution for the constellation points. In our discussion, we allow for non-uniform probability distributions. However, we assume that the distribution of probabilities of constellation points is symmetrical:

$$P(q_i) = P(q_{-i}) \quad \text{for } i = 1, 2, \dots, N.$$

Due to the symmetry of the constellation and the distribution of probabilities of the signal points, the transmitted signal has a zero-mean:

$$\sum_{\substack{i=-N \\ i \neq 0}}^N P(q_i)q_i = 0 \quad (3.6)$$

As shown in Eq. (3.5), the discrete signal at the input of the detector can be written as a sum of the desired signal, noise and the ISI. We consider a zero-mean Gaussian distribution for the noise. Since the ISI component is a weighted sum of transmitted levels, it also has a symmetrical distribution<sup>5</sup>. As a random variable, the ISI in general does not have a continuous Probability

<sup>4</sup>Note that the decision intervals corresponding to the outermost symbols are semi-infinite are only virtual boundaries of these intervals.

<sup>5</sup>We assume transmitted symbols are independent identical distributed random variables. Since transmitted sym-

Density Function (PDF) [30, p. 60]. However, the sum of noise and ISI is a random variable with a continuous PDF. We denote  $w[n]$  as the resulting additive distortion caused by noise and ISI at each sampling instance:

$$r[n] = h[n_0] a_{n-n_0} + w[n] \quad (3.7)$$

Under the following conditions (that we assume all hold),  $w[n]$  has a symmetric PDF:

- The noise component has a symmetric distribution.
- The noise and ISI components are independent.
- The PAM signal constellation is symmetrical.
- The probability distribution of the constellation points is symmetric,  $P(q_i) = P(q_{-i})$ .

### 3.2.1 Performance criterion

A basic performance measure for any digital modulation scheme is the probability of error in the presence of noise and other distortions. We use the probability of symbol error as the performance criterion by which to choose the optimal signal levels. In the absence of noise and ISI, the received signal takes a value from a PAM symbol alphabet  $\{q_i | i = \pm 1, \dots, \pm N\}$ . The probability of symbol error can be written in terms of conditional error probabilities:

$$P_e = \sum_{i=-N}^{-1} P(\text{error}|q_i)P(q_i) + \sum_{i=1}^N P(\text{error}|q_i)P(q_i) \quad (3.8)$$

Due to the symmetry of constellation and symbol probability distributions, the probability of symbol error can be written as:

$$P_e = 2 \sum_{i=1}^N P(\text{error}|q_i)P(q_i). \quad (3.9)$$

For a fixed set of symbol probabilities  $P(q_i)$  and detector thresholds  $\tau_i$ 's, we select an optimal set of signal levels  $q_i$ 's that minimize the probability of symbol error.

For the inner signal points, each conditional probability  $P(\text{error}|q_i)$  is computed as:

$$\begin{aligned} P(\text{error}|q_i) &= P(r[n] < \tau_{i-1}|q_i) + P(r[n] > \tau_i|q_i) \quad \text{for } i = 1, 2, \dots, (N-1) \\ &= 1 - \int_{\tau_{i-1}-q_i}^{\tau_i-q_i} f_W(w) dw \end{aligned} \quad (3.10)$$

---

ols have symmetrical probability distributions, the weighted sum of these random variables has also symmetrical probability distribution.

where  $f_W(w)$  is the PDF of the random variable  $w[n]$ . From Eq. (3.10), it is evident that:

$$\min_{q_i} P(\text{error}|q_i) = 1 - \max_{q_i} \int_{\tau_{i-1}-q_i}^{\tau_i-q_i} f_W(w) dw \quad \tau_{i-1} \leq q_i \leq \tau_i \quad (3.11)$$

for  $i = 1, \dots, N - 1$

In general, the value of  $q_i$  that minimizes the probability of symbol error depends on the PDF of  $w[n]$ . However, there are cases where the choice of  $q_i$  is only dependent on the values of decision boundaries (detector thresholds). For example, Fig. 3.4(a) shows a conditional PDF,  $P(r[n] < \tau_{i-1}|q_i) = f_W(w - q_i)$ , that is monotonically decreasing on each side of its mean. For this distribution, the optimal choice of the signal point  $q_i$  is the midpoint between the two closest detector thresholds<sup>6</sup>:

$$q_i = \frac{\tau_i + \tau_{i-1}}{2} \quad \text{for } i = 1, 2, \dots, N - 1 \quad (3.12)$$

Note that, in some cases, the choice of  $q_i$  as the average of two detector thresholds may not be optimal. For example, Fig. 3.4(b) shows an extreme case where the optimal value of  $q_i$  is either of the two decision boundaries. The probability of error in this case is larger than one half. Such degenerate cases can be caused by a large ISI or a relatively short distance between adjacent detector thresholds. We can trade off the number transmitted bits per symbol for a larger minimum distance between the adjacent decision boundaries. We will use pre-equalization techniques to avoid or to reduce the ISI. These methods will be described in the next chapters.

The computation of the probability of symbol error for the outermost signal points  $q_N$  is slightly different. Given that  $q_N$  is transmitted, the probability of symbol error is computed as:

$$\begin{aligned} P(\text{error}|q_N) &= P(r < \tau_{(N-1)}|q_N) \\ &= \int_{-\infty}^{\tau_{(N-1)}-q_N} f_W(w) dw \end{aligned} \quad (3.13)$$

---

<sup>6</sup>Assuming that  $f_W(w)$  is a continuous function, we can verify the optimal choice of  $q_i$  by taking the derivative of the integral with respect to  $q_i$ . The value of  $q_i$  that maximizes the integral in Eq.(3.11) should satisfy the following equation:

$$\frac{\partial}{\partial q_i} \int_{\tau_{i-1}-q_i}^{\tau_i-q_i} f_W(w) dw = 0$$

By taking the derivative of the integral, we have:

$$-f_W(\tau_i - q_i) + f_W(\tau_{i-1} - q_i) = 0$$

Since  $f_W$  is symmetrical and also monotonic on each side of the center, we find that  $\tau_i - q_i = q_i - \tau_{i-1}$ . Solving this equation for  $q_i$ , we determine the optimal value of  $q_i$  as given in Eq.(3.12). By taking the second derivative of the integral in Eq.(3.11) and evaluating the result at  $q_i$ , we can verify that this point indeed corresponds to a maximum for the integral, or a minimum for the probability of symbol error.

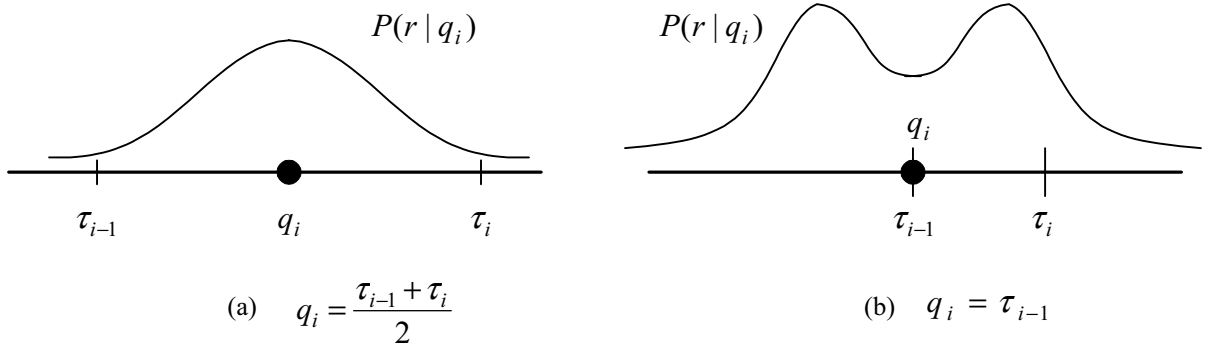


**Fig. 3.4** Two cases of conditional probability distribution functions of the received signal, given that  $q_i$  is transmitted. In case (a) the PDF has a single peak. To maximize the integral of the right-hand side of Eq. (3.11), the signal point  $q_i$  should fall midway between detector thresholds  $\tau_{i-1}$  and  $\tau_i$ . In case (b), the optimal selection of the signal level is not unique. In this particular example, the probability of symbol error for  $q_i$  is larger than  $1/2$ . Such an extreme case is caused by severe ISI and/or a short distance between detector thresholds.

From Eq. (3.13), we note that if the value of  $q_N$  increases to infinity,  $P(\text{error}|q_N)$  tends to zero. However, there is a constraint on the average transmitted signal power:

$$2 \sum_{i=1}^N P(q_i) q_i^2 \leq \mathcal{P}_{ave} \quad (3.14)$$

where  $\mathcal{P}_{ave}$  is the average transmitted power in a linear scale. The power constraint Eq. (3.14) leads to the following expression for the outermost signal point:

$$q_N = \sqrt{\frac{\frac{\mathcal{P}_{ave}}{2} - \sum_{i=1}^{N-1} P(q_i) q_i^2}{P(q_N)}}. \quad (3.15)$$

Note that we assume the detector thresholds and transmitted power are chosen such that a solution exists. We define a virtual decision boundary:

$$\tau_N = 2q_N - \tau_{(N-1)}$$

so that Eq. (3.12) also holds for the outermost signal points.

### 3.2.2 Remarks

- For a given set of detection thresholds, the optimal PAM symbols fall midway between each pair of adjacent thresholds if the PDF of the additive distortion is symmetrical and monotonic on each side of its mean. In more general cases, the PDF of additive distortion is required to identify the optimal signal levels.
- The minimum probability of symbol error is computed as:

$$\min_{q_i} P_e = 1 - 2 \left\{ \sum_{i=1}^{N-1} P(q_i) \int_{-\frac{\delta_i}{2}}^{\frac{\delta_i}{2}} f_W(w) dw + P(q_N) \int_{-\frac{\delta_N}{2}}^{\infty} f_W(w) dw \right\} \quad (3.16)$$

where  $\delta_i = \tau_i - \tau_{i-1}$  is the distance between two successive decision boundaries. From Eq. (3.16), it is clear that increasing the distance between decision boundaries will reduce the probability of error.

- The actual symbol error probability depends on the PDF of  $w[n]$ . As an example, consider a Gaussian distribution for  $w[n]$  with zero mean and a standard deviation of  $\sigma$ . The minimum probability of symbol error is simplified to:

$$\min_{q_i} P_e = 2 \left\{ 2 \sum_{i=1}^{N-1} P(q_i) Q\left(\frac{\delta_i}{2\sigma}\right) + P(q_N) Q\left(\frac{\delta_N}{2\sigma}\right) \right\} \quad (3.17)$$

where  $Q(\cdot)$  is the area under the tail of the Gaussian PDF:

$$Q(x) = \frac{1}{\sqrt{2\pi}} \int_x^{\infty} e^{-\frac{u^2}{2}} du \quad (3.18)$$

Note that, at a high signal-to-noise ratio operating point, the probability of error is determined by the minimum distance between the adjacent decision boundaries:

$$P(\text{error}) \approx K Q\left(\frac{\delta_{\min}}{2\sigma}\right) \quad (3.19)$$

where  $K$  is proportional to the number of signal levels with the minimum distance between their decision boundaries.

- The up-stream PCM channel imposes a power limit on the transmitted signal. We can take into account the energy cost of each constellation point by choosing a non-uniform probability distribution for the constellation points. Examples of non-uniform probability distribution for constellation points will be discussed later in this chapter.

- The minimum probability of error is a function of the distances between detector thresholds. In the up-stream PCM channel, the threshold levels are a subset of the PCM encoder decision boundaries. These boundaries are determined based on a non-linear companding rule (i.e. A-Law or  $\mu$ -Law) with non-uniform spacing. Although companding rules are efficient for voice communication, the choice of non-uniform spacing between threshold levels is not optimal for data communication over the PCM channel. It can be shown that for equally probable PAM constellation points with a constraint on average transmitted power, equal spacing between signal constellation points minimizes the probability of symbol error at a high signal-to-noise ratio [31].

### 3.2.3 Performance results

In this section, we examine the performance of PAM modulation with non-uniform symbol spacing over the upstream PCM channel. We model the channel distortion  $w[n]$  as an additive Gaussian component<sup>7</sup>.

As a baseline, we use conventional  $M$ -ary PAM modulation with equally spaced and equally likely constellation points. The probability of symbol error for the conventional PAM modulation over an AWGN channel is computed as [32]:

$$P_M(\text{error}) = \frac{2(M-1)}{M} Q\left(\sqrt{\frac{3\mathcal{P}_{ave}}{(M^2-1)\sigma^2}}\right) \quad (3.20)$$

where  $\sigma^2$  and  $\mathcal{P}_{ave}$  are the noise and signal power in linear scale. The average signal power is:

$$\mathcal{P}_{ave} = \frac{1}{M} \sum_{i=1}^M q_i^2 \quad (3.21)$$

The average power limit for a transmitted signal over a voiceband channel is around  $-12$  dBm0. As described in Section 2.3.4, the outermost decision boundary of a  $\mu$ -Law PCM encoder corresponds to the maximum amplitude of a sine-wave with 3.17 dBm0 power. The signal power in the dBm0 scale is computed as:

$$\mathcal{P}_{\text{dBm0}} = 3.17 + 10 \log_{10}\left(\frac{2}{(8159)^2} \mathcal{P}_{ave}\right). \quad (3.22)$$

From Eq. (3.20), it is clear that the Symbol Error Rate (SER) for uniform PAM modulation is a function of the signal-to-noise power ratio  $\mathcal{P}_{ave}/\sigma^2$ , and not the absolute value of the signal or noise power.

---

<sup>7</sup>The additive Gaussian random variable can be either a model for the noise or an approximate model for the combined noise and ISI.

In our examples, we consider PAM constellations with 32, 64 and 128 signal points. These constellations are designed for an up-stream PCM channel with a  $\mu$ -Law encoder at the receiver. Depending on the signal power, different subsets of the encoder decision levels are selected as detector thresholds. The criterion for selecting the detection thresholds is the maximization of the minimum distance between adjacent boundaries while maintaining average power constraint. As discussed in the previous section, the PAM constellation points are chosen at the mid-point of each decision interval.

Figure 3.5 shows symbol error probabilities in terms of the signal-to-noise power ratio and the average signal power for non-uniform 32-PAM modulations. As a benchmark, the probability of symbol error of a uniform 32-PAM is also depicted. For a given constellation size, the probability of symbol error for a uniform PAM is only a function of the signal-to-noise power ratio. Figure 3.5 shows that, for a non-uniform PAM (designed for the up-stream PCM channel), the probability of symbol error depends on both signal and noise power. Note that for a non-uniform PAM modulation over a PCM channel, an increase in average signal power does not necessarily cause an increase in the minimum distance between constellation points (or more precisely, detector thresholds). This point is further explained in the example described below.

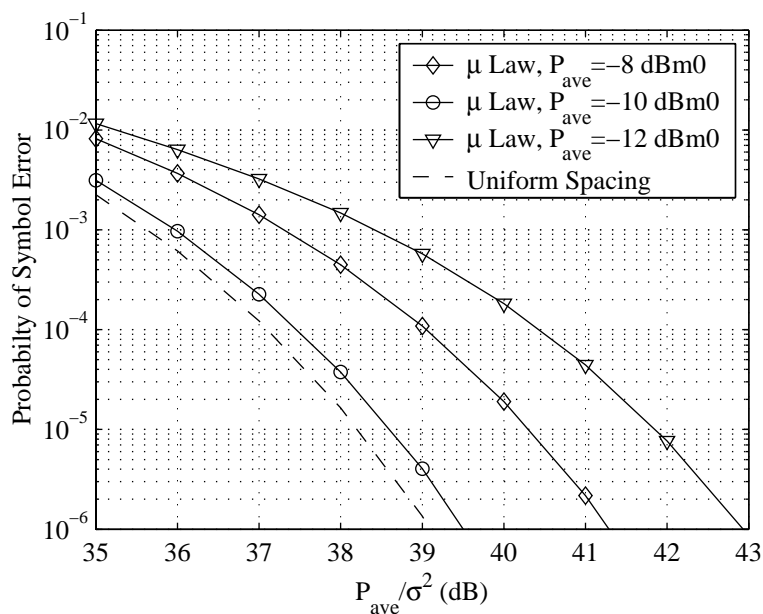


**Fig. 3.5** Performance results of 32-PAM modulation designed for the up-stream PCM channels. The performance results are compared to those of conventional 32-PAM signals. The distortion is modeled as additive white Gaussian noise. Compared to the conventional 32-PAM, the non-uniform spacing between constellation points causes performance degradations.

As shown in Eq. (3.19), at a high signal-to-noise ratio, the probability of symbol error is determined by the minimum distance between adjacent detector thresholds. Since the detector thresholds are a subset of predetermined values (i.e. the PCM encoder decision boundaries), an increase in average signal power does not always change the minimum distance between selected detector thresholds. For example, consider the performance results shown in Fig. 3.5. The minimum distance between adjacent detector thresholds are 64, 128 and again 128 unit counts while the average signal powers are  $-12$  dBm0,  $-10$  dBm0 and  $-8$  dBm0 respectively<sup>8</sup>. For the same noise power level, the performance of the two PAM constellations with  $-10$  dBm0 and  $-8$  dBm0 average signal power levels are the same. Results shown in Fig. 3.5 confirm this, since the difference between the two performance curves at a high SNR is 2 dB which accounts for the difference in signal powers. In other words, in this example, increasing the average signal power from  $-10$  dBm0 to  $-8$  dBm0 does not improve performance.

Let us now compare the performance curve of a signal with a  $-12$  dBm0 average power to that of signal with  $-10$  dBm0 average power. At  $-12$  dBm0 average signal power, the minimum distance between adjacent detector thresholds is 64 unit counts, or half of the minimum distance of the PAM signal with  $-10$  dBm0 average signal power. From Eq. (3.19), for the same probability of symbol error, the noise power for the signal with the average power of  $-12$  dBm0 is four times (or 6 dB) larger than that of the signal with  $-10$  dBm0 signal power<sup>9</sup>. The difference in signal power and noise power together account for around 4 dB difference in the SNR between the two performance curves. Results shown in Fig. 3.5 confirm this difference.

Performance results for the 64-PAM and the 128-PAM are shown in Fig. 3.6 and Fig. 3.7 respectively. The results for the 64-PAM show the same trend as those for the 32-PAM. For the 128-PAM, the minimum distance between adjacent detector thresholds is the same for all three average signal power levels. Therefore, increasing the average signal power does not improve performance. Note that the performance gap between uniform and non-uniform modulation for the 128-PAM is larger than that for the 64-PAM and the 32-PAM. For a larger constellation size, the spacing between constellation points becomes more non-uniform and the minimum distance between adjacent detector thresholds becomes relatively smaller.

Figure 3.8 compares the performance results for different constellation sizes with a fixed average signal power of  $-12$  dBm0. At a high SNR, the cost of maintaining the same performance when we add one more bit per symbol (doubling the constellation size) is around 6 dB.

<sup>8</sup>The outermost decision boundary of the PCM encoder corresponds to 8159 unit counts.

<sup>9</sup>If  $K_1 Q(\frac{\delta_1}{2\sigma_1}) \approx K_2 Q(\frac{\delta_2}{2\sigma_2})$  and  $\delta_2 = 2\delta_1$  then  $\sigma_2^2 = 4\sigma_1^2$  where the impact of  $K$  is insignificant.

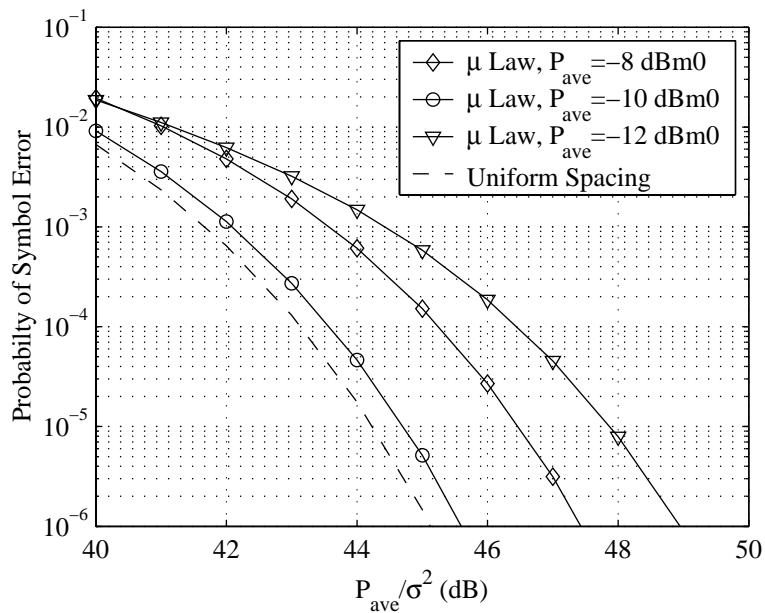


**Fig. 3.6** Performance results for non-uniform 64-PAM modulation designed for the up-stream PCM channels.

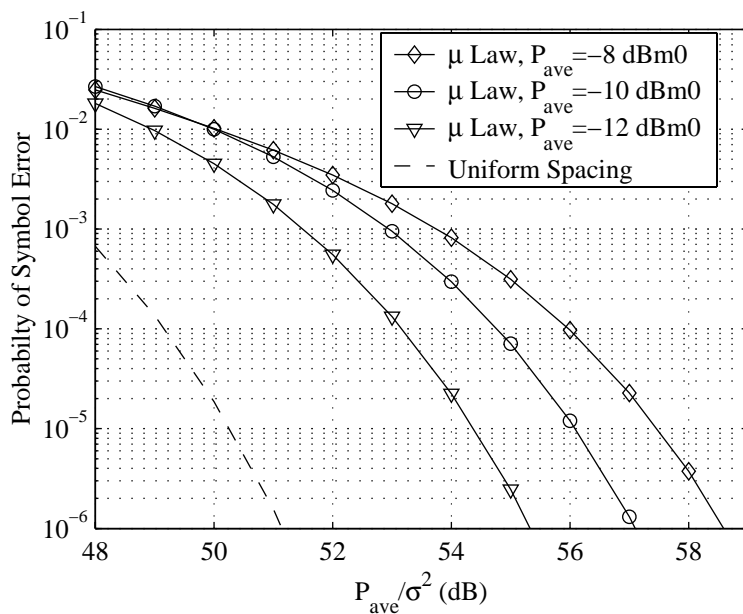


**Fig. 3.7** Performance results for the non-uniform 128-PAM designed for the up-stream PCM channels.

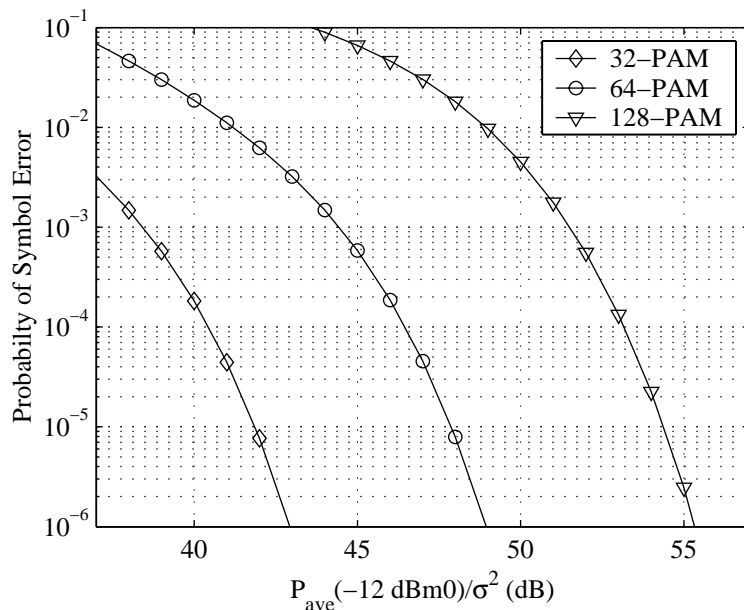


**Fig. 3.8** Performance results for non-uniform PAM modulation with an average of  $-12$  dBm0 signal power.

### 3.2.4 How to choose detector thresholds

As stated previously, detector thresholds are selected from the set of PCM encoder decision boundaries. There are several conflicting conditions effecting the selection of detector thresholds. For a given constraint on the average signal power, we wish to achieve a high transmission bit-rate while keeping a low probability of symbol error. We consider two different approaches in selecting the detector thresholds.

#### Selecting thresholds based on a given minimum distance

The minimum distance between adjacent decision thresholds determines the modulation performance (expressed in terms of the symbol error rate). For a given signal and noise power, we can set a value for the minimum distance between the detector thresholds, say  $D_{\min}$ , to obtain a desired performance. For a given value of  $D_{\min}$ , the selection of the detector thresholds can be accomplished by applying a pruning procedure to the PCM encoder decision boundaries. The procedure of selecting detector thresholds  $\tau_i$  can be described as follows:

1. Set the origin as a detector threshold  $\tau_0 = 0$ .
2. Select the smallest PCM decision boundary that is greater than  $D_{\min}$  as the first positive threshold  $\tau_1$ . For symmetry, select  $\tau_{-1} = -\tau_1$  as the first negative threshold.

3. At each stage, consider  $\tau_i$  such that  $\tau_i - \tau_{i-1} \geq D_{\min}$ . Continue until the last PCM decision boundary is reached.
4. Compute the constellation points  $q_i$  using Eq. (3.12). For a given distribution of symbol probabilities  $P(q_i)$ , compute the average signal power. Keep a subset of constellation points, so that the average signal power constraint given in Eq. (3.14), is satisfied<sup>10</sup>.

In this procedure, the number of PAM symbol levels is determined based on  $D_{\min}$  and the distribution of the symbol probabilities.

### Selecting thresholds based on a given number of symbol levels

In this approach, a fixed number of detector threshold levels is selected so that the average signal power is satisfied and the probability of symbol error is minimized. The minimum distance between adjacent detector thresholds is used as a measure of the modulation performance. For a PAM system with a large constellation size, an exhaustive search to determine the optimal set of thresholds levels is impractical. For a  $2N$ -PAM symmetrical constellation, there are  $\frac{128!}{N!(128-N)!}$  ways of selecting the thresholds.

We use a suboptimal approach in selecting thresholds. Starting from a set of equally-spaced constellation points, we adjust the levels so that the average power constraint is satisfied. A brief description of the selection algorithm is given below:

1. Design a  $2N$ -PAM constellation with equally-spaced points with average signal power below a pre-set level  $P_{\max}$ .
2. Replace each positive threshold  $\tau_i$  found in the previous stage with the nearest PCM decision boundary that is greater or equal to  $\tau_i$ .
3. It is possible that more than one threshold is mapped to a decision boundary. Select an appropriate number of the outmost unused decision boundaries that are unused to maintain  $2N$  distinct thresholds.
4. Compute the constellation point and the average signal power. If the average signal power is larger than the constraint, reduce  $P_{\max}$  and start from step 1.

---

<sup>10</sup>As we will see in the next sections, an appropriate distribution of symbol probabilities can allow for a larger constellation size while satisfying the average power constraint.

### 3.2.5 Bit-to-symbol mapping

In this section, we describe methods of mapping the binary data into symbol levels. For a  $2N$ -PAM modulation, the maximum number of bits transmitted per symbol is  $\log_2(2N)$  bits. If the constellation size  $2N$  is not an integer power of 2, the bit-to-symbol mapping on a symbol-by-symbol basis cannot reach the maximum bit rate of  $\log_2(2N)$  bits/symbol. In this case, a bit-to-symbol mapping performed on a frame-by-frame basis can increase the average number of bits transmitted per symbol. For a PCM channel, the overall increase of bit-rate due to frame-by-frame bit assignment, as opposed to symbol-based bit mapping, can be up to (but less than) 8 kbits/sec. As an example, Fig. 3.9 shows the bit-rate of a 58-PAM modulation as a function of the number of symbols per frame ( $K$ ). The maximum number of bits per symbol in this case is equal to  $\log_2(58)$ . If we choose 6 or 7 symbols per frame, the average number of bits per symbol is close to this maximum. Note that the average number of bits per symbol does not monotonically increase when we increase the number of symbols per frame<sup>11</sup>.

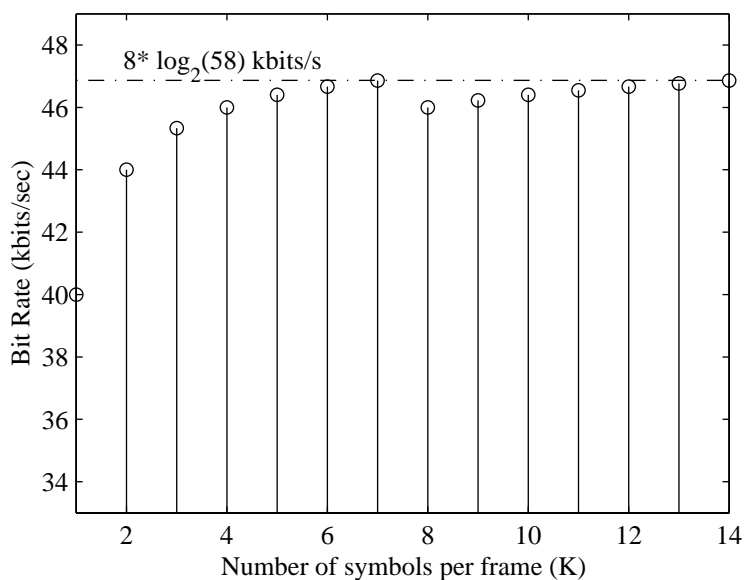


**Fig. 3.9** The average transmitted bit-rate as a function of symbols per frame on a PCM channel. The number of levels per symbol (constellation size) is 58. The bit-rate shown in this figure is based on an 8000 symbol/sec transmission.

The mapping from a string of input bits to a frame of symbols can be viewed as an index assignment problem, where each point in a  $K$ -dimensional constellation should be uniquely specified by an  $N_b$ -bit binary index. There are two important issues concerning the index assignment

<sup>11</sup>However, one can show that for a  $2N$ -PAM signal, there exists a value for  $K$  such that the average number of bits transmitted per symbol is as close as desired to  $\log_2(2N)$ .

strategy:

1. due to a large multi-dimensional constellation size  $((2N)^K)$ , the bit-to-symbol mapping should be such that it can be implemented algorithmically rather than in a look-up-table.
2. the bit-to-symbol mapping should be such that an error event due to the channel imperfections causes a small number of bit errors. In other words, we would like two constellation points with a small Euclidean distance to be assigned indices which differ in as few bit positions as possible (i.e., indices of adjacent points should have a small Hamming distance).

In the rest of this section, we first describe a simple index mapping algorithm that has been used in The V.90 Standard. We refer to this method as *natural index mapping*. Since the natural index mapping algorithm does not provide the minimum Hamming distance between adjacent points, we investigate other methods of index mapping. We propose a new index mapping algorithm that can be viewed as a generalization of Gray encoding [32, p. 175] in multi-dimensional space.

### Natural Index mapping

A simple method for index assignment is by the natural indexing of constellation points. Suppose the PAM symbol alphabet contains  $2N$  levels, each frame consists of  $K$  symbols and the frame index is an  $N_b$ -bit binary sequence. For a unique index assignment, the following inequality should hold:

$$2^{N_b} \leq (2N)^K.$$

Each index represents an  $N_b$ -digit number in base-2, while each constellation point in a  $K$ -dimensional frame is naturally represented by a  $K$ -digit number in base- $(2N)$ . A natural index assignment would be to convert the representation of the number from base-2 to base- $(2N)$ .

$$(D_{(K-1)} \dots D_1 D_0)_{(2N)} = (b_{(N_b-1)} \dots b_1 b_0)_2 \quad (3.23)$$

At the receiver, the reverse conversion from base- $(2N)$  to base-2 is used to recover the binary sequence. The natural index assignment can be implemented algorithmically using modulo arithmetics. The V.90 Standard uses this algorithm for bit-to-symbol mapping [13] described as “modulus encoding”<sup>12</sup>.

A drawback of the natural index mapping is that the average Hamming distance of the indices of the adjacent points can be relatively high<sup>13</sup>. In an extreme case, a pair of constellation points

<sup>12</sup>A similar method of bit-to-symbol mapping has been proposed for recommendation V.92.

<sup>13</sup>In our discussion, we consider two constellation points in a  $K$ -dimensional space to be adjacent if their coordinate positions are the same except for one coordinate that their values differ with a minimum amount.

with a small Euclidean distance might correspond to two indices with a maximum Hamming distance (bits in all positions in the two indices are different). When we use the natural index mapping, the average Hamming distance between adjacent constellation points increases when the number of symbols per frame increases. As an example, we consider a 58-PAM modulation and investigate the average Hamming distance of indices of the adjacent points as a function of  $K$ . If we assume that channel signal-to-noise ratio is relatively high, a symbol in error is most likely detected as one of its neighbouring points. We also assume that the probability of more than one symbol error in each frame is negligible. Based on the above assumptions, the bit error rate (BER) can be approximated as a function of the probability of symbol error:

$$P_b \approx \frac{K}{N_b} d_H P_s \quad (3.24)$$

where  $K$  is the number of symbols per frame,  $N_b$  is the number of bits transmitted per frame and  $d_H$  is the average Hamming distance between the indices of the adjacent points.

Figure 3.10 shows the average Hamming distance of indices of adjacent points as a function of  $K$ . For a natural index mapping, the Hamming distance between adjacent points increases when the number of symbols per frame ( $K$ ) increases. A more efficient index mapping strategy can reduce the probability of bit error by reducing the Hamming distance between the indices of adjacent points.

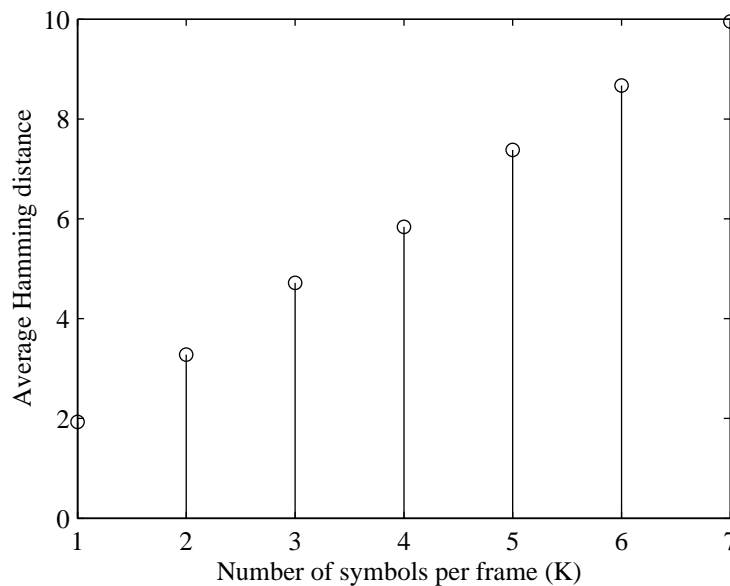


**Fig. 3.10** The average Hamming distance between indices of adjacent points is shown as a function of  $K$  for a 58-PAM modulation

### A Hybrid Gray-Natural (HGN) index mapping

The mapping of information bits to a one-dimensional PAM signal can be performed by a Gray encoding [32, p. 175], in which the indices of adjacent symbols differ by only one bit (a Hamming distance of one). However, the conventional Gray encoding is not directly applicable to a frame of symbols when the number of bits assigned to each symbol is not integer.

Here, we introduce a Hybrid Gray-Natural (HGN) index mapping that partitions the constellation points into two regions: one region where indices are assigned by using Gray encoding, and a second region where indices are obtained by a mapping similar to natural index mapping. Compared to the natural index mapping, the HGN index mapping reduces the Hamming distance between indices of adjacent points. The HGN index mapping can be implemented algorithmically, without using a large look-up table.

We describe the HGN mapping by a simple example. Consider a frame of 2 symbols ( $K = 2$ ) with a 6-PAM ( $2N$ -PAM) constellation per symbol. The number of bits transmitted per frame is  $N_b = 5$ . Each 2-dimensional constellation point in a frame can be specified by a number in base-6 as  $(D_1 D_0)_6$  where  $D_1$  and  $D_0$  take integer values between 0 and  $2N - 1 = 5$ . Figure 3.11 shows the 2-dimensional constellation points in each frame (region(A) and region(C)).

Each 5-bit index is parsed into two segments (corresponding to two symbols). The first three bits of each index are mapped into an 8-level Gray encoded symbol  $G_0$ . The last two bits of each index are used to specify a 4-level Gray encoded symbol  $G_1$ .

If  $G_0$  is less than  $2N = 6$ , the combination of  $(G_1 G_0)$  can be used directly to represent a constellation point in the frame:

$$(D_1 D_0)_6 = (G_1 G_0)$$

This constellation is in region (A) (see Fig. 3.11).

If  $G_0$  is greater or equal to  $(2N = 6)$ , the combination of  $(G_1 G_0)$  is not a legitimate constellation index (i.e., a point in region (B)). We need to apply a second mapping to project points in region (B) into points in region (C). Points in region (B) and (C) are separately labeled. A point from region (B) is mapped to a point in region (C) which has the same integer label<sup>14</sup>.

<sup>14</sup>In order to specify the mapping, we define new coordinates for region (B) and region (C). The new coordinates are constructed by a simple shift of axis. For region (B) we define:

$$\begin{aligned} E_0 &= G_0 - 5 \\ E_1 &= G_1 \end{aligned} \tag{3.25}$$

where  $0 \leq E_0 \leq 1$  and  $0 \leq E_1 \leq 3$ . We present each point in region (C) with a new coordinate  $(F_1 F_0)$  where  $0 \leq F_0 \leq 5$  and  $0 \leq F_1 \leq 1$ . In order to specify  $F_1$  and  $F_0$ , we use the following equation:

$$6F_1 + F_0 = E_1 + 4E_0 \tag{3.26}$$

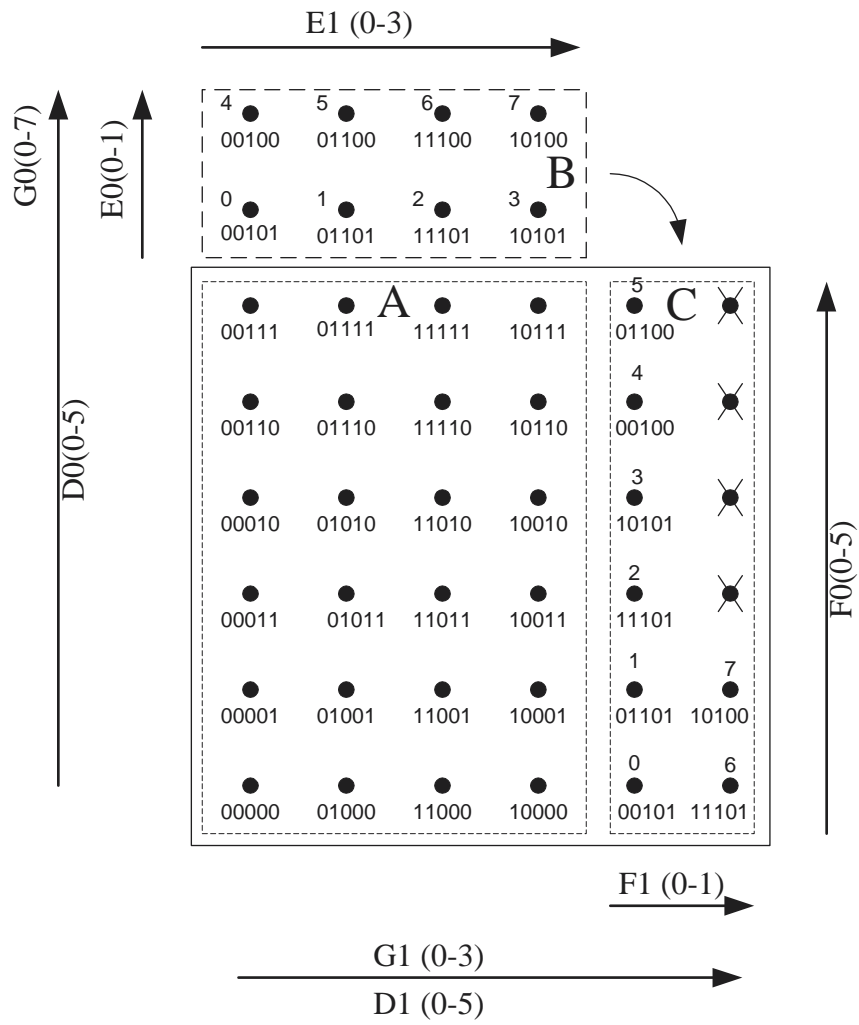


Fig. 3.11 Bit-to-symbol mapping based on hybrid natural-Gray encoding.

Since region (C) contains more points than region (B), some points in region (C) are not used. Figure 3.11 shows the index of each constellation point. For this particular example, there are four unused constellation points in region (C).

As shown in the above example, the HGN index mapping creates a Gray encoded region (A) where the indices of adjacent points have a Hamming distance of one. For points in region (C), the Hamming distance between adjacent points can be larger than one.

In general, the proposed index mapping can be summarized in the following steps:

*Step 1* For a given constellation  $2N$ -PAM and a frame size  $K$ , the number of bits per each frame index is computed as:  $N_b = \lfloor K \log_2(2N) \rfloor$ . We parse each  $N_b$  index bits into  $K$  segments. The number of bits assigned to each segment is  $N_{b_i}$  which takes an integer value equal to  $\lfloor \log_2(2N) \rfloor$  or  $\lceil \log_2(2N) \rceil$  while:

$$N_b = N_{b_1} + N_{b_2} + \cdots + N_{b_K}.$$

We choose the first  $M$  segments to have  $\lfloor \log_2(2N) \rfloor$  bits per segment and the last  $K - M$  segments to have  $\lceil \log_2(2N) \rceil$  bits per segment<sup>15</sup>. For example, for a 58-PAM with 6 symbols per frame, the number of bits per each frame index is 35. Each frame index is parsed into 6 segments where the first segment contains 5 bits and the next 5 segments contain 6 bits per segment.

*Step 2* We use a Gray encoding to map  $K$  segments into  $K$  indices. If these  $K$  indices are all less than  $2N$ , they represent a valid point in the constellation space (region (A) in Fig. 3.11).

If one or more indices are greater or equal to  $2N$ , we will use a second index mapping, as described in the next step.

*Step 3* If the indices generated by Gray encoding do not represent a valid constellation point (region (B) in Fig. 3.11), we use a natural index mapping to convert the Gray encoded indices into indices of a valid constellation point (region (C)). We label each point in region (B) and region (C) by an integer number. The labeling is performed by natural indexing of points in each region. A point from region (B) is mapped into a point in region (C) that has the same integer label.

At the receiver, a constellation point that belongs to the Gray-mapping region (region (A))

---

<sup>15</sup>It is easy to show that the number of segments with  $\lfloor \log_2(2N) \rfloor$  bits is:

$$M = K - \lfloor K \log_2(2N) \rfloor + K \lceil \log_2(2N) \rceil$$

can be easily decoded to a sequence of bits. For points in region (C), a reverse mapping of Step 3 should be applied.

We use the hybrid mapping for a 58-PAM signal. Figure 3.12 shows the average Hamming distance of the indices of adjacent point as a function of  $K$ . Compared to the previous results presented in Fig. 3.10, the average Hamming distance between adjacent points is significantly reduced. We investigated the impact of the index mapping on the probability of bit error. As an example, we applied the natural index mapping and the HGN index mapping to a 58-PAM signal. Figure 3.13 shows that the HGN index mapping outperforms the natural index mapping. As a lower bound of the probability of error, we assume there exists an index mapping that can maintain a Hamming distance of one between the indices of the adjacent points. The minimum probability of bit error can be expressed as:

$$\min P_b \approx \frac{K}{N_b} P_s \quad (3.27)$$

where  $K$  is the the number of symbols per frame,  $N_b$  is the number of bits transmitted per frame and  $P_s$  is the probability of symbol error. This lower bound is also presented in Fig. 3.13. The question of the existence of a better index mapping with reasonable computation complexity and storage size to recover the gap between the probability of the bit error and its lower bound is a subject for further study.

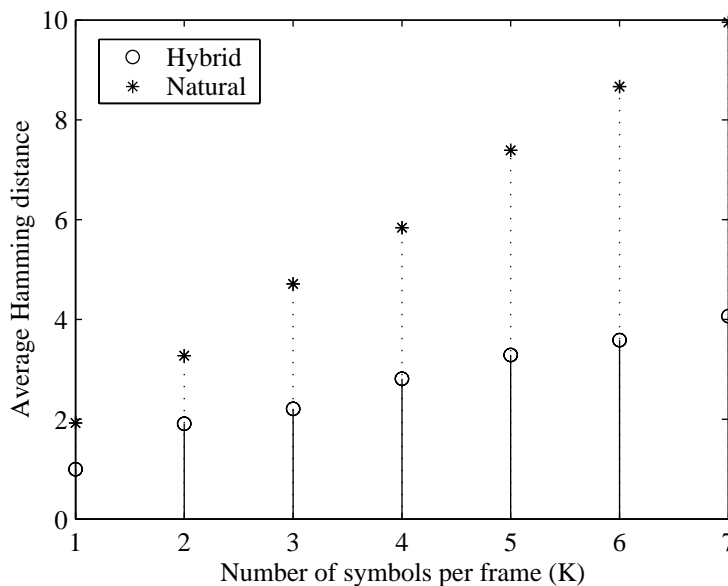


**Fig. 3.12** Compare the average Hamming distance generated by the natural index mapping with that generated by the Hybrid Gray-Natural index mapping. The number of levels per symbol is 58.

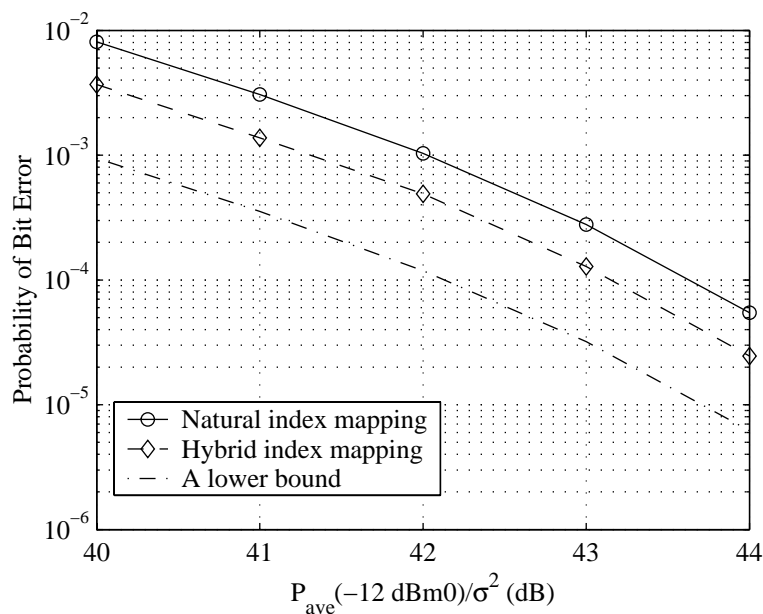


**Fig. 3.13** Probability of bit error for a 58-PAM modulation over a PCM up-stream channel. The probability of bit error based on natural index mapping and hybrid natural-Gray index mapping is compared with a lower bound. The lower bound is based on this assumption that the Hamming distance between the indices of the adjacent points is equal to one.

### Related work on index assignment

In quantization theory, problems similar to what we described here as index mapping have been investigated. In a vector quantization of an analog source, a proper index assignment to codevectors can reduce the distortion caused by an error in the bits representing each index. The index error is caused by a noisy transmission channel.

Simulated annealing [33], pseudo Gray codes via binary switching [34] and Hadamard Transform [35] [36] are several techniques suggested for the index assignment.

Despite the fact that there are similarities between the index assignment problem and the bit-to-symbol mapping, there are subtle but significant differences between the two problems:

- The constellation points specified in frame of symbols are structured over a grid. Although signal levels may not be equally spaced, the spacing is the same for different symbols. On the other hand, the codevectors specified by a vector quantizer do not follow a specific structure. Therefore, the only way to specify the distance between two codevectors is Euclidean distance.

- In general, in a vector quantization problem, the codevectors are stored in memory (unless structured VQ is used). In that case the index assignment can be seen as re-ordering the codebooks in the memory. In a bit-to-symbol mapping we would like to avoid any extensive use of memory or a look-up table for index mapping.

Although we do not rule out any potential use of the above techniques in the index mapping problem (or the possible use of HGN in the index assignment problem), we defer establishing these links to future studies.

### 3.3 Non-uniform probability distributions for constellation points

In our performance analysis of PAM modulation, we assumed equally probable constellation points. Here, we discuss a potential performance improvement that can be achieved by using a non-uniform probability distribution for the PAM symbols. For a given PAM constellation size, the average number of bits per symbol is maximized if the constellation points are equally probable (i.e. maximum entropy per symbol). However, constellation design based on equally-probable symbols does not take into account the energy cost of the outer constellation points.

Choosing constellation points with a smaller energy more often than points with a higher energy reduces the average transmitted power. As a result, we can choose a larger constellation size while maintaining the same average signal power. We will show that the overall impact of increasing the constellation size with unequally-probable constellation points is an increase in the average number of bits per symbol for a given average signal power.

In this section, we first describe the optimal probability distribution that maximizes the average number of bits per symbol, given a constraint on the average signal power. We apply the probability distribution to our previous examples of PAM modulation over the PCM channel to quantify the increase in the bit rate. As a baseline, we compute the upper bound of average transmitted bits per symbol for a PAM modulation over an AWGN channel. Finally, we describe the use of Huffman coding to map the information bits to a set of PAM symbols with non-uniform probability distribution.

#### 3.3.1 Maximizing the entropy

Considering the constraint on the average signal power, we would like to find the probability distribution of a set of PAM symbols that maximizes the average transmitted bit-rate. From the information theory point of view, the information content of a random signal is measured by

entropy. The entropy  $H(X)$  of a discrete random variable  $X$  is defined as [37]:

$$H(X) = - \sum_{x \in \mathcal{X}} P_X(x) \log_2(P_X(x)) \quad \text{bits}$$

For a PAM signal with  $2N$  constellation points, the entropy of transmitted symbols is computed as:

$$H = - \sum_{\substack{i=-N \\ i \neq 0}}^N P(q_i) \log_2 P(q_i) \quad (3.28)$$

where  $P(q_i)$  is the probability of symbol  $q_i$ . The entropy  $H(P)$  is maximized if all symbols are equally probable [37]:

$$\max_P H(P) = \log_2(2N)$$

For a PAM signal with power constraint, the maximum entropy principle [37, p. 267] leads to the following probability distribution, known as Maxwell-Boltzmann distribution, that maximizes the number of bits received per symbol:

$$P(q_i) = \frac{\exp(-\lambda q_i^2)}{\sum_i \exp(-\lambda q_i^2)} \quad (3.29)$$

where  $\lambda$  is a positive parameter chosen such that the average signal power constraint is satisfied:

$$\frac{\sum_i q_i^2 \exp(-\lambda q_i^2)}{\sum_i \exp(-\lambda q_i^2)} \leq \mathcal{P}_{ave} \quad (3.30)$$

The left hand-side is a monotone decreasing function of  $\lambda$ . If the inequality does not hold for  $\lambda = 0$ , we will solve Eq. (3.30) for  $\lambda$  under equality condition.

### 3.3.2 Examples of maximum entropy distributions for a PAM signal

Considering PAM modulation design for a PCM channel, we apply the maximum entropy distribution discussed above to the PAM constellation points. From Eq. (3.19), the probability of symbol error is a function of the minimum distance between the adjacent detector thresholds. By controlling the minimum distance, we can maintain a desired probability of symbol error at a given signal-to-noise ratio.

As an example, we consider a PCM channel with a  $\mu$ -Law compander. We choose a PAM constellation with 156 points and a minimum distance of 32 unit counts between detector thresh-

olds. Note that the maximum decision level is normalized at 8159 unit counts. Figures 3.14 and 3.15 show the maximum entropy probability distributions with average power constraints of  $-10$  dBm0 and  $-12$  dBm0 respectively. As shown in these figures, reduction of the average signal power reduces the probability of selecting the outer signal points. Since the probability of selecting the outer points is significantly smaller than that of the inner points, we can eliminate a few outmost points from the constellation without any significant change in the bit rate. The average numbers of bits per symbol are 6.82 and 6.64 bits/symbol for average signal power of  $-10$  dBm0 and  $-12$  dBm0 respectively.

To quantify the impact of maximum entropy distribution on the bit rate, we consider a PAM constellation with equally-probable symbols and an average signal power of  $-12$  dBm0. We maintain the same minimum distance between detector thresholds as that given in the above example. Figure 3.16 confirms that for the SNR range in which we are interested, the SER performance of the two schemes is similar.

The constellation size of the PAM modulation with uniform probability distributions is 90 which accounts for  $\log_2(90) = 6.49$  bits/symbol. Since the symbol rate for the up-stream PAM channel is 8000 symbols/sec, the bit-rate of the PAM modulation with uniform probability distribution is 1.22 kbits/sec lower than the bit-rate of a PAM modulation with the maximum entropy probability distribution.

Figure 3.17 shows the bit-rate versus the SNR for an average signal power of  $-12$  dBm0. Results are shown for the uniform probability distribution of constellation points as well as the maximum entropy distribution. As shown in this figure, the maximum entropy probability distribution can increase the bit rate by up to 1.8 kbits/sec. This can account for up to 1.5 dB performance improvement. In fact, it can be shown that maximum performance improvement due to optimal probability distribution for constellation points is  $\pi e/6$  or 1.53 dB [38] [39]. Note that at higher transmission bit-rates, the performance difference between the uniform probability distribution and the maximum entropy distribution becomes smaller. For PAM modulation on a PCM channel, the maximum constellation size is limited to 256 points. At a high bit-rate most of these points are in use. Therefore, there is no gain by using a maximum entropy distribution at high transmission bit-rates since there are no extra signal points available to be added to the constellation.

### 3.3.3 Channel capacity for non-uniform PAM modulation

In this section, we compute the channel capacity for the up-stream PCM voiceband channel. The channel capacity can be defined as an upper bound for information transmission rate which allows for transmission with an arbitrary small probability of error [37]. We compare three

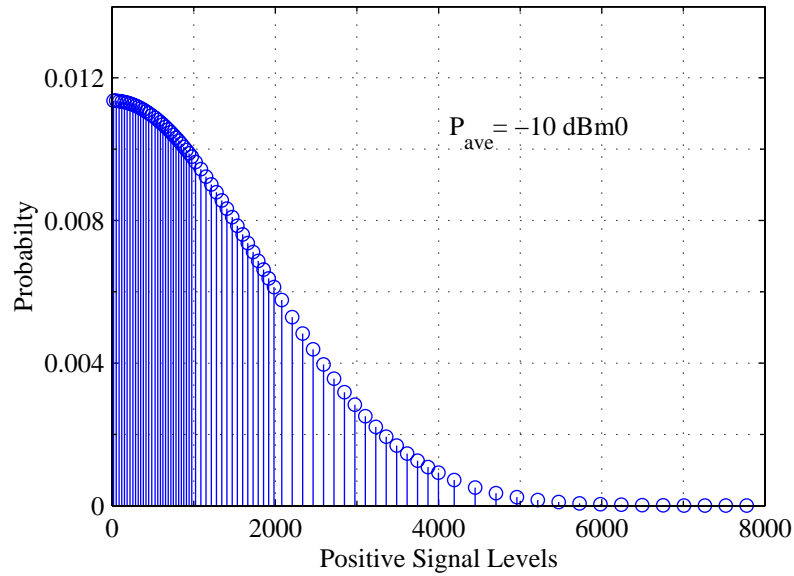


**Fig. 3.14** Probability distribution of the PAM symbols. The average signal power is limited to  $-10$  dBm0. Since the distribution is symmetrical, only positive constellation points are shown. Constellation points with low probability can be eliminated without any significant change in the average number of bits transmitted per symbol.

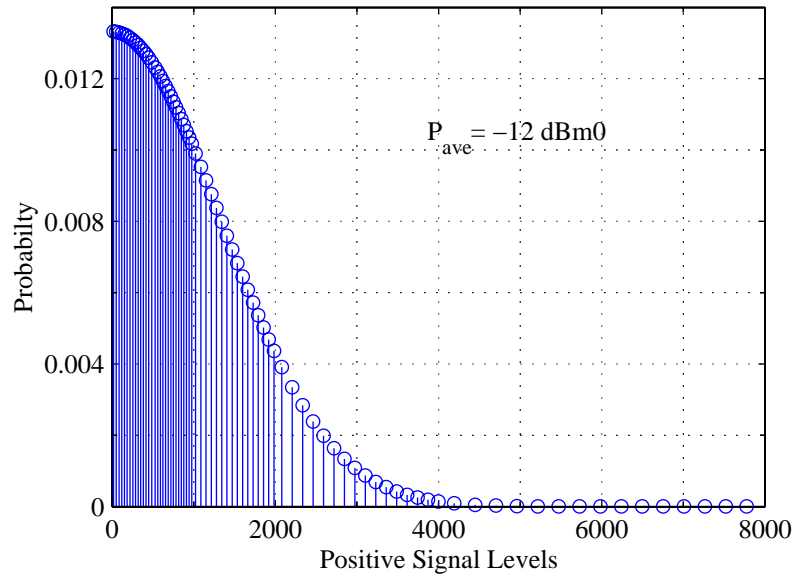


**Fig. 3.15** Probability distribution of the PAM symbols. The average signal power is  $-12$  dBm0. Compared to the probability distribution shown in Fig 3.14 for  $P_{ave} = -10$  dBm0, the probability distribution shown here is obtained by using a larger value of  $\lambda$  in Eq. 3.30.

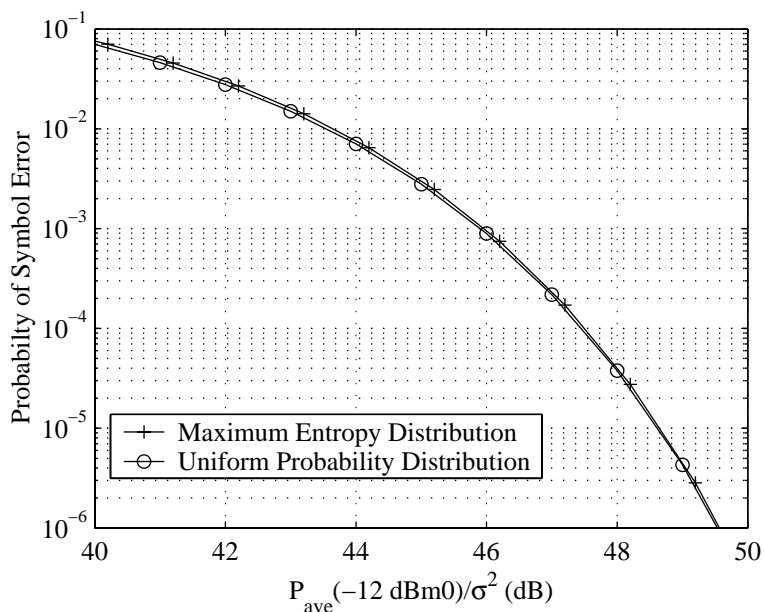


**Fig. 3.16** Probability of symbol error for PAM constellations with a maximum entropy distribution and uniform probability distribution. Note that the average signal power and the minimum distance between detector thresholds are the same for both constellations.

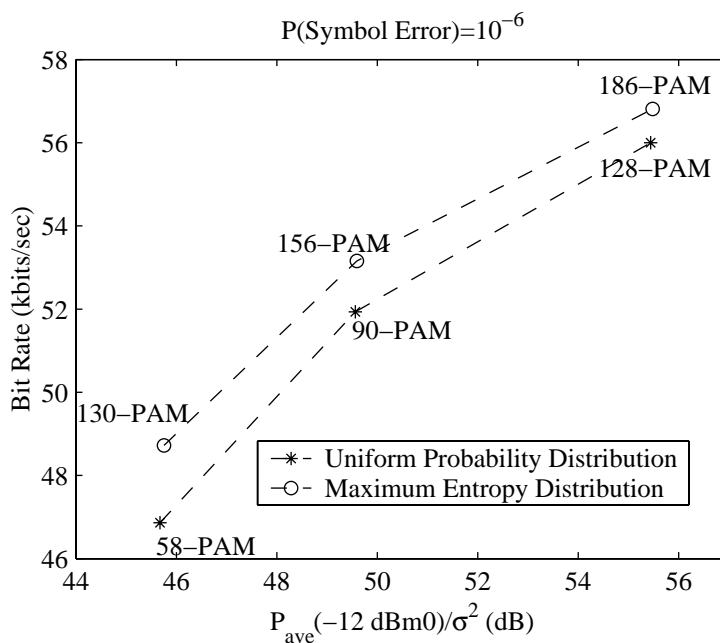


**Fig. 3.17** Transmitted bit rates of PAM modulation over a PAM channel. The average signal power is limited to -12 dBm0 and the probability of symbol error is set to  $10^{-6}$ . Results are shown for uniform probability distributions and maximum-entropy distribution. The symbol rate is 8000 symbols/sec.

different bounds for the information rate. Bounds are derived based on three different channel assumptions:

- 1 Continuous AWGN channel,
- 2 PAM signalling over AWGN channel,
- 3 PAM signalling over AWGN channel with a Hard-decision detector.

The capacity of a Gaussian channel with a constraint average input signal power of  $\mathcal{P}_{ave}$  and a noise power of  $\sigma^2$ . The capacity of this channel is computed as [37]:

$$C = \frac{1}{2} \log_2 \left( 1 + \frac{\mathcal{P}_{ave}}{\sigma^2} \right) \quad \text{bits per transmission.} \quad (3.31)$$

Since the transmission rate over the PCM channel is  $R_s = 8000$  symbols/sec, the capacity of the Gaussian channel is shown in:

$$R_{\max} = \frac{R_s}{2} \log_2 \left( 1 + \frac{\mathcal{P}_{ave}}{\sigma^2} \right) \quad \text{bits/sec.}$$

The output of a PCM up-stream channel at each sampling instant can be written as<sup>16</sup>:

$$r[n] = a[n] + w[n] \quad (3.32)$$

where  $a[n]$  is a PAM symbol and  $w[n]$  is assumed to be additive white Gaussian noise. The capacity can be expressed as the maximum difference between the entropy of the received signal and the conditional entropy of the received signal.

$$C = \max_{P(q_i)} \left\{ H(R) - H(R|A) \right\}. \quad (3.33)$$

In our discussion, the transmitted signal  $a[n]$  is chosen from a set of PAM constellation points. We also assume that the *a priori* probability associated with each constellation point is given (equally probable or maximum-entropy distribution). The capacity of a channel with M-ary PAM modulation can be written as [40, 41]:

$$\begin{aligned} C_{\text{PAM}} &= \sum_{i=1}^M P(q_i) \int_{-\infty}^{\infty} P(r|a = q_i) \log_2 \left( \frac{P(r|a = q_i)}{P(r)} \right) dr \\ &= \sum_{i=1}^M P(q_i) \int_{-\infty}^{\infty} P(r|a = q_i) \log_2 \left( \frac{P(r|a = q_i)}{\sum_{i=1}^M P(q_i) P(r|a = q_i)} \right) dr \end{aligned} \quad (3.34)$$

---

<sup>16</sup>Note that compared to Eq. (3.7), here we assume  $n_0 = 0$  and  $h[n_0] = 1$ .

For a given set of  $P(q_i)$ , we can simplify the capacity as:

$$C_{\text{PAM}} = -\frac{1}{2} \log_2(2\pi\sigma^2 e) + \sum_{i=1}^M \frac{P(q_i)}{\sqrt{2\pi\sigma^2}} \int_{-\infty}^{\infty} \exp\left(\frac{(r - q_i)^2}{-2\sigma^2}\right) \log_2\left(\sum_{j=1}^M \frac{P(q_j)}{\sqrt{2\pi\sigma^2}} \exp\left(\frac{(r - q_j)^2}{-2\sigma^2}\right)\right) dr \quad (3.35)$$

where  $\sigma$  is the standard deviation of the noise. Since the integral on the right-hand side of Eq. (3.35) does not have a closed form, the channel capacity is computed numerically. Following the method suggested in [40] to compute the above integral, we replace the integration by expectation over the Gaussian distributed noise variable and use Monte Carlo averaging method to evaluate the capacity.

The capacity bound computed above does not include the hard decision detector at the receiver. For the up-stream PCM channel, the receiver front-end structure is predetermined. This channel can be modeled as a channel with discrete input and discrete output. To compute the capacity of this channel, we can compute the transmission probabilities  $P(r = r_j | a = q_i)$  and replace the result in Eq. (3.34). Note that the integral is replaced by a sum.

Figure 3.18 shows the maximum bit rate for PAM modulations over PCM channels. Two cases of symbol probability distributions are considered: uniform and maximum entropy. For each PAM modulation with a given bit-rate<sup>17</sup>, the SNR at which the probability of symbol error reaches  $10^{-6}$  is also depicted. Figure 3.18 compares three upper bounds for the channel information rate.

As shown in Fig. 3.18, at a given bit-rate there is a SNR gap between the curve associated with the Gaussian channel capacity and the one associated with the channel capacity for a PAM modulation. This gap is smaller when we use maximum entropy probability distribution for the PAM constellation rather than uniform distribution.

We use the channel capacity of the PAM modulation as a baseline for our comparison. For an acceptable probability of symbol error (e.g.,  $10^{-6}$ ), there is a significant SNR difference between what we achieve by using symbol-by-symbol detection and the bound provided by the channel capacity for the PAM modulation. In order to reduce this difference, error correction coding techniques should be employed. Here, we do not discuss any particular error-correcting method for the PCM channels.

### 3.3.4 The Huffman algorithm for bit-to-symbol mapping

In the preceding section, we showed that the maximum entropy distribution for the PAM symbols improves the maximum achievable transmission rate. In this section, we describe a method which will almost achieve the maximum entropy distribution by appropriate mapping of input bits to

<sup>17</sup>The PAM constellation size along with the probability distribution of the constellation points determines the bit-rate.

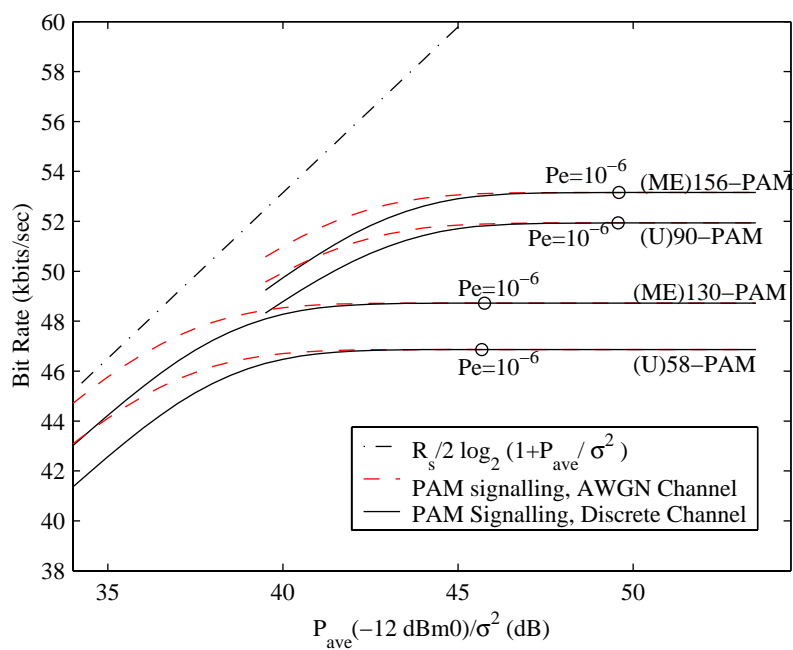


**Fig. 3.18** Channel capacity of a Gaussian channel with a continuous input signal and a PAM-modulated input signal is presented. We consider two types of probability distributions for the input PAM signal: uniform(U) and maximum entropy (ME). The average signal power is limited to  $-12 \text{ dBm0}$ . At each bit-rate, the SNR values corresponding to a probability symbol error of  $10^{-6}$  for an uncoded system are also depicted. The symbol rate is set to 8000 symbols/sec.

PAM constellation points. The input is assumed to be a random binary sequence of independent and identically distributed samples with equal probabilities of zeros and ones. The input sequence of bits is parsed into codewords and each codeword is mapped to a PAM symbol<sup>18</sup>. Since the probability of occurrence of a codeword of length  $l_i$  is  $2^{-l_i}$ , codewords with variable length can produce a non-uniform probability distribution for the constellation points.

Suppose  $C(q_i)$  is a codeword of length  $l_i$  that is mapped to a PAM constellation point  $q_i$ . We consider the following two sets of conditions as design requirements for the bit-to-symbol mapping. The first set of conditions are used to ensure that all combinations of bits are uniquely represented by PAM symbols:

1. Different symbols should be represented by different codewords:

$$q_i \neq q_j \quad \Rightarrow \quad C(q_i) \neq C(q_j)$$

2. A sequence of input bits should be uniquely mapped to a string of PAM symbols.
3. Each codeword  $C(q_i)$  should be instantaneously decodable to a symbol. In other words, no codeword should be a prefix of any other codeword.
4. The set of codewords should be complete, i.e., for any random sequence of input bits there should be one, and only one string of output symbols.

The second set of conditions ensure bit-to-symbol mapping does not change the signal mean and average power:

5. The resulting probability distribution of the PAM constellation should be symmetrical, i.e.  $P(q_i) = P(q_{-i})$ . We consider this condition to ensure the PAM signal has a zero mean.
6. The average signal power should satisfy the constraint given in (3.14).

Note that bit-to-symbol mapping can be viewed as a dual problem of encoding a discrete memoryless source of information. In a source coding problem, we are interested in an efficient (e.g. minimum number of bits, or minimum amount of redundancy) representation of a sequence of symbols as a binary sequence. In bit-to-symbol mapping, we start from a sequence of bits with no redundancy with a view to generate a set of symbols with the desired probability distributions. Bit-to-symbol mapping is in fact equivalent to decoding an encoded source. From this point of view, the design of a bit-to-symbol mapper is similar to the design of source coding for a

---

<sup>18</sup>In a more general case, a frame of input bits is mapped to a set of PAM symbols. In our discussion in this section, we assume that the bit-to-symbol mapping is performed in a symbol-by-symbol basis.

memoryless discrete source with a given probability distribution. In fact, by default, a complete prefix code [42] satisfies the first four conditions given above.

As suggested in [39], we use the Huffman algorithm [37] to generate a complete set of codewords representing constellation points. Since a Huffman code [37, p. 92] is a prefix code, it satisfies the first three requirements. From Kraft inequality [42], a set of codewords is complete if the codeword lengths  $l_i$  satisfy the following condition:

$$\sum_{i=1}^M 2^{-l_i} = 1 \quad (3.36)$$

where  $M$  is the number of codewords. It is easy to show that the Huffman algorithm generates a complete set of codewords if all the initial probabilities used in the algorithm correspond to valid symbols.

We apply the Huffman algorithm only to positive symbols to generate a symmetrical probability distribution. We will add an extra bit to each codeword to represent the sign of each symbol. Adding a sign bit to each codeword is the same as duplicating the codewords that are generated for positive symbols and adding one extra stage of bit assignment to the Huffman algorithm. The result is still a complete prefix code.

The probability of occurrence of any codeword is a negative power of two. This probability does not always match the desired maximum entropy probability distribution. The mismatch between the actual probability assigned to a symbol and the desired probability can cause an increase in the average signal power. In order to satisfy the average signal power constraint, the parameter  $\lambda$  in (3.30) should be re-adjusted.

The procedure for bit-to-symbol mapping can be summarized as follows:

1. Compute the probability distribution of PAM symbols using Maxwell-Boltzmann distributions. Compute  $\lambda$  so that the average power constraint is satisfied.
2. Use the Huffman algorithm to generate a set of codewords for PAM constellations.
3. Compute the average signal power based on the actual probability distribution of constellation points. If the power constraint is not satisfied, go to step 1 and adjust the parameter  $\lambda$  to obtain a lower average signal power.

Figure 3.19 compares the achievable bit-rates using maximum entropy, the Huffman algorithm and uniform probability distributions. As shown in this figure, the difference between bit-rates achieved by the maximum entropy distribution and that of Huffman algorithm is not significant. Table 3.1 shows codewords designed for a set of PAM symbols using the above procedure. Signal

levels with a very low probability of occurrence are discarded from the constellation. The final constellation includes 98 points. The codewords corresponding to the positive PAM symbols are shown in this table. By altering the most significant bit of each codeword presented in Table 3.1, we can specify a negative constellation point.

**Table 3.1** Huffman algorithm for bit-to-signal mapping. The bit sequence associated with each constellation is presented. Note that for negative constellation points only the sign bits should be altered. The constellation size is limited to 98 since the constellation points with a very low probability (and a high energy) are not included.

$i$	$q_i$	$P(q_i)$	$\hat{P}(q_i)$	$C(q_i)$	$i$	$q_i$	$P(q_i)$	$\hat{P}(q_i)$	$C(q_i)$
1	26	0.021654	$2^{-5}$	00101	25	1471	0.009422	$2^{-7}$	0100101
2	77	0.021610	$2^{-5}$	00100	26	1535	0.008750	$2^{-7}$	0100001
3	127	0.021526	$2^{-5}$	00011	27	1599	0.008100	$2^{-7}$	0100000
4	175	0.021406	$2^{-5}$	00010	28	1663	0.007475	$2^{-7}$	0011010
5	227	0.021235	$2^{-5}$	00001	29	1727	0.006877	$2^{-8}$	01101011
6	279	0.021021	$2^{-5}$	00000	30	1791	0.006306	$2^{-8}$	01101010
7	327	0.020787	$2^{-6}$	011110	31	1855	0.005765	$2^{-8}$	01011010
8	375	0.020519	$2^{-6}$	011101	32	1919	0.005253	$2^{-8}$	01001001
9	423	0.020219	$2^{-6}$	011100	33	1983	0.004772	$2^{-8}$	00110111
10	479	0.019830	$2^{-6}$	011011	34	2079	0.004107	$2^{-8}$	00110110
11	543	0.019337	$2^{-6}$	011001	35	2207	0.003326	$2^{-9}$	010110110
12	607	0.018798	$2^{-6}$	011000	36	2335	0.002659	$2^{-9}$	010010000
13	671	0.018215	$2^{-6}$	010111	37	2463	0.002100	$2^{-10}$	0101101110
14	735	0.017596	$2^{-6}$	010101	38	2591	0.001637	$2^{-10}$	0100100011
15	799	0.016943	$2^{-6}$	010100	39	2719	0.001261	$2^{-11}$	01011011111
16	863	0.016264	$2^{-6}$	010011	40	2847	0.000958	$2^{-11}$	01001000101
17	927	0.015563	$2^{-6}$	010001	41	2975	0.000720	$2^{-12}$	010110111101
18	1007	0.014664	$2^{-6}$	001111	42	3103	0.000533	$2^{-12}$	010010001001
19	1087	0.013749	$2^{-6}$	001110	43	3231	0.000391	$2^{-13}$	0101101111001
20	1151	0.013012	$2^{-6}$	001100	44	3359	0.000282	$2^{-13}$	0101101111000
21	1215	0.012275	$2^{-7}$	0111111	45	3487	0.000202	$2^{-13}$	0100100010000
22	1279	0.011544	$2^{-7}$	0111110	46	3615	0.000142	$2^{-14}$	01001000100010
23	1343	0.010823	$2^{-7}$	0110100	47	3743	0.000099	$2^{-15}$	010010001000110
24	1407	0.010114	$2^{-7}$	0101100	48	3871	0.000068	$2^{-16}$	0100100010001111
					49	3999	0.000046	$2^{-16}$	0100100010001110

### 3.4 Chapter Summary

- The choice of modulation scheme for the up-stream PCM channel is baseband PAM modulation. This choice is based on the assumption that the transmitter modem can be synchronized to the network clock at the central office using the signal received in the downstream

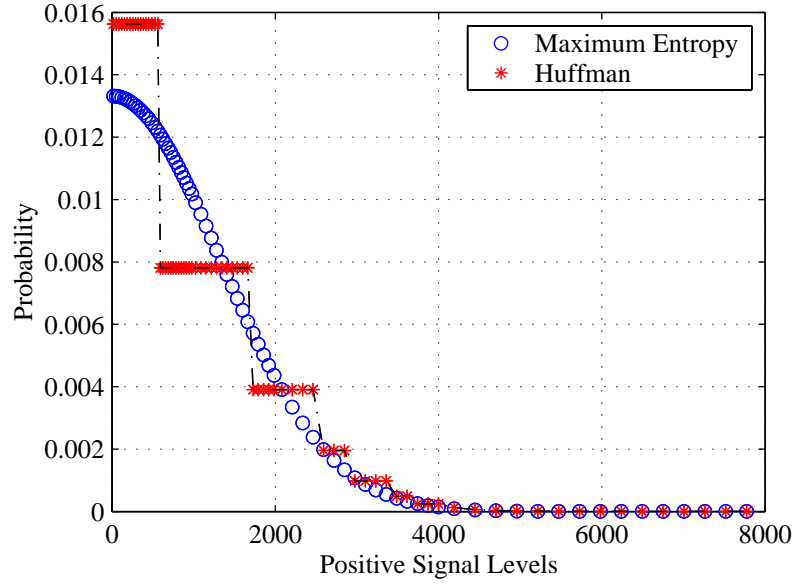


Fig. 3.19 Probability distributions of a constellation point with Huffman bit assignments compared to the maximum entropy distributions.

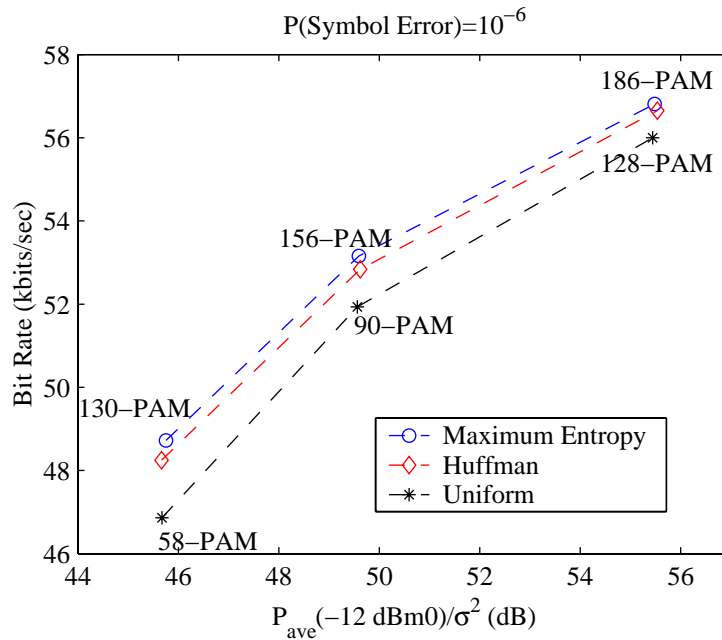


Fig. 3.20 Transmitted bit-rates as a function of SNR for three different probability distributions: maximum entropy, the Huffman algorithm and uniform distributions.

direction.

- The PCM encoder at the central office acts as the front-end of the receiver for the PCM upstream channel. The ADC circuit can be viewed as a slicer or as a detector for the PAM signal.
- The detector thresholds are selected as a subset of the ADC decision boundaries. Assuming that the distortion caused by the channel ISI is not severe, the optimal signal constellation points are midway between the adjacent detector thresholds.
- For a PAM modulation over a PCM channel with a non-linear compander, the spacing between the constellation points is non-uniform. For the same signal and noise power, the non-uniform PAM modulation shows some performance degradation compared to a uniform PAM modulation.
- In the up-stream PCM channel, the PAM constellation points are not scalable. That is, increasing the signal power does not necessarily increase the minimum distance between the detector thresholds. As a result, for a given noise power, the performance of the PAM modulation might remain the same even if we increase the signal power.
- In order to increase the constellation size by a factor of two and maintain the same performance and average transmitted power, the signal-to-noise ratio should be increased by 6 dB.
- Non-uniform probability distribution for constellation points can reduce the energy cost of the outer points. Non-uniform probability distribution can increase the bit-rate by 1.5 kbits/sec, at the same signal and noise power compared to that of a PAM modulation with a uniform probability distribution.

## Chapter 4

# Transmitter Design for the Up-stream PCM Channel

In Chapter 3, we discussed a PAM modulation design for the up-stream PCM channel. As a model for channel impairment, an additive random component was used to represent the combined effect of noise and residual ISI at the receiver. Due to the lack of control on the receiver front-end design in the up-stream PCM channel, the channel impairments can only be compensated for at the transmitter. Although the transmitter has no impact on the additive noise introduced by the channel, a proper transmitter design can eliminate or reduce the effect of ISI introduced by the channel memory.

Since the characteristics of a subscriber loop and a receiver filter do not change rapidly, we consider a linear time-invariant model for the PCM channel. We also assume that an equivalent filter model for the overall channel and receiver filters is estimated at the receiver and is fed back to the transmitter<sup>1</sup>.

A straightforward solution for channel compensation is a linear filter structure implemented at the transmitter. Such a transmitter filter can be specified based on different optimization criteria. With a constraint on transmitted power, a transmitting filter may not provide adequate ISI reduction. In particular, for channels with ISI, there is a trade-off between the average transmitted power and ISI compensation. We introduce spectrum shaping techniques along with the transmitter filter to control the transmitted power.

Section 4.1 describes a framework for designing optimal transmitter filters. Using this framework, we consider three structures for the transmitter design. In Section 4.2, we present per-

---

<sup>0</sup>This chapter has been reported in part in [43].

<sup>1</sup>Prior to data transmission, the channel can be estimated by using a training sequence known to the receiver. The down-stream PCM channel is used to return the channel estimate to the transmitter.

formance results obtained by applying an optimal filter design to the up-stream PCM channels. Section 4.3 introduces spectrum shaping and its impact on the transmitted power. In Section 4.4, we describe precoding techniques which add redundancy to transmitted symbols. We generalize the idea of Tomlinson-Harashima precoding to accommodate the requirements for pre-filtering of the PCM channel. A summary of pre-filtering methods for the PCM channels is presented in Section 4.5.

#### 4.1 Optimal transmitter filter design

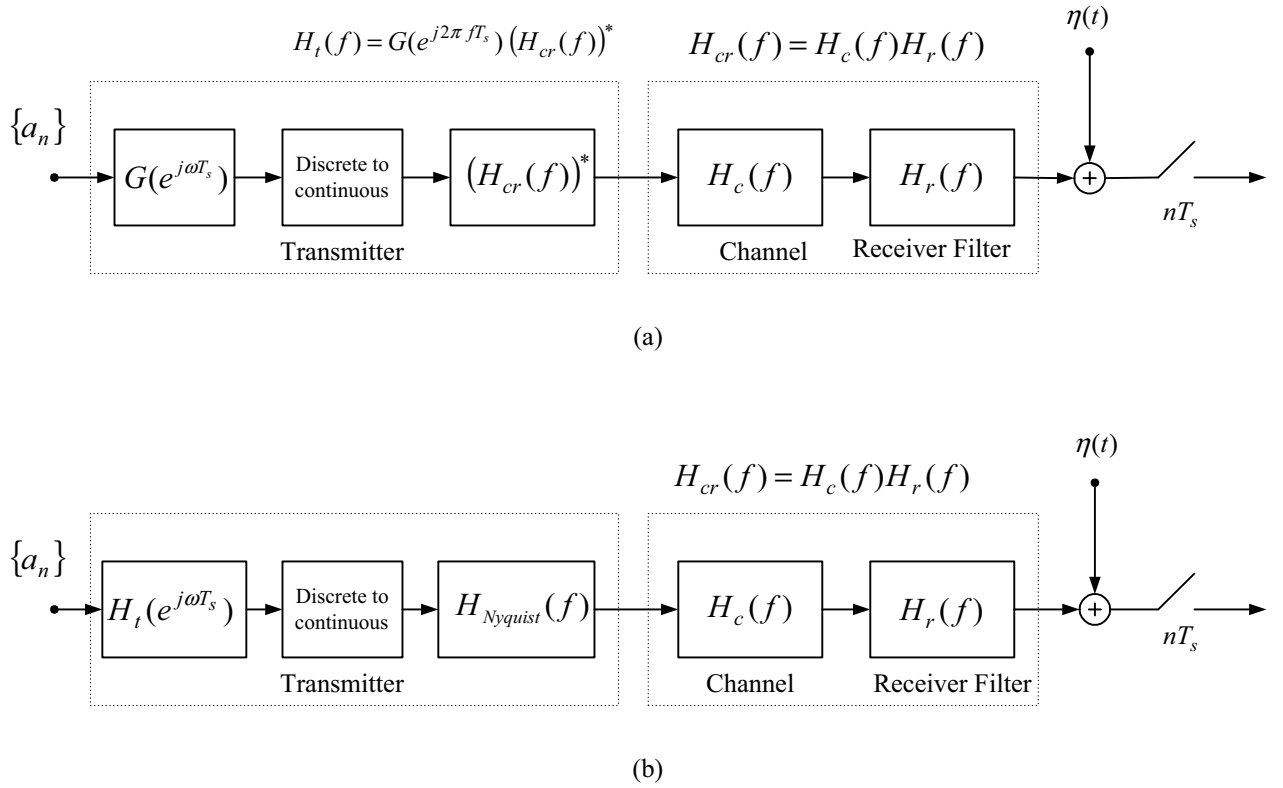
The design of an optimum transmitting filter for a fixed receiving filter and a given channel filter has been studied in [30, 32, 44, 45]. There are several optimization criteria, such as minimum probability of error, minimum mean-square error and minimum peak distortion error, that can be used for the optimal transmitter filter design [30, p. 113]. The design of an optimum transmitting filter is subject to a transmit power constraint in order to avoid a solution with an unbounded average power.

Although different optimization criteria result in different transmitter filters, these filters share a common structure. For any reasonable optimization criterion, an optimum linear transmitting filter subject to an average transmitted power constraint has the following structure:

$$\begin{aligned} H_t(f) &= G(f)(H_c(f)H_r(f))^* \\ &= G(f)H_{cr}^*(f) \end{aligned} \tag{4.1}$$

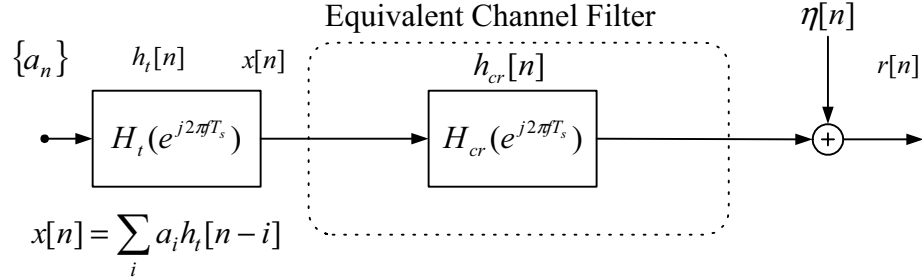
where  $G(f)$  is a periodic transfer function,  $G(f) = G(f + 1/T_s)$ , that can be implemented as a discrete-time filter with an underlying sampling frequency of  $1/T_s$ . The transfer function  $H_{cr}^*(f)$  represents a filter matched to the cascade of the channel filter and the receiver filter. We provide a proof for the above statement in Appendix A, similar to that given in [46] for the receiver filter.

Figure 4.1(a) presents the arrangement of the transmitter, the channel and the receiver filter. The matched filter  $H_{cr}^*(f)$  is a continuous-time filter. Implementing a continuous-time (analog) matched filter in a transmitter modem is impractical since the characteristics of channels vary from one subscriber line to another. Since the matched filter  $H_{cr}^*(f)$  has a limited bandwidth ( $W < 4000$  Hz), this continuous-time filter can be approximated by a symbol-synchronous (a sampling frequency equal to  $1/T_s$ ) discrete-time filter. In this case, the only continuous-time filter required at the transmitter is an interpolating (reconstruction) filter following the digital-to-analog converter. We defer further discussion regarding the choice of the interpolating filter to Chapter 6. Here, we assume the frequency response of the interpolating filter is accounted for as part of the channel filter.



**Fig. 4.1** A general structure of an optimal transmitter filter is shown in (a) where the transmit filter consists of an continuous-time filter matched to the channel and receiver filter, and a discrete-time filter  $G(e^{j\omega T_s})$ . Since the equivalent channel-receiver filter has a band-limited spectrum ( $< 1/2T_s$ ), a sub-optimal structure for the transmitter filter consists of a discrete-time filter  $H_t(e^{j\omega T_s})$ , and a fixed pulse shaping filter that replaces the analog matched filter, as shown in (b). The discrete-time transmit filter can be determined based on different optimization criteria.

As shown in Fig. 4.1(b), the input and output of the up-stream PCM channel are discrete-time signals while the channel itself is modeled as a continuous-time filter. When we design the transmitter filter, it is convenient to work with a discrete-time model for the entire system. As shown in [47], for a PAM modulation over an AWGN channel, there exists an equivalent discrete-time model for the channel filter. Figure 4.2 shows a discrete-time model of the transmitter, the channel and the receiver. Note that the additive noise sample  $\eta[n]$  represent the contribution of thermal noise, echo and cross-talks. Although different components of the noise are added to the transmitted signal at different points in the channel, due to linear assumption about the channel filters, we can add the noise to the channel output. In general, the noise samples can be correlated.



**Fig. 4.2** A discrete-time model of the up-stream PCM channel with a discrete-time transmitter filter.

The equivalent discrete-time model of the channel-receiver filter can be expressed as  $H_{cr}(e^{j2\pi f T_s})$ :

$$H_{cr}(e^{j2\pi f T_s}) = \frac{1}{T_s} \sum_k H_c(f + \frac{k}{T_s}) H_r(f + \frac{k}{T_s}) \quad (4.2)$$

We discuss the optimum design of the filter  $H_t(e^{j\omega T_s})$  based on different criteria. The probability of error is the most meaningful criterion for the optimal transmitter design. However, in many cases, there is no general solution for such an optimization problem. In our discussion, we consider two other criteria: one being the peak distortion criterion (or zero ISI criterion) and the other being the Mean Square Error (MSE) criterion.

#### 4.1.1 Peak distortion criterion

The peak distortion criterion is defined as the worst-case ISI at the sampling instants. As shown in Fig. 4.2, samples at the receiver can be written as:

$$r[n] = a_{(n)} h[0] + \sum_{\substack{i=-\infty \\ i \neq 0}}^{\infty} a_i h[n-i] + \eta[n] \quad (4.3)$$

where  $h[n]$  is the overall impulse response of the transmitter, channel and receiving filter. The peak value of the ISI is the sum of the absolute values of the ISI terms:

$$\mathcal{D}(h_t) = \sum_{\substack{n=-\infty \\ n \neq 0}}^{\infty} |h[n]| = \sum_n \left| \sum_k h_t[k] h_{cr}[n-k] \right| \quad (4.4)$$

The smallest value of peak distortion is obtained if all the overall impulse response coefficients, except for the central one, are zero. This condition implies that the ISI can be completely avoided

if the transmitting filter is a stable inverse of the overall channel-receiver filter:

$$H_t(e^{j\omega T_s}) = \frac{1}{H_{cr}(e^{j\omega T_s})} \quad (4.5)$$

The transmitter filter has a straightforward expression in terms of the channel filter. However, if the channel filter contains spectral nulls, a signal with bounded power at the input of the inverse filter can create an output signal with unbounded power (i.e., the inverse filter is not BIBO stable [48, p. 209]).

#### 4.1.2 Mean-Square Error (MSE) criterion

A commonly used criterion for an optimal linear filter design is mean-square error. According to this criterion, filter coefficients are determined so that the mean-square value of the error at sampling instants is minimized. In general, the mean-square value of error has two components, one is caused by additive noise and the other is caused by the ISI. Note that the optimal transmitter filter design can only minimize the error caused by the ISI. As a result, in our computation of optimal transmitter filter, the contribution of the additive noise in MSE is not included. The error caused by additive noise can always be added to the computed MSE. In the absence of noise, we define:

$$\min_{h_t}(\text{MSE}) = \min_{h_t}(\mathcal{E}\{(r[k] - a_k)^2\}) \quad (4.6)$$

where  $\mathcal{E}\{x\}$  denotes the mean of a random variable  $x$ . The impulse response of the transmitting filter at sample  $n$  is denoted as  $h_t[n]$ . Unless otherwise stated, we assume that the transmitting filter has an infinite length impulse response.

We assume that the data symbols  $a_n$  form a wide-sense stationary random sequence [49], taking values from a set of PAM symbols. We denote the autocorrelation function of the data symbol sequence as:

$$\phi_a[k] = \mathcal{E}\{a_i a_{i+k}\} \quad (4.7)$$

Consequently, the power spectrum density (PSD) of the input sequence is defined as:

$$\Phi_a(e^{j\omega T_s}) = \sum_{k=-\infty}^{\infty} \phi_a[k] e^{-j\omega T_s k} \quad (4.8)$$

We consider a constraint on the average transmitted power as:

$$\mathcal{E}\{|x[k]|^2\} \leq \mathcal{P}_t \quad (4.9)$$

where  $\mathcal{P}_t$  is a constant and  $x[\cdot]$  is the discrete-time sequence at the output of the transmitting filter (see Fig. 4.2). Since the input sequence to the transmitter filter is wide-sense stationary, the output sequence  $x[n]$  is also wide-sense stationary [49, p. 193]. The PSD of the signal at the output of the transmitter filter is:

$$\Phi_x(e^{j\omega T_s}) = |H_t(e^{j\omega T_s})|^2 \Phi_a(e^{j\omega T_s}) \quad (4.10)$$

The average power constraint is expressed in terms of  $H_t(e^{j\omega T_s})$  and  $\Phi_a(e^{j\omega T_s})$  as follows:

$$\frac{T_s}{2\pi} \int_{-\pi/T_s}^{\pi/T_s} \Phi_a(e^{j\omega T_s}) |H_t(e^{j\omega T_s})|^2 d\omega \leq \mathcal{P}_t \quad (4.11)$$

In Appendix B, we derive the optimum linear transmitter filter that provides the Minimum Mean-Square Error (MMSE) solution with an average transmitter power constraint. The frequency response of the optimal filter is:

$$H_t(e^{j\omega T_s}) = \frac{H_{cr}(e^{-j\omega T_s})}{|H_{cr}(e^{j\omega T_s})|^2 + \lambda} \quad (4.12)$$

where  $\lambda$  is a non-negative parameter that is determined based on the power constraint. From Eq. (4.11) and Eq. (4.12), the average power constraint is

$$\frac{T_s}{2\pi} \int_{-\pi/T_s}^{\pi/T_s} \frac{|H_{cr}(e^{j\omega T_s})|^2}{(|H_{cr}(e^{j\omega T_s})|^2 + \lambda)^2} \Phi_a(e^{j\omega T_s}) d\omega \leq \mathcal{P}_t \quad (4.13)$$

The left hand-side of Eq. (4.13) is a monotonically decreasing function of  $\lambda$ . We are interested in the smallest non-negative value of  $\lambda$  that satisfies this condition. If  $\lambda = 0$  does not satisfy the power constraint, the minimum value of  $\lambda$  is determined by solving Eq. (4.13) as an equality.

As shown in Appendix B, the minimum mean-square value of error is computed as:

$$\text{MMSE} = \frac{\lambda^2 T_s}{2\pi} \int_{-\pi/T_s}^{\pi/T_s} \frac{\Phi_a(e^{j\omega T_s})}{(|H_{cr}(e^{j\omega T_s})|^2 + \lambda)^2} d\omega \quad (4.14)$$

Equation (4.12) corresponds to the transmitter filter with an infinite length impulse response. This solution establishes the ultimate ISI reduction that can be expected from an optimal linear transmitter filter with a given power constraint.

The actual implementation of the transmitter filter can be a Finite Impulse Response (FIR) filter. An FIR filter can be formed as the truncation of the IIR filter impulse response. Alternatively, the MMSE problem can be defined to obtain directly the optimal solution as an FIR filter.

In this case, the filter coefficients are the solution of the following set of equations:

$$\mathbf{C}_{opt} = \mathbf{\Gamma}^{-1}\xi \quad (4.15)$$

where  $\mathbf{\Gamma}$  is a square matrix and  $\xi$  is a column vector. The derivation of Eq. (4.15), and the expression of  $\mathbf{\Gamma}$  and  $\xi$  are presented in Appendix B.

The MSE criterion provides a general framework for several transmitter structures. In our discussion, we investigate three different scenarios for the transmitter design.

### (1) Optimal filtering with a flat data spectrum

For a random sequence of independent and identically distributed (i.i.d.) transmitted symbols, the power spectral density  $\Phi_a(e^{j\omega T_s}) = \sigma_a^2$  is constant. In this case, Eq. (4.13) is simplified to:

$$\frac{T_s \sigma_a^2}{2\pi} \int_{-\pi/T_s}^{\pi/T_s} \frac{|H_{cr}(e^{j\omega T_s})|^2}{(|H_{cr}(e^{j\omega T_s})|^2 + \lambda)^2} d\omega \leq \mathcal{P}_t \quad (4.16)$$

For a given equivalent discrete-time filter  $H_{cr}(e^{j\omega T_s})$ , we can only reduce the MMSE by increasing the average transmitted power  $\mathcal{P}_t$ . Examples of transmitter filter design for the up-stream PCM channel are presented in Section 4.2.

### (2) Spectrum shaping followed by the linear filtering

The MMSE value in Eq. (4.14) is a function of the PSD of the filter input. We can shape the PSD of the input symbols to control the average transmitted power. In Eq. (4.11), spectrum shaping can reduce the value of parameter  $\lambda$  while satisfying the average power constraint.

The data symbols  $\{a_n\}$  take values from a PAM symbol alphabet. We introduce correlations among the symbols in order to create a desired power spectrum density at the input of the transmitting filter while maintaining the underlying PAM signal structure. Assuming the data symbols  $\{a_n\}$  are i.i.d. random variables, we map the data symbols to a new sequence  $\{s_n\}$  which contains a form of redundancy in signal levels or added symbols. The new sequence  $\{s_n\}$  has a power spectrum density close to a desired PSD, say  $\Phi_d(e^{j\omega T_s})$ . We will discuss different methods of creating such correlations in Section 4.3.

### (3) Precoding: A combined spectrum shaping and filtering

The spectrum shaping and optimal filtering can be combined into one operation, known as *precoding*. Tomlinson-Harashima (TH-) precoders [50, 51] are examples of channel compensation performed at the transmitter. A TH-precoder creates an inverse channel filter whose output is

limited to a finite range. Each symbol at the input of a TH-precoder is represented by more than one signal level. Among all signal levels representing a symbol, the precoder chooses a signal level that provides an output in a preset range. A further discussion regarding TH-precoders and their limitations for use in an up-stream PCM channel appears in Section 4.4.

## 4.2 Optimal transmitting filter design for the up-stream PCM channels

We can apply the optimal filter design to the PCM up-stream channels to compensate for the filtering effect of the subscriber line and the anti-aliasing filter in the PCM line card. Examples of typical equivalent channel-receiver filter are given. In order to evaluate system performance, we compute the MSE at the sampling instants (theoretically and also by simulation). We also use the symbol error rate of the PAM modulation over the up-stream channel as a measure of performance. The characteristics of telephone channels vary from line to line. Two examples of PCM channel filters are considered. In both cases, the PCM anti-aliasing filters satisfy Recommendation G.712 [25].

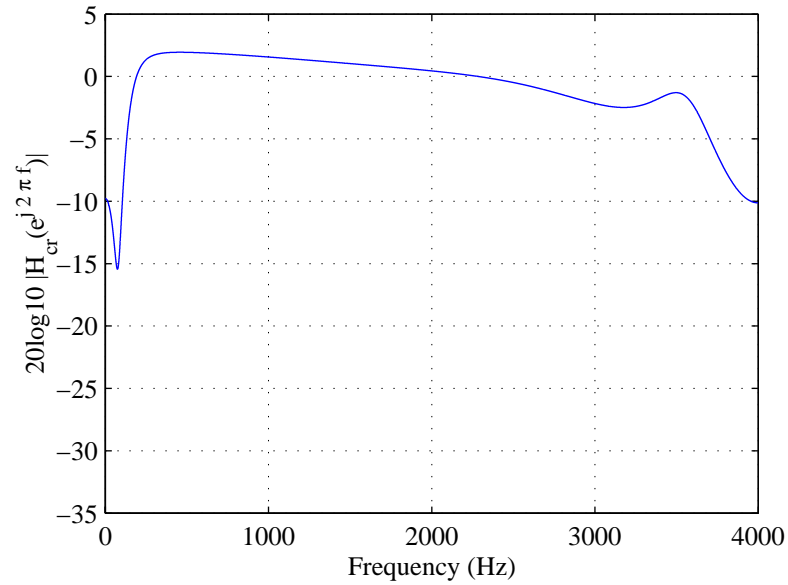
### Example 1

Figure 4.3 shows the magnitude response of an equivalent discrete-time receiver-channel filter in the up-stream PCM channel<sup>2</sup>. The frequency response of the analog anti-aliasing filter corresponding to this channel is shown in Fig 2.7. The receiver filter consists of a 5<sup>th</sup>-order elliptic lowpass filter cascaded with a bi-quad highpass filter. Due to aliasing (caused by sampling), the stopband attenuation of the equivalent discrete-time filter is significantly lower than that of the analog filter. Figure 4.4 shows the impulse response of the equivalent discrete-time filter and Fig. 4.5 shows the pole-zero locations of the equivalent channel filter transfer function. The equivalent channel filter is non-minimum phase and contains nulls near the zero frequency.

We use a linear transmitter filter structure to compensate for the channel filter. The performance of the transmitter filter design is evaluated based on the signal-to-interference ratio at the receiver, the average transmitted power and the probability of symbol error in the presence of (noise and) ISI. Note that we define the signal-to-interference ratio (SIR) as the ratio of the signal power to the MSE caused by the ISI at the receiver.

As an example, consider a PAM modulated signal with an average power of  $\sigma_a^2 = -12$  dBm<sub>0</sub> at the input to the transmitter filter. The signal power at the output of the transmitter filter is determined by the power gain of the transmitter filter. Figure 4.6 shows the variation of the

<sup>2</sup>In this example, we assume that the linear distortion in the up-stream channel is caused mainly by the receiver filter. Signal attenuation due to the subscriber line or the hybrid circuit will further increase the required transmitter power.



**Fig. 4.3** The magnitude response of the channel equivalent filter as discussed in Example 1.

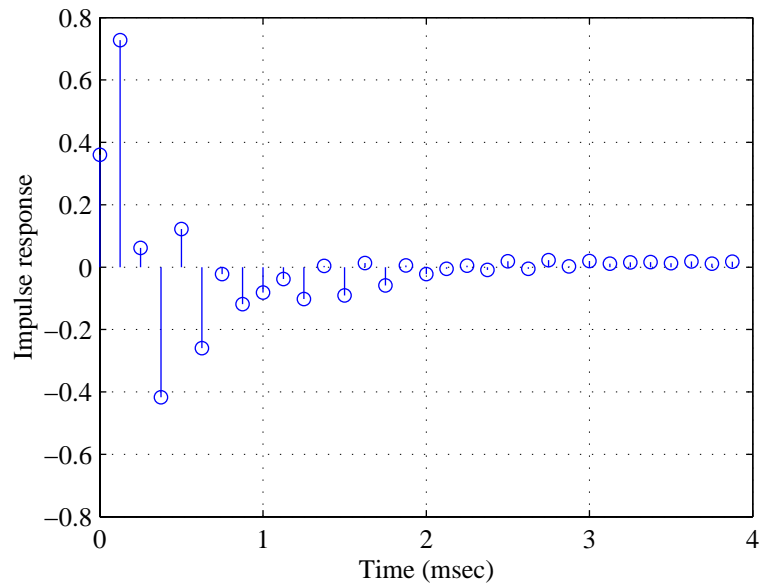


**Fig. 4.4** The impulse response of the channel discussed in Example 1.

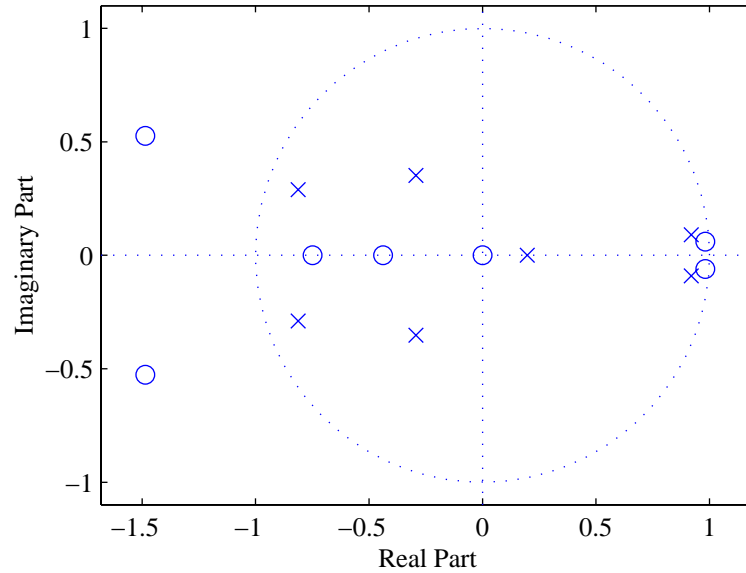


Fig. 4.5 Pole-Zero locations of a channel-receiver filter transfer function of Fig. 4.3.

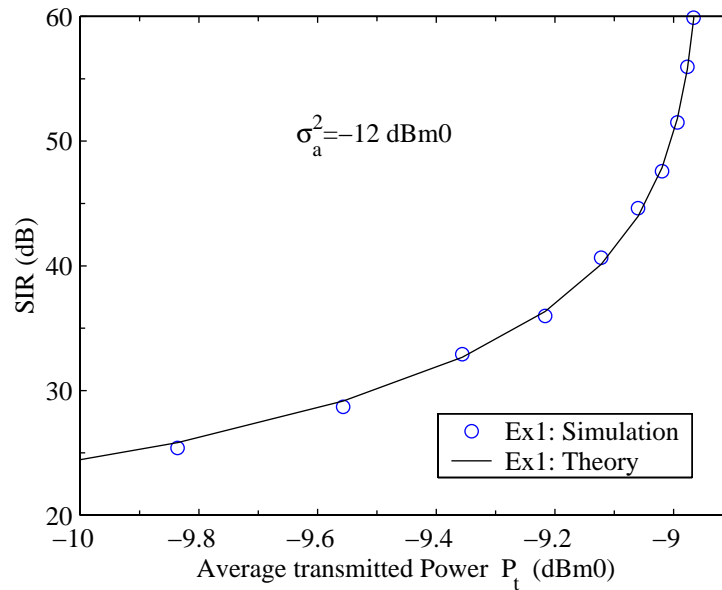


Fig. 4.6 Signal-to-interference ratio as a function of the average transmitted power for the PCM channel described in Example 1. The PAM signal power at the input of the transmitting filter is  $\sigma_a^2 = -12\text{dBm0}$ .

signal-to-interference ratio as a function of the average transmitted power  $\mathcal{P}_t$ . The SIR at the receiver increases by increasing the allowed transmitter power. The result shown in this figure holds for different PAM constellation sizes, assuming that the average power of the PAM signal is maintained at  $-12$  dBm0.

If we assume that ISI is the dominant cause of distortion at the receiver, the probability of symbol error can be characterized as a function of SIR. Figure 4.7 shows the probability of symbol error as a function of SIR for different PAM constellation sizes. The PAM constellations are designed for the up-stream PCM channels. The design procedure for the PAM constellation was discussed in Chapter 3.

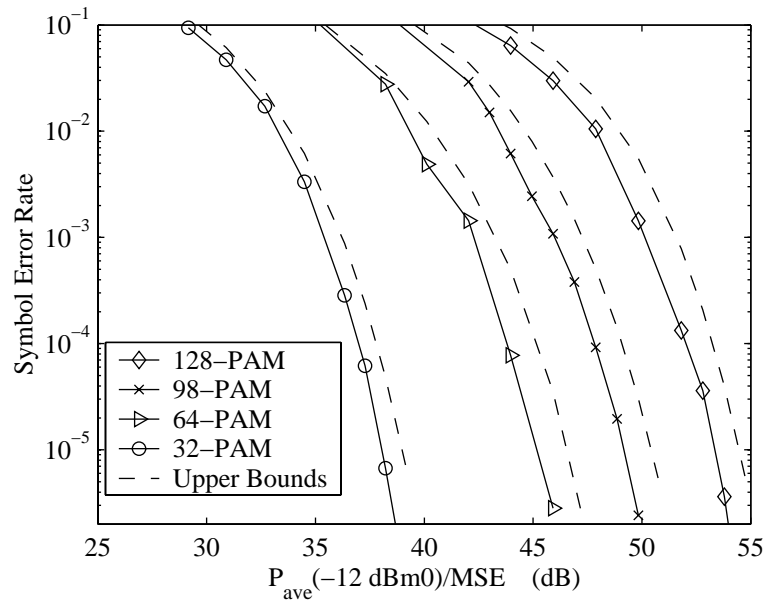
We can determine an upper bound for the probability of symbol error based on a Gaussian approximation of the residual ISI distribution.

Figure 4.7 compares the upper bound with the simulation results. The ISI has a limited peak and its tail distribution is far from being Gaussian. For the larger values of SIR (i.e., a smaller values of MSE), the probability of symbol error is roughly determined by the tail of the ISI distribution. Hence, the Gaussian assumption of the ISI distribution becomes less accurate. While the Gaussian approximation holds at low signal-to-interference levels, it provides a loose upper bound at higher values of SIR. There are methods to compute tighter bounds for the probability of symbol error [41, 52, 53, 54]. However, we can use direct simulation to compute the symbol error probabilities.

The ISI may not be the only source of distortion over the PCM channels. We consider the combination of residual ISI and an additive Gaussian noise in the up-stream channel for a given PAM modulation. As an example, Fig. 4.8 shows the probability of symbol error as a function of the signal-to-noise ratio for a 98-PAM modulation with an average power of  $-12$  dBm0 at the input of the transmitter. This figure shows that a small change in the average transmitted power (less than 0.1 dBm0) can significantly change the probability of symbol error, especially at a high signal-to-noise ratio. This observation is in line with what is shown in Fig. 4.6 where the change of average transmitter power from  $-9.05$  dBm0 to  $-8.95$  dBm0 increases the signal-to-interference ratio by more than 20 dB.

### Example 2

We consider a receiver filter that consists of a  $7^{th}$ -order elliptic lowpass filter cascaded with a bi-quad highpass filter. Compared to the receiver filter in Example 1, the filter in this example has a larger attenuation in the stopband. As a result, the equivalent discrete filter has greater attenuation at DC and at  $1/(2T_s) = 4000$  Hz. Figure 4.9 shows the magnitude frequency response and the impulse response of the discrete-time filter. The pole-zero plot of the filter is shown in



**Fig. 4.7** The probability of symbol error is shown as a function of SIR for several PAM signals for the channel filter discussed in Example 1. Assuming that the residual ISI as a Gaussian random variable, we can approximate the probability of symbol error.

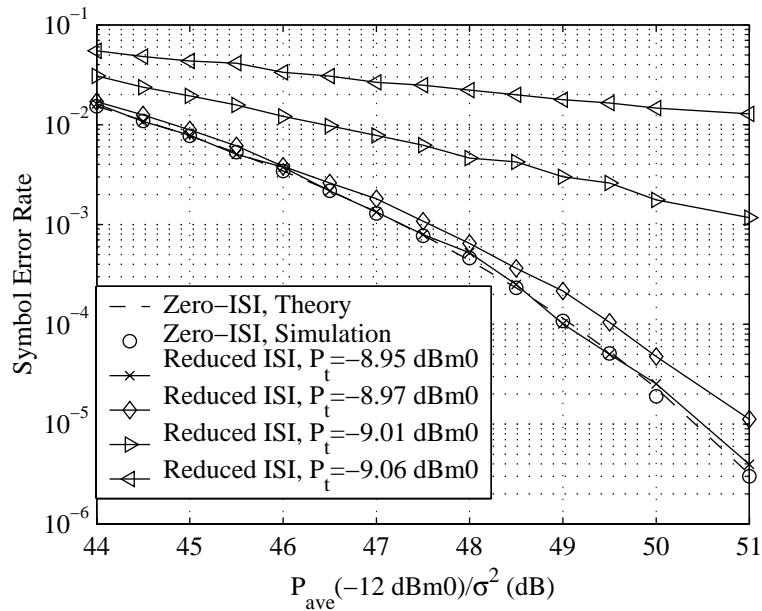


**Fig. 4.8** Probability of symbol error is shown as a function of SNR for a 98-PAM signal with an average power of  $-12 \text{ dBm0}$ . The performance of different transmitter filters is compared to the ideal channel filter with Gaussian additive noise.

Fig. 4.10.

Figure 4.11 shows the signal-to-interference ratio as a function of transmitted power. The input of the transmitter filter is a PAM signal with an average power of  $-12$  dBm0. Due to spectral nulls in the frequency response of the channel-receiver filter, the power gain of the transmitter filter is impractically large. The probability of symbol error as a function of the signal-to-interference ratio is depicted in Fig. 4.12.

Figure 4.13 shows the symbol error-rate of a 98-PAM signal transmitted over this channel. The average signal power at the input of the transmitter filter is  $-12$  dBm0. Compared to Example 1, the average transmitted power is significantly larger for a given symbol error rate.

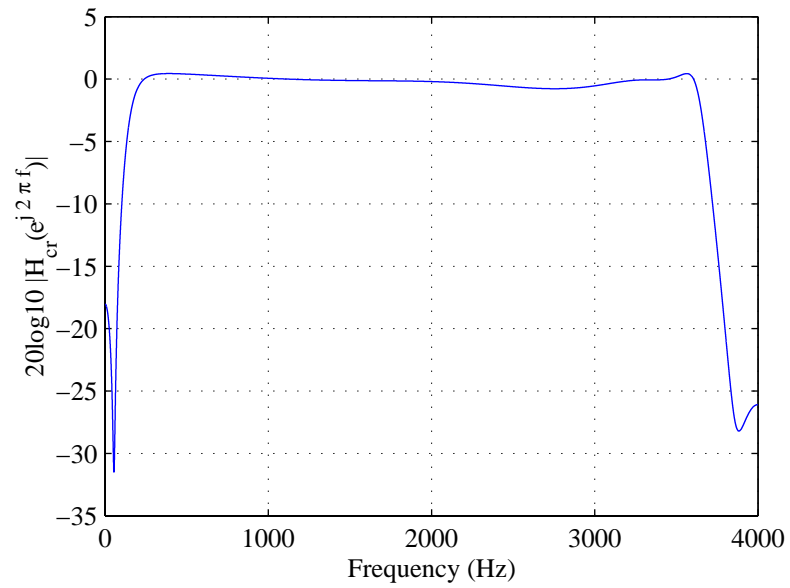
#### 4.2.1 Observations and remarks

Since the ISI does not have the same effect on the probability of error as additive noise, minimizing the MSE does not necessarily lead to the minimum probability of error. By using the MSE criterion for the transmitter filter design, we treat the combination of noise and residual ISI as an additive random variable, and ignore the information that we could obtain from the ISI regarding the transmitted data sequence. However, due to the fixed structure of the receiver front-end in the up-stream PCM channel, the information on transmitted data cannot be extracted from the ISI. Furthermore, the MSE criterion provides a simple way to combine the effect of noise and ISI with a straightforward solution for the optimal filter design.

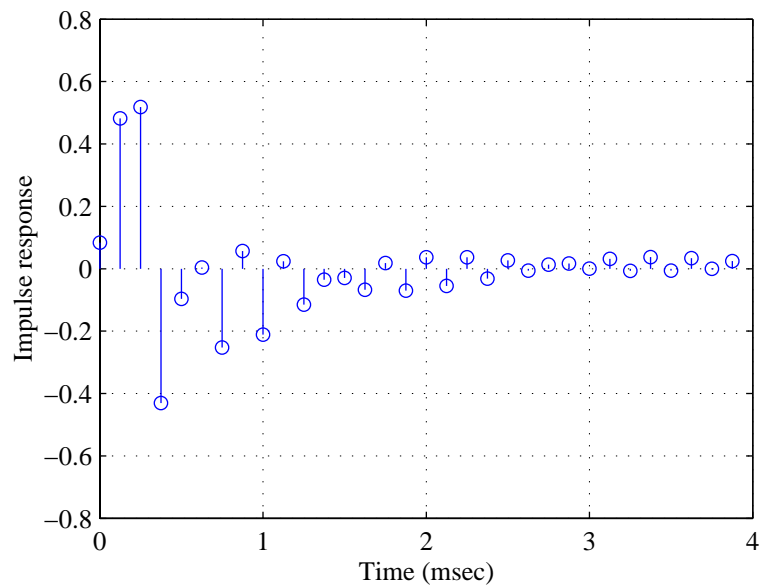
Two examples discussed above illustrate that an optimal transmitter filter can reduce the effect of the ISI. However, there is a trade-off between the residual ISI and the transmitted signal power. For some channel filter characteristics, such as the filter we discussed in Example 2, the required transmitted power to obtain an acceptable performance is significantly large. The main cause of such a requirement for the signal power is spectral nulls in the equivalent channel filter characteristics.

Apart from the average transmitted power, spectral nulls in the frequency response of the equivalent channel cause a slower decay in the impulse response of the transmitting filter. The portion of transmitting filter that correspond to the spectral nulls can only be implemented as an IIR filter.

Figure 4.11 indicates that for the SIR range in which we are interested, a small change in the average transmitted power can drastically change the SIR. As shown in Fig. 4.7 and Fig. 4.12, a slight increase in the average transmitted power can change the system performance. These examples suggest that for a PAM modulation with a large alphabet, the required signal-to-interference ratio is relatively high. As a result, the transmitting filter should be designed to provide almost



(a) Magnitude Response



(b) Impulse Response

**Fig. 4.9** Channel characteristics in Example 2.

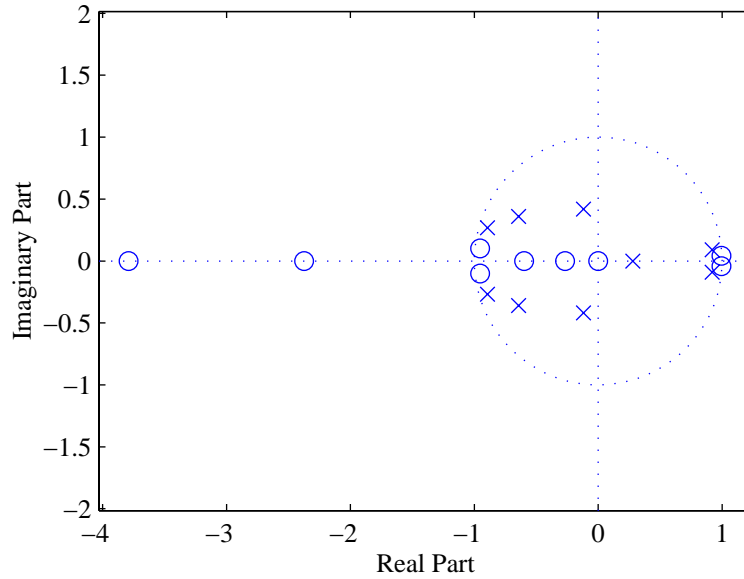


**Fig. 4.10** Pole-zero locations of a channel-receiver filter transfer function discussed in Example 2.

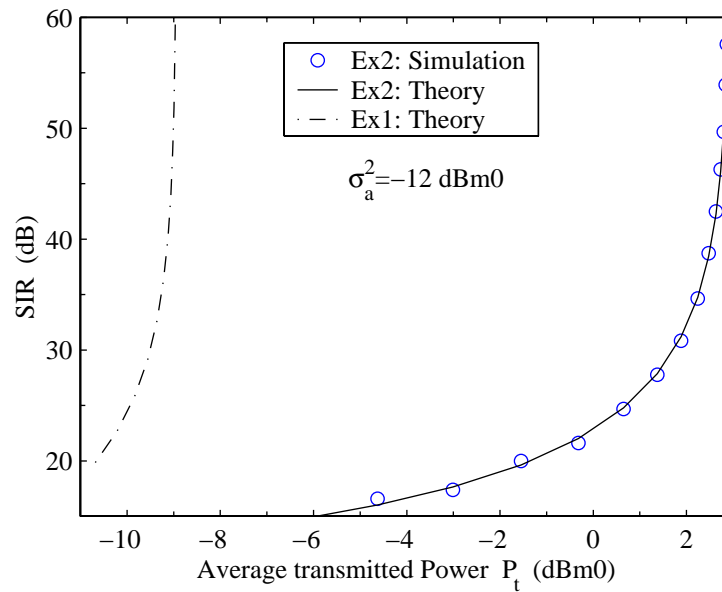


**Fig. 4.11** Signal-to-ISI ratio as a function of the average transmitted power in Example 2. Compared to Example 1, a significant increase in the average transmitted power is required to obtain the same SIR.

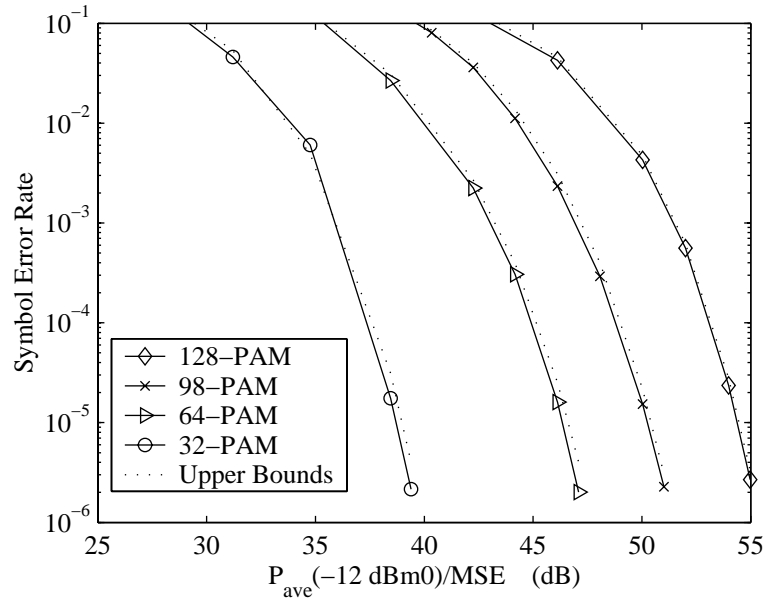


**Fig. 4.12** The probability of symbol error is shown as a function of SIR for several PAM signals for the channel filter discussed in Example 2.

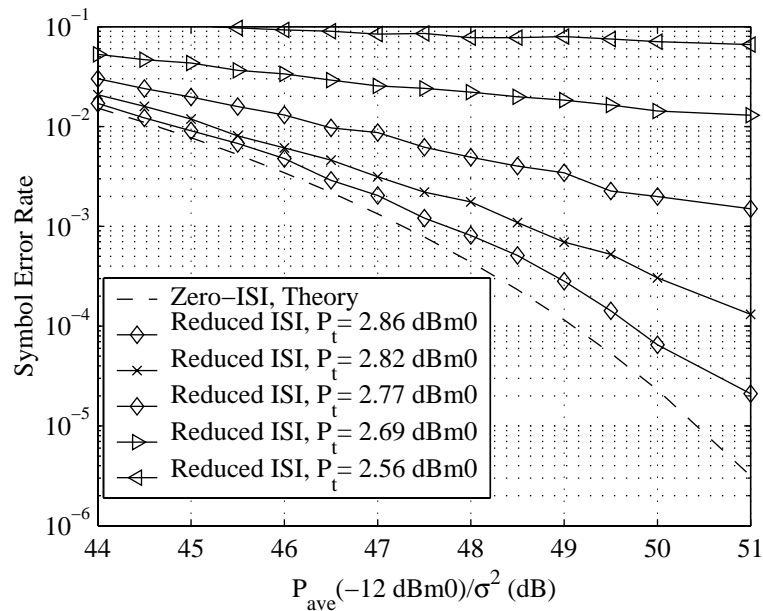


**Fig. 4.13** Probability of symbol error as a function of SNR in Example 2. The performance of different transmitter filters is compared to the ideal channel filter with Gaussian additive noise.

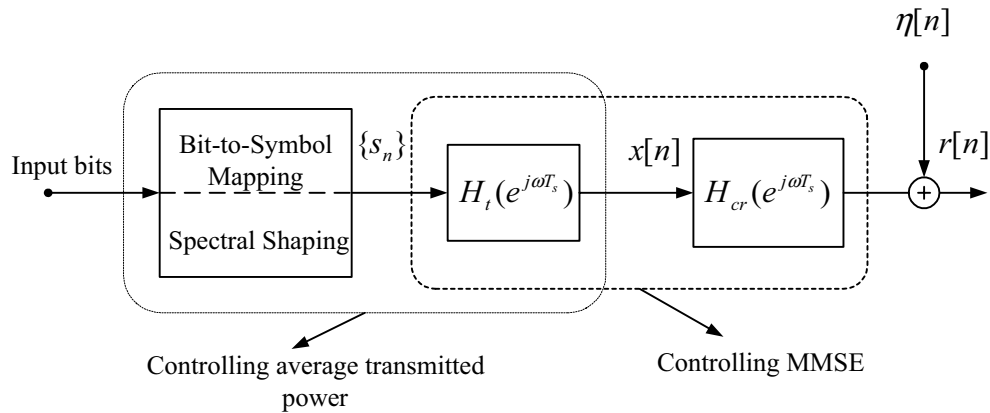


**Fig. 4.14** Spectrum shaping cascaded with an optimal filtering to control MMSE while maintaining the limit on the average transmitted power.

an ISI-free channel<sup>3</sup>. Such a design requires a large average transmitted power. For channels with spectral null, the required transmitted power can be unbounded.

In order to overcome above problems, we examine transmitter structures that can reduce the average transmitted power while maintaining an acceptable level of signal-to-interference ratio.

### 4.3 Spectrum shaping and filtering

In this section, we investigate spectrum shaping methods that can be applied to the data sequence in order to reduce the average transmitted power while maintaining an acceptable signal-to-interference ratio. Figure 4.14 shows schematically a cascade of spectrum shaping and linear filtering. The stream of incoming bits is mapped into a sequence of symbols  $\{s_n\}$  with a power spectrum density that is close to a desired spectrum.

Prior to describing spectrum shaping methods, we determine the desired power spectrum density  $\Phi_d(e^{j\omega T_s})$  that reduces the average transmitted power. There are different solutions for  $\Phi_d(e^{j\omega T_s})$ , depending on assumptions about the channel model.

#### (1) An arbitrary channel frequency response

The magnitude response of the equivalent channel-receiver filter is specified as a function of frequency  $|H_{cr}(e^{j\omega T_s})|$ . In this model, no underlying structure for the transfer function is considered. We investigate the power constraint in Eq. (4.13) and the MMSE in Eq. (4.14) to identify the desired PSD of the input signal so that the MMSE is reduced while the power constraint on the

<sup>3</sup>In other words, for a PCM channel, the MMSE transmitter filter solution should provide almost zero ISI that corresponds to  $\lambda \approx 0$  in Eq. (4.12).

transmitted signal still holds. We denote the desired power spectrum density as  $\Phi_d(e^{j\omega T_s})$ . From Eq. (4.14), it is clear that if  $\lambda$  approaches zero, the MMSE will tend to zero. For  $\lambda = 0$ , the transmitter filter given in Eq. (4.12) is simplified to the channel inverse filter  $1/H_{cr}(e^{j\omega T_s})$ .

From Eq. (4.13), we wish to determine the power spectrum density so that the power constraint is satisfied with a smaller value of  $\lambda$ . Let us examine Eq. (4.13) when  $\lambda$  approaches zero. The left hand side of Eq. (4.13) can be approximated as:

$$\frac{T_s}{2\pi} \int_{-\pi/T_s}^{\pi/T_s} \frac{|H_{cr}(e^{j\omega T_s})|^2}{(|H_{cr}(e^{j\omega T_s})|^2 + \lambda_0)^2} \Phi_d(e^{j\omega T_s}) d\omega \approx \frac{T_s}{2\pi} \int_{-\pi/T_s}^{\pi/T_s} \frac{\Phi_d(e^{j\omega T_s})}{|H_{cr}(e^{j\omega T_s})|^2} d\omega \quad (4.17)$$

where  $\lambda_0 \approx 0$ . If we choose the power spectrum density as:

$$\Phi_d(e^{j\omega T_s}) = K |H_{cr}(e^{j\omega T_s})|^2, \quad K < \mathcal{P}_t \quad (4.18)$$

the power constraint will be satisfied with a zero value of  $\lambda$ .

Equation(4.18) indicates that by spectrum shaping we wish to compensate for the power gain of the transmitting filter. Equation (4.18) sets a target spectrum for the PSD at the transmitter filter input. We aim to create a signal at the input of the transmitter filter with a PSD close to the target spectrum<sup>4</sup>.

Note that obtaining the target spectrum given in Eq. (4.18) may not be feasible since the amount of redundancy added to the PAM signal to create such a power spectrum density can be large. The constraint on the scaling factor  $K$  in Eq. (4.18) effects average power  $\sigma_a^2$  of the PAM signal before the spectrum shaping. Such a constraint limits the data transmission rate.

## (2) A rational transfer function for the channel filter

Let us assume that the transfer function of the channel-receiver filter is expressed as a rational function:

$$H_{cr}(e^{j\omega T_s}) = \frac{\sum_{k=0}^M \beta_k e^{-j\omega T_s k}}{1 + \sum_{k=1}^N \alpha_k e^{-j\omega T_s k}} = \frac{B(e^{j\omega T_s})}{A(e^{j\omega T_s})} \quad (4.19)$$

<sup>4</sup>We expect that the closer  $\Phi_a(e^{j\omega T_s})$  is to the target spectrum, the smaller the MMSE value will be. As a measure of the distance between the two spectra, we can use the following:

$$\mathcal{D} = \frac{T_s}{2\pi} \int_{-\pi/T_s}^{\pi/T_s} |\Phi_a(e^{j\omega T_s}) - \Phi_d(e^{j\omega T_s})|^2 d\omega$$

It is easy to show that when  $\lambda$  approaches zero in Eq. (4.13), the following spectrum can reduce the average transmitted power:

$$\Phi_d(e^{j\omega T_s}) = K|B(e^{j\omega T_s})|^2 \quad (4.20)$$

From Eq. (4.13), we can show that for  $\lambda = 0$ , the average power constraint is satisfied if we have:

$$K \leq \frac{\mathcal{P}_t}{\frac{T_s}{2\pi} \int_{-\pi/T_s}^{\pi/T_s} |A(e^{j\omega T_s})|^2 d\omega} = \frac{\mathcal{P}_t}{1 + \sum_{k=1}^N \alpha_k^2} \quad (4.21)$$

As shown in Eq. (4.20), one solution for the desired spectrum is based on the numerator of the transfer function  $H_{cr}(e^{j\omega T_s}) = \frac{B(e^{j\omega T_s})}{A(e^{j\omega T_s})}$ . Suppose the polynomial  $B(z)$  is written in terms of its  $M$  roots:

$$B(z) = \beta_0 (1 - z_1 z^{-1}) (1 - z_2 z^{-1}) \cdots (1 - z_M z^{-1}) \quad (4.22)$$

It is evident from Eq.(4.13) that for small values of  $\lambda$ , those roots of  $B(z)$  in the vicinity of the unit-circle or on the unit-circle are the dominant terms that determine the average transmitted power.

Depending on the average power constraint, it might be adequate to consider only a portion of  $|B(e^{j\omega T_s})|^2$  as the desired power spectrum. We decompose  $B(e^{j\omega T_s})$  into a product of two terms:

$$B(e^{j\omega T_s}) = B_1(e^{j\omega T_s})B_2(e^{j\omega T_s}) \quad (4.23)$$

where  $B_1(e^{j\omega T_s})$  contains zeros close to (or on) the unit circle. The desired power spectrum density is written as:

$$\Phi_d(e^{j\omega T_s}) = K'|B_1(e^{j\omega T_s})|^2 \quad (4.24)$$

### 4.3.1 Methods of Spectrum Shaping

The data symbol sequence at the input of the transmitter filter has a flat spectrum. Spectrum shaping can be defined as adding a form of redundancy to the input sequence to create a desired statistical correlation among the symbols. There are a variety of methods of creating such a correlation. Line codes are typical examples of spectrum shaping that control the “running digital sum” to create spectral nulls at DC and can be extended to create spectral nulls at non-zero frequencies [38, Chapter 12]. There are also trellis coding techniques that can create spectral nulls in the spectrum at desired frequencies [55]. Partial response signalling [56] [38] is an alternative method of spectrum shaping via inverse filtering and a modulo arithmetic operation.

Due to predetermined structure of the receiver, these spectrum shaping techniques are not directly applicable to the up-stream PCM channel.

The spectral shaping method used in the V.90 Standard for the down-stream PCM channel is based on Convolutional Spectral Shaping (CSS) [14]. The CSS algorithm controls the sign bits of the transmitted symbols. The sign bits are selected on a frame by frame basis. Each frame contains six symbols. In each frame, the sign bits are selected based on  $r$  bits of redundancy ( $0 \leq r \leq 3$ ) and  $6 - r$  bits of information. The sign bit sequence is selected so that the mean square error between the signal PSD and a desired spectrum is minimized.

Convolutional spectrum shaping is designed for the down-stream PCM channel where the transmitter can only determine the transmitted bits. The actual PAM modulation is performed by the PCM decoder at the central office. In [18], the application of convolutional spectrum shaping in the up-stream PCM channel is investigated. Although the results provided in [18] show the merits of applying spectrum shaping for the up-stream channel, the use of CSS is not necessarily the best choice of spectrum shaping method for the up-stream PCM channel. In the up-stream PCM channel, the analog modem controls the transmitted signal. Compared to the down-stream PCM channel, the control on the transmitted signal in the up-stream channel can reduce the amount of redundancy required for spectrum shaping.

#### 4.3.2 Spectrum shaping by inserting redundant symbols

We can perform spectrum shaping by adding redundant symbols to the input sequence. The input symbols are parsed into non-overlapping blocks of  $K$  symbols. Although the redundant symbols can be inserted at different locations among the data symbols, we consider a set of  $N - K$  symbols that is added to the end of each block. Values of redundant symbols are computed so that the power spectrum density of each block is close to the target spectrum. As shown in Fig. 4.15, the operator  $F(k, n)$  takes in a block of  $K$  data symbols and computes the redundant  $N - K$  symbols. Note that the redundant symbols are not necessarily taken from the PAM symbol alphabet. As we will discuss below, the redundant symbols do not carry any information; they are only added to create the desired spectrum shaping.

#### A spectral null at DC

Let us assume that the desired spectrum contains a spectral null at zero frequency (DC). Each input block of length  $K$  is padded by one symbol ( $N = K + 1$ ). The output sequence  $s[n]$  is

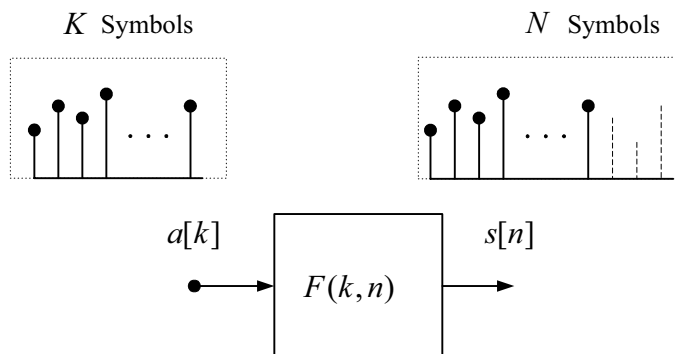


**Fig. 4.15** Spectrum shaping by inserting redundant symbols into a block of data symbols.

represented as:

$$s[mN + n] = \begin{cases} a[mK + n] & \text{for } n = 0, \dots, K - 1 \\ -\sum_{l=0}^{K-1} a[mK + l] & \text{for } n = K \end{cases} \quad (4.25)$$

The  $z$ -transform of the output signal  $s[n]$  can be written in terms of the  $z$ -transform of its non-overlapping blocks of length  $N$ :

$$\begin{aligned} S(z) &= \sum_{n=-\infty}^{\infty} s[n]z^{-n} \\ &= \sum_{m=-\infty}^{\infty} \sum_{l=0}^{N-1} s[mN + l]z^{-(mN+l)} \\ &= \sum_{m=-\infty}^{\infty} \left( \sum_{l=0}^{N-1} s[mN + l]z^{-l} \right) z^{-mN} \\ &= \sum_{m=-\infty}^{\infty} S_m(z)z^{-mN} \end{aligned} \quad (4.26)$$

From Eq. (4.25),  $S_m(z)$  can be written as:

$$\begin{aligned}
S_m(z) &= \sum_{l=0}^{N-1} s[mN + l]z^{-l} \\
&= \sum_{l=0}^{N-2} s[mN + l]z^{-l} (1 - z^{-(N-1-l)}) \\
&= \sum_{l=0}^{N-2} s[mN + l]z^{-l} (1 - z^{-1})(1 + z^{-1} + \dots + z^{-(N-l-2)})
\end{aligned} \tag{4.27}$$

From Eq. (4.27), it is evident that  $S_m(z)$  contains a zero at DC.

We would like to compute the power spectrum density  $\Phi_s(e^{j\omega T_s})$  as a function of the block size. The input sequence is assumed to be i.i.d. random variable with zero mean and variance of  $\sigma_a^2$ . Due to inserted redundant symbols, the sequence  $s[n]$  is not stationary. The autocorrelation function of  $s[n]$  is defined as:

$$\phi_s(k, l) = \mathcal{E}\{s[k]s[l]\} \tag{4.28}$$

From Eq. (4.25), the autocorrelation function can be characterized as:

$$\phi_s(k, l) = \begin{cases} \sigma_a^2 & \text{for } k = l, k \neq mN - 1 \\ (N - 1)\sigma_a^2 & \text{for } k = l, k = mN - 1 \\ 0 & \text{for } k \neq l, k \neq mN - 1, l \neq mN - 1 \\ -\sigma_a^2 & \text{for } 0 < |k - l| < N, \quad k \text{ (or } l) = mN - 1 \end{cases} \tag{4.29}$$

From Eq. (4.29), we can show that:

$$\phi_s(k + N, l + N) = \phi_s(k, l) \tag{4.30}$$

The average value of the autocorrelation function over a period  $N$  can be written as:

$$\bar{\phi}_s(m) = \frac{1}{N} \sum_{k=0}^{N-1} \phi_s(k, m + k) \tag{4.31}$$

From Eq. (4.29),  $\bar{\phi}_s(m)$  is computed as:

$$\bar{\phi}_s(m) = \begin{cases} \frac{2N - 2}{N} \sigma_a^2 & m = 0 \\ \frac{-1}{N} \sigma_a^2 & m = \pm 1, \pm 2, \dots, \pm(N - 1) \\ 0 & \text{elsewhere} \end{cases} \tag{4.32}$$

The power spectrum density of  $s[n]$  can be expressed as the discrete-time Fourier-transform of  $\bar{\phi}_s(m)$ . In this example, the power spectrum density can be computed as:

$$\begin{aligned}\Phi_s(e^{j\omega T_s}) &= \sum_{m=-\infty}^{\infty} \bar{\phi}_s(m) e^{-j\omega m T_s} \\ &= \frac{\sigma_a^2}{N} \left\{ (2N-1) - \frac{\sin(2N-1)\frac{\omega T_s}{2}}{\sin\frac{\omega T_s}{2}} \right\}\end{aligned}\quad (4.33)$$

In Eq. (4.33),  $\Phi_s(e^{j\omega T_s})$  is a positive definite function with double zeros at DC. Figure 4.16 shows  $\Phi_s(e^{j\omega T_s})$  as a function of frequency (with  $1/T_s = 8000$  Hz) for different values of block size  $N$ . As shown in this figure, the power attenuation at frequencies near DC depends on the block size.

Compared to the convolutional spectrum shaping results reported in [14], the insertion of redundant symbols can provide more attenuation at DC with less redundancy. The amount of redundancy added to the signal is controlled by the length of each block.

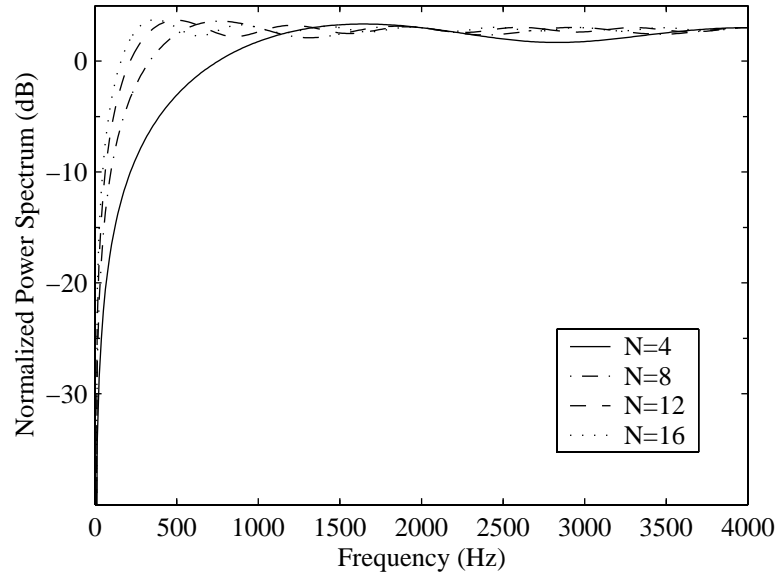
Figure 4.17(a) shows a transmitter with spectrum shaping followed by a linear transmitter filter. The channel contains a spectral null at DC. The spectrum shaping is performed by inserting a redundant symbol to each block of  $N - 1$  data symbols. The input symbols are taken from a 64-PAM constellation with an average power of  $-12$  dBm0. Figure 4.17(b) shows the average transmitted power as a function of the block size. For comparison, the required transmitter power without spectrum shaping is also depicted. As shown, the spectrum shaping can significantly reduce the average transmitted power. By changing the block size  $N$  we can control the trade-off between the average transmitted power and the information symbol rate  $K/N$ .

Ideally, spectrum shaping creates nulls that cancel the poles of the transmitter filter. However, such a pole cancellation may not be perfect due to a mismatch between the zeros created by the spectrum shaping and the poles of the transmitter filter. A realizable transmitter filter cannot include poles on the unit-circle. A non-zero value of  $\lambda$  in the optimal transmitter filter given in Eq. (4.12) can prevent such a problem.

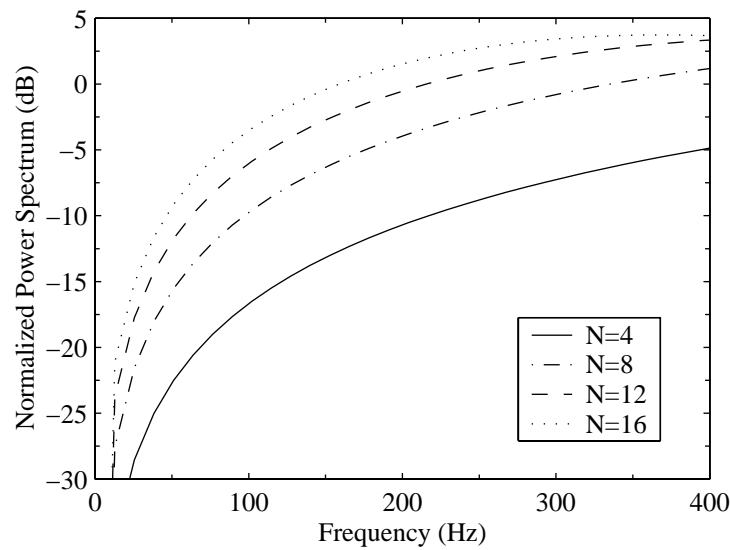
### Nulls at a set of desired frequencies

The previous example can be extended to create nulls in more than one frequency. We use a set of  $N - K$  redundant symbols in a block of  $N$  output symbols to create the desired spectral nulls. Assuming  $S_m(z)$  is the  $z$ -transform of each block, we choose the redundant symbols such that the following equations are satisfied:

$$S_m(z_i) = 0 \quad \text{for} \quad i = 1, 2, \dots, M \quad (4.34)$$

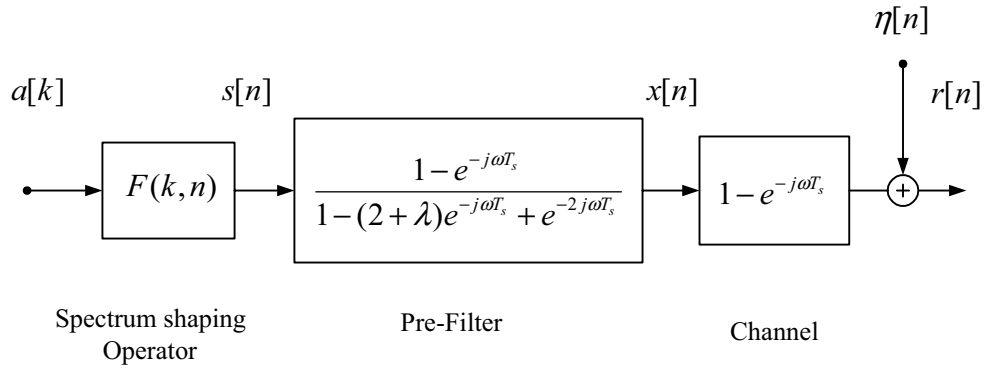


(a) Power spectrum in the 0–4000 Hz frequency range.

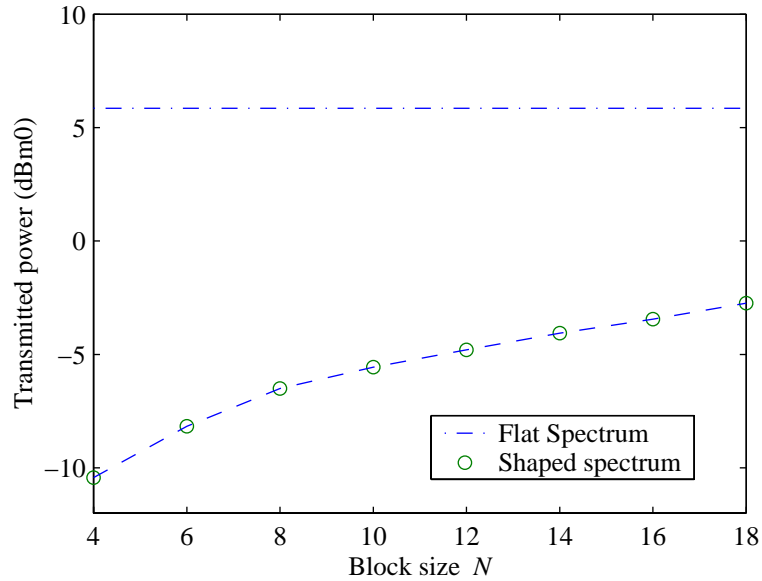


(b) Zoomed in on the 0–400 Hz frequency range.

**Fig. 4.16** Power spectrum after spectrum shaping. It is evident that the spectrum contains a spectral null at DC. The input signal power  $\sigma_a^2$  is normalized to one.



(a) A transmitter design for channel with a spectral null.



(b) The average transmitted power as a function of the block size.

**Fig. 4.17** An optimal MMSE linear transmitter filter is designed to compensate for a channel with spectral null at DC as shown in (a). The input symbols  $a[k]$  are taken from a 64-PAM constellation with an average power of  $-12$  dBm0. We choose  $\lambda = 10^{-5}$ . The average transmitted power with and without spectrum shaping is presented in (b).

where  $z_i$  corresponds to a set of desired zeros in  $S(z)$ . The first  $K$  symbols in each block are data symbols followed by  $N - K$  redundant symbols. From Eq. (4.34), we obtain the following set of equations specifying redundant symbols:

$$\begin{bmatrix} z_1^{-K} & z_1^{-(K+1)} & \dots & z_1^{-(N-1)} \\ z_2^{-K} & z_2^{-(K+1)} & \dots & z_2^{-(N-1)} \\ \dots & \dots & \dots & \dots \\ z_M^{-K} & z_M^{-(K+1)} & \dots & z_M^{-(N-1)} \end{bmatrix} \begin{bmatrix} s[mN + K] \\ s[mN + K + 1] \\ \dots \\ s[mN + N - 1] \end{bmatrix} = - \begin{bmatrix} \sum_{l=0}^{K-1} a[mK + l] z_1^{-l} \\ \sum_{l=0}^{K-1} a[mK + l] z_2^{-l} \\ \dots \\ \sum_{l=0}^{K-1} a[mK + l] z_M^{-l} \end{bmatrix} \quad (4.35)$$

If the desired zeros  $z_i$  are distinct and their number is equal to the number of redundant symbols per block ( $M = N - K$ ), then Eq. (4.35) has a unique solution<sup>5</sup>. For a set of distinct zeros  $z_i$ , the determinant of this matrix is non-zero<sup>6</sup>.

If the number of redundant symbols is less than the number of equations, the set of equations in Eq. (4.35) is over-determined. In this case, the least square solution for the redundant symbols can be selected [58]. As a result, Eq. (4.34) holds only in the mean-square-error sense.

The proposed arrangement of redundant symbols at the end of each block is arbitrary. Other patterns of redundancy insertion can be analyzed the same way. However, Eq. (4.35) may not provide a finite solution for an arbitrary pattern of inserted symbols in a block.

To show the effect of spectrum shaping in the up-stream PCM channel, we apply the redundancy insertion method to a PCM channel as discussed in Example 2 of Section 4.2. Figure 4.19 shows the average transmitted power when spectral shaping is applied to data sequence. Symbols  $a[k]$  are selected from, in this case, a 90-PAM constellation with an average power of  $-12$  dBm0. The spectrum shaping in this example creates zeros at DC and at 4000 Hz ( $1/2T_s$ ). Compared to the case where the input signal has a flat spectrum, the redundancy insertion method provides a significant reduction in the transmitted power. However, the required power to maintain an acceptable data transmission rate is still high. In order to reduce the average power, we can reduce the power of the average power of the input symbols<sup>7</sup>. Figure 4.19 shows the average transmitted power when spectral shaping is applied to data sequence. Symbols  $a[k]$  are selected

<sup>5</sup>The determinant of the coefficient matrix in the left-hand-side of Eq. (4.35) is similar to that of a Vandermonde Matrix [57, p.266]. It can be shown that if  $z_i$ 's are distinct, then the determinant of this matrix is non-zero.

<sup>6</sup>In order to create repeated roots for  $S_m(z)$ , the set of equations given above is not adequate. We should consider the derivatives of the polynomials as well.

<sup>7</sup>Note that by reducing the average signal power while maintaining the same number of constellation points, reduces the minimum distance between adjacent constellation points. In the present of additive noise, the system is susceptible to a higher probability of error.

from a 90-PAM constellation with an average power of  $-18$  dBm0.

Figure 4.20 shows the data transmission rate as a function of the transmitted power. If we assume that ISI is the dominant source of error, the transmitted filter is designed to provide symbol error rate close to  $10^{-6}$ . The required signal-to-interference ratio is around 47 dB. Results shown in Fig. 4.20 are only examples of the trade-off between the data transmission rate and the average transmitted power. Depending on the channel filter, the constellation size, the value of transmitted power constraint, the block size and the number of redundant symbols per block can be determined.

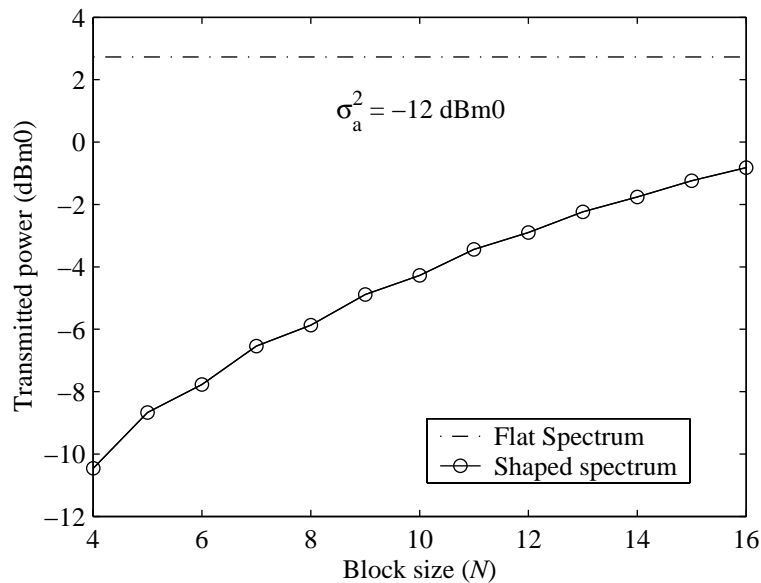


**Fig. 4.18** Spectrum shaping reduces the average transmitted power for a 90-PAM modulated signal with  $\sigma_a^2 = -12$ dBm0.

Spectrum shaping of symbols requires adding redundancy to the input sequence. Since the symbol rate and the maximum number of signal levels in the up-stream PCM channel are predetermined, adding redundancy causes a reduction in the data transmission rate over the channel. With a constraint on the average transmitted power, several factors should be considered in order to maximize the net bit-rate at a given probability of symbol error:

- the constellation size,
- the probability distribution of the constellation,
- the average power of constellation points and the block size.

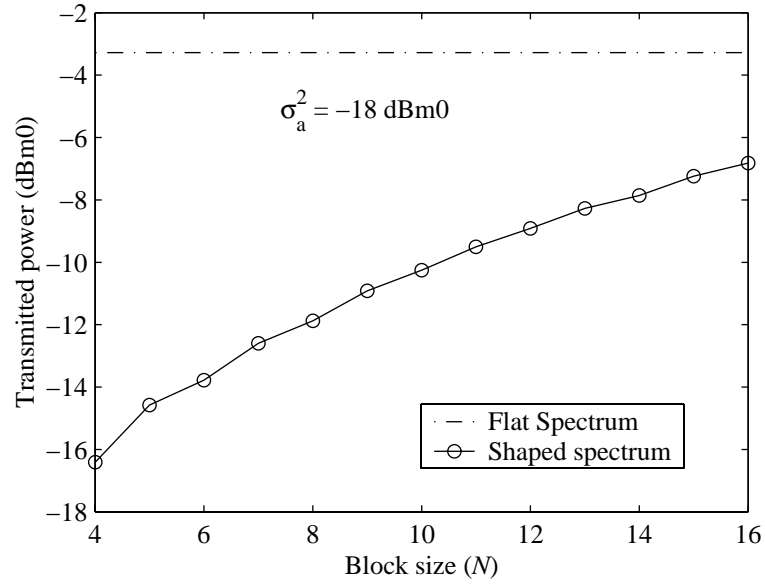


**Fig. 4.19** Average transmitted power as a function of the block size for a 90-PAM signal. Applying spectrum shaping to a PCM channel with spectral nulls reduces the average transmitted power.

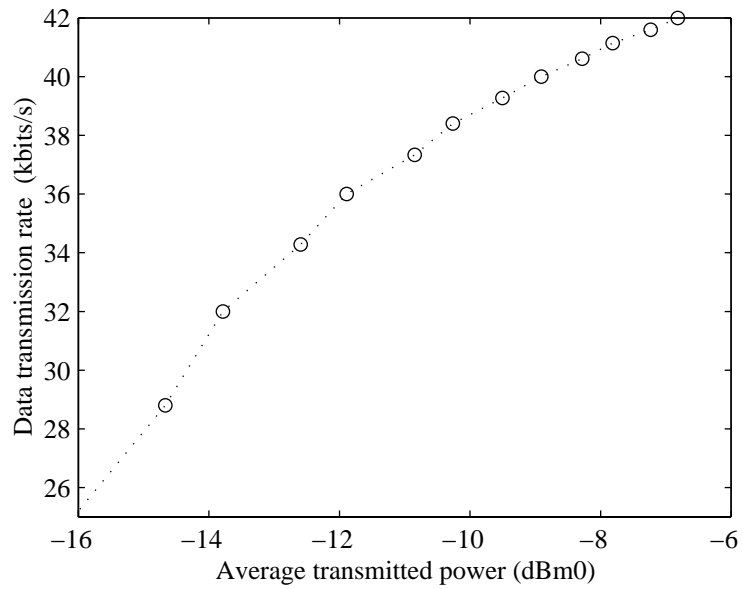


**Fig. 4.20** Data transmission rate as a function of transmitted power

#### 4.4 Precoding: combined filtering and spectral shaping

In this section, we describe precoding methods to combine linear filtering and spectrum shaping. We explain the properties and limitations of the classical precoding techniques for use in the up-stream PCM channels. Alternative precoding methods that are more suitable for the up-stream PCM channels will be described.

##### 4.4.1 Tomlinson-Harashima Precoding

Tomlinson [50] and Harashima/Miyakawa [59] invented independently a channel compensation technique known as precoding. Basically, a precoder compensates for ISI at the transmitter. By performing channel equalization at the transmitter, two known problems of receiver equalizers can be avoided: noise enhancement, as in a linear equalizer, and error propagation, as in a decision feedback equalizer [38].

Straightforward pre-filtering of channels has problems of its own; it increases the transmit signal power, especially for channels with spectral nulls. *Tomlinson-Harashima* Precoding ( TH-precoding) provides a solution for channel compensation while maintaining the transmitted signal level in a preset interval<sup>8</sup>. TH-precoding generalizes the idea of precoding used in partial-response signalling. In a partial-response signalling, precoding is used to compensate for the controlled ISI that is introduced by the transmitter. In partial response signalling, the exact model of introduced ISI is known at the transmitter. In other applications where the ISI is introduced by channel, a precoding can be applied if the filtering effect of the channel is known at the transmitter.

Figure 4.21 shows a model for the TH-precoding operation. In this model, an equivalent channel filter with an FIR impulse response  $h[n]$  is considered. We assume  $h[n]$  is known at the transmitter. The impulse response  $h[n]$  is monic (i.e.,  $h[0] = 1$ ) and causal. A TH-precoder acts as an inverse filter, compensating for  $h[n]$  at the transmitter. The inverse filter is realized as a direct form all-pole filter. In order to limit the range of transmitted signal levels, a modulo operation maps the inverse filter output to a finite interval. The modulo operator limits the output signal to a preset interval  $[-V_{max}/2, +V_{max}/2]$ . At the receiver, another modulo operation is required to reverse the mapping performed at the transmitter. The signal  $x[n]$  at the input of the TH-precoder is limited to  $\pm V_{max}/2$  in order to maintain the one-to-one mapping between the input  $x[n]$  and the output  $r[n]$ <sup>9</sup>.

The operation of a TH-precoder can be interpreted as combined spectral shaping and pre-filtering. Figure 4.22 illustrates a TH-precoder where we expand the input signal to an inverse

<sup>8</sup>In our discussion, we only consider one-dimensional signals. The TH-precoding technique can also be used for complex signals [60].

<sup>9</sup>Note that for our discussion in this section  $x[n]$  is not necessarily a PAM signal.

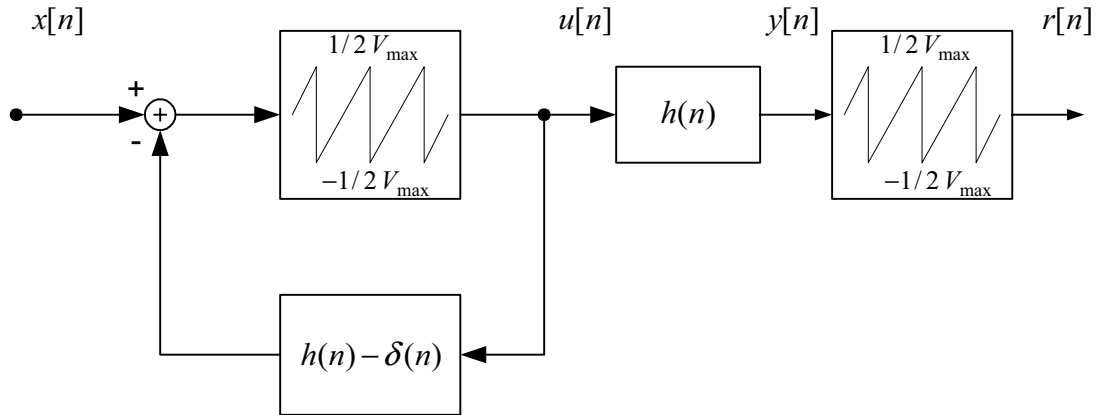


Fig. 4.21 Tomlinson-Harashima Precoder.

filter so that the output of this filter always remains in a finite range.

Taking real values in  $(-V_{max}/2, +V_{max}/2]$  interval, the input signal  $x[n]$  is mapped to  $s[n]$  via the following operation:

$$s[n] = x[n] + V_{max}k_n \quad (4.36)$$

where the integer  $k_n$  is selected so that the filter output  $u[n]$  satisfies:

$$\frac{-V_{max}}{2} < u[n] \leq \frac{+V_{max}}{2}$$

Since the inverse filter fully compensates for the channel filter, the channel output  $y[n]$  is identical to the inverse filter input  $s[n]$ . In order to extract the original signal  $x[n]$ , we use a modulo operation at the receiver:

$$\begin{aligned} r[n] &= y[n] - V_{max}k_n \\ &= \text{mod}(y[n], V_{max}) \end{aligned} \quad (4.37)$$

It is straightforward to show that  $r[n]$  is identical to  $x[n]$  [50].

A TH-precoder introduces redundancy by a multi-level representation of a signal point. The redundancy is used to shape the signal spectrum and to control the peak and average power of the transmitted signal. There are however, several (potentially restrictive) issues in TH-precoder designs that require further attention:

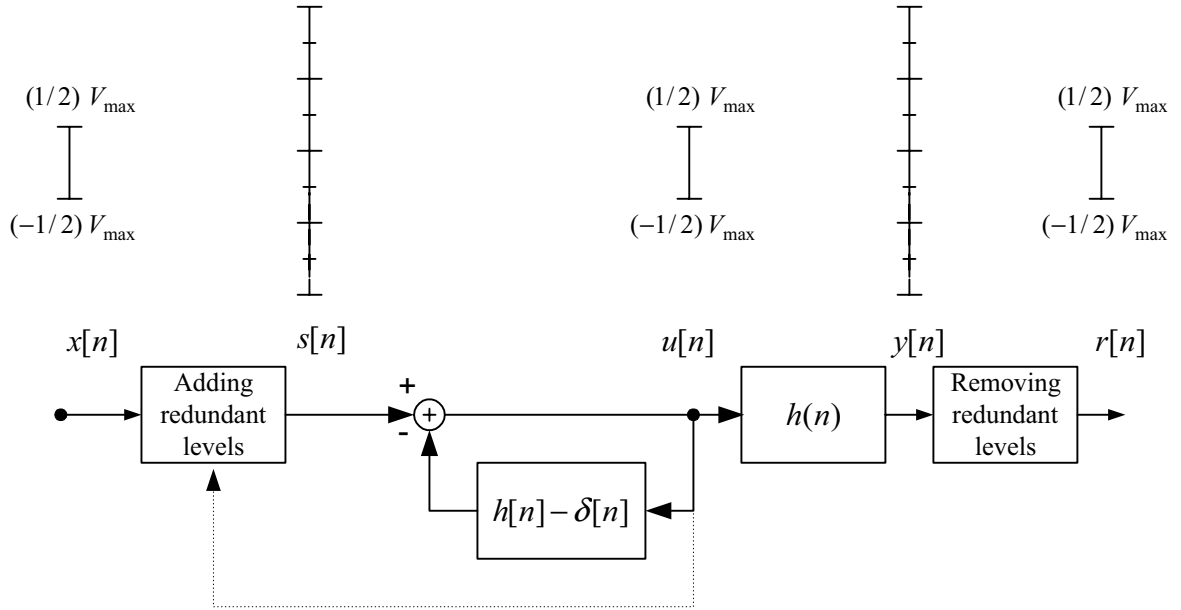


**Fig. 4.22** A TH precoder can be viewed as a combined filtering and spectrum shaping. The modulo arithmetic operation is used to add (and remove) redundant signal levels to the signal to maintain the transmitted signal in the  $(-V_{max}/2, +V_{max}/2]$  range.

### Increasing the Dynamic range of the received signal

As shown in Fig. 4.22, TH-precoding increases the dynamic range of the channel output  $y[n]$ . We determine an upper bound for the absolute value of the channel output  $|y[n]|$  as a function of the impulse response  $h[n]$ . For each sample at the output of the TH-precoder, we have:

$$-\frac{V_{max}}{2} \leq x[n] + V_{max}k_n - \sum_{l=1}^M h[l]u[n-l] \leq \frac{V_{max}}{2} \quad (4.38)$$

where  $M$  is the memory length of the channel filter impulse response  $h[n]$  and  $k_n$  is an integer number determined by the modulo operator. We assume the integer value  $k_n$  has a maximum denoted as  $K_{max}$ :

$$-K_{max} \leq k_n \leq K_{max} \quad (4.39)$$

Since the input signal  $x[n]$  and the precoder output  $u[n]$  are limited to  $\pm \frac{V_{max}}{2}$  range,  $K_{max}$  satisfies the following conditions:

$$-\frac{V_{max}}{2} \leq -\frac{V_{max}}{2} + V_{max}K_{max} - \frac{V_{max}}{2} \sum_{l=1}^M |h[l]| \leq \frac{V_{max}}{2} \quad (4.40)$$

The two inequalities expressed above result in the following expression for  $K_{max}$ :

$$K_{max} = 1 + \left\lfloor \frac{1}{2} \sum_{l=1}^M |h[l]| \right\rfloor \quad (4.41)$$

where  $\lfloor x \rfloor$  denotes the largest integer number that is less than or equal to  $x$ . At the channel output, the received signal  $y[n]$  can be written as:

$$y[n] = x[n] + k_n V_{max} \quad (4.42)$$

From Eq. (4.41), an upper bound for the received signal is determined as:

$$|y[n]| \leq V_{max} K_{max} = V_{max} \left( 1 + \left\lfloor \frac{1}{2} \sum_{l=1}^M |h[l]| \right\rfloor \right) \quad (4.43)$$

The maximum value of  $y[n]$  is obtained when  $x[n] = 0$  and  $k_n = K_{max}$ . Assuming that the upper bound given in Eq. (4.43) follows closely the signal, we can conclude that a TH-precoder increases the dynamic range of the received signal at least by a factor of two. As shown in Eq. (4.41), the upper bound is a function of the channel impulse response.

### Non-minimum-phase channel filters

Although a TH-precoder can compensate for any channel with a causal and monic impulse response, the precoding of a non-minimum phase impulse response can cause a significant increase in the receiver dynamic range. For example, consider a channel with the following impulse response:  $h[n] = \delta[n] - \rho \delta[n - 1]$ . From Eq. (4.41), we have:

$$K_{max} = 1 + \lfloor \rho/2 \rfloor$$

It is evident that increasing the value of  $\rho$  increases the dynamic range of the TH-precoding. While the dynamic range increase for minimum-phase filters ( $\rho < 1$ ) is minimal ( $K_{max} = 1$ ), a non-minimum-phase filter ( $\rho \geq 1$ ) may cause a significant increase in the dynamic range of the received signal.

### Expansion of the slicer circuit for a PAM signal detection at the receiver

In our discussion, we assume the input data symbols  $x[n]$  are taken from a  $2N$ -PAM signal alphabet. A TH-precoder increases the dynamic range of the input signal in order to control the transmitted power. At the receiver, each PAM symbol alphabet  $s_i$  has more than one represen-

tation. At The signal levels that correspond to the same symbol  $s_i$  are related as:

$$c_{ij} = s_i + k_j V_{max} \quad (4.44)$$

where  $k_j$  is an integer number chosen so that the precoder output remains in a preset range. For a receiver with a fixed dynamic range (such as the up-stream PCM channel), Eq. (4.44) indicates that TH-precoding reduces the effective number of constellation points that can be detected at the receiver. A portion of threshold levels at the receiver are used to detect redundant signal levels. If the original PAM constellation points are uniformly spaced, with an appropriate choice of  $V_{max}$ , the expanded PAM constellation can be uniformly spaced as well [38, p. 462].

If the original PAM constellation points are non-uniformly spaced, the expanded constellation points are derived from Eq.(4.44) and the detection thresholds of the expanded slicer are determined accordingly<sup>10</sup>.

#### 4.4.2 Precoding design for the up-stream PCM channels

The TH-precoding technique is not directly applicable to the up-stream PCM channels. The restrictions imposed by the PCM channel on the precoder design are as follows:

1. The up-stream PCM channel has a pre-determined receiver front end. The maximum number of constellation points at the receiver is limited by the number of ADC decision levels. The actual number of useful signal levels is smaller than the number of ADC levels in order to create enough margin against the channel signal distortions (additive noise, echo, etc.). As a result, a constellation expansion by a TH-precoder will reduce the PAM constellation size and the data transmission rate over the channel.
2. As we discussed in Section 4.2, the equivalent channel filter is typically a non-minimum phase filter.
3. In general, the estimate of a channel filter transfer function is a rational function<sup>11</sup>. The TH-precoder only compensates for an FIR channel filter.
4. In Chapter 2, we discussed the PAM constellation design for the up-stream PCM channel. The constellation points are determined based on a subset of the ADC decision boundaries in the PCM encoder. Due to the  $\mu$ -Law (or A-Law) companding used in the PCM encoder,

<sup>10</sup>For a given set of constellation points, the detector thresholds that minimize the probability of error are the midpoints of adjacent constellation points.

<sup>11</sup>Since the impulse response of the channel filter is relatively long, an IIR filter model reduces the number of parameters required to specify the channel impulse response. In recommendation V.90 and in the proposed draft of Recommendation V.92, the channel is modelled as an IIR filter.

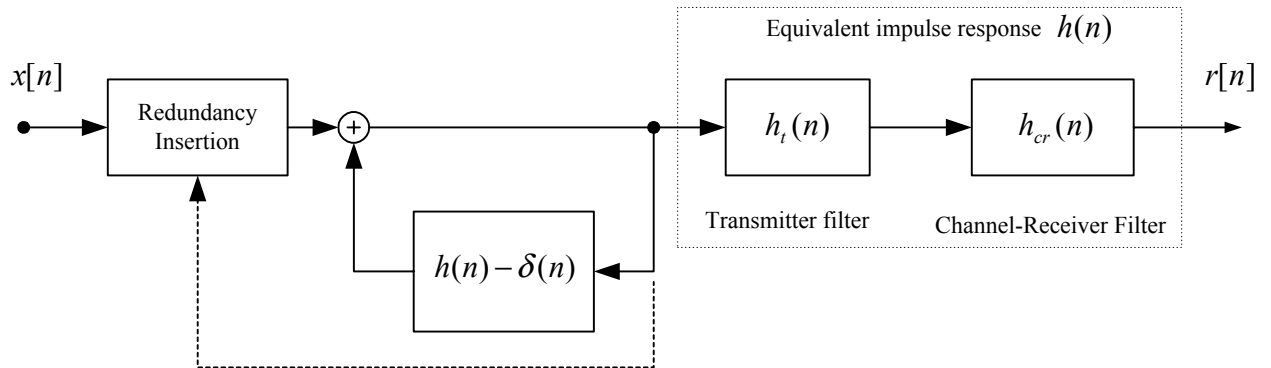


**Fig. 4.23** A precoding followed by linear filter at the transmitter.

the spacing between the constellation points is non-uniform. A TH-precoder requires a set of “modulo- $V_{max}$  equivalent” constellation points to represent a data symbol. The PAM constellation points designed for a PCM channel do not generally satisfy such requirements.

In order to compensate for a non-minimum phase channel filter, we consider a linear filter cascaded with the precoder. Figure 4.23 shows the cascade structure of a precoder and a linear filter at the transmitter. The linear transmitter filter is used to compensate for the poles of the channel filter as well as for the zeros that are not in the vicinity of the unit circle. The equivalent impulse response of the transmitter filter, the channel and the receiver filter is denoted as  $h[n]$ . The precoder is designed to compensate for a filter with the impulse response  $h[n]$ .

We investigate an alternative method of pre-filtering to accommodate non-uniform spacing between the PAM constellation points by inserting redundancies as extra symbols instead of extra signal levels.

#### 4.4.3 Linear block-by-block pre-filtering

In this section, we consider a block-by-block data transmission to allow for redundancy insertion between data symbols. In the present approach, we combine the spectrum shaping described in Section 4.3.2 with a linear channel inverse filter.

Figure 4.24 shows the cascade of spectrum shaping and the channel inverse filter. The equivalent channel impulse response and transfer function are denoted as  $h[n]$  and  $H(z)$  respectively. The impulse response  $h[n]$  is causal and monic. The causal inverse filter  $1/H(z)$  is realized as a direct form all-pole filter. The spectrum shaping is performed by a linear time-varying operator  $F(k, n)$ , as introduced in Section 4.3.2. For each block of non-overlapping  $K$  data symbols,  $F(n, k)$  specifies a block of  $N$  output symbols. The number of redundant symbols added to each

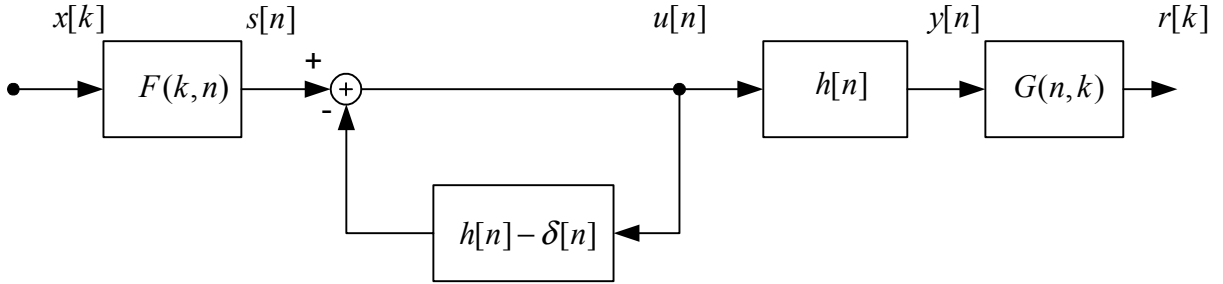


**Fig. 4.24** A block-by-block process combines spectrum shaping and channel inverse filtering.

block is equal to the memory length of the channel filter  $M = N - K$ . At the receiver, the  $M$  redundant symbols in each block are discarded by the  $G(n, k)$  operator. Since the inverse filter compensates for the channel filter  $h[n]$ , the input  $x[k]$  and the output  $r[k]$  are identical.

The redundant symbols in each block are determined such that the  $z$ -transform of each output block,  $S_m(z)$ , has a factor  $H(z)$ :

$$S_m(z) = H(z)U_m(z) \quad (4.45)$$

where  $U_m(z)$  is a finite length polynomial. In Section 4.3.2, we explained a method to compute the redundant symbols as linear functions of the data symbols in each block (see Eq. (4.35)). Here, we use the structure of the inverse filter to satisfy Eq. (4.45) without actually computing the redundant symbols.

Since there are  $N$  symbols in each block,  $S_m(z)$  a polynomial of the degree  $N - 1$  in terms of  $z^{-1}$ . The transfer function  $H(z)$  is a polynomial of the degree  $M$ . We specify the redundant symbols in each block such that  $U_m(z)$  can be written as a polynomial of the degree  $N - M - 1$ :

$$\begin{aligned} U_m(z) &= \frac{S_m(z)}{H(z)} \\ &= \sum_{n=0}^{N-M-1} u_m[n]z^{-n} \end{aligned} \quad (4.46)$$

We use series expansion of  $1/H(z)$  to compute the first  $K$  coefficients of  $U_m(z)$ . The causal inverse of  $H(z)$  can be expressed as:

$$\frac{1}{H(z)} = \sum_{k=0}^{\infty} h_{inv}[k]z^{-k} \quad (4.47)$$

where the sequence  $h_{inv}[k]$  will not be convergent if  $H(z)$  is a non-minimum phase filter. The

first  $K$  symbols of  $s_m[n]$  are taken from the input data symbols:

$$s_m[n] = x[Km + n] \quad \text{for} \quad n = 0, \dots, K - 1 \quad (4.48)$$

From Eq. (4.46), Eq. (4.47) and Eq. (4.48), the first  $K = N - M$  coefficients of  $U_m(z)$  are determined as:

$$u_m[n] = \sum_{k=0}^n h_{inv}[k] s_m[n - k] = \sum_{k=0}^n h_{inv}[k] x[Km + n - k] \quad \text{for} \quad 0 \leq n < K \quad (4.49)$$

The last  $M$  redundant symbols in each block are specified such that the output of the inverse filter satisfies the following condition:

$$u_m[n] = 0 \quad \text{for} \quad K \leq n \quad (4.50)$$

Redundant symbols can be computed from the difference equation that describes the inverse filter:

$$s_m[n] - \sum_{k=1}^M h[k] u_m[n - k] = u_m[n] = 0 \quad \text{for} \quad K \leq n < N \quad (4.51)$$

or equivalently:

$$s_m[n] = \sum_{k=1}^M h[k] u_m[n - k] \quad \text{for} \quad K \leq n < N \quad (4.52)$$

Equation (4.52) specifies  $M = N - K$  redundant symbols in each block. Equation (4.52), together with Eq. (4.48) completely specifies the input  $s[n]$  to the inverse filter. It is evident that only  $M$  redundant symbols in each block are required to create the desired spectrum shaping for  $S_m(z)$ .

From Eq. (4.49) and Eq. (4.50), we can identify  $u[n]$  as:

$$u[mN + n] = \begin{cases} \sum_{k=0}^n h_{inv}[k] x[Km + n - k] & \forall m \text{ and } 0 \leq n < K \\ 0 & \forall m \text{ and } K \leq n < N \end{cases} \quad (4.53)$$

It is clear from Eq. (4.53) that the actual values of the redundant symbols at the input of the inverse filter do not contribute to the inverse filter output. This observation suggests that we should be able to perform spectrum shaping without computing the redundant symbols.

Figure 4.25 shows an implementation of the block-by-block linear inverse filtering. The non-uniform up-sampling block parses the input symbols into blocks of  $K$  symbols and pads  $M$  zero symbols to the end of each block. Switch S1 disconnects the feedback loop and enforces the last  $M$  values of  $u_m[n]$  to be zero. In other words, at the end of each block, Switch S1 resets the

memory of the feedback loop one symbol at a time. As a result, at the beginning of each block the inverse filter starts from a zero initial state and at the end of each block the inverse filter returns to a zero-state.

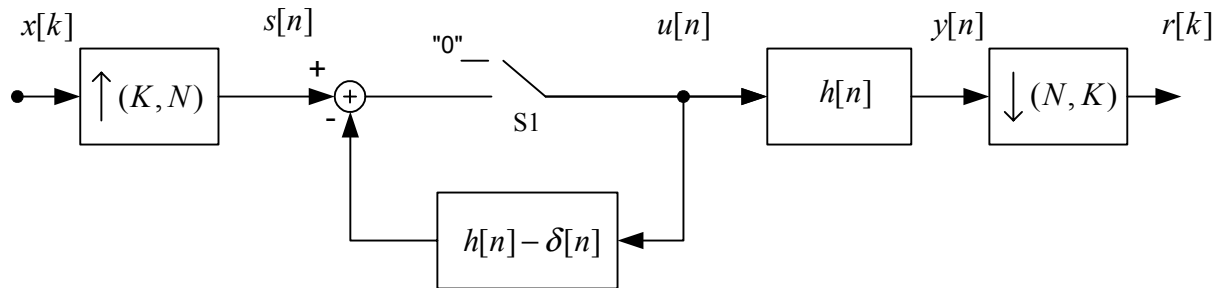


**Fig. 4.25** Redundancy insertion in a block of symbols to control the transmitted power.

The output of the inverse filter is characterized by Eq. (4.53). At the receiver, the channel output  $y[n]$  is identical to the inverse filter input  $s[n]$ . Such as for  $s[n]$ , the channel output  $y[n]$  contains non-overlapping blocks of  $K$  data symbols and  $M$  redundant symbols. To obtain the final output symbols  $r[n]$ , we discard the  $M$  redundant symbols at the end of each block using a non-uniform down-sampling process.

We illustrate the effect of the block-by-block inverse filtering by an example. Suppose that the equivalent channel transfer function is:

$$H(z) = 1 - z^{-2}$$

Since  $H(z)$  is not minimum-phase, the inverse filter is not BIBO stable. However, a block-by-block inverse filtering can be used to control the transmitted output power.

In this example, we choose a PAM input signal  $x[\cdot]$  with an average power of  $\sigma_x^2 = -12$  dBm0. The block-by-block process requires two redundant symbols per block to reset the feedback memory. Figure 4.26 shows the average signal power  $\sigma_u^2$  at the output of the inverse filter as a function of the block size  $N$ . Note that there are  $N - 2$  data symbols in each block. Reducing the block size will reduce the average transmitted power as well as the data symbol rate over the channel.

The signal power at the output of the inverse filter can be expressed in terms of the input power, the impulse response  $h_{inv}[n]$  of the causal inverse filter  $1/H(z)$  and the number of data symbols  $K$  in each block. Assuming the input signal  $x[n]$  forms an i.i.d. sequence with an average

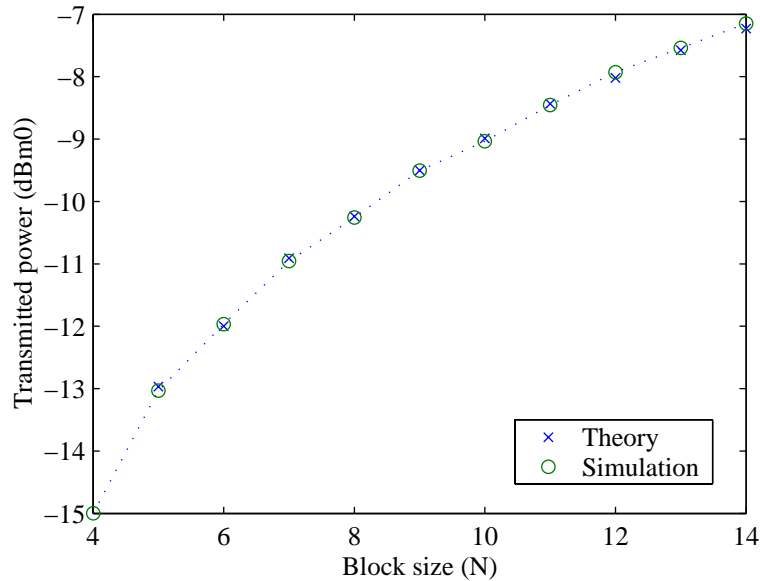


**Fig. 4.26** The average signal power at the output of the inverse filter is shown as a function of the block size. The input is a PAM signal with an average power of  $-12$  dBm0. The channel filter is specified as:  $H(z) = 1 - z^{-2}$ . There are 2 redundant symbols in each block. The values of signal power computed from Eq. (4.55) and the simulation results are similar.

power of  $\sigma_x^2$ , we have:

$$\begin{aligned}\sigma_u^2 &= \mathcal{E}\{|u[n]|^2\} \\ &= \frac{1}{N} \mathcal{E}\left\{\sum_{n=0}^{N-1} |u_m[n]|^2\right\}\end{aligned}\quad (4.54)$$

Replacing  $u_m[n]$  from (4.49) and (4.50), we can express the signal power  $\sigma_u^2$  as:

$$\sigma_u^2 = \frac{\sigma_x^2}{N} \sum_{n=0}^{K-1} (K-n) |h_{inv}[n]|^2 \quad (4.55)$$

Equation (4.55) indicates that the impulse response of the causal inverse filter has a major influence on  $\sigma_u^2$ . The block-by-block process restricts the contribution of the impulse response to its first  $K$  samples. A linear weighting function  $(K-n)$  tapers off the effect of the  $|h_{inv}[n]|^2$  when  $n$  increases.

It is important to note that for a non-minimum phase channel,  $h_{inv}[n]$  can grow exponentially causing a significant power gain  $\sigma_u^2/\sigma_x^2$  for the inverse filter. For channels with spectral nulls the location and the order of the spectral nulls affect the power gain of the inverse filter significantly.

In particular, if the channel has a repeated zero at a certain frequency, the impulse response grows linearly and creates a larger power gain. To illustrate this point, we compare the power gain of the block-by-block inverse filters for  $H_1(z) = 1 - z^{-2}$  and  $H_2(z) = (1 - z^{-1})^2$ . Figure 4.27 illustrates the power gain as a function of the block size. In both cases, the number of redundant symbols per block is 2.

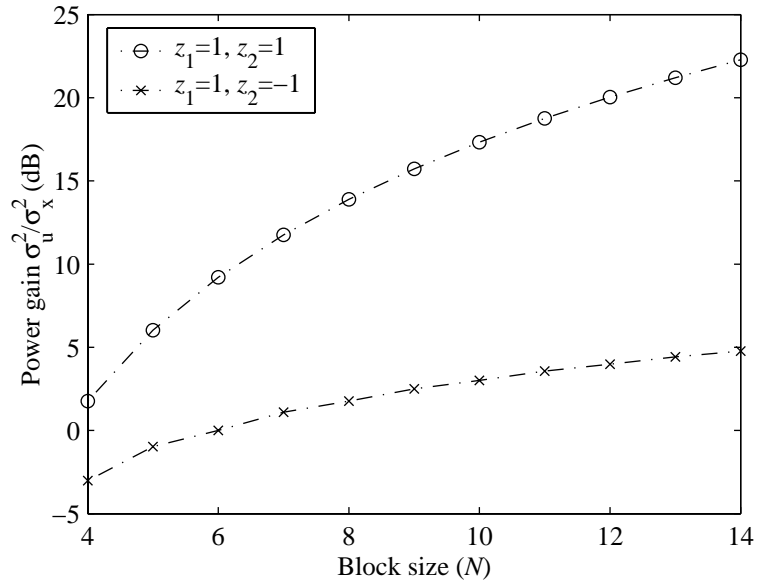


**Fig. 4.27** the power gain of two inverse filters are compared. It is evident that filters with repeated nulls require a larger transmitted power.

#### 4.5 Concluding Remarks

In this chapter, we developed a framework for pre-equalization techniques applicable for the up-stream PCM channels. It was shown that a linear pre-equalizer should provide almost an ISI free condition in order to support the transmission of  $2N$ -PAM signals with a desired constellation size ( $2N > 64$ ). For typical PCM channel filters, implementing a zero-ISI pre-equalizer requires a large transmitted power.

We investigated power spectrum methods to reduce the required transmitted power while maintaining a pseudo ISI-free solution for the pre-equalizer. A spectrum shaping technique based on redundant symbol insertion was investigated. It was shown that spectrum shaping can significantly reduce the average transmitted power. However, this technique requires to compute redundant symbols per each block of transmitted symbols.

As an alternative method, we proposed a block-by-block pre-filtering. The implementation

of the pre-filter employs a single switch in the feed-forward path of the transmitter filter to reset the channel memory. Assuming that the number of redundant symbols per block is the same as the memory length of the (FIR) channel filter, we can show that the block-by-block pre-filtering has the same performance as the spectrum shaping method obtained by redundancy insertion. Compared to a TH-precoder, the block-by-block pre-filtering does not expand the dynamic range of the data symbols, instead it adds appropriate redundancies to the input signal to cancel undesired poles of the pre-filter. The price to be paid for stabilizing the system is a reduction in the effective symbol rate.

We developed a theoretical ground for linear block-by-block pre-filtering. The average power gain of this structure can be determined in terms of the channel impulse response (Eq. (4.55)). We also determined an upper bound for the required signal level redundancy for a TH-precoder as a function of the impulse response of the channel filter (Eq. (4.55)). The power gain of a TH-precoder is almost one especially for PAM signals with a large alphabet [38, 60]. For a given channel impulse response and a fixed transmitted power, we can compare the effective bit-rate that can be obtained by a TH-precoder and a block-by-block pre-filter. In many cases the result is in the favor of the TH-precoder, especially if the channel filter includes repetitive zeros (e.g.,  $H(z) = 1 - z^{-2}$ ). This observation suggests that having redundant signal levels can be more effective than adding redundant symbols. However, as we discussed, a TH-precoder is not directly applicable to a PCM up-stream channel since the spacing between the constellation points are not uniform in general. It is important to note that the modulo arithmetic is only one way to create redundant signal levels. Other methods of creating redundant levels is a subject for our future studies.

## Chapter 5

# Filterbank Structures for ISI Channel Pre-Equalization

As described in Chapter 4, the up-stream PCM channel requires channel pre-equalization in order to avoid performance degradation due to ISI. A straightforward inverse filter is not feasible since spectral nulls of the channel filter can cause a high power gain in the pre-equalizer. We presented methods of adding redundancy to the transmitted signal in order to control the average transmitted power while compensating for the channel filter.

In this chapter, we discuss channel pre-equalization methods based on filterbank structures. A filterbank structure can provide a natural way of creating patterns of redundancy in a block of transmitted symbols. The filterbank pre-equalizer can compensate for channel filters even if they have a non-minimum phase impulse response. We compare the performance of the filterbank structure with that of the inverse pre-filtering methods presented in Chapter 4.

### 5.1 Signal design based on non-uniform sampling

Nyquist's first criterion for signal design implies that for an ISI-free data transmission over a bandlimited channel with a one-side bandwidth of  $W$  Hz, the symbol rate should be less than  $2W$  samples/sec. For an up-stream PCM channel, the symbol timing is determined by the fixed sampling rate of the A/D converter set to  $f_s = 8000$  Hz at the central office. Since the effective bandwidth of an up-stream PCM channel is less than 4000 Hz, the basic Nyquist signal design for this channel cannot prevent ISI distortion.

In a conventional Nyquist signalling, modulated waveforms carrying data symbols are trans-

mitted regularly at uniformly distributed time instants:

$$x(t) = \sum_{k=-\infty}^{\infty} a_k g(t - kT_s + \tau) \quad (5.1)$$

where  $a_k$  are transmitted symbols and  $g(\cdot)$  is a Nyquist waveform. There is a fixed timing interval of  $T_s$  sec between two consequent transmissions.

For a signalling scheme in general, the intervals between consequent transmissions do not need to be the same. According to the dimensionality theorem [61, p. 294], the maximum number of independent symbols transmitted over a channel with  $W$  Hz bandwidth is  $2W$  symbols/sec, regardless of the arrangement of symbols in a time interval. The conventional Nyquist signal design is only a special case of signalling over bandlimited channels. We review other signalling methods that can provide non-uniform symbol timing.

Inspired by non-uniform sampling methods such as those described in [62], we design a set of bandlimited waveforms that can be modulated by data symbols at non-uniformly distributed time instants. Data symbols are expected to be detectable at the receiver without any ISI distortion. For an up-stream PCM channel in particular, we would like to have symbol intervals of integer multiples of  $T_s = 1/8000$  sec. However, only a subset  $K$  of every  $N$  consecutive timing instants is permitted in order to maintain an average transmission rate of less than or equal to  $2W$  symbols/sec. We choose  $K$  and  $N$  such that:

$$\frac{K}{N} \leq 2WT_s \quad (5.2)$$

Figure 5.1 shows the transmitter structure based on the set of  $K$  linear time-invariant filters with  $K$  distinct impulse responses  $p_0(t)$  to  $p_{K-1}(t)$ . The transmitted signal  $u(t)$  can be written as:

$$u(t) = \sum_{n=-\infty}^{\infty} \sum_{k=0}^{K-1} s_k[n] p_k(t - nNT_s) \quad (5.3)$$

where  $s_0[n]$  to  $s_{K-1}[n]$  are  $K$  data symbols transmitted in a time interval of  $NT_s$  sec. At the receiver, sampling instants are integer multiples of  $T_s$ . However, out of every  $N$  consecutive samples,  $K$  samples correspond to data symbols and  $N - K$  samples are redundant.

Each waveform  $p_k(t)$  has a limited bandwidth of  $K/(2NT_s)$  Hz and is designed to avoid ISI at certain sampling instants. For an ISI-free signalling, these waveforms should satisfy the following conditions:

$$p_k(nT_s) = \begin{cases} 1 & n = k \\ 0 & n = Nm + l \end{cases} \quad (5.4)$$

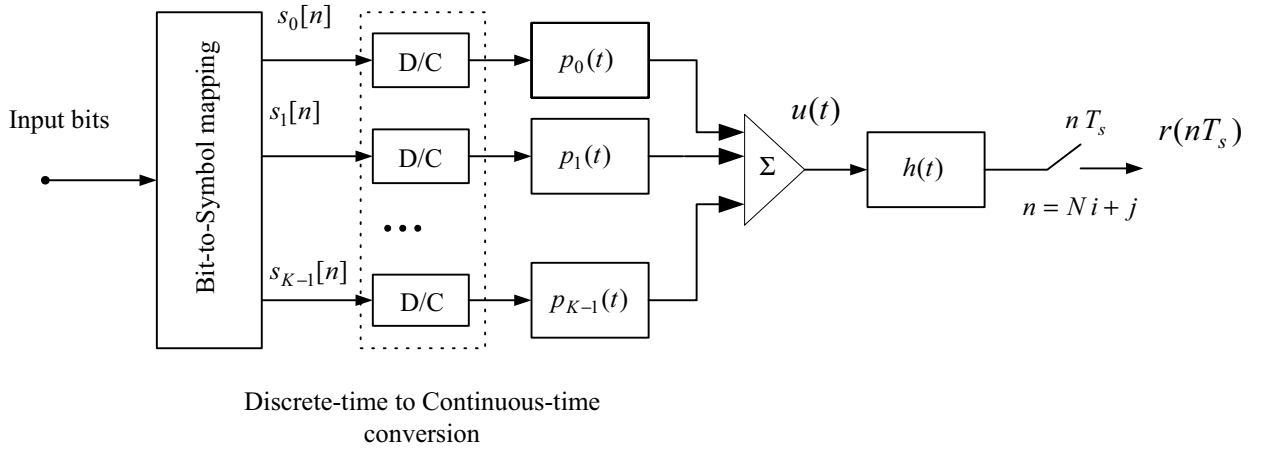


**Fig. 5.1** Signal design for a bandlimited channel with non-uniform symbol timing distribution.

where the index  $Nm + l$  points to a subset  $K$  of each  $N$  consecutive samples. Compared to a Nyquist pulse that has regular zero-crossings,  $p_k(t)$  has no constraints at a subset of sampling instants. By relaxing the constraints, we allow for ISI at particular sampling instants while reducing the required bandwidth of each waveform<sup>1</sup>.

### Example

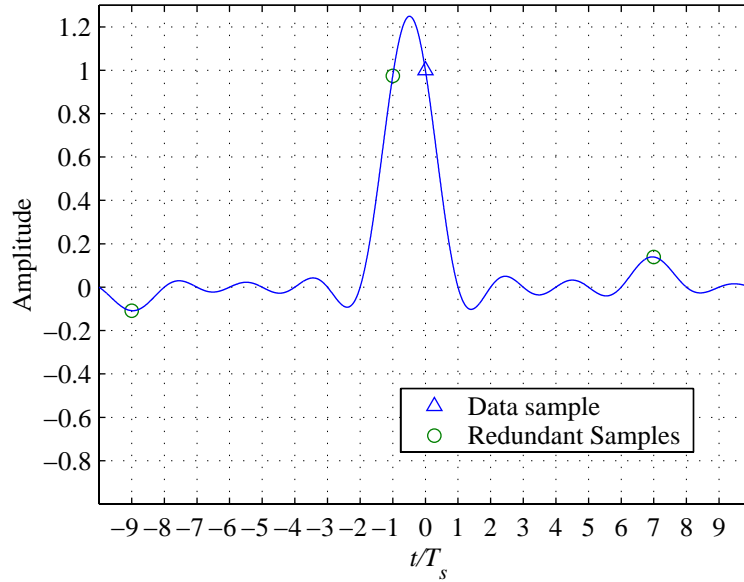
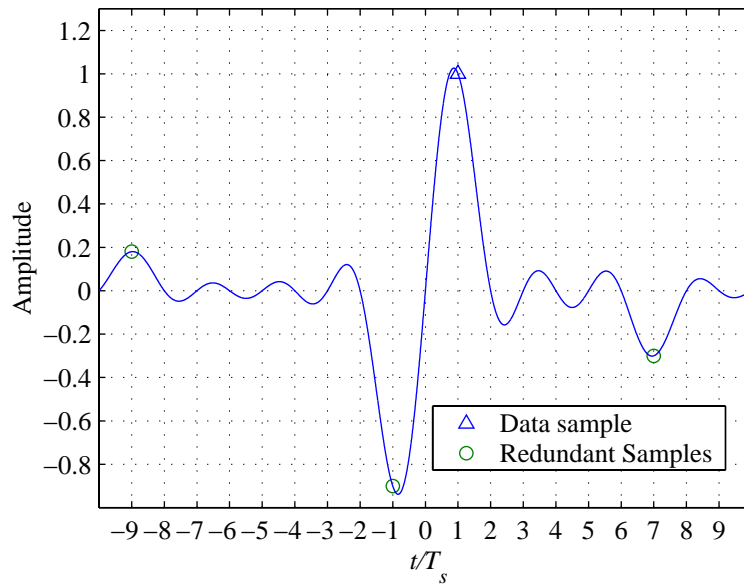
Let us assume that an up-stream PCM channel filter is modeled as an ideal brick-wall low pass filter, strictly bandlimited to 3500 Hz. We would like to design a signalling scheme for this channel that is compatible with channel bandwidth limitation and the fixed sampling rate at the receiver. By choosing  $K = 7$  and  $N = 8$  in Eq. (5.3), seven waveforms that construct the transmitted signal are determined as follows [62, 5]:

$$p_k(t) = C_k \operatorname{sinc}\left(\frac{t - kT_s}{8T_s}\right) \prod_{\substack{i=0 \\ i \neq k}}^{K-1} \sin \frac{\pi(t - iT_s)}{8T_s} \quad \text{for } k = 0, 1, \dots, 6 \quad (5.5)$$

where  $C_k$  is a normalization factor to ensure  $p_k(kT_s) = 1$ . Figure 5.2 shows two waveforms  $p_0(t)$  and  $p_1(t)$  that satisfy conditions given in Eq. (5.4). As shown, both these waveforms share the same redundant sampling instants<sup>2</sup>.

<sup>1</sup>Note that waveforms  $p_k(t)$  are different from signals with controlled ISI used in partial-response signalling. The important feature of signals  $p_k(t)$  is that the required bandwidth for these signals is less than  $1/(2T_s)$ .

<sup>2</sup>Note that other redundant samples occur outside the range shown in these figures.

(a)  $p_0(t)$ (b)  $p_1(t)$ 

**Fig. 5.2** Signal design for an up-stream PCM channel with  $W = 3500$  Hz bandwidth and sampling rate of  $1/T_s = 8000$  Hz.

### 5.1.1 Pre-equalizer design for the up-stream PCM channel

Signal design with non-uniform sampling intervals is proposed in [4] for signalling over PCM channels. The work on non-uniform signalling for PCM up-stream and down-stream channels is further studied in [5]. Assuming a brick-wall frequency response for the channel filter, the work presented in [5] describes a condition for permissible patterns non-uniform symbol intervals. In practice, the effect of the up-stream PCM channel on the transmitted signal is far from a brick-wall filter. In [5], the ideal continuous filters are replaced by discrete-time FIR filters. The coefficients of these filters are computed at the receiver by using training sequence sent by the transmitter. Filter coefficients are then fed back to the transmitter. However, such training is problematic since there is no direct access to the channel output at the up-stream receiver. Furthermore, there are no results reported on the required transmitted power for such a filterbank structure.

In the rest of this chapter we discuss filterbank structures that are specifically designed to compensate for a known FIR channel filter. We evaluate the required transmitted power for the filterbank structure and compare the results with those obtained for the block-by-block pre-filtering method described in the previous chapter.

## 5.2 Non-maximally decimated filterbanks

In this section, We discuss a filterbank structure to pre-compensate for the channel filter at the transmitter. To obtain zero ISI, the pre-equalizer should act as channel inverse filter. As discussed in Chapter 4, a direct inverse filtering for a non-minimum phase channel may require an unacceptably large transmitted power. A filterbank can provide a simple method of adding redundancy to the transmitted signal. Such filterbank structure is known as non-maximally decimated filterbanks [63, 64]. We determine conditions to obtain FIR filters for a non-maximally decimated filterbank.

Assuming that the channel is FIR and is known at the transmitter, we consider a filterbank structure that can accommodate redundant symbols along with the information-carrying symbols in the transmitted signal. Figure 5.3 shows the filterbank structure at the transmitter, the equivalent discrete-time channel with impulse response  $h[n]$ , and the sample selection process at the receiver. As shown, the input signal  $a[.]$  is parsed into  $K$  non-overlapping sequences  $a_0[.]$  to  $a_{K-1}[.]$ . Sequence  $a_i[.]$  is up-sampled by a factor of  $N(> K)$ . We design filters such that ISI in one branch and Inter-Channel Interference (ICI) between different branches are avoided.

Each branch of the filterbank contains a filter  $g_k[n]$ . We will show that these filters can be chosen to be FIR, even though the inverse filter  $1/H(z)$  is an IIR filter. Since only a subset of the received samples carry data symbols, the system can allow ISI at redundant sampling instants.

Figure 5.4 illustrates the contribution of each branch of the filterbank in the overall system

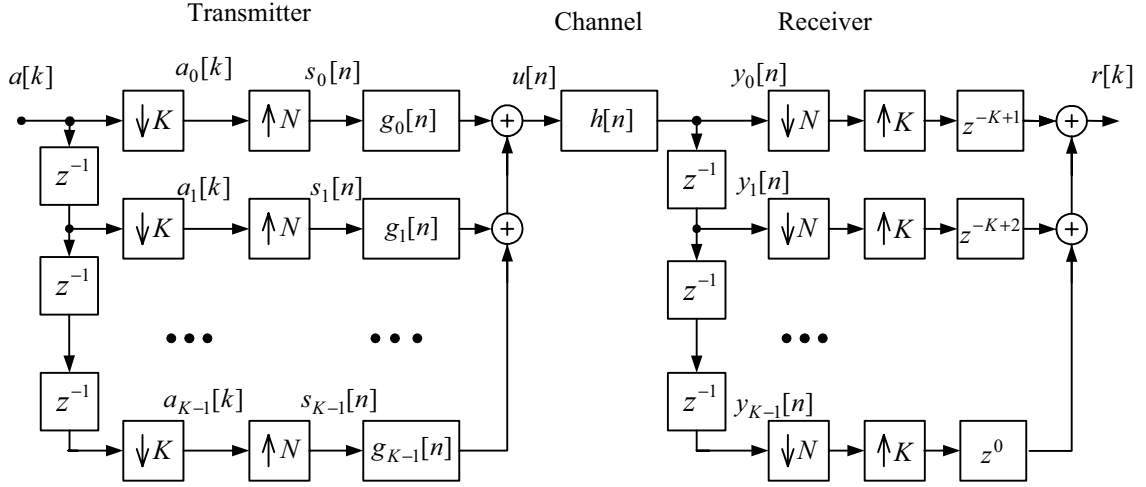


**Fig. 5.3** A non-maximally decimated filterbank structure is used to pre-equalize the channel filter. The redundant symbols are discarded at the receiver by a non-uniform down-sampler. Note that the filterbank structure at the receiver is only used to show a non-uniform down-sampling process which discards  $N - K$  redundant symbols from a block of  $N$  symbols.

response. Note that structure shown in Fig. 5.4 is functionally equivalent to the filterbank structure. Conditions imposed on the  $k^{\text{th}}$  filter to avoid ISI and ICI distortion can be formulated as:

$$g_k[n] \otimes h[n] = \begin{cases} 1 & n = k \\ d_k(i, j) & n = Ni + j, \quad 0 \leq i \leq L, \quad j \in \mathcal{S} \\ 0 & \text{otherwise} \end{cases} \quad (5.6)$$

where  $\mathcal{S}$  is a set of  $N - K$  distinct indices selected between 0 and  $N - 1$ . Note that redundant symbols  $d_k(i, j)$  are spread over  $L+1$  symbol blocks. Figure 5.4 shows an example where redundant symbols are at the end of block of  $N$  symbols. In this example we have:

$$\mathcal{S} = \{K, K + 1, \dots, N - 1\}$$

Coefficients  $d_k(i, j)$  correspond to the sampling instants that no data symbol is transmitted.

We wish to determine coefficients  $d_k(i, j)$  such that pre-equalizer filters have FIR impulse

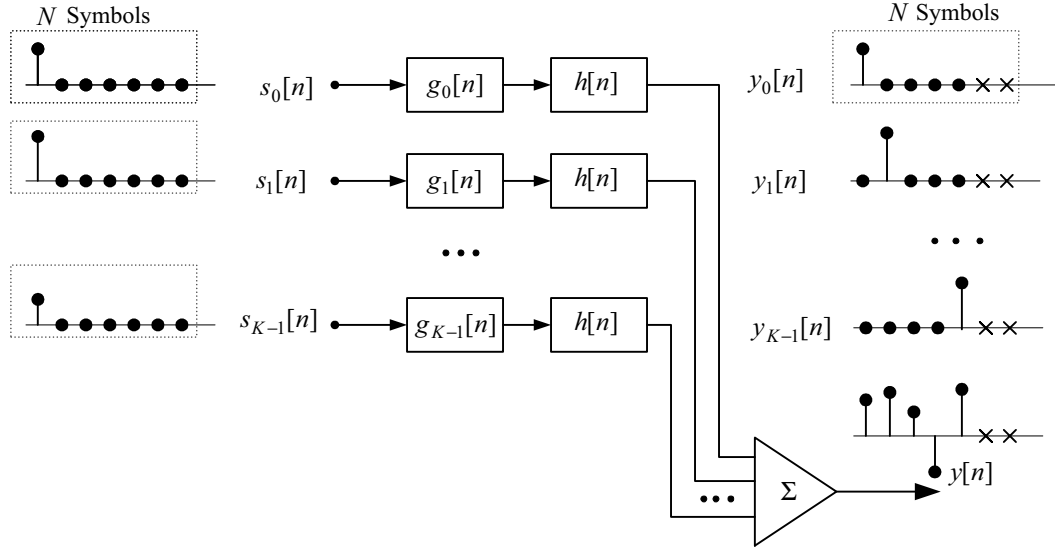


**Fig. 5.4** A set of FIR filters can partially invert the channel filter. The redundant samples are used to allow for FIR inverse filters.

response. From Eq. (5.6), we obtain:

$$\begin{aligned}
 G_k(z) &= \frac{z^{-k} + \sum_{i=0}^L \sum_{j \in \mathcal{S}} d_k(i, j) z^{(-Ni-j)}}{1 + \sum_{i=1}^M h[i] z^{-i}} \\
 &= \frac{z^{-k} + \sum_{i=0}^L \sum_{j \in \mathcal{S}} d_k(i, j) z^{(-Ni-j)}}{\prod_{i=1}^M (1 - z_i z^{-1})} \\
 &= \sum_{i=0}^{M_k-1} g_k(i) z^{-i}
 \end{aligned} \tag{5.7}$$

In order to have an FIR filter in each branch,  $G_k(z)$  should be a finite length polynomial in  $z^{-1}$ . Since  $H(z)$  has a finite number of roots, say  $M$ , the number of coefficients  $d_k(i, j)$  required for pole-zero cancellation is at least  $M$ . Assuming that polynomial  $H(z)$  has no repetitive roots,

coefficients  $d_k(i, j)$  should satisfy the following set of equations:

$$\underbrace{\begin{bmatrix} z_1^{-j_1} & z_1^{-j_2} & \dots & z_1^{-j_{N-K}} & \dots & z_1^{-(NL+j_m)} \\ z_2^{-j_1} & z_2^{-j_2} & \dots & z_2^{-j_{N-K}} & \dots & z_2^{-(NL-j_m)} \\ \dots & \dots & \dots & \dots & \dots & \dots \\ z_M^{-j_1} & z_M^{-j_2} & \dots & z_M^{-j_{N-K}} & \dots & z_M^{-(NL-j_m)} \end{bmatrix}}_{\geq M} \mathbf{d}_k = - \begin{bmatrix} z_1^{-k} \\ z_2^{-k} \\ \dots \\ z_M^{-k} \end{bmatrix} \quad (5.8)$$

where  $\{j_1, j_2, \dots, j_{N-K}\}$  are indices of redundant symbols in each block. There are at least  $M$  unknown values in the system of  $M$  equations in Eq. (5.8). As a result, there can be more than one solution for the coefficients  $d_k(i, j)$ . Among all these solutions we are interested in one that can provide a minimum transmitted power. Depending on the roots of  $H(z)$  and the pattern of redundancy, there may or may not be a solution for these equations. Below, we discuss examples to illustrate these cases.

**Example 1:**  $H(z) = 1 + z^{-1}$

Consider a channel filter with a signal null at  $z_1 = -1$ . We examine a filterbank structure with  $K=3$  branches and a block size of  $N=4$ . Since the channel filter has one root, only one redundant symbol per block is required to obtain the FIR filter in each branch. Filters of different branches are determined as follows:

$$\begin{aligned} G_0(z) &= \frac{1 + z^{-3}}{1 + z^{-1}} = 1 - z^{-1} + z^{-2} \\ G_1(z) &= \frac{z^{-1} - z^{-3}}{1 + z^{-1}} = z^{-1} - z^{-2} \\ G_2(z) &= \frac{z^{-2} + z^{-3}}{1 + z^{-1}} = z^{-2} \end{aligned} \quad (5.9)$$

For a channel filter with a single root, Eq. (5.8) has always a solution for the coefficient  $d_k(1)$ .

**Example 2:**  $H(z) = 1 - z^{-2}$

We investigate different patterns of added redundancy for different block sizes. First, we consider symbols blocks with two redundant symbols. In this case, Eq. (5.8) has always a solution for  $d_k$  since the determinant of the matrix in the left-hand side is always non-zero. Filter coefficients for

$K = 3$  and  $N = 5$  can be determined as:

$$\begin{aligned} G_0(z) &= \frac{1 - z^{-4}}{1 - z^{-2}} = 1 + z^{-2} \\ G_1(z) &= \frac{z^{-1} - z^{-3}}{1 - z^{-2}} = z^{-1} \\ G_2(z) &= \frac{z^{-2} - z^{-4}}{1 - z^{-2}} = z^{-2} \end{aligned} \quad (5.10)$$

Next, we consider one redundant symbol at the end of each block ( $N = K + 1$ ). Depending on the number of symbols  $N$  in each block, there may or may not be solution for  $d_k$ . Equation (5.8) can be written as:

$$\underbrace{\begin{bmatrix} (1)^{N-2} & (1)^{2N-2} & \dots & (1)^{NL-2} \\ (-1)^{N-2} & (-1)^{2N-2} & \dots & (-1)^{NL-2} \end{bmatrix}}_{\geq 2} \mathbf{d}_k = - \begin{bmatrix} (1)^{-k} \\ (-1)^{-k} \end{bmatrix} \quad (5.11)$$

When  $N$  is an even number, Eq. (5.11) does not provide a solution for  $\mathbf{d}_k$ . If the block length  $N$  is an odd number, there is at least one solution for the filters. For example, the set of filters for  $N = 5$  and  $K = 4$  can be computed as:

$$\begin{aligned} G_0(z) &= \frac{1 - z^{-4}}{1 - z^{-2}} = 1 + z^{-2} \\ G_1(z) &= \frac{z^{-1} - z^{-9}}{1 - z^{-2}} = z^{-1} + z^{-3} + z^{-5} + z^{-7} \\ G_2(z) &= \frac{z^{-2} - z^{-4}}{1 - z^{-2}} = z^{-2} \\ G_3(z) &= \frac{z^{-3} - z^{-9}}{1 - z^{-2}} = z^{-3} + z^{-5} + z^{-7} \end{aligned} \quad (5.12)$$

This example shows for a non-maximally decimated filterbanks there exists FIR solutions for the branch filters even if the number of redundant symbols per block is smaller than the number of zeros of the channel filter.

### Example 3: Minimum redundancy per block

We are interested in maintaining a minimum amount of redundancy per symbol block since it corresponds to a smaller reduction in the data symbol rate. For a block of  $K$  data symbols, we consider adding only one redundant symbol  $N = K + 1$ . As shown in the previous example, there are cases where no solution exists for branch filters. Here, we derive conditions under which

Eq. (5.8) has at least a solution for minimum added redundancy. Assuming that one redundant symbol is added to the end of each block of  $N - 1$  symbols, we can write Eq. (5.8) as:

$$\underbrace{\begin{bmatrix} z_1^{-(N-2)} & z_1^{-(2N-2)} & \cdots & z_1^{-(NL-2)} \\ z_2^{-(N-2)} & z_2^{-(2N-2)} & \cdots & z_2^{-(NL-2)} \\ \cdots & \cdots & \cdots & \cdots \\ z_M^{-(N-2)} & z_M^{-(2N-2)} & \cdots & z_M^{-(NL-2)} \end{bmatrix}}_{L \geq M} \mathbf{d}_{\mathbf{k}} = - \begin{bmatrix} z_1^{-k} \\ z_2^{-k} \\ \cdots \\ z_M^{-k} \end{bmatrix} \quad (5.13)$$

Note that each block of  $N$  symbols contains only one redundant symbols. We need at least  $M$  redundant symbols  $d_k(i, j)$  in order to compensate for  $M$  roots of  $H(z)$ . To ensure that at least one solution for  $\mathbf{d}_{\mathbf{k}}$  exists, the matrix in the left-hand side of Eq. (5.13) should be a full rank matrix. A condition for this matrix to be full-rank is that:

$$z_i^N \neq z_j^N \quad \text{for } 1 \leq i, j \leq M \quad (5.14)$$

The above statement can be proved by examining the determinant of the first  $M$  columns of the left-hand side matrix in Eq. (5.13). Using the properties of the determinant of Vandermonde matrix, we can show that if Eq. (5.14) holds, then the determinant of this matrix is non-zero.

### 5.2.1 IIR implementation of the FIR filters

Equation (5.7) indicates that the coefficients of each FIR filter  $G_k(z)$  are computed based on the values of  $d_k(i, j)$ . It is possible to implement filters in each branch without actually computing the coefficients  $g_k[i]$  of these FIR filters.

Let us assume that the inverse filter  $1/H(z)$  has an impulse response  $h_{inv}[n]$ . Equation (5.7) can be written in time domain as:

$$g_k[n] = h_{inv}[n - k] + \sum_{i=0}^L \sum_{j \in \mathcal{S}} d_k(i, j) h_{inv}[n - Ni - j] \quad (5.15)$$

The value of  $g_k[n]$  is forced to zero after a finite number of samples. To eliminate the tail of the inverse channel impulse response  $h_{inv}[n]$ , the impulse response is delayed, scaled and subtracted from the original impulse. In the context of FIR filter implementation, this technique has been used to implement an FIR filter as a tail-cancelling IIR filter [65].

The recursive difference equation that describes each IIR filter can be written as:

$$u_k[n] = s_k[n - k] + \sum_{i=0}^L \sum_{j \in \mathcal{S}} d_k(i, j) s_k[n - Ni - j] - \sum_{i=1}^M u_k[n - i] \quad (5.16)$$

For an IIR implementation of the filter  $g_k[n]$ , the actual coefficients of the filter are not required.

### 5.2.2 Average transmitted power

In this section, we compute the average signal power at the output of the filterbank as a function of the input signal power  $\sigma_a^2$  and filter coefficients. Input signal  $a[n]$  is assumed to be an i.i.d. random variable. As shown in Fig. 5.3, the output of the filterbank is a sum of signals from different branches. Since the input signals to these branches are independent, the output power can be written as a sum of the power at the output of each branch:

$$\mathcal{E}\{u^2[n]\} = \sum_{k=0}^{K-1} \mathcal{E}\{u_k^2[n]\} \quad (5.17)$$

The average power at the output of each branch can be written as:

$$\mathcal{E}\{u_k^2[n]\} = \frac{\sigma_a^2}{N} \sum_{i=0}^{M_k-1} |g_k(i)|^2 \quad (5.18)$$

where  $M_k$  is the length of the filter impulse response  $g_k$  in the  $k^{\text{th}}$  branch. Due to the up-sampling in each branch, the sum of squared coefficients is normalized by  $N$ . As a result, the average signal power at the output of the filterbank can be written as:

$$\mathcal{E}\{u^2[n]\} = \frac{\sigma_a^2}{N} \sum_{k=0}^{K-1} \sum_{i=0}^{M_k-1} |g_k(i)|^2 \quad (5.19)$$

This equation relates the average output power to the input signal power, filter coefficients and the block size  $N$ .

### Example

Let us consider the following channel filter:

$$H(z) = (1 - z^{-1})(1 + z^{-1})(1 - e^{j0.8\pi} z^{-1})(1 - e^{-j0.8\pi} z^{-1}) \quad (5.20)$$

We design a pre-equalizer using the filterbank structure. Several block sizes  $N$  and symbol sizes  $K$  are considered. We would like to gain the maximum throughput from the channel. The decimation ratio  $K/N$  is directly related to the data symbol-rate. As a measure of transmitted power, we use the power gain derived from Eq. (5.19). Table 5.1 shows the results. Since the filterbank structure contains only FIR filters, the transmitter power is always bounded. However, depending on the channel filter and the choice of up-sampling and down-sampling factors, the total filter gain varies widely. As shown in the previous section, for some combinations of  $N$  and  $K$ , there is no solution for the filters. From the results shown in Table 5.1, it is evident that if the number of redundant symbols per block is reduced, the average transmitted power can increase significantly.

**Table 5.1** Comparison of decimation rates and the average filterbank power gain.

$K$	$N$	Decimation Rate	$\frac{1}{N} \sum_{k=0}^{K-1} \sum_{i=0}^{M_k}  g_k(i) ^2$
4	8	0.500	4.05
5	8	0.625	35.9
6	8	0.750	36.2
7	8	0.875	no solution
5	9	0.556	6.28
6	10	0.600	8.33
7	11	0.637	10.10

### 5.3 Performance Comparison

The filterbank structure is capable of creating a zero-ISI pre-equalizer for a channel with spectral nulls. A non-maximally decimated filterbank can include different patterns of redundancy in a block of data symbols. In many cases, the number of redundant symbols can be chosen to be less than the length of the channel filter. A block-by-block pre-filtering, as discussed in Chapter 4, requires the same number of redundant symbols per block as the number of roots of the channel filter. In this section we investigate whether the more flexible pattern of redundancy provided by the filterbank can improve the performance in terms of the average transmitted power for a given data symbol-rate.

As a measure of the effective data symbol-rate, the system sampling rate is normalized by effective ratio of data symbols per block. For a system with a sampling rate of  $1/T_s$ , the effective symbol rate is  $K/(NT_s)$  symbols/sec. In examples below, we use the sampling rate corresponding to a PCM channel,  $1/T_s = 8000$  Hz.

For a channel transfer function with a single root, it is expected that the filterbank structure and block-by-block pre-filtering have equivalent performance since the number of redundant symbols per block is minimal. As an example, we consider a channel with a null at zero frequency ( $H(z) = 1 - z^{-1}$ ). Figure 5.5 shows the power gain of both filters as a function of the effective symbol-rate. The power gain for the block-by-block filter structure is computed based on Eq. (4.55). As shown, the required power gain of both structures is the same at a given data symbol rate.

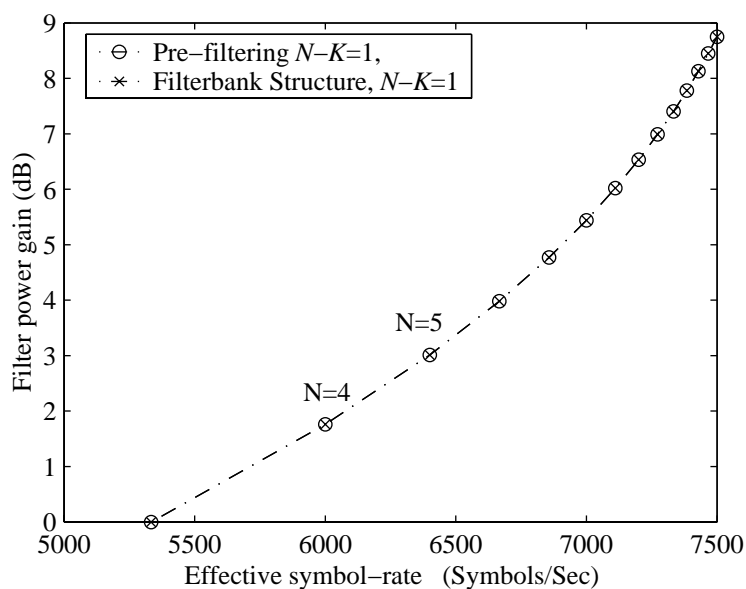


**Fig. 5.5** Power gain as a function of the effective symbol rate for  $H(z) = 1 - z^{-1}$ . The power gain for filterbank structure is similar to that of the pre-filtering structure.

When the memory length of the channel filter is larger than one, a filterbank structure can accommodate more than one pattern of redundancy. For example for a channel with a transfer function  $H(z) = 1 - z^{-2}$ , we can have one or two redundant symbols per block. Figure 5.6 shows the power gain of the filterbank structure for these two cases and compares it with that of a block-by-block pre-filtering structure. In this particular example, the power gain of the filterbank is the same for two different patterns of redundancy.

The same analysis is performed for a channel filter with transfer function:

$$H(z) = (1 + z^{-1})(1 - e^{j0.8\pi} z^{-1})(1 - e^{-j0.8\pi} z^{-1})$$

Figure 5.7 shows that the overall effect of reducing the number of redundant symbols per block to one symbol is an increase in required power for a given data symbol rate.

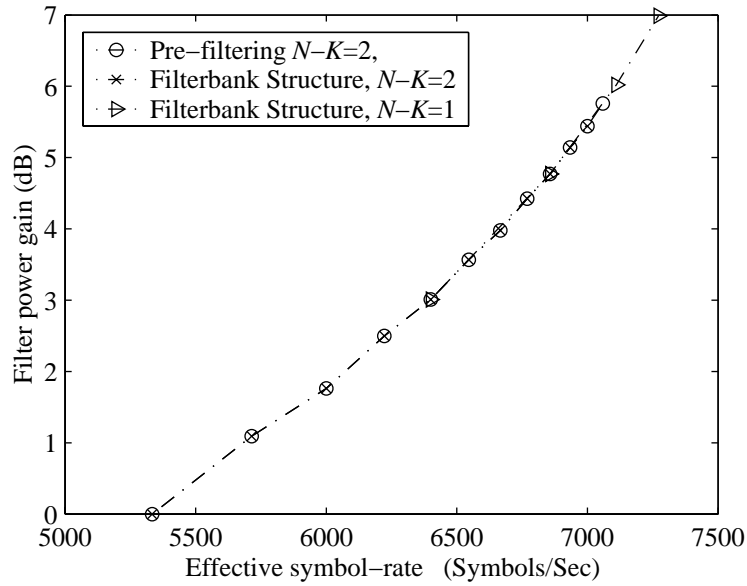


**Fig. 5.6** Power gain as a function of the effective symbol rate for  $H(z) = 1 - z^{-2}$ . The power gain for filterbank structure is similar to that of the pre-filtering structure.

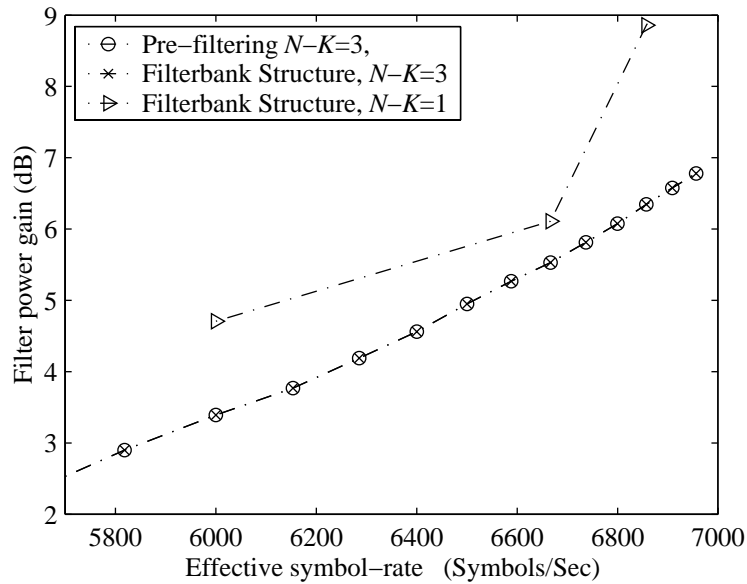


**Fig. 5.7** Power gain as a function of the effective symbol rate for  $H(z) = (1 + z^{-1})(1 - e^{j0.8\pi} z^{-1})(1 - e^{-j0.8\pi} z^{-1})$ .

The examples above suggest that although the filterbank structure is capable of accommodating more flexible patterns of redundancy in a block of symbols, the overall effect of different redundancy pattern does not reduce the required transmitted power at a given data symbol rate.

#### 5.4 Remarks

We investigated pre-equalizer structures for the up-stream PCM channel. The pre-equalizer is implemented as FIR filters within a filterbank structure. The non-maximally decimated filterbank provides a natural way of inserting redundant symbols in blocks of data symbols. Compared to block-by-block redundancy insertion discussed in Chapter 4, the filterbank structure offers more flexibility in choosing the pattern of redundancy. However, in terms of the required transmitted power, there is no gain in having patterns different than those we discussed in Chapter 4.

## Chapter 6

# A New Family of Pulse Shaping Filters

Data transmission over bandlimited channels requires pulse shaping to eliminate or control Inter-Symbol Interference (ISI). Nyquist filters provide ISI-free transmission. Here, we introduce a phase compensation technique to design Nyquist filters. Phase compensation can be applied to the square-root of any zero-phase bandlimited Nyquist filter with a normalized excess bandwidth of less than or equal to one. The resulting phase-compensated square-root filter is also a Nyquist filter. In the case of a raised-cosine spectrum, the phase compensator has a simple piecewise linear form. Such a technique is particularly useful to accommodate two different structures for the receiver, one with a filter matched to the transmitting filter and one without a matched filter.

In this chapter, a general relationship between the phase and amplitude responses of a bandlimited Nyquist filter is presented. We also show that a bandlimited zero-phase Nyquist filter can always be split into two cascaded Nyquist filters matched to one another. The special case of the square-root raised-cosine spectrum is investigated. We quantify the SNR degradation due to replacing the matched filter with a lowpass filter.

We also introduce a new family of Nyquist filters which subsumes raised-cosine filters. These “generalized raised-cosine filters” offer more flexibility in filter design. Design examples are provided to illustrate the applications of the new Nyquist filters.

### 6.1 Pulse shaping filters for voiceband PCM channels

In Section 4.1, we explained that the transmitter filter can be implemented as a discrete time filter and the only continuous-time filter required is an interpolating filter. In order for an interpolating

---

Parts of this chapter have been reported in [66] and [67]

filter not to add any ISI to the transmitted signal, the impulse response of the filter should have regular zero crossings at integer multiples of the sampling times. As we describe in the next section, filters with this property are known as Nyquist filters.

Here, we consider two scenarios for data transmission over a PCM channel: the up-stream channel, and the end-to-end PCM channel that consists of a cascade of an up-stream and a down-stream channel. Figure 6.1 shows these two scenarios. For an up-stream PCM channel, the Nyquist pulse shaping should be implemented entirely at the transmitter since there is no access to the receiver front end of this channel. In Fig. 6.1(a) the pulse shaping filter is shown as  $G_T(f)$ . For an end-to-end PCM channel<sup>1</sup>, we assume that the signal conversion from continuous-time to discrete-time and back to continuous-time, performed in the CODEC in the central office, does not cause any significant distortion. This assumption is valid only if the quantization error in the CODEC can be avoided. Figure 6.1(b) shows an end-to-end PCM channel. For the end-to-end PCM channel, we use the same filter  $G_T(f)$  at the transmitter<sup>2</sup>. We would like to use a filter matched to  $G_T(f)$  at the receiver front-end in order to maximize the signal-to-noise ratio at the sampling instants. At the same time, the cascade filter  $G_T(f)G_R(f)$  should be a Nyquist filter.

The phase compensation technique described in this chapter, provides a method of performing pulse shaping at the transmitter of an analog PCM modem, complying with two different channels: the end-to-end PCM channel where a matched filter can be implemented at the receiver, and the up-stream PCM channel where the receiver filter is fixed.

## 6.2 Nyquist filters

A conventional baseband Pulse Amplitude Modulation (PAM) signal can be represented as

$$x(t) = \sum_{k=-\infty}^{\infty} a_k g(t - kT_s) \quad (6.1)$$

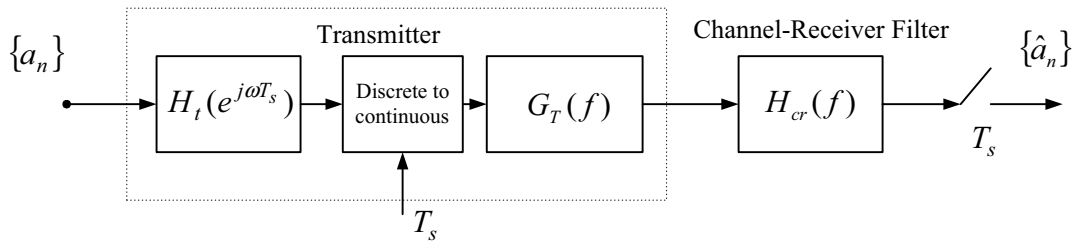
where  $a_k$ 's are the transmitted symbols and  $g(\cdot)$  is a real-valued ‘‘Nyquist pulse’’ which satisfies Nyquist’s first criterion,

$$g(kT_s) = \begin{cases} 1 & \text{for } k = 0 \\ 0 & \text{for } k = \pm 1, \pm 2, \dots \end{cases} \quad (6.2)$$

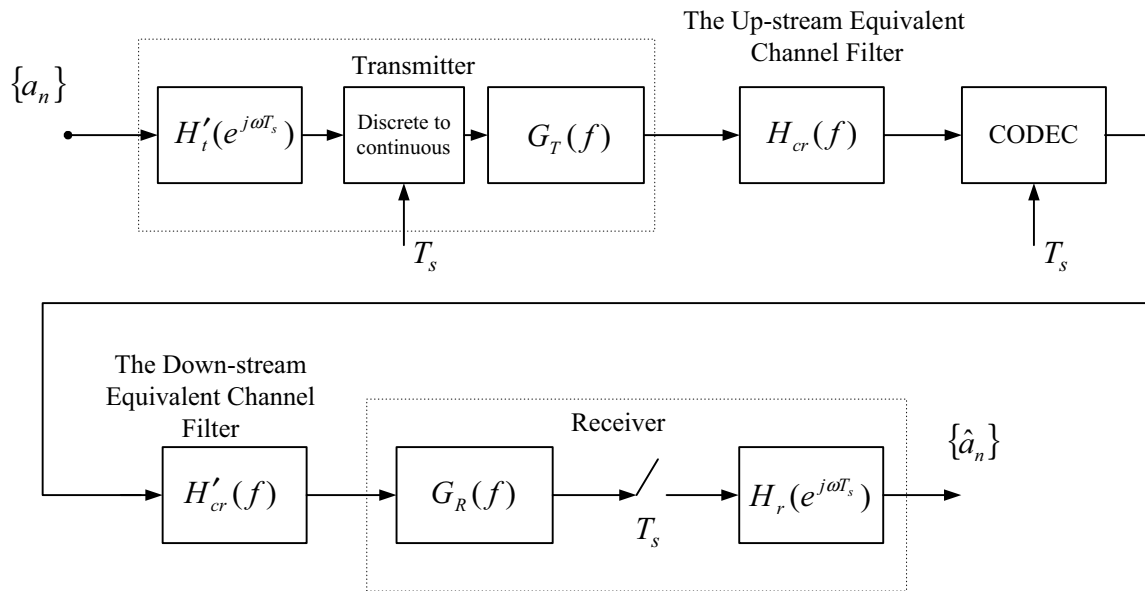
$g(\cdot)$  represents the overall impulse response of the transmitting filter, the receiving filter and the communication channel. Each transmitted symbol  $a_k$  can be recovered from the received signal

<sup>1</sup>Note that for an end-to-end PCM channel, we assume that sample timing and channel estimates are known.

<sup>2</sup>Note that the digital transmitter filter  $H'_t(f)$  can be different from the filter  $H_t(f)$  used in the up-stream channel.



(a) The up-stream PCM channel



(b) End-to-end PCM channel

**Fig. 6.1** The pulse shaping design for a PCM channel should consider two scenarios: (a) the up-stream PCM channel, where the pulse shaping is performed entirely at the transmitter as a Nyquist filter  $G_T(f)$  and, (b) an end-to-end PCM channel, where the receiving filter  $G_R(f)$  is matched to the transmitting filter  $G_T(f)$  and, at the same time, the cascaded filter of the two  $G_T(f)G_R(f)$  is also a Nyquist filter.

$x(t)$ , by taking samples of  $x(t)$  at the time instants  $kT_s$ . In other words, choosing  $g(\cdot)$  as a Nyquist pulse avoids Inter-Symbol-Interference (ISI) and allows sample-by-sample detection at the receiver. In the frequency domain, Nyquist's first criterion is written as:

$$\sum_{n=-\infty}^{\infty} G(f - \frac{n}{T_s}) = T_s \quad (6.3)$$

where  $G(f)$  is known as a Nyquist filter. A particular Nyquist filter with wide practical applications is the *raised-cosine* filter

$$G_{rc}(f) = \begin{cases} T_s & |f| \leq \frac{1-\alpha}{2T_s} \\ T_s \cos^2\left(\frac{\pi T_s}{2\alpha}\left(|f| - \frac{1-\alpha}{2T_s}\right)\right) & \frac{1-\alpha}{2T_s} \leq |f| \leq \frac{1+\alpha}{2T_s} \\ 0 & |f| > \frac{1+\alpha}{2T_s} \end{cases} \quad (6.4)$$

where  $\alpha$  is called the *roll-off factor* and takes values between zero and one. The parameter  $\alpha$  also represents the normalized *excess bandwidth* occupied by the signal beyond the Nyquist frequency  $1/2T_s$ .

In practical applications, the overall magnitude response of the Nyquist filter is split evenly between the transmitter and receiver. The phase response of the receiving filter compensates for the transmitting filter phase so that the overall filter has a linear phase:

$$\begin{aligned} G(f) &= G_T(f)G_R(f) \\ |G_T(f)| &= |G_R(f)| = \sqrt{|G(f)|} \\ \angle G_R(f) &= -2\pi f\tau_0 - \angle G_T(f) \end{aligned} \quad (6.5)$$

$G_T(f)$  and  $G_R(f)$  are the transfer functions of the transmitting and receiving filters accordingly. The receiving filter in this case is matched to the transmitting filter to maximize the signal-to-noise ratio (SNR) at the sampling time instants at the receiver [32]. The transmitting and receiving filters are typically considered to be linear phase with a nominal delay of  $\tau_0/2$  that is required to make the filters physically realizable.

### 6.2.1 Nyquist Filters with compensated phase

For Nyquist filter design a constraint on the magnitude is adequate to provide regular zero-crossing property. The phase response of the filter can be designed independently.

We consider more general phase responses for the transmitting and receiving filters. The phase

compensated transmitting filter satisfies Nyquist's first criterion. As a result, with or without a matched filter at the receiver, we obtain ISI free transmission. The ability to use a simple receiver filter (not a matched filter) is particularly useful to reduce the cost of the receiver [68].

### 6.3 Extension of Nyquist's first criterion

The transfer function of a filter  $G(f)$  with real impulse response  $g(t)$  can be expressed in terms of its magnitude and phase responses:

$$G(f) = |G(f)| \cdot e^{j\phi(f)} \quad (6.6)$$

where  $\phi(\cdot)$  is a real-valued odd function and  $|G(\cdot)|$  is a real-valued function with even symmetry. In our discussion we assume  $G(f)$  is bandlimited to  $|f| < 1/T_s$ . We consider the relationship between  $|G(f)|$  and  $\phi(f)$  such that  $G(f)$  satisfies Nyquist's first criterion. For a Nyquist filter with normalized excess bandwidth less than or equal to one, Nyquist's first criterion is written as:

$$|G(f)| \cdot e^{j\phi(f)} + |G(f - 1/T_s)| \cdot e^{j\phi(f-1/T_s)} = K \quad 0 \leq f \leq \frac{1}{T_s} \quad (6.7)$$

where  $K$  is a real constant. Following Gibby and Smith [69], we decompose Eq. (6.7) into the real and imaginary parts:

$$|G(f)| \cdot \cos \phi(f) + |G(f - 1/T_s)| \cdot \cos \phi(f - 1/T_s) = K \quad (6.8)$$

$$|G(f)| \cdot \sin \phi(f) + |G(f - 1/T_s)| \cdot \sin \phi(f - 1/T_s) = 0 \quad (6.9)$$

As shown in [69], one can combine Eq. (6.8) and Eq. (6.9) to express  $\phi(f)$  in terms of the magnitude response of  $G(f)$ :

$$\phi(f) = \arccos \left( \frac{K^2 + |G(f)|^2 - |G(f - 1/T_s)|^2}{2K|G(f)|} \right) \quad 0 \leq f \leq \frac{1}{T_s} \quad (6.10)$$

Note that for  $-1/T_s \leq f \leq 0$  the phase response  $\phi(f)$  is determined using its odd symmetry property  $\phi(-f) = -\phi(f)$ . Since the argument of the  $\arccos(\cdot)$  should be limited to one in absolute value, there may not be a real solution for  $\phi(f)$ .

#### 6.3.1 Square-root Nyquist filters

For the case of a zero-phase Nyquist filter, we can design a phase compensator for the square-root filter such that the compensated square-root filter also satisfies Nyquist's criterion. To show this,

consider the zero-phase Nyquist filter  $|G(f)|^2$ :

$$|G(f)|^2 + |G(f - 1/T_s)|^2 = T_s \quad 0 \leq f \leq \frac{1}{T_s} \quad (6.11)$$

The phase compensated square-root filter is:

$$G(f) = |G(f)| \cdot e^{j\theta(f)} \quad (6.12)$$

The phase compensator  $\theta(f)$  is chosen such that  $G(f)$  is Nyquist filter. From Eq. (6.10),  $\theta(f)$  can be expressed in terms of  $|G(f)|$  as:

$$\theta(f) = \arccos \left( \frac{A^2 + |G(f)|^2 - |G(f - 1/T_s)|^2}{2A|G(f)|} \right) \quad 0 \leq f \leq \frac{1}{T_s} \quad (6.13)$$

where  $A$  is a real constant. If we choose  $A = \sqrt{T_s}$ , the phase compensator simplifies:

$$\theta(f) = \arccos \left( \frac{|G(f)|}{\sqrt{T_s}} \right) \quad 0 \leq f \leq \frac{1}{T_s} \quad (6.14)$$

From Eq. (6.11) it is evident that  $0 \leq \frac{|G(f)|}{\sqrt{T_s}} \leq 1$ , therefore there is always a real solution for  $\theta(f)$  in Eq. (6.14).

The phase compensator can fully characterize the zero-phase Nyquist filter and the phase compensated square-root filter:

$$|G(f)|^2 = T_s \cos^2 \theta(f) \quad (6.15)$$

$$G(f) = \sqrt{T_s} \cos \theta(f) \cdot e^{j\theta(f)} \quad (6.16)$$

Note that  $|G(f)|^2$  is to within a scaling factor, the real part of  $G(f)$ :

$$|G(f)|^2 = \sqrt{T_s} \operatorname{Re}[G(f)] \quad (6.17)$$

### 6.3.2 Phase compensated square-root raised-cosine filter

The standard raised-cosine spectrum as defined in Eq. (6.4) is zero phase and satisfies Nyquist's criterion. To find the phase compensator  $\theta(f)$ , we substitute the square-root of the raised-cosine spectrum into Eq. (6.14). The resulting phase response  $\theta(f)$  is a piecewise linear function, as

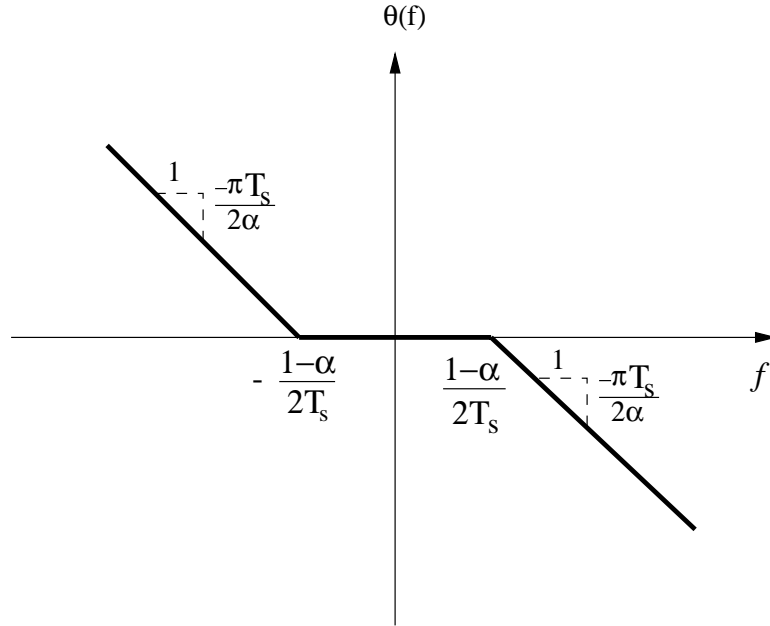


**Fig. 6.2** Piece-wise linear phase compensator for square-root raised-cosine filter.

shown in Fig. 6.2 and expressed below:

$$\theta(f) = \begin{cases} \frac{\pi T_s}{2\alpha} \left( -f - \frac{1-\alpha}{2T_s} \right) & \text{for } -\frac{1+\alpha}{2T_s} \leq f \leq -\frac{1-\alpha}{2T_s} \\ 0 & \text{for } |f| < \frac{1-\alpha}{2T_s} \\ \frac{\pi T_s}{2\alpha} \left( -f + \frac{1-\alpha}{2T_s} \right) & \text{for } \frac{1-\alpha}{2T_s} \leq f \leq \frac{1+\alpha}{2T_s} \end{cases} \quad (6.18)$$

Note that  $-\theta(f)$  can also be used for phase compensation. Therefore, for the transmitting and receiving filters, we can use  $G_T(f) = \sqrt{|G_{rc}(f)|} e^{j\theta(f)}$  and  $G_R(f) = \sqrt{|G_{rc}(f)|} e^{-j\theta(f)}$  which are individually Nyquist filters and matched to one another. Throughout our discussion here, we assume the time delay  $\tau_0$ , introduced in Eq. (6.5), is zero. A time delay can always be added to an appropriately truncated filter response to make it causal and physically realizable.

The impulse response of the phase-compensated square-root raised-cosine filter has a simple closed form:

$$g(t) = \mathcal{F}^{-1} \{ \sqrt{|G_{rc}(f)|} e^{j\theta(f)} \} = \frac{\pi}{2\sqrt{T_s}} \operatorname{sinc}\left(\frac{t}{T_s}\right) \cdot \operatorname{sinc}\left(\frac{\alpha t}{T_s} - \frac{1}{2}\right) \quad (6.19)$$

where  $\mathcal{F}^{-1}$  is the inverse Fourier transform and  $\operatorname{sinc}(x) = \sin(\pi x)/\pi x$ . The filter impulse response is expressed as a product of two terms where the first term  $\operatorname{sinc}(t/T_s)$ , provides the regular zero

crossings at integer multiples of  $T_s$ . In general, adding the phase compensator to the square-root filter changes the filter impulse response and the pulse shape may no longer be symmetric. The zero-phase square-root raised-cosine filter has a closed form impulse response with an even symmetry around the center:

$$\mathcal{F}^{-1}\{\sqrt{|G_{rc}(f)|}\} = \frac{\sin(\pi(1-\alpha)t) + 4\alpha t \cos(\pi(1+\alpha)t)}{\pi(1-(4\alpha t)^2)t} \quad (6.20)$$

Using the inverse Fourier transform of the Eq. (6.17), we can show that the impulse response of a standard raised-cosine filter is within to a scaling factor the even part of  $g(t)$ :

$$\begin{aligned} g_{rc}(t) &= \frac{\sqrt{T_s}}{2} (g(t) + g(-t)) \\ &= \frac{\pi}{4} \operatorname{sinc}\left(\frac{t}{T_s}\right) \cdot \left(\operatorname{sinc}\left(\frac{\alpha t}{T_s} - \frac{1}{2}\right) + \operatorname{sinc}\left(\frac{\alpha t}{T_s} + \frac{1}{2}\right)\right) \end{aligned} \quad (6.21)$$

which is consistent with the result given in [70, p. 62].

### 6.3.3 Special Case: Full excess bandwidth

In the case of full excess bandwidth, i.e.  $\alpha = 1$ ,  $\theta(f)$  is a linear function over the whole frequency range of the filter:

$$\theta(f) = -\frac{\pi T_s}{2} f \quad \text{for } |f| \leq \frac{1}{T_s} \quad (6.22)$$

The zero-phase square-root raised-cosine filter (no phase compensation) has the following impulse response:

$$\mathcal{F}^{-1}\{\sqrt{|G_{rc}(f)|}\} = \frac{\pi}{2\sqrt{T_s}} \operatorname{sinc}\left(\frac{t}{T_s} + \frac{1}{4}\right) \cdot \operatorname{sinc}\left(\frac{t}{T_s} - \frac{1}{4}\right) \quad (6.23)$$

The zero-crossings of the impulse response do not occur in the correct places. Adding the phase response  $\theta(f)$  to the filter delays the impulse response by a quarter of the sampling period  $T_s$ :

$$\mathcal{F}^{-1}\left\{\sqrt{|G_{rc}(f)|} e^{j\theta(f)}\right\} = \frac{\pi}{2\sqrt{T_s}} \operatorname{sinc}\left(\frac{t}{T_s}\right) \cdot \operatorname{sinc}\left(\frac{t}{T_s} - \frac{1}{2}\right) \quad (6.24)$$

Figure 6.3 shows the two impulse responses where both pulses are normalized by  $1/\sqrt{T_s}$ . Since  $\theta(f)$  causes only a pure time delay, the phase compensation does not change the pulse shape. Thus, in the case of full excess bandwidth, with or without a matched filter at the receiver, one can achieve ISI free transmission using the square-root full raised-cosine filter by merely shifting the sampling points at the receiver.

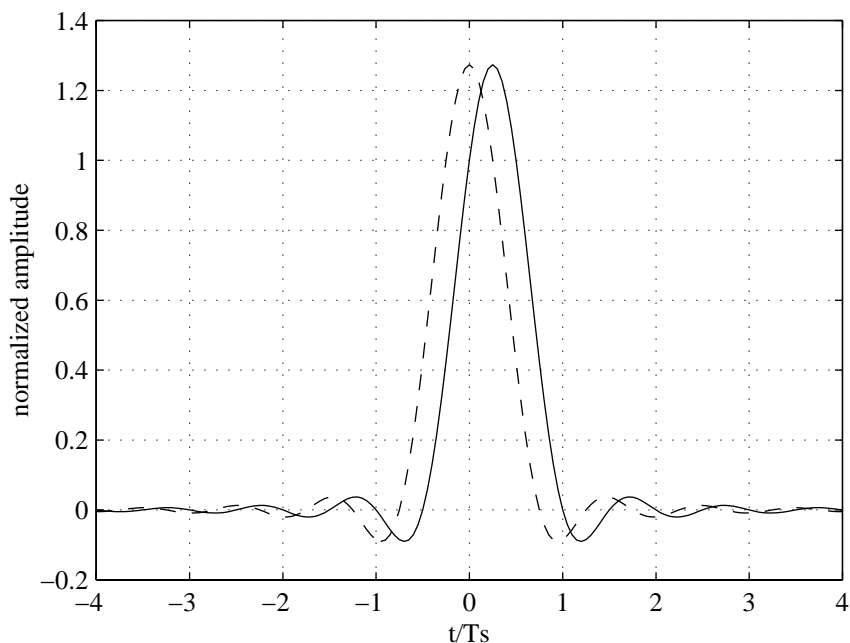


**Fig. 6.3** Normalized impulse responses of the square-root raised-cosine filter with  $\alpha=1$ , (dashed line). The phase compensated filter has a delayed impulse response (solid line).

### 6.3.4 Eye pattern diagram

Eye pattern diagrams provide a simple and effective way to measure and visualize the noise immunity of a pulse shaping scheme. Using an eye pattern, one can also assess the effect of errors in the timing phase and the sensitivity to phase jitter [38]. Here, we use the eye pattern diagrams to compare conventional raised-cosine filters with the phase-compensated square-root raised-cosine filters.

First consider a raised-cosine filter with  $\alpha=1$ ; Figure 6.4(a) shows the eye pattern of the pulse shape modulated by binary data. At integer multiples of the sampling period, each transmitted symbol can be recovered without any ISI. Figure 6.4(b) shows the eye pattern of a square-root full raised-cosine spectrum. Note that the center of the eye in Fig. 6.4(b) coincides with peak of the impulse response. For zero ISI, the sampling points should be shifted by one quarter of sampling time. However, for the special case of binary data, the center of the eye has the widest vertical opening. In fact, in Appendix C we show that the lower boundaries of the eye pattern stay constant, equal to 1 and  $-1$  for half of the sampling period around the center. The boundaries are shown in Fig. 6.4(b) as dotted lines. Compared to the eye pattern of the conventional full raised-cosine filter, the eye pattern of the square-root filter shows that it is insensitive to sampling

phase error over a large interval.

Note however, that the above results are based on the binary PAM signaling and do not generalize to a multi-level PAM signaling. Figure (6.5) illustrates the eye patterns of the same filters with 4 level input data. To avoid ISI, the sampling points for the square-root raised-cosine filter should be shifted by a quarter of sampling period.

As another example, consider the raised-cosine filter with  $\alpha=0.5$ ; Figure 6.6 shows the eye diagram for the raised-cosine and phase-compensated square-root raised-cosine filters. Due to the non-symmetric impulse response of the filter, the eye pattern of the modified square-root raised-cosine is not symmetric around the sampling points.

### 6.3.5 SNR degradation

It is well known that the use of matched filter at the receiver of an additive white Gaussian noise (AWGN) channel maximizes the signal-to-noise ratio at the sampling instants [32]. Here, we quantify the SNR degradation due to the use of a non-matched filter at the receiver.

Assume that the transmitter uses a modified square-root raised-cosine filter. The received signal is passed through a filter  $H(f)$  and is sampled at integer multiples of  $T_s$ . Let us also assume the channel adds only white Gaussian noise to the transmitted signal. The noise power at the output of the receiving filter is calculated as:

$$\sigma_n^2 = \frac{N_0}{2} \int_{-\infty}^{\infty} |H(f)|^2 df, \quad (6.25)$$

where  $N_0/2$  is the power spectral density of the noise. The signal power at the sampling instant can be written as:

$$\sigma_s^2 = \left| \int_{-\infty}^{\infty} G_T(f)H(f)df \right|^2 \quad (6.26)$$

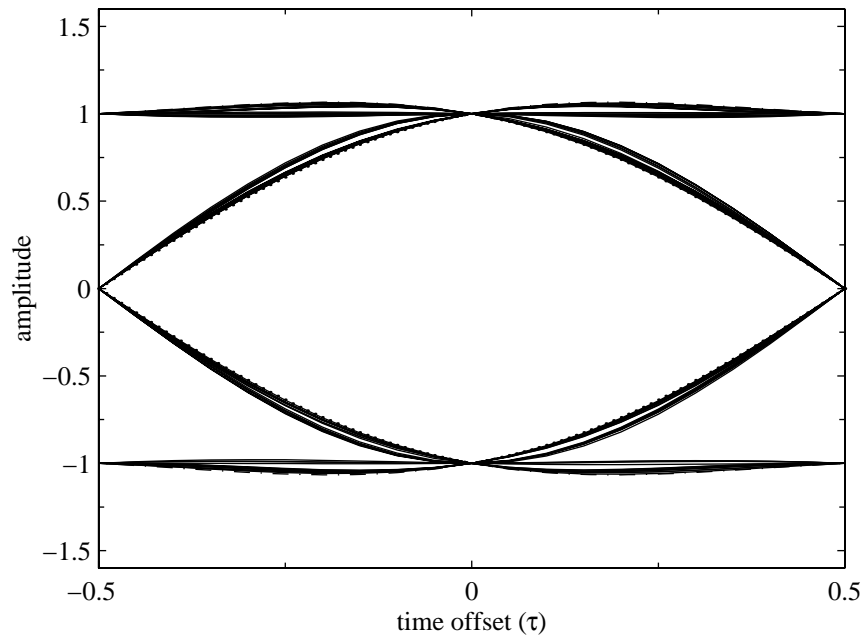
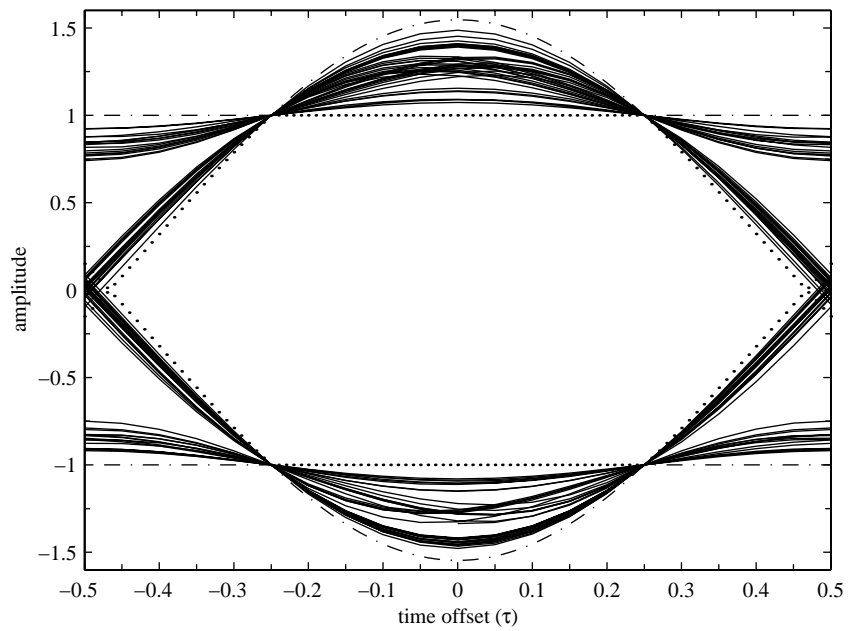
where  $G_T(f)$  is the transmitting filter. We consider two different receiving filters:

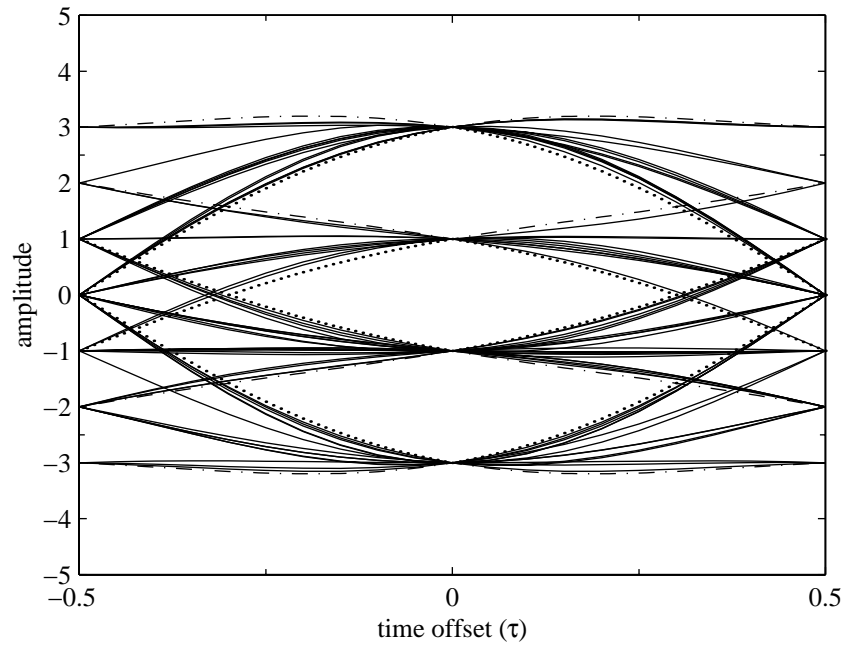
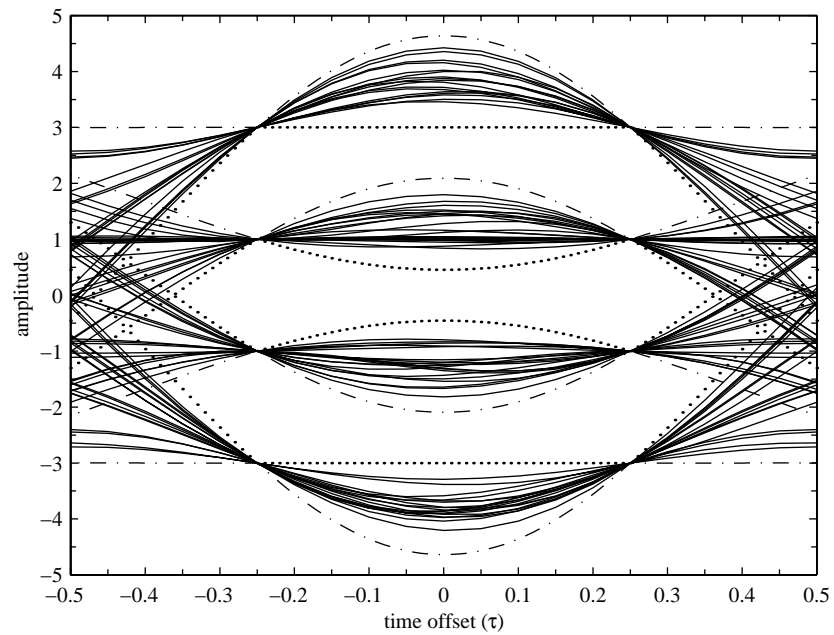
1. A filter matched to the transmitting filter:  $H(f) = G_T^*(f)$ .
2. A brick-wall filter with a pass-band region  $|f| \leq \frac{1+\alpha}{2T_s}$ .

Using the fact that the transmitting filter is normalized, the SNR after sampling is

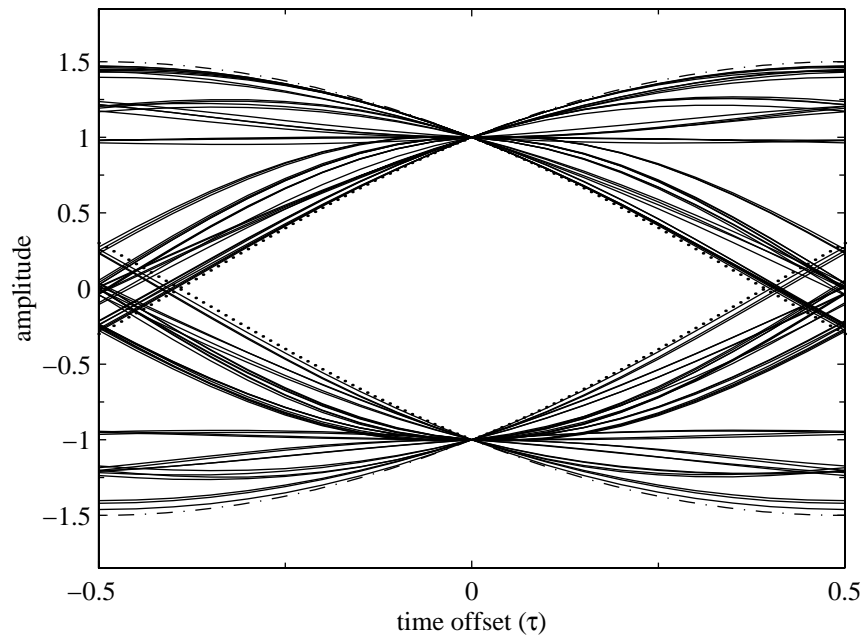
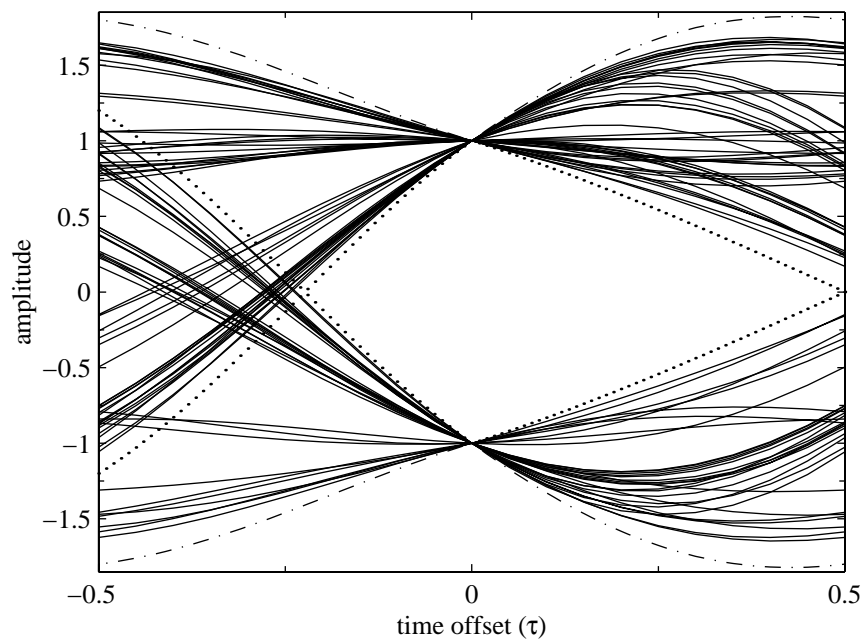
$$\text{SNR (matched)} = \frac{2}{N_0} \quad (6.27)$$

$$\text{SNR (brick-wall)} = \frac{2}{(1+\alpha)N_0} \quad (6.28)$$

(a) Raised-cosine filter with  $\alpha = 1$ .(b) Square-root raised-cosine filter with  $\alpha = 1$ .**Fig. 6.4** Binary eye patterns for a raised-cosine filter and a square-root raised-cosine filter.

(a) Raised-cosine filter with  $\alpha = 1$ .(b) Square-root raised-cosine filter with  $\alpha = 1$ .

**Fig. 6.5** Eye patterns (4 level PAM) for a raised-cosine filter and a square-root raised-cosine filter.

(a) Raised-cosine filter with  $\alpha = 0.5$ .(b) phase-compensated square-root raised-cosine filter with  $\alpha = 0.5$ .**Fig. 6.6** Binary eye patterns for a raised-cosine filter and a phase compensated square-root raised-cosine filter.

Equations (6.27) and (6.28) show that there will be a  $10 \log_{10}(1 + \alpha)$  dB loss if the matched filter is replaced by an ideal brick-wall filter. For instance, for  $\alpha = 0.5$  the loss is 1.76 dB.

## 6.4 Generalized Raised-Cosine Filters

We use the phase compensation technique, discussed in Section 6.3, to characterize a more general family of Nyquist filters. Compared to the conventional raised-cosine filters, the new filters offer more flexibility in filter design. For instance, the rate of asymptotic decay of the filter impulse response may be increased, or the residual ISI introduced by truncation of the impulse response may be minimized.

### 6.4.1 Nyquist filter design using phase compensation

We derive a sufficient condition for a real-valued odd function  $\theta(f)$  so that the zero-phase bandlimited filter in Eq. (6.15) and the phase compensated square-root filter in Eq. (6.16) satisfy Nyquist's first criterion. Note that the filters are bandlimited to  $|f| < 1/T_s$ . The ISI-free condition for both filters can be expressed as:

$$\sqrt{T_s} \cos \theta(f) \cdot e^{j\theta(f)} + \sqrt{T_s} \cos \theta(f - 1/T_s) \cdot e^{j\theta(f-1/T_s)} = \sqrt{T_s} \quad 0 \leq f \leq \frac{1}{T_s} \quad (6.29)$$

Solving for  $\theta(f)$ , we obtain the following condition:

$$\theta(f) + \theta(1/T_s - f) = n\pi + \frac{\pi}{2} \quad 0 \leq f \leq \frac{1}{T_s} \quad (6.30)$$

where  $n$  is an integer. Note that we use the odd symmetry of  $\theta(f)$  to obtain this result.

Using the condition developed for the phase compensator in Eq. (6.30), we introduce a general family of Nyquist filters. The standard raised-cosine filter for any normalized excess bandwidth can be regarded as a special case of this family of filters.

Let us define a real-valued monotonic odd function  $V(x)$  which satisfies the following conditions:

$$\begin{aligned} V(x) &= -V(-x) \\ V(x) &= 1 \quad x \geq 1 \end{aligned} \quad (6.31)$$

Consider a real-valued odd function  $\phi(f) = -\phi(-f)$  defined as:

$$\phi(f) = -\frac{\pi}{4} V\left(\frac{2T_s}{\alpha} \left(f - \frac{1}{2T_s}\right)\right) - \frac{\pi}{4} \quad f \geq 0 \quad (6.32)$$

It can be verified that  $\phi(f)$  satisfies Eq. (6.30) therefore, the following filters satisfy Nyquist's first criterion:

$$\begin{aligned} H_G(f) &= T_s \cos^2 \phi(f) \\ H_{s\text{qrt}}(f) &= \sqrt{T_s} \cos \phi(f) e^{j\phi(f)} \end{aligned} \quad (6.33)$$

We call  $H_G(f)$  a generalized raised-cosine filter. If  $V(x)$  is a increasing function for  $-1 < x < 1$ ,  $H_G(f)$  corresponds to a low-pass filter with monotonically decreasing spectrum. The phase-compensated square-root of  $H_G(f)$  is denoted by  $H_{s\text{qrt}}(f)$ . The standard raised-cosine filter, defined in Eq. (6.4), is a special case of  $H_G(f)$  where

$$V(x) = \begin{cases} -1 & x < -1 \\ x & -1 \leq x \leq 1 \\ +1 & x > +1 \end{cases} \quad (6.34)$$

The impulse response of  $H_{s\text{qrt}}(f)$  does not have a closed form in general. In Appendix D, we show that:

$$\begin{aligned} h_{s\text{qrt}}(t) &= \mathcal{F}^{-1}\{H_{s\text{qrt}}(f)\} \\ &= \frac{1}{\sqrt{T_s}} \text{sinc}\left(\frac{t}{T_s}\right) \cdot \left( \cos\left(\frac{\pi t \alpha}{T_s}\right) + \frac{\pi \alpha t}{T_s} \int_0^1 \cos\left(\frac{\pi}{2} V(x) - \frac{\pi t \alpha}{T_s} x\right) dx \right) \end{aligned} \quad (6.35)$$

The first term,  $\text{sinc}(t/T_s)$ , provides regular zero crossings at integer multiples of  $T_s$  except at  $t = 0$ . In the case of conventional raised-cosine filter, the impulse response has a closed form as shown in Eq.(6.19). In more general cases, the impulse response must be evaluated numerically. Decomposing the impulse response into two terms as shown in Eq. (6.35) facilitates the numerical evaluation.

The impulse response of  $H_G(f)$ , denoted by  $h_G(t)$ , is to within a scaling factor the even part of  $h_{s\text{qrt}}(t)$  (see Eq. (6.17)):

$$\begin{aligned} h_G(t) &= \frac{\sqrt{T_s}}{2} \left( h_{s\text{qrt}}(t) + h_{s\text{qrt}}(-t) \right) \\ &= \text{sinc}\left(\frac{t}{T_s}\right) \cdot \left( \cos\left(\frac{\pi t \alpha}{T_s}\right) + \frac{\pi \alpha t}{T_s} \int_0^1 \sin\left(\frac{\pi}{2} V(x)\right) \cdot \sin\left(\frac{\pi t \alpha}{T_s} x\right) dx \right) \end{aligned} \quad (6.36)$$

A family of Nyquist filters is also presented in [68] which with or without a matched filter at the receiver satisfy the ISI-free conditions. Each filter in this family is characterized by a real-valued continuous function  $\nu(x)$  which ‘‘controls the transfer band of the filters’’. We can rewrite the family of filters presented in [68] in the form of a phase-compensated square-root filter, described

in Eq. (6.16). In fact, Xia's Nyquist filters belong to the family of generalized raised-cosine filters in Eq. (6.33) with  $\alpha \leq 1/3$ .

## 6.5 Design examples

In this section, we provide examples of Nyquist filter design using generalized raised-cosine filters. In practice, it is important that the transmitting and receiving filters be well approximated with short impulse responses [71, 72]. From this point of view, the standard raised-cosine filter is not necessarily the best choice for Nyquist filter design. We consider two design examples. First, a family of Nyquist pulses is designed such that these pulses have faster asymptotic decay than the raised-cosine filter impulse responses. In the second example, Nyquist filters are designed such that the inter-symbol interference (ISI) caused by truncation of the transmitting and receiving filters is minimized.

### 6.5.1 Nyquist filters with smoother spectra

It is a well known result that if the amplitude response of a filter along with its first  $(K-1)$  derivatives are all continuous but its  $K$ th derivative is discontinuous, the filter impulse response asymptotically decays as  $1/|t|^{K+1}$  [56]. Based on this result, the impulse response of a raised-cosine filter decays asymptotically as  $1/|t|^3$ . Using the generalized raised-cosine spectrum, we can design filters with higher rates of decay of their impulse responses. We use a family of polynomials  $P_n(x)$  to design the generalized raised-cosine spectra of Eq. (6.33) with higher degrees of continuity:

$$V(x) = \begin{cases} -1 & x < -1 \\ P_n(x) & -1 \leq x \leq 1 \\ 1 & x > 1 \end{cases} \quad (6.37)$$

where  $V(x)$  specifies the phase compensator in Eq. (6.32). To satisfy condition Eq. (6.31),  $P_n(x)$  should be an odd function of  $x$ :

$$P_n(x) = \sum_{k=1}^n a_k \cdot x^{2k-1}$$

where  $a_k$ 's are real-valued coefficients and  $a_n$  takes on a non-zero value. Furthermore, the coefficients  $a_k$ 's are determined such that  $V(x)$  and its first  $(n-1)$  derivatives are continuous at

$x = \pm 1$  which results in the following expression:

$$P_n(x) = \frac{\int_0^x (1-u^2)^{n-1} du}{\int_0^1 (1-u^2)^{n-1} du} \quad n = 1, 2, 3, \dots \quad (6.38)$$

The first derivative of  $P_n(x)$  is a polynomial of degree  $(2n-2)$  with  $(n-1)$  repeated roots at  $x=1$  and by symmetry  $(n-1)$  repeated roots at  $x = -1$ . Since the first derivative of  $P_n(x)$  has no roots in  $-1 < x < 1$  interval,  $P_n(x)$  is monotonic in this interval. Figure 6.7 illustrates the first five polynomials of this family<sup>3</sup>. The actual polynomials  $P_n(x)$  are given in Table 6.1. Note that  $P_1(x)$  generates the standard raised-cosine filter. Using a Taylor series, we can show that the generalized raised-cosine spectrum corresponding to  $P_n(x)$  has  $(2n-1)$  continuous derivatives and its impulse response decays asymptotically as  $1/|t|^{2n+1}$ .

The rate of decay describes only the asymptotic behavior of the impulse response and does not characterize the impulse response for the first few lobes around the center. Figure 6.8 compares the impulse responses of two generalized raised-cosine filters generated from polynomials  $P_1(x)$  and  $P_2(x)$ . The excess bandwidth in this case corresponds to  $\alpha=0.5$ . Figure 6.8(a) shows that for the first few lobes  $|h_2(t)|$  is larger than  $|h_1(t)|$ . As shown in Fig. 6.8(b), only for the lobes farther away from the center is  $h_2(t)$  smaller than  $h_1(t)$ .

Apart from the rate of decay of the filter impulse response, there are other issues to be considered. Since timing recovery at the receiver is not always perfect, we encounter timing phase jitter. The eye pattern diagram of a pulse shape can be used to assess the immunity of the pulse to timing phase jitter. Using polynomials given in Table 6.1, we design five generalized raised-cosine filters with  $\alpha = 1$  and normalized sampling period. Figure 6.9 shows the inner boundaries of the binary eye diagrams associated with the impulse responses of these filters. As we increase the number of continuous derivatives of the spectrum, the width of the eye diagram decreases (see Table 6.1).

**Table 6.1** Comparison of several generalized raised-cosine filters with  $\alpha = 1$ .

n	$P_n(x)$	Decay	Eye-width
1	$x$	$ t ^{-3}$	1.000
2	$2^{-1}(-x^3 + 3x)$	$ t ^{-5}$	0.911
3	$2^{-3}(3x^5 - 10x^3 + 15x)$	$ t ^{-7}$	0.843
4	$2^{-4}(-5x^7 + 21x^5 - 35x^3 + 35x)$	$ t ^{-9}$	0.791
5	$2^{-7}(35x^9 - 180x^7 + 378x^5 - 420x^3 + 315x)$	$ t ^{-11}$	0.750

<sup>3</sup> $P_1(x)$  and  $P_3(x)$  correspond to examples presented by Xia [68]

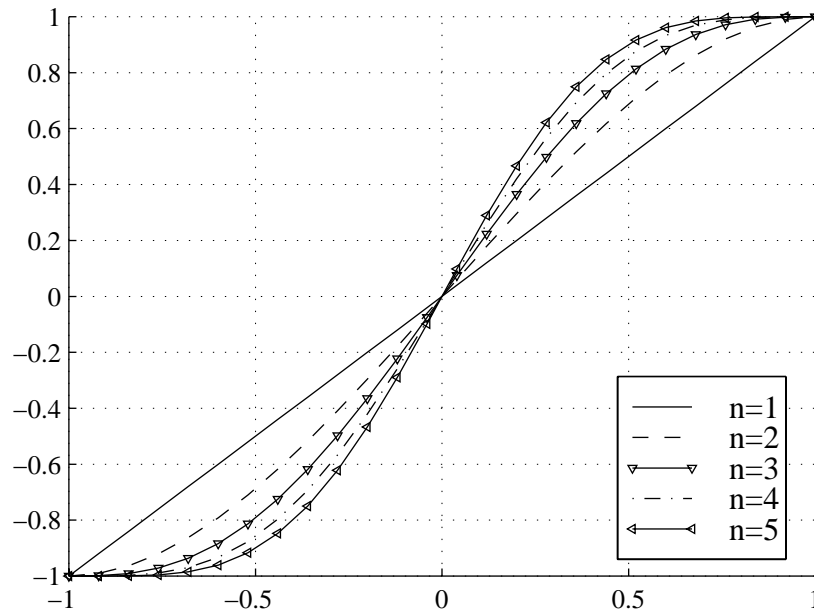


Fig. 6.7 Polynomials  $P_n(x)$  to generate the generalized raised-cosine filter.

### 6.5.2 Nyquist filters with reduced ISI due to truncation

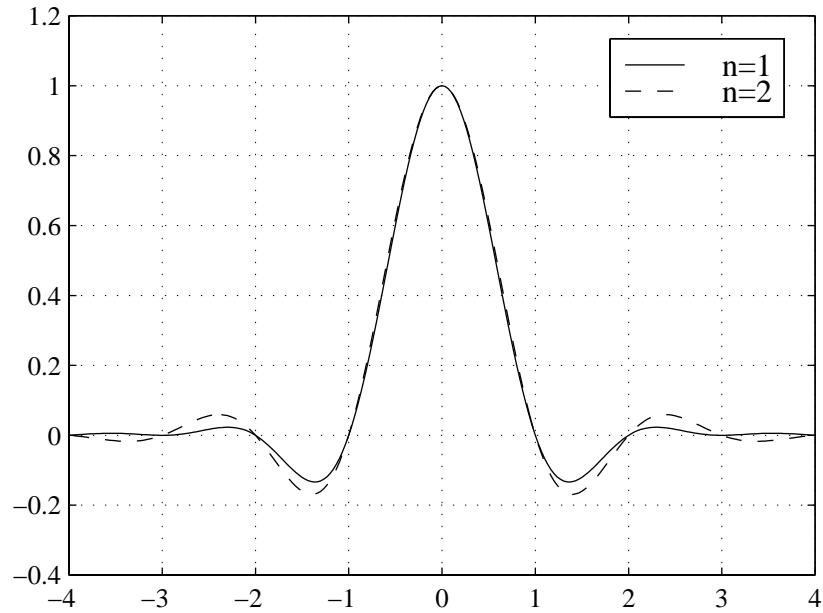
As shown in Section 1, pulse shaping can be split between the transmitter and the receiver so that the overall response satisfies Nyquist's first criterion (see Eq. (6.5)):

$$g(t) = g_T(t) * g_R(t) \quad (6.39)$$

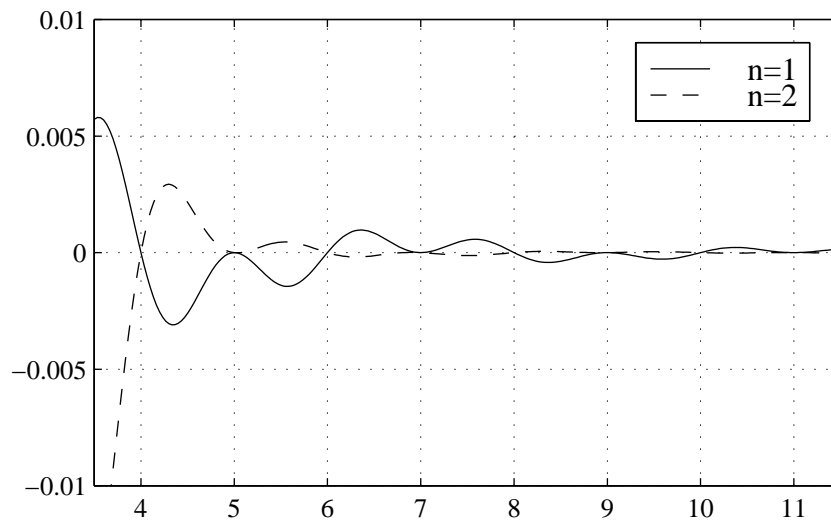
Truncating a Nyquist pulse does not affect its Nyquist zero-crossing property. However, the convolution of the truncated responses will in general no longer satisfy Nyquist's first criterion.

Here we use generalized raised-cosine filters to design Nyquist filters with minimized ISI due to impulse response truncation. To study the effect of truncating the impulse response of the square-root filter, we consider the following conditions:

- We assume that the compensated square-root generalized raised-cosine filters are used at the transmitter and the receiver. In this example we assume the channel is ideal with additive noise.



(a) The main lobes of the impulse responses



(b) Extended scale view of the tails

**Fig. 6.8** Impulse responses of generalized raised-cosine filters generated by  $P_1(x)$  and  $P_3(x)$  are compared.

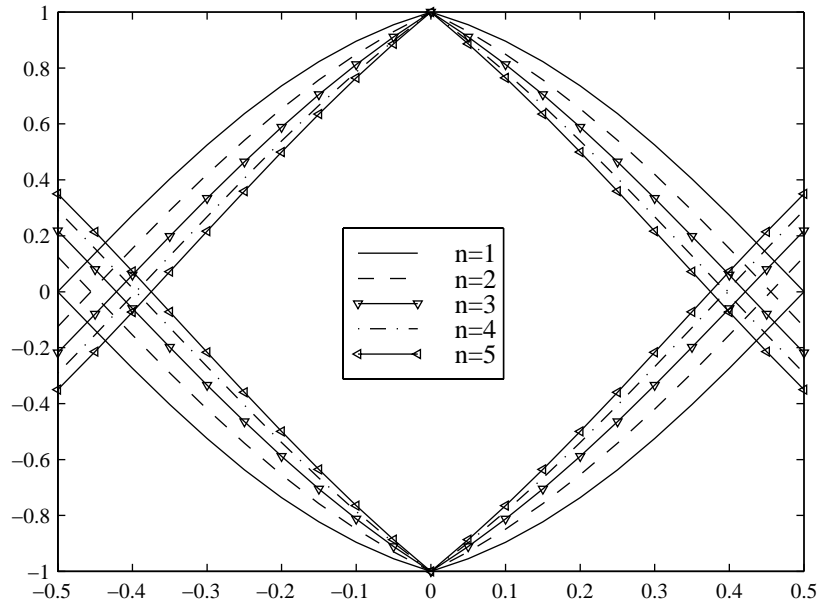


**Fig. 6.9** Inner boundaries of the eye diagram for several generalized raised-cosine filters with  $\alpha = 1$ .

- To specify the generalized raised-cosine filter of Eq. (6.33), we define  $V(x)$  as follows:

$$V(x) = \begin{cases} -1 & x < -1 \\ P(x) & -1 \leq x \leq 1 \\ 1 & x > 1 \end{cases} \quad (6.40)$$

where  $P(x)$  is a polynomial defined as:

$$P(x) = \frac{\int_0^x (1 + p_1 u^2)(1 + p_2 u^2) du}{\int_0^1 (1 + p_1 u^2)(1 + p_2 u^2) du} \quad (6.41)$$

To obtain a monotonic function  $V(x)$ , both  $p_1$  and  $p_2$  should be greater than or equal to  $-1$ . Note that for  $p_1 = p_2 = 0$ ,  $P(x) = x$  which generates the phase compensated standard raised-cosine filter. For  $p_1 = p_2 = -1$ ,  $P(x) = P_3(x)$  as defined in Eq. (6.38).

- To calculate samples of the impulse response of the transmitting and receiving filters, we evaluate Eq. (6.35) numerically. Each impulse response is calculated for  $N \cdot M$  points where  $M$  is the up-sampling ratio and  $N$  is the number of lobes in each truncated impulse response. Numerical results are presented for  $M=20$ .

- The overall impulse response is determined by convolving the impulse responses of the truncated transmitting and receiving filters.
- To measure the ISI caused by truncation, we use the peak distortion criterion [41]:

$$D_{peak} = \frac{1}{h(0)} \sum_{\substack{n=-N \\ n \neq 0}}^N |h(nT_s)| \quad (6.42)$$

where  $h(t)$  is the overall impulse response.

Table 6.2 shows the results for several values of normalized excess bandwidth  $\alpha$ . In each case the parameters  $p1$  and  $p2$  are found using an optimization procedure to minimize  $D_{peak}$ . The corresponding polynomial  $P(x)$  is given in the second column of the table. For each  $\alpha$  two values of  $D_{peak}$  are presented. The “Minimized  $D_{peak}$ ” value corresponds to the filter generated by  $P(x)$  and the “Standard  $D_{peak}$ ” value corresponds to the filter generated by  $P(x) = x$  which is a phase compensated square-root of the standard raised-cosine filter. In all cases the optimized filters produce less ISI due to truncation of the impulse responses.

To calculate probabilities of error, we assume a white Gaussian additive noise corrupts the transmitted signal. An upper bound for probability of error for binary data can be found in terms of  $D_{peak}$  [41]:

$$\hat{P}_e = Q\left(\frac{1 - D_{peak}}{\sigma}\right) \quad (6.43)$$

where  $\sigma$  is the standard deviation of the noise and  $Q(x) = \frac{1}{\sqrt{2\pi}} \int_x^\infty e^{-t^2/2} dt$ . For example, consider the second row of Table 6.2. If the probability of error with zero ISI ( $D_{peak}=0$  for  $N=\infty$ ) is  $10^{-6}$ , then with  $D_{peak}=0.104$ , the worst case bound for the probability of error is  $\hat{P}_e=1.02 \times 10^{-5}$ . For  $D_{peak}=0.192$ , we obtain  $\hat{P}_e=6.13 \times 10^{-5}$ .

Table 6.2 also shows that for smaller values of  $\alpha$ , truncating the filter impulse response causes a larger distortion. Comparing different rows of the table, we notice that filters with smaller excess bandwidth have larger ISI due to truncation even though they have larger truncation lengths.

## 6.6 Remarks

We have shown that any zero-phase bandlimited Nyquist filter with normalized excess bandwidth can be split into two cascaded Nyquist matched filters. Each filter consists of the square-root of the overall response along with a phase compensator. We have expressed the phase compensator in terms of the square-root magnitude response of the overall filter.

The phase compensation can be applied to the square-root of a standard raised-cosine spectrum. The required phase response in this case is a simple piecewise linear function. For standard

**Table 6.2** Nyquist filter design to reduce ISI due to truncation.

$\alpha$	$P(x)$	$N$	Truncation effects	
			Minimized $D_{peak}$	Standard $D_{peak}$
0.10	$0.4799x^5 + 0.3827x^3 + 0.1373x$	14	0.125	0.216
0.15	$0.3147x^5 + 0.4259x^3 + 0.2594x$	10	0.104	0.192
0.25	$0.2951x^5 + 0.4269x^3 + 0.2780x$	6	0.089	0.194
0.50	$-0.0105x^5 - 0.1775x^3 + 1.1879x$	6	0.015	0.046
0.75	$-0.0145x^5 - 0.2122x^3 + 1.2267x$	4	0.011	0.052
1.00	$0.0192x^5 + 0.1844x^3 + 0.7964x$	4	0.004	0.010

raised-cosine filter with  $\alpha=1$ , the square-root filter satisfies Nyquist's first criterion, provided an appropriate time delay is added to the impulse response.

Using the phase compensation technique, we have extended the family of raised-cosine filters to a more general family of Nyquist filters. Compared to the standard raised-cosine spectrum, the family of generalized raised-cosine filters provides more flexibility for designing Nyquist filters. As an example, we designed a family of Nyquist filters with smoother spectra. The impulse responses of these filters have higher asymptotic rates of decay. We also designed transmitting and receiving filters such that when we truncate the impulse responses of these filters, the overall impulse response has a reduced ISI.

The work reported in [66, 67] on generalized raised-cosine filters was followed by other research groups for different applications such as the relationship between orthogonal wavelet functions and Nyquist pulses [73], window design for Harmonic analysis [74], and data transmission applications [75].

## Chapter 7

# Concluding Remarks

This thesis has presented design methods which allow the data transmission rate of a PCM voiceband channel in a public switched telephone network to approach channel capacity. These methods take into account the underlying structure of the PCM encoder/decoder to avoid or reduce the distortion due to the signal conversion at the central office. PCM voiceband channels can be categorized into three different types of digital communication channels where the predetermined structural constraints appear in the transmitter back-end (as in the down-stream PCM channels), the receiver front-end (as in the up-stream PCM channels), or the tandem connection of two channels (as in the end-to-end PCM channels).

Our particular interest is the up-stream PCM channel in which the communication system designer has no control on the receiver front-end. Such a constraint creates many unconventional questions in the theory and practice of the modem design. We tackle several problems in modulation, channel equalization and pulse shaping filter design for this channel.

In the PCM voiceband channel, the appropriate choice of modulation scheme is a baseband PAM modulation that matches the structure of the PCM encoder at the receiver. We have described constellation design methods to satisfy the average signal power constraint and minimize the probability of symbol error. For a reliable communication over the up-stream channel the average number bits per information symbol should be less than 7.1 bits/symbol.

We have investigated the problem of index mapping and its potential contribution in the probability of bit error. Our new design method of index mapping can reduce the bit error rate without reducing the transmission data rate. As an example, the proposed hybrid bit-to-symbol mapping algorithm can reduce the probability of bit error by a factor of 2-3 for a frame of 7 symbols.

We have considered a non-equally-probable signal constellation design to obtain a shaping gain in the constellation design. We have also investigated the application of the Huffman algorithm

to implement the bit-to-symbol mapping to obtain a shaping gain. The resulting system has a variable rate due to the variable number of bits assigned to symbols. The overall effect of non-equally probable constellation design is an increase in the transmission rate in the range of 1–2 kbits/sec.

A PCM up-stream channel has a limited bandwidth and a fixed sampling rate at the receiver. The sampling rate is larger than twice the effective bandwidth of the channel. The combination of these constraints leads to inter-symbol interference at the sampling instants at the receiver. We have investigated design techniques to compensate for the channel at the transmitter. With an average power constraint, a linear transmitter filter alone is not adequate to fully compensate for the channel in all cases. We have proposed methods to add redundancy to the transmitted data.

The redundancy is added so that the power spectrum density of the transmitted symbols at the input of the transmitter filter closely follows a desired shaping function. We have also identified three different solutions for the desired shaping function in terms of the channel frequency response. Spectral shaping is used to control the average signal power by appropriately distributing the signal power density at different frequencies. We have also proposed precoding techniques to combine spectral shaping and filtering.

As an alternative method for adding redundancy to the transmitted signal, we have considered non-maximally decimated filterbanks. A pre-equalizer design based on the non-maximally decimated filterbanks can be used to compensate for channels. The channel filter can be non-minimum phase and its frequency response can contain special nulls. Adding redundancy using pre-filtering or non-maximally decimated filterbank is an effective way to avoid or reduce ISI. For a typical up-stream PCM channel, the required rate of redundancy is 1-2 symbols in a block of 8 transmitted symbols.

By using a baseband PAM modulation scheme, an optimum constellation design, an appropriate bit-to-symbol mapping, and the block-by-block pre-filtering the maximum achievable rate over the up-stream PCM channel can be increased to 49 kbits/sec which is 50% higher than that provided by recommendation V.90 in the up-stream direction. Many of the proposed methods can be used as part of the Recommendation V.92 to improve the performance and increase the maximum bit-rate of the up-stream PCM channel.

In Chapter 6, we introduced a phase compensation for the family of square-root raised-cosine filters so that the resulting filters satisfy Nyquist's first criterion. As a result, a raised-cosine filter can be used in two different scenarios: in the up-stream PCM channel as an interpolating filter, and in an end-to-end PCM channel as a pair of transmitter/receiver filters matched to one another.

We also introduced a new family of Nyquist filters that includes the raised-cosine filters.

Using this new family of filters, we can characterize filters with smoother spectra (compared to the standard raised-cosine spectra) which result in a faster decay of the pulse shape. This family of filters can provide more flexibility in the design of digital Nyquist filters as an approximation to the truncated analog filters.

## 7.1 Contributions

- Three types of PCM voiceband channels are characterized. The structural constraints of the up-stream channel are identified and a communication model for the up-stream channel is established (Chapter 2 and [43])
- The optimal constellation design for the up-stream PCM channel is presented and the modulation performance under the average signal power constraint is analyzed. Two methods of selecting a subset of PCM decision boundaries as detector thresholds are presented. The criterion for the subset selection is to maximize the minimum distance between adjacent thresholds while maintaining a constraint on the average signal power (Section 3.1).
- A new algorithm for index mapping over a frame of symbols is described. Its performance of the new method is compared to the existing index mapping algorithm used in the V.90 Standard and in the proposed V.92 Standard (Section 3.2.5).
- A non-equally-probable constellation design is presented. The performance improvement due to this probability assignment is analyzed. The maximum achievable data rate of a PAM modulation with non-uniform spaced and non-equally probable constellation points is computed (Section 3.3).
- A bit-to-symbol mapping method for the up-stream PCM channels based on the Huffman algorithm is presented. The shaping gain obtained via this method is compared to the maximum shaping achievable on the up-stream PCM channel (Section 3.3.4).
- A framework of the transmitter design for the up-stream PCM channel is presented. In this work, we consider MMSE as the optimization criterion and describe three different structures for the transmitter as a combination of filtering and spectral shaping (Section 4.1).
- The performance of the optimal filter design for an up-stream PCM channel is analyzed. It is shown that a reliable data transmission over the up-stream PCM channel requires almost ISI-free channel.

- A new spectral shaping method based on redundant symbol insertion is proposed (Section 4.3).
- A new block-by-block pre-filtering structure for the up-stream PCM channel is presented (Section 4.4 and [43]).
- A non-maximally filterbank structure for adding redundancies to transmitted symbols is proposed. The non-maximally decimated filterbank structure provides a natural way of adding redundancy to the symbols. The filterbanks can be composed of FIR filters even if the channel filter contains spectral nulls. The complexity of such a filter is compared with the spectral shaping and precoding techniques (Section 5.2 and [76]).
- A phase compensation technique for pulse shaping filter designs is investigated. The resulting pulse shaping filters act both as an interpolating filter in the transmitter back-end of an up-stream PCM channel and as a pair of matched filters in the end-to-end PCM channels. (Section 6.3 and [66, 67]).
- A family of generalized raised-cosine filters is presented. The new family of filters provides more flexibility in the design of pulse shaping filters, particularly in the design of digital filters as an approximation of the continuous pulse shaping filters (Section 6.4 and [66, 67]).

## 7.2 Future Work

We introduced an index mapping algorithm that can reduce the Hamming distances between adjacent points. However, this algorithm does not necessarily provide the minimum Hamming distance. Further studies regarding a generalized Gray encoding in general and a possible modification to the proposed algorithm in particular should be considered. The link between the index assignment problem in vector quantization and the modulation index mapping should be studied further. The proposed solutions for either of these problems may provide insight for the other.

In Section 3.3.3, the maximum achievable rate for an up-stream PCM channels was presented. The performance gap between the maximum achievable rate and the actual PAM performance is significant. The use of appropriate channel coding techniques over the up-stream PCM channel can reduce this gap. Furthermore, channel coding can be particularly useful to combat the residual echo that is not cancelled by the echo canceller.

The non-equally-probable distribution of constellation points results in variable length code-words for transmitted symbols. A variable-rate data transmission can be more sensitive to symbol errors. The actual number of output bits can change even if one symbol error occurs. There are

possible solutions to reduce this sensitivity. For example, the transmitted bits can be categorized into two separate channels, one with a fixed-rate as a primary channel and another with a variable-rate as secondary channel. The impact of variable rate bit-to-symbol mapping obtained via the Huffman algorithm requires further investigation.

The modulation design and channel equalization work described here is mainly concerned with the up-stream PCM channel. Many of proposed techniques can also be applied to the end-to-end PCM channels. At the end points of an end-to-end PCM channel, only a partial knowledge regarding the up-stream and the down-stream channel might be available. The sensitivity of channel equalization techniques to a mismatch between the actual channel characteristics and the estimated channel should be further investigated.

## Appendix A

# Optimal Linear Transmitter Structure

For a given channel filter  $H_c(f)$  and receiving filter  $H_r(f)$ , we derive the structure of the linear transmitter filter which for a given sequence of sampled outputs minimizes the average transmitted power. The steps are similar to those described in [46] for the receiver design.

We assume that the sequence of the transmitted symbols  $\{a_k\}$ , form a wide-sense stationary random sequence. The power spectrum density of the input sequence is denoted as  $\Phi_a(f)$ . We show that among all transmitter filters, a filter of the following form minimizes the average transmitted power,

$$\begin{aligned} H_t(f) &= G(f)(H_c(f)H_r(f))^* \\ &= G(f)H_{cr}^*(f). \end{aligned} \tag{A.1}$$

The overall filtering effect of the transmitter, channel and receiver filters at the sampling instants can be combined as an equivalent filter. The equivalent filter at the output of the sampler can be expressed as:

$$X_{eq}(f) = \sum_{k=-\infty}^{\infty} Z(f - \frac{k}{T_s}) H_{cr}(f - \frac{k}{T_s}) \tag{A.2}$$

where  $H_{cr}(f) = H_c(f)H_r(f)$  and  $Z(f)$  is an arbitrary transmitter filter.

Here we show that, for any transmitting filter  $Z(f)$ , there exists a transmitter filter in the form given in Eq. (A.1) that can produce the same output as  $Z(f)$  at the sampling instants. Replacing

the transmitter filter from Eq. (4.1) into Eq. (A.2), we have:

$$X'_{eq}(f) = G(f) \sum_{k=-\infty}^{\infty} |H_{cr}(f - \frac{k}{T_s})|^2 \quad (\text{A.3})$$

Note that in the above equation,  $G(f)$  is periodic with a period of  $1/T_s$ , hence it can be factored out from the sum. Now we choose  $G(f)$  so that  $X_{eq}(f) = X'_{eq}(f)$ . If we choose  $G(f)$  as:

$$G(f) = \frac{\sum_{k=-\infty}^{\infty} Z(f - \frac{k}{T_s})H_{cr}(f - \frac{k}{T_s})}{\sum_{k=-\infty}^{\infty} |H_{cr}(f - \frac{k}{T_s})|^2} \quad (\text{A.4})$$

the equivalent filters given by Eq. (A.2) and Eq. (A.3) will be the same.

Now we compare the average transmitted power for both filters and show that the average transmitted power for the structure given in Eq. (A.1) is less than or equal to that of  $Z(f)$ . The average transmitted power are computed as:

$$P_1 = \int_{-\frac{1}{T_s}}^{\frac{1}{T_s}} \Phi_a(f) \left( \sum_{k=-\infty}^{\infty} |Z(f - \frac{k}{T_s})|^2 \right) df \quad (\text{A.5})$$

and

$$P_2 = \int_{-\frac{1}{T_s}}^{\frac{1}{T_s}} \Phi_a(f) |G(f)|^2 \left( \sum_{k=-\infty}^{\infty} |H_{cr}(f - \frac{k}{T_s})|^2 \right) df \quad (\text{A.6})$$

Replacing  $G(f)$  from Eq. (A.4) and using the Schwarz inequality, we have

$$\begin{aligned} |G(f)|^2 \left( \sum_{k=-\infty}^{\infty} |H_{cr}(f - \frac{k}{T_s})|^2 \right) &= \frac{\left( \sum_{k=-\infty}^{\infty} Z(f - \frac{k}{T_s})H_{cr}(f - \frac{k}{T_s}) \right)^2}{\sum_{k=-\infty}^{\infty} |H_{cr}(f - \frac{k}{T_s})|^2} \\ &\leq |Z(f - \frac{k}{T_s})|^2 \end{aligned} \quad (\text{A.7})$$

From Eq. (A.7), the average power for the system of Eq. (A.1) is less or equal to the average power for general filter of Eq. (A.2). Since the channel output for both filters is the same, any reasonable optimization criterion would choose the filter with a lower average transmitted power.

## Appendix B

# Optimal MMSE Transmitting Filters

Here we derive the minimum mean square error (MMSE) solution for a discrete time transmitter filter. Figure 4.2 shows a discrete time model of the filters. As we discussed in Chapter 4, the contribution of the additive noise  $\eta[\cdot]$  in MSE is independent of the transmitter filter design. Therefore, we do not include the additive noise in our computation. In the absence of noise, the MMSE criterion for minimizing the ISI is stated as:

$$\text{MMSE} = \min_{h_t} \mathcal{E}\{(r[k] - a_k)^2\} \quad (\text{B.1})$$

We assume input symbols  $a_k$  form a stationary random sequence. The autocorrelation function and power spectrum density of  $a_k$ 's are defined in Eq. (4.7) and Eq. (4.8) respectively. We derive the MMSE solution of the transmitting filter, subject to an average transmit power constraint.

### B.1 Transmitting filter with infinite length impulse response

We consider an infinite length impulse response  $h_t[n]$  for the transmitting filter. Using the Lagrange multiplier method, we determine the optimal transmitting filter based on the following objective function:

$$\mathcal{F}_{h_t} = \mathcal{E}\{(r[k] - a_k)^2\} + \lambda(\mathcal{E}\{(x[k])^2\} - \mathcal{P}_t) \quad (\text{B.2})$$

Expanding the right-hand side of Eq. (B.2), we obtain:

$$\begin{aligned} \mathcal{F}_{h_t} = & \sum_i \sum_j \phi_a[i-j] h_t[i] h_t[j] - 2 \sum_i \phi_a[i] h_t[i] + \phi_a[0] \\ & + \lambda \left( \sum_i \sum_j \phi_a[i-j] h_t[i] h_t[j] - \mathcal{P}_t \right) \end{aligned} \quad (\text{B.3})$$

where the overall transmitter, channel and receiver filter impulse response is:

$$h[n] = \sum_i h_t[i] h_{cr}[n - i]$$

To compute the MMSE, we take the derivative of the objective function with respect to the transmitting filter coefficients  $h_t[k]$ . For all values of  $k$ , we have<sup>1</sup>:

$$\begin{aligned} \frac{\partial}{\partial h_t[k]}(\mathcal{F}_{h_t}) &= \sum_{i=-\infty}^{\infty} \sum_{j=-\infty}^{\infty} \phi_a[i - j] \left( \frac{\partial}{\partial h_t[k]}(h[i] h[j]) \right) \\ &\quad - 2 \sum_{i=-\infty}^{\infty} \phi_a[i] \frac{\partial}{\partial h_t[k]}(h[i]) \\ &\quad + \lambda \sum_{i=-\infty}^{\infty} \sum_{j=-\infty}^{\infty} \phi_a[i - j] \left( \frac{\partial}{\partial h_t[k]}(h_t[i] h_t[j]) \right) \end{aligned} \quad (\text{B.4})$$

To minimize the objective function, the derivatives with respect to the coefficients  $h_t[k]$  should be zero. The resulting equations for all values of  $k$  are:

$$2\phi_a[k] \otimes h_t[k] \otimes h_{cr}[k] \otimes h_{cr}[-k] - 2\phi_a[k] \otimes h_{cr}[-k] + 2\lambda\phi_a[k] \otimes h_t[k] = 0 \quad (\text{B.5})$$

where “ $\otimes$ ” denotes the discrete convolution. Equation B.5 can be simplified to:

$$h_t[k] \otimes \left( h_{cr}[k] \otimes h_{cr}[-k] + \lambda \right) = h_{cr}[-k] \quad (\text{B.6})$$

In the frequency domain, Eq. (B.6) corresponds to the following expression for the transmitting filter transfer function:

$$H_t(e^{j\omega T_s}) = \frac{H_{cr}(e^{-j\omega T_s})}{|H_{cr}(e^{j\omega T_s})|^2 + \lambda} \quad (\text{B.7})$$

where  $\lambda$  is determined from the average power constraint. Replacing  $H_t(e^{j\omega T_s})$  in the power constrain equation Eq. (4.11), we obtain:

$$\frac{1}{2\pi} \int_{-\pi}^{\pi} \frac{|H_{cr}(e^{j\omega T_s})|^2}{(|H_{cr}(e^{j\omega T_s})|^2 + \lambda)^2} \Phi_a(e^{j\omega T_s}) d\omega = \mathcal{P}_t \quad (\text{B.8})$$

The MSE can be written in terms of the transfer function of the filters and power spectrum density

---

<sup>1</sup>Note that in our discussion  $h[n]$  is an impulse response with real coefficients. Optimization of real function with respect to complex coefficients is discussed in [77]

of the input data:

$$\begin{aligned}
\text{MSE} &= E\{(r[k] - a_k)^2\} \\
&= \frac{1}{2\pi} \int_{-\pi}^{\pi} \Phi_a(e^{j\omega T_s}) H(e^{j\omega T_s}) H(e^{-j\omega T_s}) d\omega \\
&\quad - \frac{1}{\pi} \int_{-\pi}^{\pi} \Phi_a(e^{j\omega T_s}) H(e^{j\omega T_s}) d\omega + \frac{1}{2\pi} \int_{-\pi}^{\pi} \Phi_a(e^{j\omega T_s}) d\omega
\end{aligned} \tag{B.9}$$

where  $H(e^{j\omega T_s}) = H_t(e^{j\omega T_s})H_{cr}(e^{j\omega T_s})$ . Substituting the optimal transmitting filter of Eq. (B.7) into this expression, we compute the minimum mean square error (MMSE) as:

$$\text{MMSE} = \frac{\lambda^2}{2\pi} \int_{-\pi}^{\pi} \frac{\Phi_a(e^{j\omega T_s})}{(|H_{cr}(e^{j\omega T_s})|^2 + \lambda)^2} d\omega \tag{B.10}$$

## B.2 Finite Impulse Response

We consider a finite impulse response of length  $2K + 1$  for the transmitting filter. The filter coefficients are denoted as  $c_k$ .

$$h_t[k] = \begin{cases} c_k & \text{for } |k| \leq K \\ 0 & \text{elsewhere} \end{cases} \tag{B.11}$$

We also assume the channel impulse response  $h_{cr}[n]$  has finite length with  $L$  non-zero coefficients:

$$h_{cr}[n] = 0 \quad \text{for } n < 0 \quad \& \quad n \geq L \tag{B.12}$$

The objective function given in Eq. (B.2) is given by:

$$\begin{aligned}
\mathcal{F}_C &= \sum_{i=-K}^{K+L-1} \sum_{j=-K}^{K+L-1} \phi_a[i-j] h[i] h[j] - 2 \sum_{i=-K}^{K+L-1} \phi_a[i] h[i] \\
&\quad + \phi_a[0] + \lambda \left( \sum_{i=-K}^K \sum_{j=-K}^K \phi_a[i-j] c_i c_j - \mathcal{P}_t \right)
\end{aligned} \tag{B.13}$$

where the overall impulse response  $h[n]$  can be computed as:

$$h[n] = \sum_{i=-K}^K c_i h_{cr}[n-i] \quad \text{for } -K \leq n \leq L+K-1 \tag{B.14}$$

The derivative of Eq.( B.2) with respect to  $c_k$  for  $|k| \leq K$  can be written as:

$$\begin{aligned} \frac{\partial}{\partial c_k}(\mathcal{F}_C) = & 2 \sum_{l=-K}^K \sum_{i=-K}^{K+L-1} \sum_{j=-K}^{K+L-1} \phi_a[i-j] h_{cr}[j-k] h_{cr}[i-l] \\ & - 2 \sum_{l=K}^K \phi_a[l] h_{cr}(l-k) + 2\lambda \sum_{l=-K}^K \phi_a[k-l] c_l \end{aligned} \quad (\text{B.15})$$

These equations can be simplified to:

$$\sum_{l=-K}^K \Gamma_{kl} c_j = \xi_k \quad \text{for } |k|, |l| \leq K \quad (\text{B.16})$$

where

$$\Gamma_{kl} = \sum_{i=-K}^{K+L-1} \sum_{j=-K}^{K+L-1} \phi_a[i-j] h_{cr}[j-k] h_{cr}[i-l] + \lambda \phi_a[k-l] \quad (\text{B.17})$$

and

$$\xi_k = \sum_{m=-K}^K h_{cr}[m-k] \phi_a[m] \quad \text{for } |k| \leq K \quad (\text{B.18})$$

Equation (B.16) has the following matrix form

$$\mathbf{\Gamma} \mathbf{C}_{opt} = \boldsymbol{\xi} \quad (\text{B.19})$$

## Appendix C

# Inner boundaries of the eye pattern for the square-root filter

To find the lower boundaries of the eye pattern diagram of the square-root full raised-cosine filter, we first determine the maximum ISI for a PAM signal. From Eq. (6.1), we obtain:

$$x(\tau) = a_0 g(\tau) + \sum_{\substack{n=-\infty \\ n \neq 0}}^{\infty} a_k g(\tau - n) \quad (\text{C.1})$$

where  $\tau$  is the time offset relative to the sampling instances  $nT_s$ . The second term in this equation is due to ISI. In the case of binary PAM signal with  $a_k = \pm 1$ , the maximum ISI for a Nyquist pulse is calculated as:

$$D(\tau) = \sum_{\substack{n=-\infty \\ n \neq 0}}^{\infty} |g(\tau - n)| \quad (\text{C.2})$$

therefore, the eye-pattern boundaries are:

$$\begin{aligned} \text{Lower Boundaries:} &= \pm (g(\tau) - D(\tau)) \\ \text{Upper Boundaries:} &= \pm (g(\tau) \pm D(\tau)) \end{aligned} \quad (\text{C.3})$$

Substituting Eq. (6.23) into Eq. (C.2), we obtain

$$g(\tau) - D(\tau) = \frac{-\cos(2\pi\tau)}{4\pi(\tau + 1/4)(\tau - 1/4)} - \frac{\cos(2\pi\tau)}{4\pi} \sum_{\substack{n=-\infty \\ n \neq 0}}^{\infty} \left| \frac{1}{(\tau + n + 1/4)(1/4 - \tau - n)} \right| \quad (\text{C.4})$$

For  $|\tau| \leq 1/4$ , the above expression simplifies to:

$$g(\tau) - D(\tau) = -\frac{\cos(2\pi\tau)}{4\pi} \sum_{n=-\infty}^{\infty} \frac{1}{(\tau + n + 1/4)(\tau + n - 1/4)} \quad \text{for } |\tau| \leq \frac{1}{4} \quad (\text{C.5})$$

Consider the following identity

$$\sum_{k=-\infty}^{\infty} \frac{1}{(x + k + 1/4)(x + k - 1/4)} = \frac{-4\pi}{\cos(2\pi x)}. \quad (\text{C.6})$$

Therefore, the lower boundaries of the eye pattern are

$$\pm(g(\tau) - D(\tau)) = \pm 1 \quad \text{for } |\tau| \leq \frac{1}{4} \quad (\text{C.7})$$

## Appendix D

# The impulse response of $H_{sqr}(f)$

To obtain the impulse response given in Eq. (6.35), we note that  $H_{sqr}(f)$ , as defined in Eq. (6.33), has Hermitian symmetry. The inverse Fourier transform of  $\sqrt{T_s} H_{sqr}(f)$  can be written as:

$$\begin{aligned}
 \mathcal{F}^{-1}\{\sqrt{T_s} H_{sqr}(f)\} &= 2T_s \int_0^{\frac{1-\alpha}{2T_s}} \cos(2\pi ft) df + 2T_s \int_{\frac{1-\alpha}{2T_s}}^{\frac{1+\alpha}{2T_s}} \cos(\phi(f)) \cdot \cos(\phi(f) + 2\pi ft) df \\
 &= 2T_s \int_0^{\frac{1-\alpha}{2T_s}} \cos(2\pi ft) df \\
 &\quad + T_s \int_{\frac{1-\alpha}{2T_s}}^{\frac{1+\alpha}{2T_s}} \cos(2\pi ft) df + T_s \int_{\frac{1-\alpha}{2T_s}}^{\frac{1+\alpha}{2T_s}} \cos(2\phi(f) + 2\pi ft) df
 \end{aligned} \tag{D.1}$$

where  $\phi(f)$  is defined in Eq. (6.32). The first two terms of Eq. (D.1) can be combined as follows:

$$2T_s \int_0^{\frac{1-\alpha}{2T_s}} \cos(2\pi ft) df + T_s \int_{\frac{1-\alpha}{2T_s}}^{\frac{1+\alpha}{2T_s}} \cos(2\pi ft) df = \text{sinc}\left(\frac{t}{T_s}\right) \cdot \cos\left(\frac{\pi t \alpha}{T_s}\right) \tag{D.2}$$

By introducing a new variable  $x = \frac{2T_s}{\alpha}(f - \frac{1}{2T_s})$ , we simplify the third integral in Eq. (D.1) to:

$$\begin{aligned}
 T_s \int_{\frac{1-\alpha}{2T_s}}^{\frac{1+\alpha}{2T_s}} \cos(2\phi(f) + 2\pi ft) df &= \frac{\alpha}{2} \int_{-1}^1 \sin\left(\frac{\pi}{2}V(x) - \frac{\pi t \alpha}{T_s}x + \frac{\pi t}{T_s}\right) dx \\
 &= \alpha \sin\left(\frac{\pi t}{T_s}\right) \int_0^1 \cos\left(\frac{\pi}{2}V(x) - \frac{\pi t \alpha}{T_s}x\right) dx
 \end{aligned} \tag{D.3}$$

Combining Eq. (D.2) and Eq. (D.3), we obtain the result as given in Eq. (6.35).

## References

- [1] K. Pahlavan and J. L. Holsinger, "Voiceband data communication modems – a historical review 1919–1988," *IEEE Commun. Mag.*, vol. 26, pp. 16–27, Jan. 1988.
- [2] ITU-T Recommendation V.34, "A Modem Operating at Data Signalling Rates of Up to 28,800 bit/s for Use on the General Switched Telephone Network and on Leased Point-to-Point 2-Wire Telephone-Type Circuits," *ITU-T V Series Recommendations*, 1994.
- [3] G. D. Forney, L. Brown, M. V. Eyuboglu, and J. L. Moran III, "The V.34 high-speed modem standard," *IEEE Commun. Mag.*, vol. 34, pp. 28–33, Dec. 1996.
- [4] I. Kalet, J. E. Mazo, and B. R. Saltzberg, "The capacity of PCM voiceband channels," *Proc. IEEE Int. Conf. Commun.*, pp. 507–511, 1993.
- [5] E. Ayanoglu, N. R. Dagdeviren, G. D. Golden, and J. E. Mazo, "An equalizer design technique for the PCM modem: A new modem for the digital public switched network," *IEEE Trans. Commun.*, vol. 46, pp. 763–774, June 1998.
- [6] H. Herzberg and B. R. Saltzberg, "Coding for a channel with quantization in the presence of an estimable interference," *IEEE Trans. Commun.*, vol. 45, pp. 45–51, Jan. 1997.
- [7] E. Ayanoglu, N. R. Dagdeviren, J. E. Mazo, and B. R. Saltzberg, "A high-speed modem synchronized to a remote codec," *United States Patent*, no. 5 394 437, Feb. 1995.
- [8] E. Ayanoglu, G. D. Golden, R. K. Jones, and J. E. M. D. G. Shaw, "High speed quantization-level-sampling modem with equalization arrangement," *United States Patent*, no. 5 528 625, June 1996.
- [9] N. R. Dagdeviren, "Modem with received signals and transmitted signals comprising signal sets," *United States Patent*, no. 5 406 583, Apr. 1995.
- [10] H. Herzberg and B. R. Saltzberg, "Communication arrangement with improved echo and noise suppression in a channel containing quantization," *United States Patent*, no. 5 710 790, Jan. 1998.
- [11] B. Townshend, "High speed communications system for analog subscriber connections," *United States Patent*, no. 5 801 695, Sept. 1998.

- 
- [12] P. A. Humblet and M. G. Troulis, "The information driveway," *IEEE Communications Magazine*, vol. 34, pp. 64–68, Dec. 1996.
- [13] ITU-T Recommendation V.90, "A digital modem and analogue modem pair for use on the public switched telephone network (PSTN) at data signalling rates of up to 56 000 bit/s downstream and up to 33 600 bits upstream," *ITU-T V Series Recommendations*, 1998.
- [14] D. Kim and V. Eyuboglu, "Convolutional spectral shaping," *IEEE Commun. Lett.*, vol. 3, pp. 9–11, Jan. 1999.
- [15] B. Barazesh, "PCM upstream considerations for the US Interim Standard," *Telecommunication Industry Association (TIA), Technical Committee TR-30 Meetings*, January 1997.
- [16] N. Dagdeviren, "Estimated Coverage with PCM Upstream," *Telecommunication Industry Association (TIA), Technical Committee TR-30 Meetings*, January 1997.
- [17] V. Eyuboglu, "Upstream transmission in PCM modems," *Telecommunication Industry Association (TIA), PCM Modem Ad-Hoc Group Contribution*, January 1997.
- [18] N. Warke and M. Ali, "On the next generation of high-speed voiceband modems," *Proc. IEEE Int. Conf. Commun.*, pp. 256–260, 1999.
- [19] W. D. Reeve, *Subscriber Loop Signaling and Transmission Handbook, Analog*. IEEE Press, New York, NY, 1992.
- [20] W. D. Reeve, *Subscriber Loop Signaling and Transmission Handbook, Digital*. IEEE Press, New York, NY, 1995.
- [21] T. Starr, J. M. Cioffi, and P. Silverman, *Understanding Digital Subscriber Line Technology*. Prentice-Hall, Upper Saddle River, NJ, 1999.
- [22] Members of Technical Staff, *Transmission Systems for Communications*. Bell Telephone Laboratories, New York, NY, Fifth ed., 1982.
- [23] S. Ramo, J. R. Whinnery, and T. Van Duzer, *Fields and Waves in Communication Electronics*. Wiley, New York, NY, Second ed., 1984.
- [24] ITU-T Recommendation V.56bis, "Network transmission model for evaluating modem performance over 2-wire voice grade connect," *ITU-T V Series Recommendations*, August 1995.
- [25] Recommendation G.712, "Transmission performance characteristics of Pulse Code Modulation channels," *ITU-T G series Recommendations*, November 1996.
- [26] A. V. Oppenheim and R. W. Schaffer, *Discrete-Time Signal Processing*. Prentice-Hall, Englewood Cliffs, NJ, 2nd ed., 1998.
- [27] Recommendation G.711, "Pulse code modulation (PCM) of voice frequencies," *ITU-T G Series Recommendations*, 1988.

- 
- [28] J. E. Mazo, "Quantization noise and data transmission," *The Bell System Technical Journal*, vol. 47, pp. 1737–1753, Oct. 1968.
- [29] C. E. Shannon, "A mathematical theory of communication," *Bell System Technical Journal*, vol. 61, pp. 379–423 and 623–656, July and Oct. 1948.
- [30] R. Lucky, J. Salz, and E. Weldon, *Principles of Data Communication*. McGraw-Hill, Book Company, New York, NY, 1968.
- [31] N. Warke and M. Ali, "Optimum CODEC companding for high-speed PCM data transmission in telephone networks.," *IEEE Int. Conf. on Acoustics, Speech, Signal Processing*, pp. 2679–2682, March 1999.
- [32] J. G. Proakis, *Digital Communications*. McGraw-Hill, New York, NY, third ed., 1995.
- [33] N. Farvardin, "A study of vector quantization for noisy channels," *IEEE Trans. Inform. Theory*, vol. 36, pp. 799–809, July 1990.
- [34] K. Zeger and A. Gersho, "Pseudo-Gray coding," *IEEE Trans. Commun.*, vol. 38, pp. 2147–2158, Dec. 1990.
- [35] P. Knagenhjelm and E. Agrell, "The Hadamard transform – a tool for index assignment," *IEEE Trans. Inform. Theory*, vol. 42, pp. 1139–1151, July 1996.
- [36] P. Knagenhjelm, "How good is your index assignment?," *IEEE Int. Conf. on Acoustics, Speech, Signal Processing*, pp. 423–426, vol. II, Apr. 1993.
- [37] T. M. Cover and J. A. Thomas, *Elements of Information Theory*. Wiley, New York, NY, 1991.
- [38] E. A. Lee and D. G. Messerschmitt, *Digital Communication*. Kluwer Academic Publishers, Boston, MA, 1994.
- [39] F. R. Kschischang and S. Pasupathy, "Optimal nonuniform signaling for gaussian channels," *IEEE Trans. Inform. Theory*, vol. 39, pp. 913–929, May 1993.
- [40] G. Ungerboeck, "Channel coding with multilevel/phase signals," *IEEE Trans. Inform. Theory*, vol. 28, pp. 55–67, Jan. 1982.
- [41] R. D. Gitlin, J. F. Hayes, and S. B. Weinstein, *Data Communications Principles*. Plenum Press, New York, NY, 1992.
- [42] R. E. Blahut, *Digital Transmission of Information*. Addison-Wesley, Reading, MA, 1990.
- [43] N. S. Alagha and P. Kabal, "Linear time varying precoder applied to ISI channel," *IEEE Pacific Rim Conf. Commun., Computers and Sig. Processing*, pp. 36–39, Aug. 1997.
- [44] D. W. Tufts, "Nyquist's problem—The joint optimization of transmitter signal and receiver in pulse amplitude modulation," *Proc. IEEE*, vol. 53, pp. 248–259, Mar. 1965.

- 
- [45] J. W. Smith, "The joint optimization of transmitted signal and receiving filter for data transmission systems," *Bell System Technical Journal*, vol. 44, pp. 2363–2392, Dec. 1965.
- [46] T. Ericson, "Structure of optimum receiving filters in data transmission systems," *IEEE Trans. Inform. Theory*, vol. 17, pp. 352–353, May 1971.
- [47] T. Ericson, "Optimum PAM filters are always band limited," *IEEE Trans. Inform. Theory*, vol. 19, pp. 570–573, July 1973.
- [48] J. G. Proakis and D. G. Manolakis, *Digital Signal Processing*. Prentice-Hall, Englewood Cliffs, NJ, Third ed., 1996.
- [49] W. Gardner, *Introduction to Random Processes*. McGraw-Hill, New York, NY, Second ed., 1989.
- [50] M. Tomlinson, "New automatic equaliser employing modulo arithmetic," *Electron. Lett.*, vol. 7, pp. 138–139, Mar. 1971.
- [51] H. Harashima and H. Miyakawa, "Matched-transmission technique for channels with intersymbol interference," *IEEE Trans. Commun.*, vol. 20, pp. 774–780, Aug. 1972.
- [52] B. R. Saltzberg, "Intersymbol interference error bounds with application to ideal bandlimited signaling," *IEEE Trans. Inform. Theory*, vol. 14, pp. 563–568, July 1968.
- [53] K. Yao and R. M. Tobin, "Moment space upper and lower bounds for digital systems with intersymbol interference," *IEEE Trans. Inform. Theory*, vol. 22, pp. 65–74, Jan. 1976.
- [54] F. E. Glave, "An upper bound on the probability of error due to intersymbol interference for correlated digital signals," *IEEE Trans. Inform. Theory*, vol. 18, pp. 356–263, May 1972.
- [55] A. Calderbank, T. Lee, and J. E. Mazo, "Baseband trellis codes with spectral null at zero," *IEEE J. Selected Areas Communications*, vol. 34, pp. 425–434, May 1988.
- [56] P. Kabal and S. Pasupathy, "Partial-response signaling," *IEEE Trans. Commun.*, vol. 23, pp. 921–934, Sept. 1975.
- [57] F. A. Graybill, *Matrices with Applications in Statistics*. Wadsworth International Group, Belmont, California, Second ed., 1983.
- [58] G. H. Golub and C. F. Van Loan, *Matrix Computations*. John Hopkins University Press, Baltimore, 1996.
- [59] H. Harashima and H. Miyakawa, "Matched-transmission technique for channels with intersymbol interference," *IEEE Trans. Commun.*, vol. 20, pp. 774–780, Aug. 1972.
- [60] J. E. Mazo and J. Salz, "On the transmitted power in generalized partial response," *IEEE Trans. Commun.*, vol. 24, pp. 348–352, Mar. 1976.
- [61] J. M. Wozencraft and I. M. Jacobs, *Principles of Communication Engineering*. Wiley, New York, NY, 1965.

- 
- [62] J. L. Yen, "On the non-uniform sampling of bandwidth-limited signals," *IRE transactions on Circuit Theory*, vol. CT-3, pp. 251–257, Dec. 1956.
- [63] P. Vaidyanathan, *Multirate Systems and Filter banks*. Prentice-Hall, Englewood Cliffs, NJ, 1993.
- [64] T. Li and Z. Ding, "Joint transmitter-receiver optimization for partial response channels based on nonmaximally decimated filterbank precoding technique," *IEEE Trans. Commun.*, vol. 47, pp. 2407–2414, Sept. 1999.
- [65] A. Wang and J. Smith, "On fast FIR filters implemented as tail-canceling IIR filters," *IEEE Trans. Signal Processing*, vol. 45, pp. 1415–1427, June 1997.
- [66] N. S. Alagha and P. Kabal, "Generalized raised-cosine filters," *IEEE Trans. Commun.*, vol. 45, pp. 989–997, July 1999.
- [67] N. S. Alagha and P. Kabal, "A family of Nyquist filters based on generalized raised-cosine spectra," *Proc. 19th Biennial Symp. Commun.*, pp. 131–135, July 1998.
- [68] X.-G. Xia, "A family of pulse-shaping filters with ISI-free matched and unmatched filter properties," *IEEE Trans. Commun.*, vol. 45, pp. 1157–1158, Oct. 1997.
- [69] R. A. Gibby and J. W. Smith, "Some extensions of Nyquist's telegraph transmission theory," vol. 44, pp. 1487–1510, Sept. 1965.
- [70] J. A. C. Bingham, *The Theory and Practice of Modem Design*. Wiley, New York, NY, 1988.
- [71] P. Kabal and E. Dubois, "Interpolating and Nyquist filters with constraints at certain frequencies," *Signal Processing*, vol. 24, pp. 117–126, Aug. 1991.
- [72] R. P. Ramachandran and P. Kabal, "Minimax design of factorable Nyquist filters for data transmission systems," *Signal Processing*, vol. 18, pp. 327–339, Nov. 1989.
- [73] C. J. Zarowski, "Orthogonal wavelet packet functions and Nyquist pulses," *Proc. 19th Biennial Symp. Commun.*, pp. 136–139, June 1998.
- [74] José A. de la O, "On the use of amplitude shaping pulses as windows for harmonic analysis," *IMTC*, pp. 1388–1393, 2000.
- [75] C. Tan and N. Beaulieu, "An investigation of transmission properties of Xia Pulses," *Proc. IEEE Int. Conf. Commun.*, 1999.
- [76] N. S. Alagha and P. Kabal, "A filterbank structure for voice-band PCM channel pre-equalization," *IEEE Int. Conf. on Acoustics, Speech, Signal Processing*, pp. 2793–2796, June 2000.
- [77] S. Haykin, *Adaptive Filter Theory*. Prentice-Hall, Englewood Cliffs, NJ, 3 ed., 1996.